Stimuli-Responsive Microgel-Based Systems and Their Application for Controlled Drug Release

by

Yongfeng Gao

A thesis submitted in partial fulfillment of the requirements for the degree of

Doctor of Philosophy

Department of Chemistry
University of Alberta

Abstract

Stimuli-responsive polymers have found their way into numerous materials and devices for myriad applications that can solve problems related to human health and the environment. In this dissertation, the work covers the general scope of stimuli-responsive polymers, with a special focus on thermo-responsive poly (*N*-isopropylacrylamide) (pNIPAm)-based microgels and their co-functional composites, and their applications in controlled drug delivery.

Chapter 1 gives a brief introduction about stimuli-responsive polymers and Chapter 2 discusses the applications of stimuli-responsive polymers in controlled drug delivery. In Chapter 3, the study of rate control, by varying the thickness of a membrane (device Au layer) was shown to control the rate of release from the device. With the increase of Au layer thickness, the drug release rate is able to slow down and the release could be triggered by temperature and pH. After that, the modification of the devices membrane layer was investigated for its ability to control the release behavior (Chapter 4). Subsequently, a multi-drug releasing system was developed by incorporating two different microgels, which has the ability to sequential release drugs by changing the pH (Chapter 5). Free-standing assemblies of microgels were then generated by simply applying a sacrificial layer under the film and this film was transferable to other substrates, whether flat or curve surface, and even human skin (Chapter 6). In Chapter 7, the optical properties and drug releasing behavior were studied on this developed device by light-induced pH change, which makes this platform versatile for developing smart systems based on other stimuli. Furthermore, by tuning the chemistry of microgels, we were able to generate microgel-based aggregates for drug delivery applications from microgels with opposite charges (Chapter 8). In Chapter 9, novel microgels from supramolecular crosslinker were firstly prepared

with the degradable properties. The characterizations of this microgel promote it as a great candidate for degradable drug delivery system.

Finally, in Chapter 10, conclusion and future outlook are presented to illustrate the future direction of this research topic.

Preface

This thesis is an original work by Yongfeng Gao (Y. Gao) under the supervision from Dr. Michael J. Serpe (M. J. Serpe).

Chapter 3 of this thesis has been published as Y. Gao, G. P. Zago, Z. Jia, and M. J. Serpe, Study of Controlled and Triggered Small Molecule Release from a Confined Polymer Film. *ACS Appl. Mater. Interfaces,* 2013, 5, 9803-9808. I was responsible for the data collection and analysis as well as the manuscript composition. G. P. Zago and Z. Jia assisted with the data collection. M. J. Serpe was the supervisory author and was involved with research design and manuscript composition.

Chapter 4 of this thesis is based on publication as S. Guo, Y. Gao, M. Wei, Q. Zhang and M. J. Serpe, Surface Modification of Microgels Assemblies Systems for Controlled Drug Release. *J. Mater. Chem. B*, 2015, 3, 2516-2521. I was responsible for the experiment design, data analysis as well as the manuscript composition. S. Guo and I were contributing equally to this publication. M. Wei, Q. Zhang assisted with the manuscript composition. M. J. Serpe was the supervisory author and was involved with research design and manuscript composition.

Chapter 5 of this thesis has been published as Y. Gao, K. Wong, A. Ahiabu and M. J. Serpe with the study of Sequential and Controlled Release of Small Molecules from Poly (*N*-isopropylacrylamide) Microgel-Based Reservoir Devices. *J. Mater. Chem. B*, 2016, 4, 5144-5150. I was responsible for the experiment design, data collection and analysis as well as the manuscript composition. K. Wong was responsible for the data collection and we were contributing equally to this study. A. Ahiabu assisted with the manuscript composition. M. J. Serpe was the supervisory author and was involved with research design and manuscript composition.

Chapter 6 of this thesis is based on the publication as Y. Gao, W. Xu and M. J. Serpe, Study of Free-standing poly (*N*-isopropylacrylamide) microgel-based etalons. *J. Mater. Chem. C*, 2014, 2, 5878-5884. I was responsible for the experiment design, data collection and analysis as well as the manuscript composition. W. Xu assisted with the data collection. M. J. Serpe was the supervisory author and was involved with research design and manuscript composition.

Chapter 7 of this thesis is based on the publication of Light-Induced Color Changes of Microgel-Based Etalons, *ACS Appl. Mater. Interfaces*, 2014, 6, 8461-8466, by Y. Gao and M. J. Serpe. I was responsible for the experiment design, data collection and analysis as well as the manuscript composition. M. J. Serpe was the supervisory author and was involved with research design and manuscript composition.

Chapter 8 of this thesis has been published as Y. Gao, A. Ahiabu, and Michael J. Serpe, Controlled Drug Release from the Aggregation-Disaggregation Behavior of pH-Responsive Microgels. *ACS Appl. Mater. Interfaces*, 2014, 6, 13749-13756. I was responsible for the experiment design, data collection and analysis as well as the manuscript composition. A. Ahiabu assisted with the data collection as well as the manuscript composition and contributes equally with me. M. J. Serpe was the supervisory author and was involved with research design and manuscript composition.

Chapter 9 of this thesis has been published as Q. Song, Y. Gao, J. Xu, B. Qin, M. J. Serpe, and X. Zhang, Study of Supramolecular Microgels Fabricated from Supramonomers. *ACS Macro Lett.,* 2016, 5, 1084-1088. Q. Song and I were contributed equally and responsible for the experiment design, data collection and analysis as well as the manuscript composition. J. Xu, B. Qin assisted with the manuscript composition. M. J. Serpe and X. Zhang were the supervisory author and was involved with research design and manuscript composition.

I would like to dedicate this thesis to my parents, Xueren Gao and Gaitang Su, my wife, Li Zhang, and my sons, Charles Gao and Anthony Gao.

Acknowledgement

I would like to express my sincere thanks to my supervisors, Dr. Michael J. Serpe, for providing me an opportunity to take this wonderful journey of exploring various topics in Polymer materials at University of Alberta. Without your constant encouragements, suggestions, and guidance, I could not have been able to achieve this degree.

I would also like to offer my sincere thanks to Dr. Xi Zhang (Tsinghua University) for providing me opportunities to work with a team of excellent chemistry scientists. Special thanks will be credited to Mr. Qiao Song, who collaborated and discussed a lot with me making supramolecules microgel works.

Many thanks to previous lab members and also my good friends: Dr. Xue Li, Dr. Molla Islam, and Mr. Gustavo P. Zago, and all current members in Dr. Serpe's group.

I would like to show my great thanks to my supervisor committee members, Dr. Jillian Buriak and Dr. Julianne Gibbs-Davis, for their valuable suggestions and comments on my research.

Thanks financial support from the Alberta Innovates Technology Futures (AITF) in Alberta.

I would like to thank my dear parents, two elder sisters and brother for your supporting and understanding, and all the encouragements, confidences, and loves that you continuously delivered in the past 30 years.

I want to express my great thanks to my lovely wife, Li Zhang, who has sacrificed so much to make my life go this far, who bring two cute angels, Charles and Anthony, with all happiness and joys. Thank you very much for your unconditional love and support for the past eight years and it truly brings me power and great enthusiasm. I love you.

Table of Contents

List of Schemes

List of Figures

List of Abbreviations

pNIPAm	poly (*N*-isopropylacrylamide)
LCST	lower critical solution temperature
AAc	acrylic acid
UCST	upper critical solution temperature
PVCL	poly (*N*-vinylcaprolactone)
ΔG	free energy of dissolution
ΔH	dissolution change
ΔS	entropy change
PDMAEMA	poly (*N, N'*-dimethylamino ethyl methacrylate)
MAAc	methacrylic acid
pOEGMAs	poly (oligo (ethylene glycol) methacrylates
pMVE	poly (methyl vinyl ether)
PAA	poly (acrylic acid)
EAPs	electroactive polymers
PEG	poly(ethylene glycol)
p(NIPAm-*co*-AAc)	poly (*N*-isopropylacrylamide-*co*-acrylic acid)
DTT	dithiothreitol
GSH	glutathione
TMBQ	Trimethyl-locked benzoquinone
TEMPO	4-*N*-amino- 2,2,6,6-tetramethylpiperidin-1-oxyl-4-yl
ROS	reactive oxygen species
PPS	poly (propylene sulfide)

PU	polyurethane
VPTT	volume phase transition temperature
p(NIPAm-*co*-MAA)	poly (*N*-isopropylacrylamide-*co*-methacrylic acid)
p(NIPAm-*co*-APBA)	poly (*N*-isopropylacrlamide-3-(acrylamido) phenylboronic acid)
BIS	*N, N'*-methylene-bis-acrylamide
PEGDA	poly (ethylene glycol) diacrylate
AIBN	azobisisobutyronitrile
APS	ammonium persulfate
DLS	dynamic light scattering
DIC	differential interference contrast
APBA	3-aminopenylboronic acid
APMH	*N*-3-aminopropyl methacrylamide hydrochloride
4-VP	4-vinyl pyridine
o-NB	*o*-nitro benzyl
PLA	polylactic acid
p(NIPAm-*co*-4VP-*co*-NAS)	poly (*N*-isopropylacrylamide-*co*-4-vinylpyridine-*co*-*N*-acryloxysuccinimide)
MMPs	matrix metalloproteinases
EPR	enhanced permeability and retention effect
1D	one dimensional
2D	two dimensional
3D	three dimensional

PLGA	poly (lactic-*co*-glycolic acid)
NIR	near infrared
pNIPAm-*g*-CS	poly (*N*-isopropylacrylamide)-graft-chitosan
Dox	doxorubicin
DMAPMA	*N*-[3-(dimethylamnino)propyl]methacrylamide
PDADMAC	poly (diallyl dimethyl ammonium chloride)
PSS	poly (sodium 4-styrene-sulfonate)
PAH	poly (allylamine hydrochloride)
LBL	Layer-by-layer
PDMS	polydimethylsiloxane
CV	crystal violet
MB	methylene blue
PBS	phosphate buffer solution
o-NBA	*o*-nitrobenzaldehyde
p(NIPAm-*co*-DMAPMA)	poly (*N*-isopropylacrylamide-*co*-*N*-[3-(Dimethylamino) propyl] methacrylamide
pAPBA-MG	poly (*N*-isopropylacrylamide-*co*-3-aminopenylboronic acid) microgels
pAAc-MG	poly (*N*-isopropylacrylamide-*co*-acrylic acid) microgels
CB[8]	cucurbit[8]uril
DMADA	3,5-Dimethyl-1-adamantanamine hydrochloride
TEA	triethylamine
FGG	Phe-Gly-Gly peptides

SEM	scanning electron microscope
TEM	transmission electron microscopy
NMR	nuclear magnetic resonance spectroscopy
ITC	isothermal titration calorimetry
XPS	X-ray photoelectron spectroscopy
SIMS	static secondary ion mass spectrometry
AFM	atomic-force microscopy
ESI-MS	electrospray ionization mass spectrometry

Chapter 1: Introduction

1.1 Stimuli-responsive polymers

Nature has created materials and systems with the ability to respond and adapt in response to their environmental conditions by changing their structure and/or chemistry.[1] For example, snakes facial pits are extremely sensitive to the environmental temperature change;[2] chameleons can change their color to adapt to the environment;[3] plants like *Dionaea muscipula* and *Mimosa pudica* react to mechanical stimulus allowing them to protect themselves or capture nutrients.[4, 5] Inspired by nature, materials with dynamic and tunable properties, which are typically referred as smart or stimuli-responsive materials[6-9] have been developed. Over the past few decades, polymers that can undergo physical or chemical changes as a consequence of small environmental variations (stimuli-responsive polymers), have been considered as one of the largest family of smart materials. The responses can be defined in a variety of ways depending on how the physical or chemical properties of the polymer change, e.g., a change in polymer size, structure, color, or solubility. The environment variations act as a stimulus to trigger the response of the materials. The scientific interest in stimuli-responsive polymers has persisted over the last several decades, and a tremendous amount of work has been dedicated to devising examples of environmentally sensitive polymers that can be crafted into new smart materials as shown in Figure 1-1. Stimuli-responsive polymers provide an ideal candidate to design smart materials, offering great opportunities to develop intelligent systems.

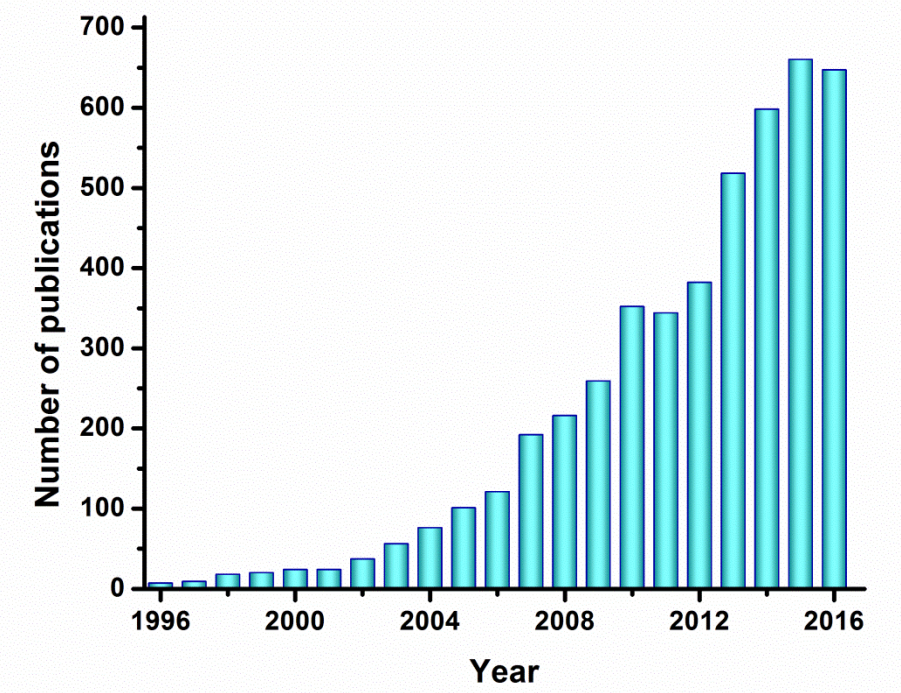

Figure 1-1. Representation of the growing interest in the field of stimuli-responsive polymers from years 1996 to 2016 inclusive, in the form of a number of publications per year. Data collected from Web of science (Term: stimuli-responsive polymers).

Different stimuli can be used to yield a response, such as physical, chemical or biological stimuli. Physical stimuli, such as light,[10, 11] temperature,[12, 13] electric,[14, 15] and pressure,[16] affect the molecular structure or interactions. Chemical stimuli, such as pH,[17-20] carbon dioxide,[21] and other chemicals,[22] interfere with the molecular interactions between polymeric chains and solutes or alternate the functional groups located in the polymers. Biological stimuli such as antigen,[23] ligand[24] and enzymes[25-27] can mimic the performance of these agents in the living system to change the structure or properties of polymers. With applied stimuli, the interactions and microenvironments of polymeric systems can be altered which cause changes in the physical state of the system. The removal of the stimuli will result in a reversion to the original physical

state. In order to better understand the relative research in this area, we will introduce some widely used stimuli-responsive polymers and illustrate their fundamental properties.

1.1.1 Temperature-responsive polymers

Temperature-responsive polymers are especially interesting since temperature variations can be applied in a non-invasive manner. Furthermore, spontaneous temperature fluctuations also occur in nature. There are different types of temperature-responsive polymers,[28] however, the most widely studied are polymers that undergo a solution liquid-liquid phase transition in response to temperature variation. This phase transition occurs from a homogeneous solution into a concentrated polymer phase, accompanied by a transition from a clear to a cloudy solution. If the phase separation occurs at an elevated temperature, it is known as lower critical solution temperature (LCST) transition[29] while the opposite phase behavior is referred to as upper critical solution temperature (UCST) transition.[30] Although the early examples of LCST and UCST behavior of polymers were reported in organic solvents,[31, 32] those with a phase transition in aqueous solution have gained the most interest since they provide high potential for application, especially in the biomedical area. Herein, we will mainly focus on the polymers with LCST since they are most prominent in water soluble polymers. The polymers are completely soluble in aqueous solution when the temperature is below the LCST, and become insoluble at a temperature above the LCST. Generally, all water soluble polymers exhibit LCST behavior in water as the enthalpy of hydration becomes less and the loss of entropy for hydrating water molecules increases with increasing temperature.[33] However, a subtle balance of hydrophilic and hydrophobic groups needs to be present in the polymer structure to tune the LCST to be applicable at ambient pressure. The most extensively studied LCST polymers include poly (*N*-isopropylacrylamide) (pNIPAm),[12] poly (*N*-vinyl caprolactam) (pVCL),[34] poly (oligo (ethylene

glycol) methacrylates) (pOEGMAs),[35] poly (methyl vinyl ether) (pMVE),[36] poly (2-oxazoline)s,[37] and their analogous polymers. Among these, the most studied during the past few decades and also most investigated in this thesis is pNIPAm,[12, 13, 18, 38-42] which present LCST of ~32 ^{o}C. It undergoes a coil-to-globule transition in water which is close to the physiological temperature range. Following, we will mainly discuss the solution behavior and thermodynamic properties of pNIPAm.

A schematic depiction of solution behavior of pNIPAm is shown in Figure 1-2. At low temperatures, pNIPAm is highly solvated due to hydrogen bonding between the amide residues on the polymer chain and the water molecules. Furthermore, there is a "cage-like" conformational arrangement of water molecules around the isopropyl groups.[43] Hence at low temperatures, the polymer-solvent interactions are stronger than the polymer-polymer interactions and pNIPAm exists in a random coil state. At elevated temperatures, the hydrogen bonds between the polymer and the water molecules are broken, leading to an entropically favored expulsion of water from the polymer network. Consequently, the polymer-polymer interactions (hydrophobic effect and hydrogen bonds) become stronger than the polymer-solvent interactions, resulting in phase separation as the polymer assumes a globule conformation. This process is an entropically driven transition, which was first proposed by Heskins and Guillet.[13] The Gibbs free energy of the system is given by the following equation:

$$\Delta G = \Delta H - T\Delta S \qquad (1\text{-}1)$$

where ΔG is the free energy of mixing, ΔH is the enthalpy change of the dissolution, T is the temperature in Kelvin and ΔS is the entropy change as a result of water association with the polymer.

ΔH favors dissolution due to hydrogen bonding of NIPAm and water molecule makes a negative contribution. However, structured water around the pNIPAm leads to a loss in entropy (negative ΔS term) and a positive entropic contribution. As T increases the positive entropic contribution to the free energy grows. When the positive entropic contribution dominates over the enthalpic contribution, phase separation begins and makes dissolution unfavorable and pNIPAm undergoes the coil to globule transition above the LCST. In this dissertation, we utilized pNIPAm to prepare temperature-responsive materials and systems to study the controlled drug release properties.

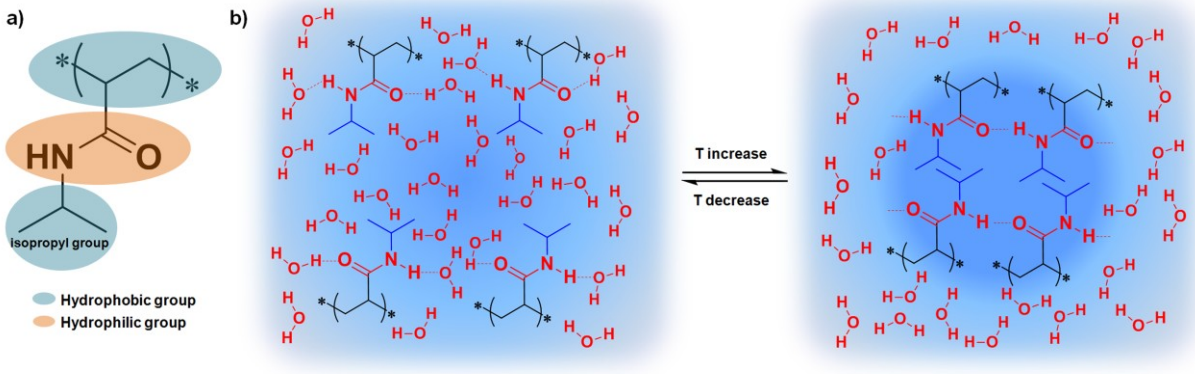

Figure 1-2. Structure and solution behavior of pNIPAm. (a) structure components on pNIPAm and (b) phase separation of pNIPAm under temperature change.

1.1.2 pH-responsive polymers

pH-responsive polymers are a group of stimuli-responsive polymers that can respond to solution pH by undergoing structural property changes such as surface activity, chain conformation, solubility, and configuration. pH-responsive polymers[20, 44] are normally polyelectrolytes with weak acidic or basic groups that either accept or release protons in response to a change in the environmental pH. Similar to acidic or basic groups of monoacid or monobasic compounds, the pH-responsive groups in polyelectrolytes can also be ionized. However,

complete ionization of these systems is more difficult due to electrostatic effects exerted by other adjacent ionized groups, which makes the apparent dissociation constant different from that of the corresponding monoacid or monobasic.[44] The physical properties, such as chain conformation, configuration, solubility, hydrophilicity and volume of pH-responsive polymers, could be tailored by manipulating the charges along the polymer backbone, resulting in electrostatic repulsion between charges on the polymer chain and allows them to expand. A large number of pH-responsive polymers can be designed using various electrolyte groups. Weak polyacid accepts protons at low pH and releases protons at high pH. Weak polybases accept protons at low pH and form a positively charged polymer chain. Figure 1-3 summarizes some of the classic pH-responsive polymers in the direction of acidic, basic and natural polymers. For example, poly (acrylic acid) (PAA) is a polymer with acidic carboxylic groups which has a dissociation constant ($pK_a \sim 4.25$) and above this pH the carboxylic group becomes ionized. This leads to electrostatic repulsion between the chains that can then associate with water to cause swelling. The cationic polyelectrolyte poly (*N, N*-dimethylamino ethyl methacrylate) (PDMAEMA) with basic amine group shows ionized behavior at low pH values. Charge status in these materials is readily reversed by returning the pH of the solution; thus the switching behavior of pH-responsive smart materials is also reversible.

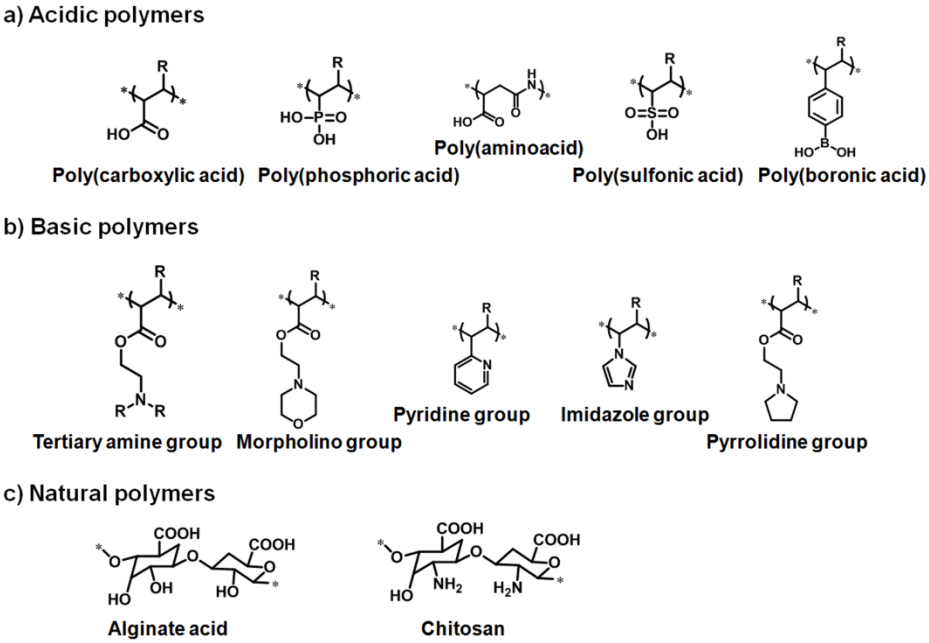

Figure 1-3. Typical pH-responsive polymers.

Most anionic pH-sensitive polymers contain moieties anionically charged at a pH above their pK_a and can attract positively charged molecules, e.g., therapeutic agents. By controlling the surface physical and chemical properties of materials, the interfacial characteristics can be altered to dictate the interactions between polymer and biological target, which makes pH-sensitive polymers interesting for biomedical applications as many biological mechanisms are strongly affected by the levels of charge. The adjustment in pH alters ionic interactions, hydrogen bonding, and hydrophobic interaction, resulting in a reversible microphase separation or self-organization phenomenon. For example, since the extracellular pH of most tumors is acidic (pH 5.8-7.2),[45] smart polymeric nano-devices can be designed for anti-cancer drug delivery, where the release of drugs can be triggered by manipulating pH. The pH triggering could be done by incorporating a pH-responsive moiety into the polymer structure, destabilizing a self-assembled polymeric aggregate or by chemical conjugation of pH-labile linkages between polymers and drugs. These strategies are particularly useful for targeted drug delivery. In this

dissertation, we utilized the ability of the pH-responsive polymer to control the release of positively charged drugs under different conditions.

1.1.3 Field-responsive polymers

Light-, electro-, magnetic- and ultrasound-sensitive polymers offering removable and dynamic controllable properties is considered as field responsive materials. Light-responsive polymers[46-48] undergo a change in their properties, like conformation, polarity, amphiphilicity, charge, optical chirality, in response to exposure to light of a particular wavelength. The light-induced molecular change is manifested as a macroscopic change of material properties like shape (i.e., contraction or bending), wettability, solubility, optical properties, conductivity, and adhesion. Light control possesses many advantages compared to temperature, pH, electric, and magnetic stimuli as it: (i) allows for remote/non-contact stimulation; (ii) can be easily dosed in order to tune the strength of the response, and (iii) allows accurate temporal and positional resolution of the response. In order to obtain light-responsive polymers, a light-responsive functional group (chromophore) needs to be incorporated into the polymer, either in backbone or side chain. Depending on the type of chromophore used, the response can be reversible or irreversible. Reversible chromophores, often named molecular switches, undergo a reversible isomerization upon light excitation at a specific wavelength. The photochromic interconversion between isomeric forms allows switching the properties of the polymer material by irradiation at two different wavelengths.

Some commonly used light-responsive groups are shown in Figure 1-4. Azobenzene derivatives undergo *trans-cis* isomerization upon exposure to specific wavelengths of light.[10, 49-51] The responsive nature of azobenzene has been applied in photoinduced deformation of liquid crystalline polymers[52] and also the optical properties of photonic materials.[53] Spiropyran can

change from an unconjugated spiroheterocycle to a charged planar merocyanine form with extended conjugation.[54-56] *O*-nitrobenzyl is one of the commonly used irreversible light-responsive groups. It can release different side groups under UV light irradiation.[57] For example, the release of a proton side group can decrease the solution's pH. The light-induced change of neutral to charged state has been applied to control wettability,[58] motion,[59] particle dissociation,[60] and molecular recognition.[61] In this dissertation, we utilized the ability of *o*-nitrobenzaldehyde to release the proton to decrease the surrounding pH in response to the UV light irradiation time.

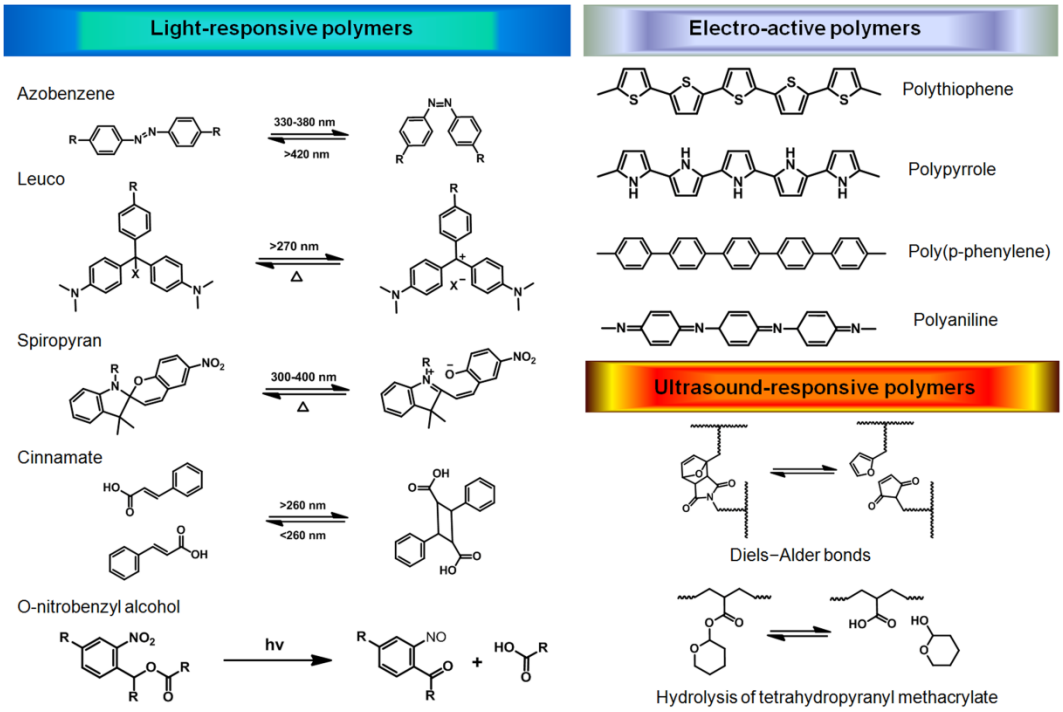

Figure 1-4. Examples of field responsive polymers.

Electroactive polymers (EAPs) are materials that respond to an applied electric field by changing their size or shape.[62-65] EAPs have attracted rapidly expanding scientific and technological interest lately due to their potential applications in sensors and actuators,[66, 67] robotics and artificial muscles,[68, 69] optical systems,[70] drug delivery,[71, 72] and energy harvesting applications.[73] Conducting polymers are one of the most extensively studied ionic electric-

responsive polymers that can create a change in the local concentration of the ions in solution under the electric field, whereas dielectric elastomers and the electroactive polymers are dielectric EAPs whose deformation is induced by electrostatic forces developed between two electrodes. They normally exhibit fast response and high deformations and operate under dry conditions, however, high activation fields are required.[74] The non-ionic polymers, poly (vinylidene fluoride),[75] polyacrylates[76] and silicone have also been shown to respond to an external electric field in the absence of charge carriers and have been employed as electro-active materials.[77] For example, an alternative electric-responsive system comprises polyelectrolyte brushes that exhibit tunable swelling behavior upon application of an electric voltage.[78] Most commonly studied EAPs are summarized in Figure 1-4 and their family is still growing. Polymer actuators and walkers, as well as electric-responsive drug delivery systems, have been developed by EAPs and their properties and functions have been studied during the past decades. Modification of the chemistry of these materials with significantly increased response rate is still being pursued and will further extend the potential application of this area.

Other fields like magnetic fields and ultrasound have also been exploited to create responses from materials. Magnetic-responsive systems[79] are polymers incorporated with magnetic materials to generate magnetic-responsive polymer materials. It provides unique capabilities as it can be spatially and temporally controlled, and can additionally be operated externally to the system, providing a non-invasive approach to remote control. There are several strategies that can be applied to generate magnetic-responsive polymer systems. For example, magnetic nanoparticles are doped into the polymer to produce highly efficient magnetic-responsive materials. They can respond to weak stimuli with a movement,[80] heat generation,[81] magnetic or optical signal.[82] Ultrasound-responsive polymers[83] use different frequency

ultrasound to induce formation transitions[84] and bond cleavage[85] based on the thermal effect, which is the transfer of acoustic energy to the tissues causing a rise of temperature, or non-thermal effect, which is the formation of tiny gas bubbles in the tissues as the result of ultrasound vibration.[86] Some of the magnetic-, ultrasound-responsive polymer systems are listed in Figure 1-4.

1.1.4 Enzyme-responsive polymers

Enzyme-responsive materials are in an early stage of development and were first described in 2006 by R. V. Ulijn. They were described as "materials that undergo reversible macroscopic transitions that are triggered by selective enzyme catalysis".[26] However, the use of enzymes to alter the materials properties dates back to 1970s.[87] The definition was broadened by Zelzer[27] in 2013 as "materials whose structure or functionality changes after the direct action of the enzyme". In nature, dynamic processes in living organisms are almost exclusively controlled by enzymes. Enzymes have evolved to be highly specific catalysts whose action and activity are naturally controlled either by regulating enzyme expression levels or the availability of cofactors. Enzymes thus present a highly attractive alternative to conventional stimuli for the development of functional biomaterials. Figure 1-5 shows the development of enzyme-responsive polymers during the past few decades. Enzyme-responsive polymers are one of the most important types of this kind of materials and stand apart from other stimuli-responsive polymers in their ability to respond to biological molecules to regulate the function of natural materials. There are many advantages for enzyme-responsive polymers. One of them is selectivity, the ability of an enzyme to convert one specific substrate in the presence of a mixture of molecules that are very similar to the target substrate. Another important advantage is the cross-reactivity of the enzyme-sensitive functionality with other enzymes. Ideally, the enzyme-sensitive functionality should react only

with the enzyme that it was designed for and show little to no sensitivity to other enzymes. Other advantages like enzyme-sensitive functional groups are easy to be chemically incorporated, a large number of enzyme/substrate pairs are available, and transitions are reversible.

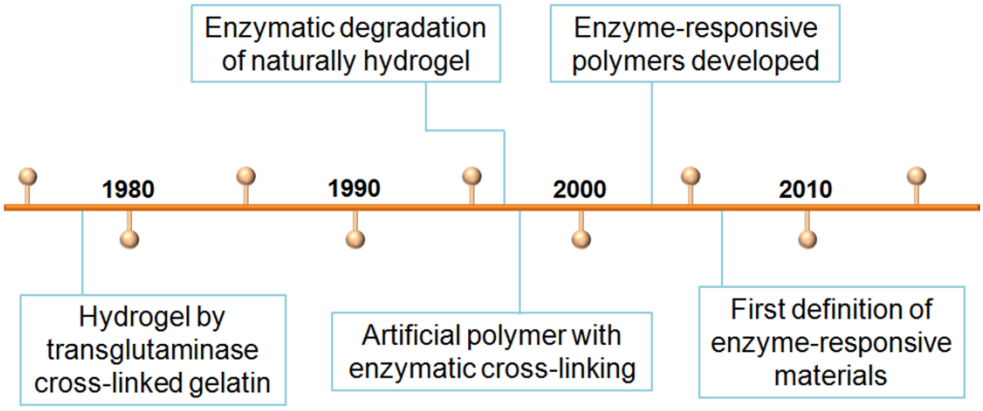

Figure 1-5. Milestones in the development of enzyme-responsive polymers. Adapted from ref. 33

Naturally derived polymers, such as gelatin and dextran hydrogels,[88] are the first developed enzymatic degradable polymers. After that, short peptide cross-links were incorporated into poly (ethylene glycol) (PEG) to create an enzyme-responsive artificial polymer that exhibits enzyme-responsive properties.[89] Till now, enzyme-responsive polymers have been developed and diversified into different architectures, divided into four classes, enzyme-responsive polymer hydrogels,[90] enzyme-responsive supramolecular polymers,[91, 92] enzyme-responsive polymer conjugates[93, 94] and enzyme-responsive self-immolation polymers.[25, 95] Enzyme-responsive polymers have found applications in areas such as cell supports, injectable scaffolds, and drug delivery systems and have been integrated with other stimuli-responsive polymers to obtain materials with closely tailored stimuli-responsive characteristics. For example, a poly (*N*-isopropylacrylamide-*co*-acrylic acid) (p(NIPAm-*co*-AAc)) hydrogel that included peptide-based cross-links was used as the stimuli-responsive polymer to create the artificial extracellular matrix.[96] It can be biodegraded by collagenase enzyme and be removed once it is no longer

required. Another example shows that polymer hydrogel particles have been designed such that exposure to the triggering enzymes causes swelling of the particle. The resulting increase in the mesh size of the polymer hydrogel allows the encapsulated proteins to diffuse out of the particle to achieve the purpose of releasing of payload.[90]

1.1.5 Redox-responsive polymers

Redox-responsive polymers[97] are polymers that contain redox-sensitive groups that can have a reduction or oxidation reaction to induce changes in structure or properties. Basically, it can be separated into two different strategies, one is reduction-responsive polymers and the other one is oxidation-responsive polymers. In reduction-responsive polymers, the most commonly developed one contains disulfide or diselenide groups.[98, 99] They are sensitive to the reduction agent with a thiol group, like dithiothreitol (DTT) and glutathione (GSH) through thiol-disulfide exchange reaction. Using disulfide group as an example, polymers with disulfide linkers[100] and disulfide pendent groups[101] are all developed during the past years. The disulfide linker is easy to break and degrade the polymer. However, the pendant disulfide can trigger the release of the attached payload. Those two strategies are very common in designing the controlled drug delivery vehicles by using this type of stimuli-responsive polymers. Other reduction-responsive polymers like reduction-responsive platinum(IV)-coordinate polymers,[102] Trimethyl-locked benzoquinone (TMBQ) polymers,[103] 4-*N*-amino- 2,2,6,6-tetramethylpiperidin-1-oxyl-4-yl (TEMPO) polymers[104] are also being pursued. In oxidation-responsive polymers,[105] the response relies on reactive oxygen species (ROS) such as hydrogen peroxide (H_2O_2) and hydroxyl radicals. Sulfide-containing polymer, like poly (propylene sulfide) (PPS), is one of the first studied oxidation-responsive polymers. Similar to sulfide, selenide is more reactive than sulfide since the lower bond energies of diselenide and the carbon-selenium bond and selenium containing

polymers[106] are developed. One of the important works was published in 2009 by Xu and Zhang's group.[107] They reported a diselenide-containing polyurethane triblock copolymer, PEG-PUSeSe-PEG, which assemblies exhibited both the reduction- and oxidation-responsive behaviors, and the results indicated that the diselenide was much more sensitive (even under 0.01 mg mL^{-1} GSH the encapsulated Rhodamine B could still be released almost entirely in only 5 h), while they were stable without redox stimuli. Besides those, there are few other oxidation-responsive polymers also studied, such as ferrocene-containing polymers,[108] which can tune the polymer property with different redox stage, poly (NiPAAm-*co*-$Ru(bpy)_3$), one can generate a chemical wave by the periodic redox change of $Ru(bpy)_3$ into an oxidized state.[109] This redox reaction alters the hydrophobic and the hydrophilic properties of the polymer chains and results in swelling and deswelling of the polymer.

The great advantage of designing and developing redox-responsive polymers is their uniqueness in biomedical applications. Since the interconversion of thiols and disulfides plays an important role in many biological processes in cells, the redox-responsive polymers have become effective candidates in controlled drug delivery systems to actively deliver the drugs.

1.2 Stimuli-responsive polymer microgels

The term microgel was first mentioned in 1949 by Baker[110] and describes a new macromolecule from cross-linked polybutadiene latex particles. The word micro referred to the size of the gel particles usually in the range of 100 nm-1000 nm. While microgels internally have the same gel structure as their macroscopic counterparts, like macrogels or hydrogels, microgels and macrogels are physically different. Microgel particles have surface to volume ratios that are several orders of magnitude larger than those existing in bulk gels. Tanaka and Fillmore (TF)

developed a theory of deswelling kinetics that was based on the concept of cooperative diffusion.[111, 112] According to the TF theory:

$$\tau \approx R^2/D \qquad (1\text{-}2)$$

where τ is the time needed for gel swelling or collapse, R is the gel size and D is the cooperative diffusion coefficient. According to this relation, the most obvious way to achieve faster response rates is to decrease the size of the gel.[113] Microgels, therefore, de-swell at rates much faster than bulk gels because of their significantly decreased size. The collapsing rates of temperature-responsive microgel are typically on the microsecond time scale.[114]

A breakthrough with responsive microgels was in 1986 when Pelton and coworkers successfully synthesized temperature-responsive pNIPAm microgels by precipitation polymerization.[38] After that, responsive microgels have received increased attention and found great potential in different areas of application. The family of responsive microgels are growing and a variety of stimuli-responsive microgels have been developed.[18, 115-120] However, pNIPAm-based microgels are still the most studied one with potential to be practically used in future. In the following sections, we will mainly focus on the pNIPAm microgels from the basic aspect. In this dissertation, all the microgels based materials and devices are prepared based on pNIPAm microgels.

1.2.1 Temperature-responsive pNIPAm microgels

Microgels constructed from pNIPAm exhibit similar temperature responsive properties to their bulk hydrogel. It has extremely solvent swollen properties, approximately 95 % by volume in their hydrated state and 20 % solvent in their de-swollen state.[12, 121-123] The size of pNIPAm microgels can range from 50 nm to 5 μm and the volume phase transition temperature (VPTT) is close to the LCST of pNIPAm. However, more parameters affect the VPTT of the microgels,

such as cross-linking density, solvent nature, microgels structure and composition, and the nature of the functional groups in the copolymer.[116] For example, charged groups in microgels having a large influence on the VPTT was proved recently by dielectric analysis on poly (*N*-isopropylacrylamide-*co*-methacrylic acid) (p(NIPAm-*co*-MAA)) microgels.[124] Most of the researchers focus on the incorporation of functional moieties within pNIPAm based microgel materials by copolymerization or post-functionalization that alter the hydrophilic/hydrophobic balance as well as swelling capacity and explored the application of pNIPAm microgels. One of the examples is copolymerization of acrylic acid monomer into the system to incorporate charged species into this microgel, which found employment in controlled uptake and release of various model drug compounds.[125, 126] There is also an increasing attention on constructing microgels in a large scale to create new functional materials or devices, like microgels assemblies based devices are developed by Asher group[127-129] and Serpe group.[130-132]

1.2.1.1 PNIPAm microgel synthesis and functionalization

Precipitation polymerization is defined as a polymerization that starts from a homogeneous monomer solution and ends when polymer dispersion is obtained and is one of the most convenient polymerization methods for microgel formation. PNIPAm microgels are usually prepared by free radical precipitation polymerization.[38, 133] The components needed for microgel synthesis are monomer, crosslinker and initiator. NIPAm served as the monomer in all of the synthesis, and comonomer can be added to increase the functionality of the microgels. Although Gao and Frisken reported self-crosslinking of pNIPAm microgels without cross-linker,[134] cross-linker is still vital to forming a uniform and stable microgels with high yield. It is versatile to choose different types of cross-linkers, such as *N, N′*-Methylenebisacrylamide (BIS), a relatively short and rigid cross-linked, poly (ethylene glycol) diacrylate (PEGDA), a more flexible

oligomeric cross-linker. Obviously, other cross-linkers can be prepared based on the required properties of microgels, like preparation of a degradable microgel using *N, N*'-(1, 2-dihydroxyethylene)-bis-acrylamide as a cleavable cross-linker.[135] There are several initiators available to be used during the synthesis such as ammonia persulfate (APS) for the aqueous system and azobisisobutyronitrile (AIBN) for the non-aqueous system.[136]

In this dissertation, free radical precipitation polymerization was used to synthesize all the microgels. Figure 1-6 illustrates the mechanism of the free radical precipitation polymerization. Microgels are formed by homogeneous nucleation in an aqueous solution. First, the polymerization temperature much higher than the LCST of pNIPAm is necessary for the formation of stable pNIPAm microgels. There are few reasons for requiring this: (i) at this temperature, the radicals can be formed to initiate the polymerization, (ii) it allows the growing pNIPAm chains to reach a critical chain length and collapse on itself to give precursor particles. Then other growing oligo radical chains can attach and thereby forming growing particles that keep maturing until all of the monomers have been exhausted. The charge imparted by the initiator stabilizes the microgels. Since the cross-linker reacts faster than NIPAm monomer, the microgels have unevenly distributed cross-links: the inner layer of the pNIPAm microgel contains more cross-links than the outer one. There is a way to generate uniformly distributed crosslinks by delaying the addition of the cross-linker during the polymerization.[137] Stable pNIPAm microgels are obtained at a low temperature when a co-solvent is used as the medium. For example, a water/ethanol mixture (7:3 v/v) enabled the precipitation polymerization of NIPAm at 40 °C. In this mixed solvent, the LCST of pNIPAm fell to 5 °C because water and ethanol interact closely and pNIPAm has a decreased affinity to both.[138-141] The size of these microgel particles can be tuned by modulating the concentration of stabilizing surfactant as well

as initiator. Typically, higher surfactant concentration results in smaller microgels and vice versa. Attributed by the convenience of precipitate polymerization, other co-monomers with functional groups have been added to give microgels with multi-functional properties.[121, 142, 143]

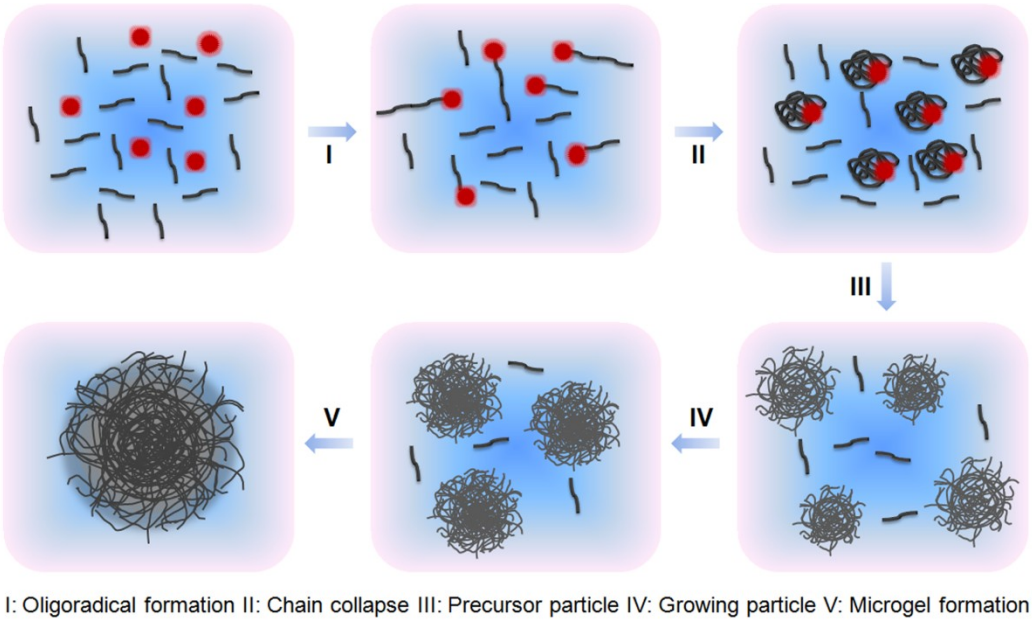

Figure 1-6. Mechanism of microgels formation in free radical polymerization.

1.2.1.2 PNIPAm microgels characterization

Several techniques are used to characterize microgel size, morphology, functional group distribution and responsive properties. They include optical microscopes, light scattering, scanning and transmission electron microscopy, UV-vis spectrometry, differential scanning colorimetry, fluorometry, small-angle neutron scattering, rheology, NMR and so on. In this dissertation, optical microscopy, UV-vis spectrometry and dynamic light scattering (DLS) are the most commonly used techniques to characterize the microgels.

Differential interference contrast (DIC) microscopy was used to characterize the synthesized microgels to evaluate the success of the synthesis and characterize the size and uniformity of the microgels. In this dissertation, an Olympus IX 70 inverted microscope

equipped with a high numerical aperture, oil immersion 100X objective was used to obtain images of the microgels adsorbed to the glass substrate as well as imaging a mask through the microgel to prove the lensing abilities of the microgels. Images were captured using a black and white CCD camera.

DLS has been used most often to study the size distribution and solution behavior of microgels. All of the DLS experiments in this dissertation were carried out on a Protein Solutions DynaPro-MS/X. The source is a semiconductor laser of λ = 784.8 nm. The light impinges on the sample through fiber optics and the scattered light at 90° to the source is collected by an avalanche photodiode. The signal from the photodiode is fed to an autocorrelator board, from which the diffusion coefficient is calculated. In DLS, the fluctuations in the scattered intensity are collected and these fluctuations are used to plot the autocorrelation function. The diffusion coefficient is then calculated from the decay of the autocorrelation function. Assuming that the particles have random Brownian motion the diffusion coefficient is used to calculate the hydrodynamic radius (R_h) of the particles from the Stoke-Einstein equation:

$$R_h = {k_b T}/{6\pi\eta D} \qquad (1\text{-}3)$$

where k_b is the Boltzman constant, T is the temperature in Kelvin, η is the solvent viscosity and D is diffusion coefficient.

The temperature-induced volume phase transition of pNIPAm microgels can be followed by detecting the scattered light. A dilute dispersion of microgels appears transparent because at T < VPTT the microgels are swollen with water and the contrast in refractive indices of the polymer and the solvent is small. At T > VPTT, the expulsion of water from the particles causes an increase in refractive index contrast between the polymer and the solvent, and the dispersion appears turbid.

1.2.1.3 PNIPAm microgel assemblies

Microgels have been applied as a building block to self-assemble into structures such as one-dimensional (1D) monolayer,[144, 145] two-dimensional (2D) films[146] and three-dimensional (3D) hydrogels,[146-149] and these structures are used in different applications, like sensing and biosensing. Microgel monolayer has been developed as non-fouling coatings to increase the biocompatibility of the biomedical devices.[150] For example, Schmidt prepared pNIPAm microgel monolayer for studying cell culture substrates.[151] Lyon group fabricated microgel 2D films as drug delivery vehicles.[126] Zhang group prepared microgels 2D colloidal crystals assemblies by a different method.[152, 153] Lyon group used microgels to create large-scale photonic crystals with tunable bandgaps.[148, 154] In our group, we originally developed a microgels based device that has excellent optical properties, called etalon.[144] In this dissertation, the main structure we used is based on the microgels monolayer assemblies.

The devices that we investigated in this dissertation are made by assembling pNIPAm-based microgels on a Cr/Au coated glass substrate. The excess microgel was washed away and another layer of Cr/Au was deposited on top of the microgels layer, sandwiching the microgels. Hence, the distance between two Au layers depends on the diameter of the microgels. The resultant device is typically referred to as a microgels-based etalon and is shown schematically in Figure 1-7 (Figure 1-7a is the structure of this device and Figure 1-7b is the typical reflectance spectrum, Figure 1-7c shows the instrument setup for collecting the reflectance spectrum).[155] This device shows visible color and characteristic multipeak reflectance spectra both of which depend on the refractive index of the microgels and the distance between the two Au mirrors based on equation (1-4).

$$\lambda m = 2nd\cos\theta \quad (1\text{-}4)$$

where *n* is the refractive index of the dielectric layer, d is the mirror–mirror distance, θ is the angle of the incident light relative to the normal, and m (an integer), is the order of the reflected peak. Because λ is directly proportional to *n*, an increase in *n* for a given peak of order *m* results in a red-shift. Similarly, because λ is also proportional to the distance between the two mirrors, *d*, an increase in *d* gives rise to a red-shift in λ for order *m*.

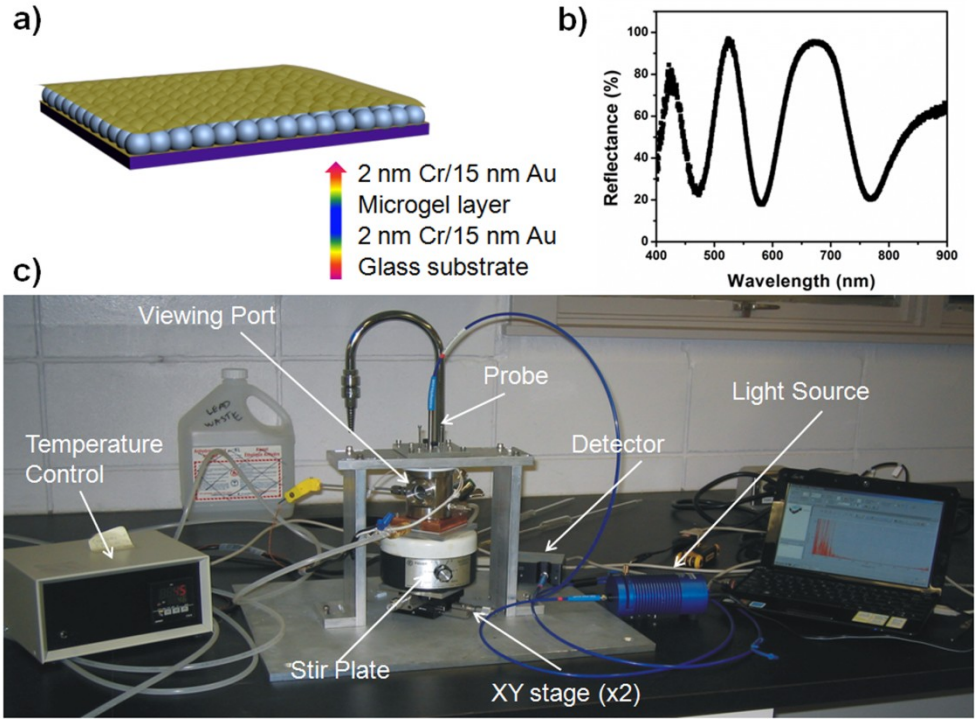

Figure 1-7. The structure of microgel-based etalon device (a) and (b) the standard optical spectrum of this device. (c) the instrument setup for collecting the reflectance spectrum. Reproduced with permission from ref. 156 Copyright 2013, Springer.

The color tunability is a result of the temperature-dependent solvation state of the microgels dynamically modulating the distance between the mirrors; the predicted red shift due to the increase in refractive index of the dielectric microgels layer with temperature (due to microgels deswelling) was dominated by the decrease in the mirror separation distance. Furthermore, when reflectance spectra were collected, multiple peaks in the visible were

observed, corresponding to different reflection orders as defined by equation 1-4. While materials that have multiple spectral peaks in the visible region can be extremely beneficial for various types of sensing, we seek a configuration that produces a single reflectance peak in the visible. This can be useful for developing sensors that have distinct colors in the absence and presence of an analyte for point-of-care and home testing devices.

1.2.2 Multi-responsive microgels systems

Multi-responsive microgels are prepared by incorporating a second functional monomer into pNIPAm microgels to generate other response properties. There are two methods can be used to achieve this, one of during the polymerization and forming of pNIPAm microgels, the second monomer was added before the reaction was initiated. In this case, during the polymerization of NIPAm and forming the precursor particles, the second monomer will be also polymerized and inserted into the polymer chains. The other method is post-functionalizing the synthesized microgels, which can give more diversity of function of microgels if there is no relative monomer exists. Many functional monomers have been studied to create multi-responsive pNIPAm microgels.[157] Negatively charged microgels with pH-responsive pNIPAm microgels are produced by copolymerization with anionic monomers, such as acrylic acid (AAc),[158] and 3-(Acrylamide)phenylboronic acid (APBA).[159] Temperature and pH-responsive microgels with a positive charge are prepared by incorporating cationic monomers like 4-vinyl pyridine (4-VP),[160] *N*-(3-aminopropyl) methacrylamide hydrochloride (APMH),[161] and *N, N*-(dimethylamino)ethyl methacrylate (DMAEMA).[143] Others multi-responsive microgels can be prepared by just incorporating the specific response unit into the microgels network, for example, by incorporating functional nanoparticles, researchers developed novel superparamagnetic microgels[162] and catalyst microgels.[163]

The architectures relative to the co-monomer of the resulting microgels can be controlled by the addition time of the monomers during the polymerization. Besides the comonomers location controllable, the microgel's structure can also be tailored by forming core-shell microgels. A stepwise addition of monomers during polymerization or a real two-step synthesis process results in core-shell structures. Researchers have studied the core-shell microgels from their basic concept of phase transition properties to the application in controlled molecules release. One of the first group of researchers who reported the synthesis of core-shell microgels using stepwise polymerization of NIPAm and acrylic acid was Lyon.[164] Recently, Richtering group synthesis the hollow microgels with different components and study the swollen and assemble behavior.[165]

There is steadily growing interested in the synthesis of copolymer microgels since the variation of the comonomer and crosslinker is a straightforward strategy to tune the properties of the obtained particles. For example, microgels based on supramolecular chemistry were successfully prepared in our group recently[166] and responsive microgel with supramolecular crosslinker developed by Pich group at the same time.[167] In addition, we observe growing interest in not-NIPAm based microgels systems.[168, 169] Meanwhile a variety of colloidal copolymer microgels is available and the volume phase transition temperature of these systems can be tuned over a wide range.[116] During the past few years, a clear tendency of research towards more complex monomer mixtures was observed and particles with a specific affinity to nanoparticles, biopolymers or drugs were made to meet the requirement of different applications.

1.3 Applications of responsive microgels

Over the past few decades, several new applications of microgels have arisen due to their stimulus-responsive nature. These include their uses as microreactors for the synthesis of

inorganic nanoparticles with predetermined properties, as carriers for targeted drug delivery, as tunable optical lenses and as building blocks of photonic crystals. This section below will briefly chart the functional roles and properties of microgels in the context of these applications.

The swelling and deswelling of responsive microgel particles open up a new mechanism for sensing and biosensing.[131] One early example of this was presented by Hoare and co-workers,[170] where they used APBA-modified microgels to detect the presence of glucose molecules in solution. Specifically, the microgel's APBA groups bind glucose, which (via equilibrium arguments) increases the microgel's anionic charge density, leading to a swelling response due to both Donnan equilibrium and direct intra-microgel charge-charge repulsion. Another early example from the Asher Group showed that the volume changes that pNIPAm undergoes as a function of temperature can be used to tune the visual color of colloidal crystals. Microgels-based etalons were able to fabricate that could detect the concentration of glucose in solution.[171] P(NIPAm-*co*-AAc) microgels based etalons could be attached to the surface to sensitive detect the solution pH.[172] Furthermore, pNIPAm microgels based etalons and etalon arrays are developed to determine the molecular weights of polymers in solution.[161] Recently, our group synthesized Triacylglycerols (TAG)-responsive microgels by conjugating lipase to poly (*N*-isopropylacrylamide-*co*-4-vinylpyridine-*co*-N-acryloxysuccinimide) (p(NIPAm-*co*-4VP-*co*-NAS)) microgels.[173] When triolein penetrated into the microgel layer, it was hydrolyzed into a long chain fatty acid ($C_{18}H_{37}COOH$) by the lipase inside the microgels. The long chain fatty acid could subsequently attach to the microgels via acid–base reactions between a fatty acid and the microgel's pyridine groups. The lipophilicity of long chain fatty acid increases the hydrophobicity of the microgels, hence water was expelled from the microgels, and they collapsed. This resulted in a blue shift of the etalon's reflectance peaks, which corresponded to

the concentration of triolein. Such devices were able to detect the physiologically relevant range of triolein.

Microgels also have shown promised advantages in water remediation application. Flocculation and coagulation have proved to be extremely important in wastewater treatment over thousands of years, with clarifying agents such as crushed seeds known to have been used in treating potable water since ancient times.[174] Today, coagulation and flocculation are key processes for removing suspended fine particles, colloids, turbidity, and inorganic/organic contaminants during most water treatment.[175] Synthetic or natural polymers (polyelectrolytes) are commonly utilized, either adsorbing to and binding adjacent colloid particles to cause bridging flocculation, or by attracting and absorbing oppositely charged materials, thereby decreasing the potential energy of repulsion between adjacent colloids and allowing flocculation to occur. As microgels are capable of the sorption/desorption of a variety of materials[116] and can also be tailored to flocculate under specific environmental conditions.[176] For example, microgels show promise in assisting in removing metal ions in wastewater treatment;[177] Microgels with affinities for many compounds and the porous structure are potentially used in water purification.[178]

One of the key areas of intensive research of microgels is in the biomedical application, such as controlled drug delivery. The open network structure of microgels can be used to incorporate small molecules such as drugs in their interiors while their large swelling-deswelling transitions may be employed as triggers to direct release of the drugs. In addition to pH, ionic strength, or temperature-triggered volume transitions, microgels loaded with a drug can interact with biological components or events such as enzymatic processes that would activate the release of the drug. Functionalization of microgels allows one to tune their volume transitions in

physiologically relevant conditions. Furthermore, by attaching receptor-specific proteins to the microgel surface, one can achieve selective targeting ability designed to treat specific diseases or specific tumor cells.

Besides these described above, there is still another application that microgels involved like emulsion stabilization,[179] micro-reactor[118] and lubrication materials.[180] We will not go through them one by one. In this dissertation, microgels and their assemblies are mainly studied in the biomedical application. The next chapter will discuss the responsive polymeric materials, specifically, microgels, in controlled drug delivery in detail.

Chapter 2: Stimuli-Responsive Polymer Materials in Controlled Drug Delivery

2.1 Background of controlled drug delivery

Drug delivery describes the method and approach to delivering drugs or pharmaceuticals to their site of action within an organism, for achieving a therapeutic outcome.[a] When employing standard drug delivery approaches, only a very small fraction of the dose actually arrives at the relevant receptors or sites of action, and most of the dose is actually wasted either by non-specificity and/or degradation before arrival at the required site. Scientists researching drug delivery seek to address these issues in order to maximize drug efficacy and minimize side effects.[181] Over the past few decades, the rise of modern pharmaceutical technology and the incredible growth of the biotechnology industry have revolutionized the approach to drug delivery systems development. Controlled drug delivery technologies have made great progress in the last six decades from the primitive delayed release forms in the 1960s to highly sophisticated self-regulated delivery systems in 2000s. Kinam Park describes the development of controlled drug delivery technologies into three generations.[182] The 1st generation (1950-1980) used to develop numerous oral delivery systems, transdermal patches and studied the drug release mechanisms. The 2nd generation (1980-2010) was dedicated to the development of zero-order release systems, self-regulated drug delivery systems, long-term depot formulations, and nanotechnology-based delivery systems. During this generation, many novel drug delivery technologies were developed. The 3rd generation (2010-2040) is yet to be established; the technologies contain target delivery, on-demand delivery and long-term delivery and so on. For

[a] From www.nature.com/subjects/drug delivery

this generation of drug delivery to be beneficial, it should address and overcome the hurdles associated with the current drug delivery systems.

Figure 2-1 shows the schematic illustration of the drug released from matrix system and the drug concentration release profiles. There is certain concentration range considered as an effective drug level for disease treatment. However, beyond (toxic) or below (ineffective) is better to be eliminated. Figure 2-1c and d are two standard controlled drug release profiles, sustained and pulsatile release, respectively.

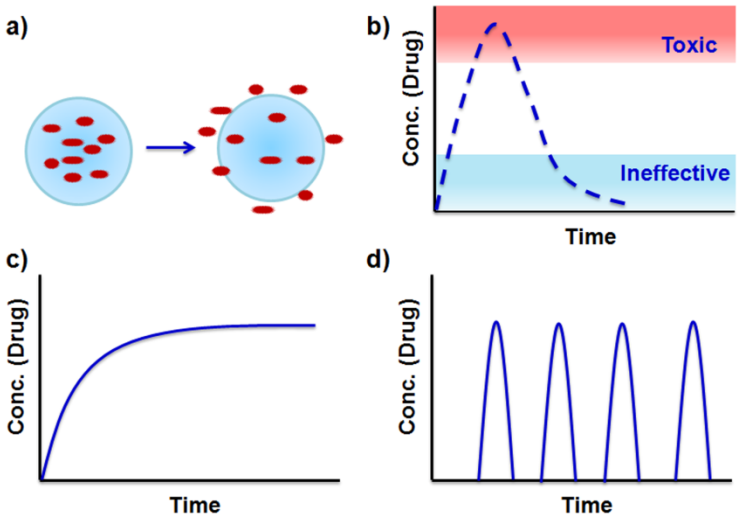

Figure 2-1. Release profiles in controlled drug delivery system.

The route of administration of therapeutics is crucially important to cure the disease. Development of alternative drug delivery methods to overcome the challenges plays an important role throughout the history of medicine. Scientists have been working on the creation of smart drug delivery system and such approaches could provide an easy route of administration, ensuring patient compliance, decreasing toxicity, improving bioavailability and achieving the precise therapeutic target. Figure 2-2 summary the typical routes of administration of therapeutics developed. The traditional delivery method like oral[183, 184] have been developed and applied for many years. Oral administration is a desirable alternative because of the convenience

and increased compliance by patients, especially for chronic diseases that require frequent administration. There are still challenges that exist for oral delivery like gastrointestinal tract, which may involve the enzymatic degradation, poor permeability and instability because of the extremely acidic pH environment. Many smart systems are developed to afford the requirement of different drugs to address these challenges.[185-187] For example, the gastric-retentive device with prolonged gastric retention of drugs is developed by pH-responsive polymer systems recently with stable properties in stomach acid condition.[188] These supramolecular polymer gels are formed by hydrogen bonds between the terminal carboxyl groups, which are protonated at the acid condition to stabilize the gel structure, however, under neutral pH, the carboxyl groups deprotonate and destroy the interaction to dissociate the gels.

Injection is a method of introducing a drug into the bloodstream via a hollow hypodermic needle and a syringe, which is pierced through the skin into the body. It provides an alternative way to admit drugs that are limited by oral delivery while providing increased efficiency. These injectable delivery systems have various advantages including easy of application, localized delivery in case of site-specific action, extended delivery periods, enhanced patient comfort and reduced body drug dosage by lessening unwanted side effects that may occur in systemic delivery.[189, 190] Polymeric hydrogel with the sol-gel transition is a great candidate to apply into injection drug delivery systems.[191] Bioactive molecules, like drug, protein, and DNA can be easily mixed with precursor solution and loaded at target site via the in situ gelatin right after the injection.[192] The release of these bioactive molecules can be performed in a sustained or triggered way on demand in response to the external stimuli. Most of the studies are focused on the hydrogel-forming strategies,[193] biocompatibility,[194] and the novel hydrogel systems.[195]

For example, Burdick and co-workers describe the synthesis of a polysaccharide-based hydrogel that can be locally injected into tissues and releases a recombinant tissue inhibitor of matrix metalloproteinases (MMPs) (such as rTIMP-3) in response to MMP activity. Specifically, rTIMP-3 is sequestered in the hydrogels through electrostatic interactions and is released as crosslinks are degraded by active MMPs. This is the first proof-of-concept demonstration of designing MMP-degradable hydrogels to release an MMP inhibitor in the presence of MMP activity to limit off the clinically problematic target effects and to provide an on-demand presentation of an inhibitor based on local MMP activity. Others, like self-healing hydrogel, is also developed with injectable properties to apply to this area. Zeng's group report a new type of injectable hydrogel based on self-assembly of a tri-block copolymer with rapid self-healing properties through mussel-inspired catechol-mediated hydrogen bonding interactions and aromatic interactions and with anti-biofouling capability.[196] Besides the design of materials and properties used in hydrogel system, the needle for injection was also interestingly studied recently by Kang and Lee.[197] They modified the surface of the needle by crosslinked catechol-functionalized chitosan that undergoes a solid-to-gel phase transition to seal punctured tissues. However, there are still some disadvantages exist for injection method, like the chance of infection, increased the chance of overdose and arterial damage.

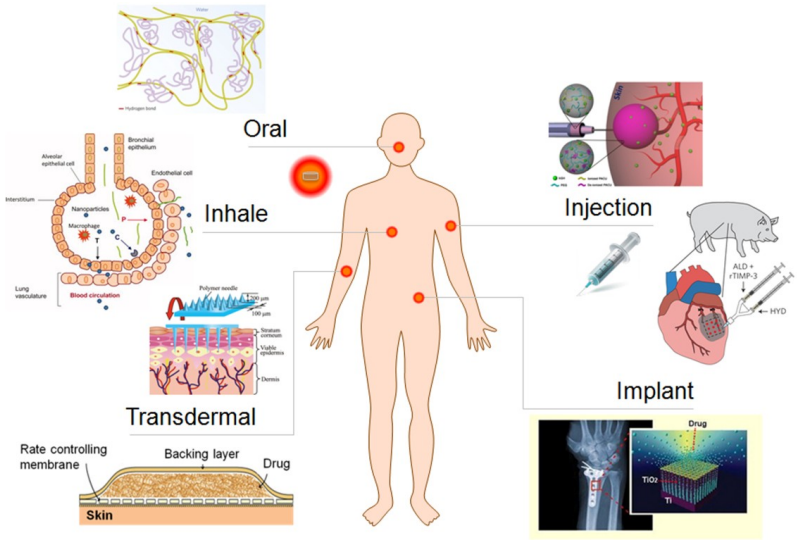

Figure 2-2. Typical routes of administration of therapeutics.

Another alternative way is the transdermal route, which has the advantages of preventing prematurely metabolize drugs, non-invasive and can be self-administered. The common structure of transdermal delivery is patch-based devices, which are a construct of a drug reservoir and rate controlling membrane. Drug reservoir works as a carrier to load the drug. The rate controlling membrane has a specific structure, like pores to control the drug release from the reservoir and penetrate the skin. The requirements of these materials are limited by biocompatibility and stability. The greatest challenge for transdermal delivery is the skin permeability that makes only limited number of drugs amenable to administration by this route, relative to the hydrophilicity of drugs and their molecular weight. To overcome this limitation, a number of different approaches were developed and studied with the same goal.

Needle-free transdermal patches have been reported to disrupt stratum corneum structure in order to create "holes" big enough for delivery of large vaccine molecules,[198] which is still a challenge for most of the traditional patches. Recently, increasing efforts are contributed to developing microneedles based patches,[199, 200] which can efficiently deliver a variety of drugs to

the skin by combing the microneedles puncture into the skin for transdermal delivery and get admirable success. At the early stage, silica microneedles were fabricated by micro electrical mechanical systems based techniques[201] to mechanically and painlessly disrupt the skin barrier and deliver vaccines epidermally. The devices effectively breach the skin barrier in humans with minimal discomfort and skin irritation.[202] Polymer microneedles were also developed recently for different purposes. For example, dissolving polyvinylpyrrolidone based microneedles[203] were fabricated to vaccination with protective immune responses superior to other methods. And this dissolving microneedle also offers additional benefits, like small storage and disposal size, inexpensive fabrication and ease of use to enable self-administration at home. Poly(L-lactic acid) (PLA) based polymer microneedles with bioresorbable properties were also employed for vaccination.[204] Gu group report a novel glucose-responsive insulin delivery device based on microneedle-array patches integrated with hypoxia-sensitive hyaluronic acid vesicles containing insulin and glucose oxidase.[205] Instead of using enzymatically-induced pH changes, for the first time they have taken advantage of the local generation of hypoxia due to the consumption of oxygen in the enzymatic reaction as a trigger for rapid insulin release in response to hyperglycemia. Modification of microneedle is an alternative to applying polymer in transdermal patches. Hammond and Irvine's group introduce a new approach to delivering a vaccine formulation by modifying the poly (lactide-*co*-glycolide) microneedle arrays with multilayer films via layer-by-layer assembly of a biodegradable cationic poly(β-amino ester) and negatively charged interlayer-cross-linked multilamellar lipid vesicles.[206] They demonstrated the potential utility of such functional multilayer coatings constructed on microneedle arrays for rapid transfer of particle-carrying multilayers into microneedle-treated skin and for the subsequent release of vesicle cargos through multilayer degradation in situ, which may ultimately serve as a potent

platform for protein vaccination providing enhanced immunogenicity, simple and safe administration, and the potential for dry-state storage.

The implant is a medical device[207] to maintain the functions of the body by replacing a missing biological structure, supporting a damaged biological structure or enhancing an existing biological structure. Implantable drug delivery devices[208] offer several advantages over other forms. First, implantable devices allow site specific drug administration where the drug is needed most. Examples include implants used in the treatment of brain tumors or prostate cancer. This may also allow for significantly lower doses of the drug, which can minimize potential side effects. Second, implantable devices allow for sustained release of a therapeutic agent. The last and perhaps most important advantage is patient compliance, as the treatment regimen associated with an implantable device is generally less burdensome than pills or injections.

There are several major factors need to be considered during the development of an implantable drug delivery system. Biocompatibility with the human environment is essential since the system is to be implanted and it should not cause any inflammatory response at the site of implantation.[209] Historically, implantable drug delivery systems have been classified into two major classes: drug implants and implantable pumps containing the drug. The first major class utilizes various types of polymers and polymeric membranes, degradable or non-degradable, to control the release kinetics of drugs from the delivery systems.[210] The second major class consists of mechanical pump-type implants which utilize an infusion pump-type action to control the release of the drug.[211] Implantable drug pumps have been used to deliver insulin in the treatment of diabetes[212] and histrelin implants[213] for the palliative treatment of prostate cancer and uterine fibroids. No matter in which types, nowadays the research contribution mainly focuses on the development of nano- or micro- scale devices that can transport inside the vessel

and move to the target site to deliver the drugs. Relay on the development of nanotechnology and 3D printing, more and more studies focused on the fabrication of micro-robot and chip-based controlled drug delivery devices. A half century of research has established that implanted "cyborg" biomaterials could be used to provide controlled, long-term release of drugs and proteins.[214, 215] Technologies that can generate biocompatible micrometer and sub-micrometer particles with precise control over the shape and some control over surface topography are in use. Both the chemical and material properties of these systems can be engineered to control parameters such as degradability, cross-linking, and swelling in order to provide fine control over the kinetics, duration, and location of drug and protein release.[216, 217] One example is a refined soft-lithography process known as PRINT,[218] which utilizes fluorinated molds and non-wetting substrates to polymerize a liquid precursor within the mold, producing particles with precise control over features and sub-50 nm resolution. Micrometer and submicrometer particles shaped as trapezoids, hex nuts, boomerangs, and arrows have been PRINT-fabricated from a range of biocompatible materials including PLA, PEG, and proteins.[219] Another emerging technology that could allow 3D printing of free-standing robot device is two-photon lithography.[220] This technology is capable of voxel-by-voxel additive construction of arbitrary 3D microstructures without requiring pre-manufactured molds. The technique is performed using ultrafast lasers with photosensitive laser-transparent materials. Using the two-photon excitation mechanism, the energy transfer from the laser to the material is spatially confined to the vicinity of the laser focus. Thus, a photoreaction in the material, often polymerization, can be confined to a very small volume using laser focusing. Therefore, it is possible to control material properties by moving the laser focus in a predefined pattern throughout the volume of the material. Materials could be used to localize the release of chemotherapeutic in order to reduce the dose of

a drug, decrease systemic side effects, and increase its site-specific tissue absorption. Implantable drug delivery systems[221] have played more and more important roles in progressing this area because of the precise fabrication and highly intelligent control properties and will continue to contribute to the developing of controlled drug delivery.

Materials used for preparing controlled drug delivery device or systems are diverse. Among that candidate, polymeric materials are the widest studies area of drug delivery in recently, and it provides a significant contribution to developing smart controlled drug delivery systems in the 2nd generation. Polymers can be manipulated to possess certain properties that can meet specific criteria for the designing of suitable delivery systems. Polymeric drug delivery systems[98, 222-227] provide advantages such increased efficacy, reduced side effects and toxicity and convenience. Like small drugs in general, therapeutic macromolecular drug requires the use of polymeric systems, since these agents have very short half-lives in blood plasma and are susceptible to physical or chemical degradation. Polymers that exhibit physicochemical responses to stimuli have been widely explored as potential drug delivery systems.[9, 228-231] Kinds of stimuli investigated to date include most of we described in Chapter 1. Among these, polymers that, in an aqueous solution, exhibit dramatic changes upon a temperature change below or above the body temperature are of particular interest in drug delivery. The application of pNIPAm and its copolymer is probably one of the best examples, and we will describe in details in the following section. Figure 2-3 summary the evolution of polymeric drug delivery systems over past 50 years. They are organized in the order of scale of the drug delivery systems contain macroscale, microscale, and nanoscale from different materials. In macroscale,[232] mostly the earliest stage of controlled drug delivery systems. In microscale, the polymeric

microstructure is developed to apply into the drug delivery system. Nanoscale drug delivery systems are most recently developed with the progress of varieties of nanotechnologies.

Three key technologies were the major factors that stimulated the immense activity and clinical success of nanotherapeutics from the late 1980s to the present. The first was the concept of “PEGylation”, which refers to polyethylene glycol conjugated drugs or drug carriers. The second is the concept of “active targeting” of the drug conjugate by conjugating cell membrane receptor antibodies, peptides or small molecule cell ligands to the polymer carrier. The third was the discovery of the “enhanced permeation and retention effect” (EPR) by Hiroshi Maeda in Kumamoto, Japan, wherein nanoscale carriers are entrapped within solid tumors due to the leaky vasculature of the fast-growing tumor. This is called “passive” targeting as contrasted with active targeting.

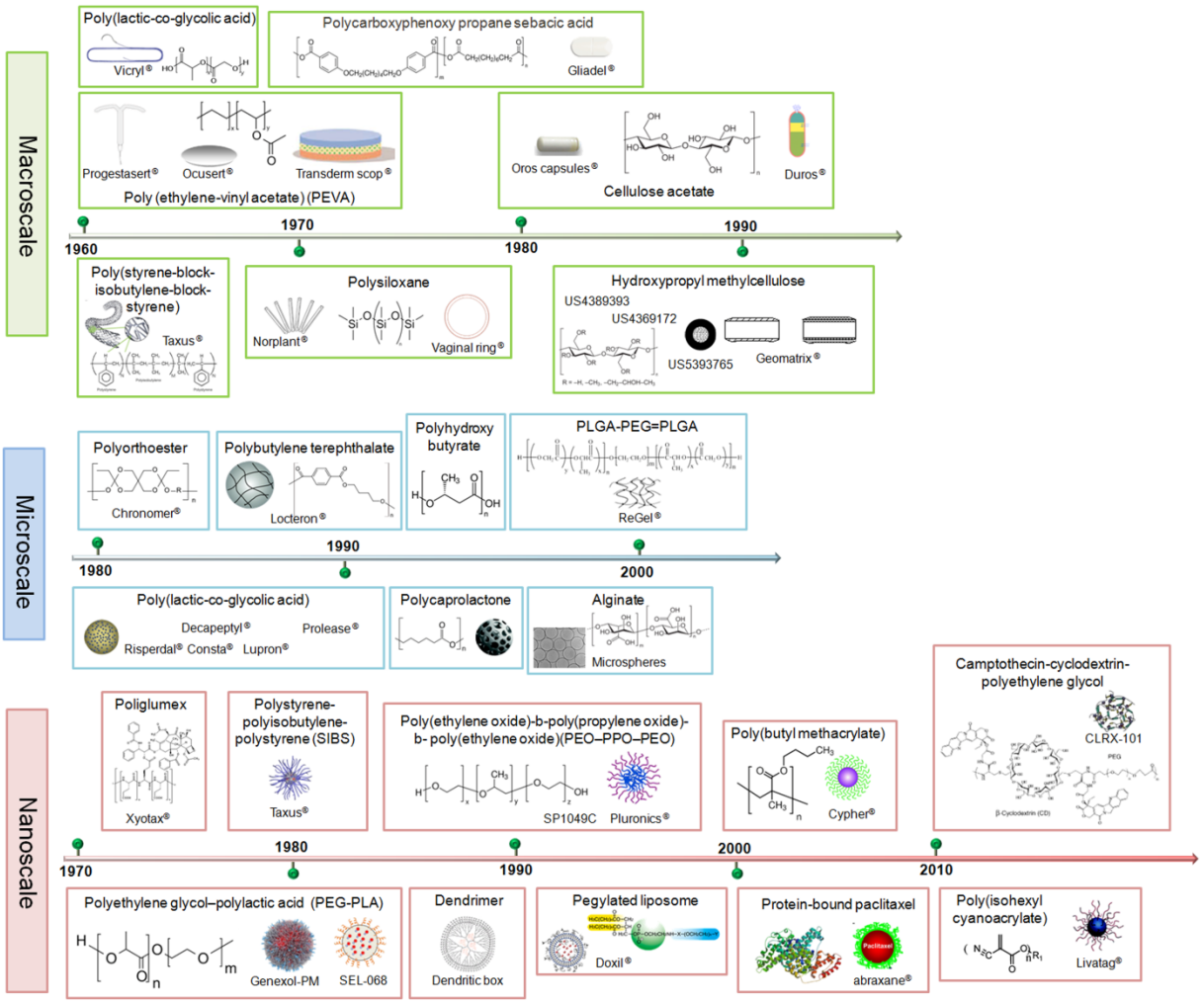

Figure 2-3. Evolution of polymeric drug delivery systems for past 50 years in the scale of macro-, micro- and nano-. (Adopted from ref. 98, 233)

2.2 Release mechanism and mathematical models in polymeric material based controlled drug delivery systems

Polymeric materials have played an integral role in the advancement of drug release technology by providing controlled release of therapeutic agents in constant dose over long periods and tunable release of both hydrophobic and hydrophilic drugs. The devices made by polymeric materials are expected to provide effective therapy, reduce toxicity and increase patient comfort levels. The versatility of polymeric materials gives these systems great

opportunity to design devices following relative principles. For examples, the degradable polymer can control the degradation process to control the drug release; porous structure on the polymer based device allows the drug molecules diffusion outside of the matrix. Study of the mechanism of polymeric controlled drug release systems[98, 234-236] can be used to predict drug releasing profile and to reduce the number of the experiments. However, the mechanisms used for describe the controlled release process are normally diverse and complex, and mostly depend on the particular application. Sometimes, multiple mechanisms may simultaneously apply to one delivery process for illustrating the different stages. Herein, this section will discuss classical drug release mechanisms based on drug diffusion, polymer degradation, and erosion. Mathematic models are used for predict the release behavior of each mechanism, providing useful information, such as release kinetics and diffusion coefficient.

2.2.1 Diffusion-based release mechanism

In these systems, a drug is dissolved or dispersed in a non-swellable or fully swollen matrix that does not degrade during its therapeutic life. Diffusion occurs due to the drug molecules motion involves concentration gradients. The drug molecules migrate through the pores or channels. Mathematic model for the simple slab-like system is derived from Fick's second law of diffusion.[98, 237-239]

$$\frac{M_t}{M_0} = 4\left(\frac{Dt}{\pi h^2}\right)^{1/2} \left(0 \leq {M_t}/{M_0} \leq 0.6\right) \qquad (2\text{-}1)$$

$$\frac{M_t}{M_0} = 1 - \left(\frac{8}{\pi^2}\right) exp\left[\frac{(-\pi^2 Dt)}{h^2}\right] \left(0.4 \leq {M_t}/{M_0} \leq 1.0\right) \qquad (2\text{-}2)$$

where M_t is the sum of drug released at time t, with M_0 being the total of the drug-loaded mass, D is the diffusion coefficient, and h is the device thickness.

This model assumes that the dimension and physical properties do not change as the drug is released; for example, there is no loss of bulk polymer material or degradation. These models have been used in many studies. For example, the diffusion coefficients of functional proteins released from peptide nanofiber hydrogel scaffold was successfully predicted[240] and in another study, measured the diffusion coefficients of small molecular-theophylline in the poly (acrylic acid-*g*-ethylene glycol) hydrogels and showed that both the early- and late-time approximations correlate with experimental data, which indicate the dominant release mechanism was Fickian diffusion in this study.[241] However, there are some limitation if diffusion of drugs having heterogeneous structure, moving boundary condition, non-Fickian diffusion and ionic species.

2.2.2 Dissolution-based release mechanism

Polymer dissolution refers to a polymer releasing its payload drug into a thermodynamically compatible medium or solvent.[242-244] The release process was controlled by drug diffusion as well as polymer dissolution.[245, 246] As an example, the one-dimensional systems, such as slabs, films, or disks the model equation for accumulative drug release is described as below:

$$\frac{M_t}{M_0} = \frac{v_{d,eq}+{v_d}^*}{l}(\sqrt{2At} + Bt) \qquad (2\text{-}3)$$

Variables A and B are designated as

$$A = D({v_{1,eq}} - {v_1}^*)\left(\frac{v_{1,eq}}{v_{1,eq}+v_{d,eq}} + \frac{1}{{v_1}^*+{v_d}^*}\right) + D_d({v_d}^* - v_{d,eq})\left(\frac{v_{d,eq}}{v_{1,eq}+v_{d,eq}} + \frac{1}{{v_1}^*+{v_d}^*}\right) \quad (2\text{-}4)$$

$$B = \frac{k_d}{v_{1,eq}+v_{d,eq}} \quad (2\text{-}5)$$

where l is the initial crystalline polymer thickness,D represents the solvent diffusion coefficient value, D_d is the drug diffusion coefficient, ${v_1}^*$ and ${v_d}^*$ are the fixed fractions of the solvent and the drug (respectively) at the polymer crystalline-rubber transition, $v_{1,eq}$ and $v_{d,eq}$ are the fixed

fractions of the solvent and drug (respectively) at the polymer rubber phase-solvent phase equilibrium, k_d is the disentanglement rate of the polymer chain, and t is time.

The model successfully captures Fickian and Case II type behavior and the transition state in between. It provides good represent to polymer dissolution as there is a good correlation between equation 2-3 and experimental data. For example, the release of cimetidine hydrochloride from a poly(vinyl alcohol) tablet was shown a zero-order release pattern and to be driven via a Fickian diffusion process using this model.[245]

2.2.3 Erosion-based release mechanism

There are several mathematic models for erosion mechanism, such as Hopfenberg model[247, 248] and Hixson-Crowell model.[249] Surface eroding polymers can be represented using Hopfenberg's model, where the zero-order surface release of the drug determines the rate-limiting step. The following equation holds true for spheres, cylinders, and slabs.

$$\frac{M_t}{M_\infty} = 1 - (1 - \frac{k_0 t}{C_0 a})^n \quad (2\text{-}6)$$

where M_t and M_∞ are the cumulative drug release at time t and infinite time, k_0 is the erosion rate constant, C_0 is the initial concentration of the drug, a is the radius of the cylinder/sphere (or half the thickness of the slab), and n is a shape factor where n = 3 for a sphere, n = 2 for a cylinder, and n = 1 for a slab. However, predicted values using this model for a cylindrical tablet did not correlate well with experimental values.[250] The next model was developed for drug release from an erodible polymer matrix, which takes into consideration axial and radial erosion factors.

$$\frac{M_t}{M_\infty} = 1 - \left(1 - \frac{k_a t}{C_0 a_0}\right)^2 (1 - \frac{2k_b t}{C_0 b_0}) \quad (2\text{-}7)$$

where k_a is the radial erosion rate constant, k_b is the axial erosion rate constant, a_0 and b_0 are the tablet's starting radius and thickness (respectively), and C_0 is the initial concentration of drug in the matrix. Under specific conditions, where $k_a \approx k_b$, the model accurately described drug release from a cylindrical tablet. After this, different models were developed to taking into account the system's different situations, like considering the hydration kinetics, dissolution and pore formation for both surface and bulk eroding materials' drug release with all the parameters were explained and expressed was described by Rothstein *et al*.[251]

2.2.4 Affinity-based release mechanism

Affinity-controlled release[232, 252-256] is an approach proposed recently to study the controlled drug release systems. Due to the strong, reversible and noncovalent interaction between a therapeutic drug and a binding ligand, this alternative strategy provides a sustained and tunable release of therapeutics. The interaction used could be electrostatic, hydrophobic or/and van der waals between two binding partners.[232, 257] This process, in contrast to degradation or erosion polymer-based release systems, is controlled through the strength of the binding interaction, the binding kinetics and the concentration of the binding partners. Recently, a mathematical model for affinity-based delivery systems was proposed by different groups.[253, 258-261] These models have broadened our understanding of the mechanisms of controlling affinity-based protein released from hydrogels.

Recently, Shoichet group proposed a mathematical model to simulate affinity-based protein release by considering the terms of kinetic constants, gel thickness, protein diffusivity, binding ligand concentration and some other factors.[253] The mass transport within the hydrogel can be described using the mass balance for protein and complex. The concentration of free

protein (C_{pro}) changes due to diffusion from the gel as well as association or dissociation with the bound peptide are describes in equation (2-8).

$$\frac{\partial C_{pro}}{\partial t} = \frac{D}{r}\frac{\partial}{\partial r}\left(r\frac{\partial C_{pro}}{\partial r}\right) + D\frac{\partial^2 C_{pro}}{\partial z^2} - k_{on}C_{pro}\left(C_{pep,T} - C_{com}\right) + k_{off}C_{com} \quad (2\text{-}8)$$

Where $\mathrm{C_{pro}}$, $\mathrm{C_{pep}}$, and $\mathrm{C_{com}}$ are the molar concentration of the free protein in the gel matrix, the uncomplexed or free peptide and the complexed or bound peptide. The concentration of the free peptide (C_{pep}) is described as a difference between the concentration of total immobilized peptide ($C_{pep,T}$) and the concentration of complex (C_{com}). D is the diffusivity of the protein and assumed that the protein diffusivity through the gel and release media were not significantly different. Parameter k_{on} and k_{off} is the rates of association and dissociation of protein binding with the hydrogel matrix, respectively.

They concluded that the protein release from affinity-based systems will fall into one of the three regimes. In regime 1, bound and free proteins are released together over a single timescale and dominant by diffusion controlled, and it requires the concentration of binding ligand must by greater than dissociation constant to achieve affinity-based release although the peptides are mostly uncomplexed. Regime 2 has a large proportion of complexed peptides relative to uncomplexed ones and represents another case of diffusion-controlled dynamics with. A two-stage release profile is obtained for this regime. In regime 3, the decomplexation of bound protein is slow relative to diffusion, and nearly all the free protein is initially released from the gel over the diffusion timescale. The initial fast diffusive release is followed by the slower decomplexation and release of the bound protein over the timescale. When involving into a real controlled drug delivery system with different materials and morphologies, the mechanism is even more complex and not all of them can be predicted by the mathematical model. And we believe there still have large spaces to make progress in this area.

In this dissertation, most of the drug loading and releasing studies were based on the controlling of electrostatic interaction between the drug molecules and polymeric microgels.

2.3 Responsive polymeric materials design for controlled drug delivery

Stimuli-responsive polymers have very promising applications in the biomedical field as delivery systems of therapeutic agents, tissue engineering scaffolds, cell culture supports, bioseparation devices, sensors or actuators systems. The concept of stimuli-responsive drug delivery system was first reported in the late 1970s with the use of thermosensitive liposomes for the local release of drugs through hyperthermia.[262] After that, a great deal of research has been carried out on stimuli-responsive materials for drug delivery, especially concerning the design and application of responsive polymers. The design of new systems and approaches of drug delivery must meet challenges associated with administration in the body, such as a simple route of administration, effective delivery to the desired biological compartment, response adapted to the pathological event, either rapid or slow, depending on the bio-specificity and use of non-toxic, biocompatible and biodegradable systems. The strategy underlying polymer-containing responsive systems is a dramatic physicochemical change caused by stimuli. At the macromolecular level, polymer chains can be altered in different ways, including changes in hydrophilic-to-hydrophobic balance, conformation, solubility, degradation, and bond cleavage, and these, in turn, will cause detectable behavioral changes to self-assembled structures. Many designs that vary the location of responsive moieties or functional groups are possible, like side chains on one of the blocks, chain end-groups, or junctions between blocks. The response may be reversible or not, depending on the strategy employed. Stimuli-responsive polymers are involved in building up the controlled drug delivery system in different ways, including microgels/nanogels, self-assembly vehicles, core-shell particles, polymer-inorganic hybrid

systems and polymer-biomacromolecules conjugates and so on. In this dissertation, we will mainly discuss the most significant progress made in the field of controlled drug delivery from responsive polymeric microgels.

2.3.1 Thermo-responsive drug release

Thermoresponsive drug delivery is among the most investigated stimuli-responsive strategies and has been widely explored in oncology.[226, 263] Thermoresponsive is usually governed by a nonlinear sharp change in the properties of at least one component of the nanocarrier material with temperature. Such a sharp response triggers the release of the drug following a variation in the surrounding temperature. Ideally, thermosensitive nanocarriers should retain their load at body temperature (~37 °C), and rapidly deliver the drug to a locally heated tumor (~40-42 °C) to counteract rapid blood-passage time and washout from the tumor.

Thermoresponsive systems are generally liposomes, or polymer micelles or nanoparticles (usually pNIPAm) that exhibit a lower critical solution temperature as we described in Chapter 1. We know that microgels are cross-linked polymeric particles, which possess high water content, biocompatibility, and desirable mechanical properties. They are faster in responding to changes in their environment than their macroscopic or bulk counterparts and can be used more efficiently in medical applications.[117, 264] Due to their much higher interfacial area per unit mass, they have greater exchange rates. They offer unique advantages, like a tunable size from nanometers to micrometers, a large surface area for multivalent bioconjugation, and an interior network for the incorporation of biomolecules. Present and future microgels applications require a high degree of control over properties. They include stability for prolonged circulation in the blood stream, novel functionality for further bioconjugation, controlled particle size with a uniform diameter, and biodegradability for sustained release of drugs for a desired period of time

and facile removal of empty devices. When systems or materials are developed for used in medical application, the primary requirement is compatible with the biological environment or human body, which is proved with the character of nontoxic and easily digestion. A significant amount of work has been directed towards developing the responsive microgels with functionalized degradable groups or cross-linkers, such as peptides,[265] anhydrides,[266] polyglycerol,[267] disulfides,[268] acetals,[269] poly (3-hydroxybutyrate),[270] and polyphosphoesters.[271] Recently, more and more attention is focused on the biomedical application of microgels. [117, 226, 264, 272-274] The functionalities of pNIPAm can be further modified by embedding micro or nanoparticles that are responsive to different types of stimulations, including magnetic fields.[275-277] Recently, an example is pNIPAm microgel with embedded iron nanowires which shows highly efficient magnetic controlled drug release.[278] These hybrid microgel particles are made from a simple microfluidic technique with a high control of the nanowire concentration and in a relatively short time compared to chemical synthesis methods. The thermoresponsive microparticles were used for the remotely triggered release of Rhodamine B (RhB). With a magnetic field of only 1 mT and 20 kHz, a drug release of 6.5 % and 70 % was achieved in the continuous and pulsatile modes, respectively, as shown in Figure 2-4. It also shows that almost no release is obtained from pNIPAm and NBC particles in a pulsatile low-power alternating magnetic field (AMF). The small release observed is due to RhB diffusion.

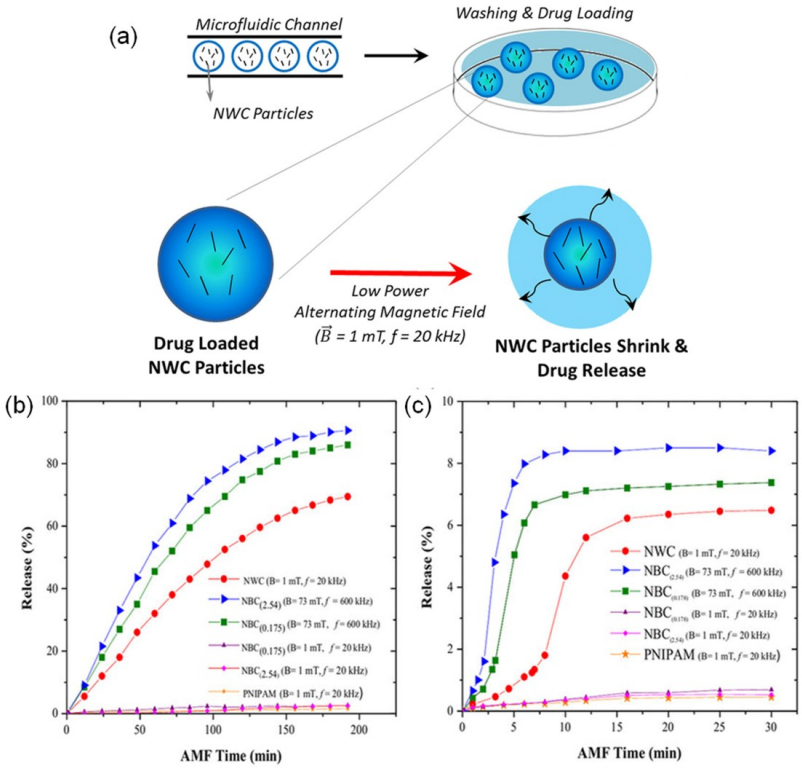

Figure 2-4. (a) The nanowire composite pNIPAm particles are fabricated in a microfluidic system and are loaded with a drug by means of diffusion. (b) The release of RhB from particles at low-power and high-power alternating magnetic fields. (c) Pulsatile release of RhB from particles exposed to an alternating magnetic field for 12 minutes separated by 5 minutes intervals. NWC means nanowire composite and NBC means nanobead composite particles. Reproduced with permission from ref. 278, Copyright 2016, Nature publication.

2.3.2 pH-responsive drug release

The pH values in various segments of the gastrointestinal tract, different organs, tissues, and cellular compartments are different have been exploited to control the delivery of drugs, as well as to trigger the release of the drug when subtle environmental changes are associated with pathological situations, such as cancer or inflammation. For example, the pH values vary in a wide range from the stomach (pH ~1.5-3.5) and small intestine (pH ~5.5-6.8) to the colon (~6.4-

7.0). The pH values in tumors and inflammatory tissues are lower than those in blood and normal tissues (~7.4), and the acidic cellular environments exhibit even lower pH values (e.g., endosomes (pH ~5.5-6.0) and lysosomes (pH ~4.5-5.0).[45] The difference in the pH value of different organs, tissues, and cellular compartments may provide a suitable physiological stimulus for pH-responsive drug delivery.[279, 280] The strongly pH-dependent drug release profile of the drug-delivery system is an ideal platform for targeted drug delivery because the drug release is inhibited during systemic circulation at the physiological pH value of 7.4 and the drug is released only in the acidic environment of cancer cells. Two main strategies exist: the use of polymers (polyacid or polybases) with ionizable groups that undergo conformational and/or solubility changes in response to environmental pH variation; and the design of polymeric systems with acid-sensitive bonds[281] whose cleavage enables the release of molecules anchored at the polymer backbone, the modification of the charge of the polymer or the exposure of targeting ligands. The polymers with a large number of ionizable groups are known as polyelectrolytes. The polymer contains acid-sensitive bonds that can undergo a cleavage of the bond to break down the drug carriers to release the payload. It usually requires the specific chemical modification of the polymeric components and the details will describe later.

Hydrogels are an important kind of material with many applications in various biomedical fields. Compared with other synthetic biomaterials, the physical properties of hydrogels resemble living tissues closely because of their relatively high water content and soft and rubbery consistency. More importantly, the ability of drug molecules with different sizes to diffuse into and out of hydrogels allows the possible use of dry or swollen polymeric networks as drug-delivery systems. Hydrogels can perceive and respond the stimuli by changing their physical or chemical behavior, which results in the controlled release of loaded drugs. The pH change

induced swelling behaviors of hydrogel have been most frequently used to develop controlled release systems.[280] For example, PAA-based hydrogels can be used to develop formulations that release drugs in a neutral pH environment.[282-284] Hydrogels crosslinked with azoaromatic crosslinkers were developed for colon-specific drug delivery.[285] pH-responsive hydrogels were also placed inside capsules[286] or silicone matrices[287] to modulate the drug release. Compare to hydrogels, as a hydrogel particles micro/nano size scale, microgels maintain all the excellent properties of hydrogels and with much faster in responding to changes in their environment, higher interfacial area, and well-defined compositional heterogeneity as we described in previous Chapter and sections. Microgels also have tremendous flexibility in terms of their composition, morphology or assembly, enabling the production of multiple types of microgels-based materials with properties not accessible by conventional hydrogel fabrication techniques. Specifically, microgels with pH responsivity have found important application in controlled drug delivery systems. Georgiou group fabricated Amphiphilic microgels of different composition based on the hydrophilic, pH-responsive acrylic acid and the hydrophobic, non-ionic *n*-butyl acrylate[288] or hydrophobic crosslinks of different compositions[289] via a microfluidic platform. Due to their amphiphilic nature, they were able to encapsulate and deliver both hydrophobic Sudan I dye and hydrophilic Trypan Blue dye. The release was influenced by both the hydrophobic content of the microgels and the pH of the surrounding solution. With increasing the hydrophilic content of the microgels and suspending them in a more basic solution, the release of the dyes was accelerated.

Other more complex systems are design based on the concept of pH-responsive properties, instead of using acidic or basic polymers, acid or base degradable or cleavable polymers have been applied into the pH-responsive drug delivery system to generate novel delivery properties. Haag's group developed a series of microgels/nanogels of labile based on crosslinks for

biomedical applications.[290-293] Recently their group[294] reported efficient and homogenous stimuli-responsive microgels to encapsulate living cells that overcome the limitation of traditional acid-cleavable systems with free radical cross-linking[295] and copper(I)-catalyzed azide-alkyne cycloaddition.[267] The process of microgels fabrication and the cell encapsulation and release were shown in Figure 2-5. These microgels were fabricated by combining bioorthogonal strain-promoted azide-alkyne cycloaddition (SPAAC) and droplet-based microfluidics. Poly (ethylene glycol)-dicyclooctyne and dendritic poly (glycerol azide) (dPG) served as bioinert hydrogel precursors, and nonspecific hydrogel-cell interactions are avoided. Azide conjugation was performed using different substituted acid-labile benzacetal linkers that allowed precise control of the microgels degradation kinetics in the interesting pH range between 4.5 and 7.4. By this means, a pH-controlled release of the encapsulated cells was achieved upon demand with no effect on cell viability and spreading. As a result, the microgels particles can be used for temporary cell encapsulation, allowing the cells to be studied and manipulated during the encapsulation and then be isolated and harvested by decomposition of the microgels scaffolds.

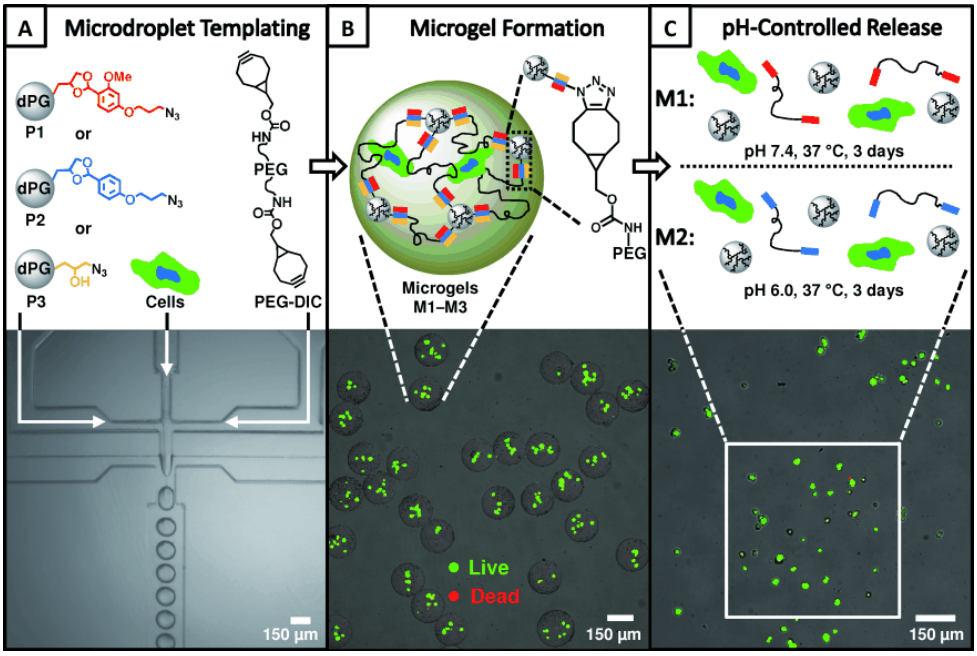

Figure 2-5. The process of microgels fabrication and cell encapsulation and release: A) A set of dPG-azide precursors P1-P3 with acid-cleavable linkers were prepared by microfluidic devices. B) Micrometer-sized, cell-laden hydrogel particles were formed with the living cells were stained green and dead cells were stained red. C) Microgel M1 degraded completely after three days at the condition of pH 7.4, 37 °C, and 5 % CO_2. Microgel M2 showed incomplete degradation and no release of cells for an observation period of two weeks under the same condition. However, incubation of microgel M2 at pH 6.0, 37 °C, and 5 % CO_2 led to complete particle degradation after three days. Microgel M3 showed no degradation between pH 6.0-7.4. Reproduced with permission from ref. 294, Copyright 2013, WILEY-VCH Verlag GmbH & Co. KGaA, Weinheim.

Microgels or hydrogels that can response to multiple stimuli are also very interesting in this area.[296] They are providing more opportunities to control the release behavior of the polymer systems. Like microgels response to both temperature and pH can be made by simply incorporating pH-responsive monomer and temperature-responsive polymer, the LCST of the

microgels or hydrogels depends on the ionization of the pendant ionizable groups. The commonly used one is p(NIPAm-*co*-AAc) microgels, which has been extensively studied in controlled drug release application.[126, 297-300]

2.3.3. Light-responsive drug release

Light-responsive systems has been engineered in the past few years to achieve on-demand drug release in response to illumination of a specific wavelength (in the UV, visible or near-infrared (NIR) regions)[301] because of the non-invasiveness and the possibility of remote spatiotemporal control. Light-induced changes at polymer level can be reflected on the macroscopic level of material properties. A large variety of different strategies available relies on either a one-time or repeatable on-off drug-release event triggered by light-sensitiveness induced structural modifications of the drug carriers. These strategies can be divided into three directions. The first one is the materials with photo-switchable groups, which can change its molecular structure reversibly by applying different wavelength light. For instance, photoisomerization of the azobenzene group and its derivatives (discussed in Chapter 1) from trans to cis on irradiation at 300-380 nm, and from *cis* to *trans* by shining light in the visible region is enabled light-regulated control of drug release. Spiropyran isomerizes to colored merocyanine form upon UV light irradiation and back to the original structure under visible light. These transitions change not only the color of the materials but also the properties of charges and can alter the hydrophilic/hydrophobic balance, which is used tune the drug release. Light-responsive polymer micro- and nano-capsules[302] with these responsive groups promising ideal light controlled drug release.[303] For example, supramolecular valves constructed by tetra-ortho-methoxy-substituted azobenzene and β-cyclodextrin were used to control drug release from mesoporous silica nanoparticles by the red light trigger.[304] The second direction is using the photocleavable groups

that can break the covalent bond with light irradiation.[305] For example, *o*-nitro benzyl (*o*-NB) and its derivatives[57, 306, 307] are efficiently cleavable upon UV exposure. Molecular with a *p*-methoxyphenyl group can light-triggered hemolysis of the carbon-oxygen bond to release the pending groups, like benzoic acid, several amino acid derivatives, and peptides. Zhao and co-workers show the first example of the potential application of *o*-NB linkers in drug delivery and phototherapeutic.[308] It was demonstrated by the controlled release of Nile Red-previously trapped inside a hydrophobic core of the micelle. Upon irradiation, the hydrolysis of the 2-nitrobenzyl moieties converts the polymer from hydrophobic to hydrophilic, which results in the disruption of the micelle and release the hydrophobic drug. The last one is combined with nanomaterials, like nanoparticles, nanosheets, and nanorod, with polymers to form hybrid materials which can response to light and control the drug release.[309-316] The mechanism behind is using the photo-thermal effect of nanomaterials to induce the properties to change of polymeric materials to trigger the release of drugs. For example, gold nanorods encapsulated pNIPAm nanogel has been reported by application of the NIR laser caused rapid shrinkage of the hydrogels and released the drug.[317]

A variety of materials and structures is designed to meet the requirement of a different situation for controlled drug release. Materials like block copolymers incorporated with photosensitive moieties and thermal-responsive polymers hybrid with nanoparticles. The structure could be macro-size hydrogels, films, micro/nanogels, micelles or vesicles, and so on. Photosensitive block copolymers have been intensively studied due to their self-assembling properties and drug delivery applications. Polymer micelles or vesicles formed through self-assembly of photo-response block copolymers can be applied as carriers for controlled drug delivery. The increase in temperature resulting from the surface plasmon resonance of gold on

NIR irradiation may also cause a phase transition in polymers or lipids, allowing the leakage of a preloaded drug. Accordingly, poly (lactic-*co*-glycolic acid) (PLGA) entirely or half coated with a gold layer,[318] gold nanoparticles are encapsulated within pNIPAM microgels,[319] polymer-coated gold nanocages,[320] gold nanoparticles coated with pNIPAm polymer shell[321] or gold nanorods combined with thermosensitive liposomes[322] have been designed, and some have shown significant antitumour activity in experimental models of breast cancer.

Light with the wavelength range of 190 nm-1000 nm, which contains the UV-vis and NIR light, is normally considered as a trigger for light-responsive controlled drug systems to release their entrapped drugs. Lots of studies focus on the UV-vis region of the spectrum (less than 700 nm),[323-325] which have rather limited tissue penetration depth (~10 mm) that results from the strong scattering properties of soft tissues and thus would be inappropriate for *vivo* applications. Alternatively, NIR light with the wavelength ranging from 700 nm to 1000 nm exhibits great tissue penetration depth owning to its obviously reduced scattering and absorption by biological tissues. This makes NIR-responsive systems extremely promising for clinical applications. The capacity of NIR-absorbing plasmonic materials to convert the photon energy absorbed during irradiation into heat has been used to trigger the release of chemotherapeutic molecules from NIR-responsive nanodevices.

Here is an example, light-sensitive composites consisting of CuS nanocrystals as a core and poly (*N*-isopropylacrylamide)-graft-chitosan (p(NIPAm-*g*-CS)) microgels as a shell was described recently.[326] After loaded with another photo-sensitive component, $Fe_4S_3(NO)^{7-}$, the microgels shows light triggered dual releasing properties. Due to the photothermal effect of CuS under NIR light (980 nm), the nanocomposites showed photo-thermal-sensitive volume shrink of p(NIPAm-*g*-CS), which release the loaded doxorubicin (Dox). Due to the visible-light response

of $Fe_4S_3(NO)^{7-}$, nitric oxide (NO) was released from photolysis. NIR and visible light respectively triggered the release of Dox and NO from the nanocarriers, as shown in Figure 2-6. Together with the photothermal effect of CuS, the nanocarriers simultaneously realized light-triggered release of dual drugs and synergistic chem-photo-thermal therapy to cancer cells. In Figure 2-6b, the release of Dox from the nanocomposites is slower at neutral than mildly acidic pH as Dox is less soluble in water at neutral pH and would, therefore, prefer to remain in the nanocomposites. Upon the increase of irradiation time (0-5 min), an obviously accelerated Dox release was found in Figure 2-6c, with almost no change when there is no irradiation.

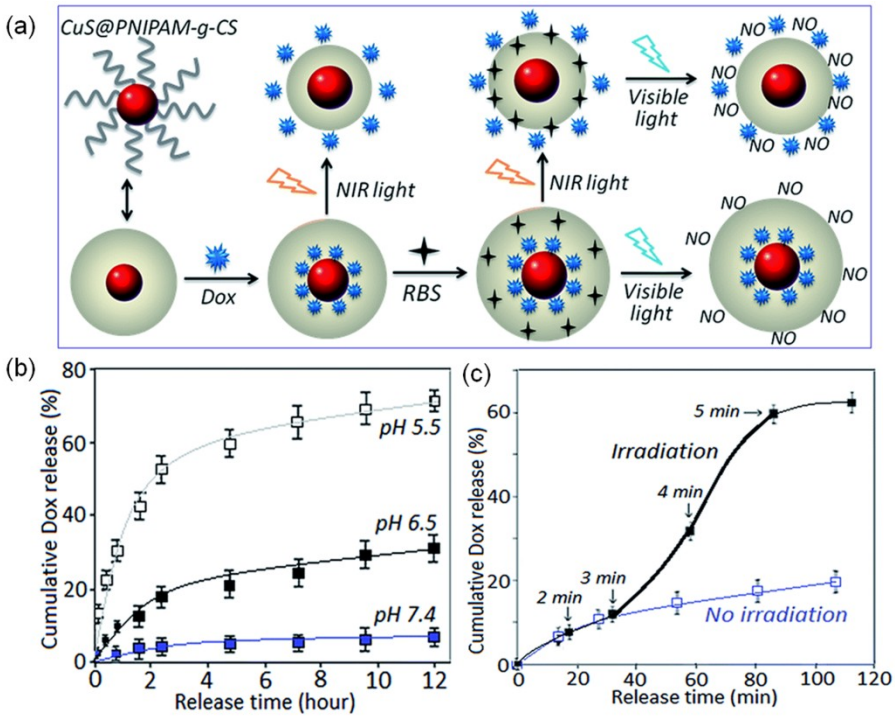

Figure 2-6. (a) Schematic illustration of the fabrication and light-regulated drug release of Dox/RBS loaded CuS@p(NIPAm-*g*-CS) nanocarriers. (b) Dox release from Dox-loaded nanocomposites in phosphate buffer solution (PBS) at different pHs. (c) Dox release in PBS (pH 6.5) without or with NIR- light irradiation (980 nm, 0.5 W). Reproduced with permission from ref. 326, Copyright 2016, Royal Society of Chemistry.

Recently, more and more interests are focused on the developing of multi-responsive systems[327-329] or multiple drugs releasing systems[330-332] to combine with more than one function of the materials to generate advanced intelligent devices for controlled drug release. A smart composite hydrogel was reported to show both pH-dependent drug release in a cancer environment and heat generation based on NIR laser exposure, for the combined application of photothermal therapy and chemotherapy.[333] The hydrogel was composed of a highly biocompatible polydopamine nanoparticle, as a near-infrared absorbing agent embedded within stimuli-sensitive poly (NIPAm-*co*-AAm) hydrogels. Bortezomib and Dox were loaded into the hydrogel through complexation with catechol groups to evaluate the multimodal treatment and multidrug release. Nanoparticles absorbed the light locally as heat to impact cancer cells via hyperthermia. Hydrogel will de-swell with the temperature increase to release Dox in an on-demand manner. Moreover, in a typical acidic cancer environment, the conjugation between catechol and bortezomib dissociates, also resulting in the controllable release of this drug. This unique system combines multi-response materials and multiple drug release behaviors for both photothermal therapy and chemotherapy can be considered as a potential future direction for cancer treatment.

2.4 Conclusion

Research in polymer therapeutics has enjoyed success over the past few decades in mediating safe and effective delivery of bioactive agents, such as small molecules, peptides, and proteins, but also newer, complex molecules such as antisense oligonucleotides, to treat an enormous variety of medical conditions. Polymer hydrogels of different chemical architecture with novel physicochemical properties have shown potential to find applications as a promising drug carrying vehicles in various drug delivery technologies. With a fundamental understanding

of biological barriers, many candidates advanced materials can be developed as carriers and devices for the delivery of pharmaceuticals. The creation of smart, stimuli-responsive systems that respond to subtle environmental changes in the local cellular environment is likely to yield long-term solutions to many of the current drug delivery problems. Although reports of dual- and multi-responsive hydrogels have shown a marked increase in recent years, challenges remain in terms of reducing synthesis complexity and ensuring excellent biocompatibility. Not only the examples we illustrated above have made great progress in controlled drug delivery area, there are still many others have excellent properties that can apply to the development of new drug delivery systems which are not described in detail in this chapter. In future, we can expect to see the advancement of self-healing hydrogels, biomimetic scaffolds, and closed-loop drug delivery systems that are sustainable over long periods of time, resulting in regenerative treatments and implants with improved efficacy to restore a high quality of life for patients.

There are still many important future challenges in drug delivery. Among the most important is the development of approaches where drugs can be targeted to specific cells for delivery of anticancer drugs. Another challenge is to develop ways to target genes or transcription factors to specific cells. In addition, the design of drug delivery systems able to cross complex barriers such as the gastrointestinal tract or brain is of great importance. Finally, increased research in materials science to understand how to improve implant biocompatibility and to achieve desired drug delivery patterns must be conducted to administer drugs optimally.

Chapter 3: Controlled and Triggered Small Molecule Release from a Confined Polymer Film[b]

In this chapter, we will discuss the small molecule controlled release behavior from the confined polymer microgel assemblies based device. The study focused on the development of microgel assemblies and tuning the release rate by varying the thickness of the covered gold layer. The results showed that the model drug could be released in a triggered fashion, turning on and off as a function of solution pH.

3.1 Introduction

Polymer-based materials that are capable of encapsulating small molecules (or drugs) and releasing them in a controlled/triggered manner are well known, pioneered by the work of the Langer group.[334] In the following years a number of functional materials composed of stimuli-responsive polymers,[6, 335, 336] micro and nanoparticles,[337-339] and porous materials[340-342] have been developed that are capable of releasing a variety of small molecules and macromolecules (e.g., DNA and RNA)[343-346] in a controlled and triggered fashion. Responsive materials have been developed that can respond to external stimuli, for example, temperature,[347] light,[348, 349] small molecules,[228] magnetic fields,[350] ultrasound[351, 352] and electric field.[14, 353] Various drug delivery systems, such as liposomes, micelles, polymeric particles, and hydrogels have shown great promise for controlled and targeted drug delivery. Among these systems, porous materials are emerging as a new category of drug delivery systems.

Great attention has been focused on the development of porous materials as controlled drug delivery matrices because they can be synthesized to have a stable uniform porous structure with

[b] This Chapter has been adapted from the previously published article: Y. Gao, P. Zago, Z. Jia, M. J. Serpe.* *ACS Appl. Mater. Interfaces,* 2013, 5, 9803-9808.

tunable pore sizes and well-defined surface properties. Of particular interest to the work here are porous materials that were used for controlled release of encapsulated species from their pores via regulation of the pore size. Recently, different porous-container materials were used for the controlled release of the small molecules in a reservoir.[340, 341, 354-361] The Willner group reported that nucleic acid modified mesoporous silica nanoparticles could be used to release a drug in a controlled and triggered fashion.[26] Specifically, they modified the mesoporous silica nanoparticles with tailored nucleic acids, which defined the pores and pore size. The nucleic acid pores could be cleaved, and thus opened, in the presence of specific ions. This results in the release of the pore-encapsulated substrates. In another example, nitrospiropyran photoisomerizable units were used to modify mesoporous SiO_2 nanoparticles.[27] Photoisomerization of the capping units to the protonated nitromerocyanine opens the channels and releases the encapsulated dye molecules in the nanoparticles. Vasiliev and co-workers developed a polymer bilayer-based platform to control the local release of drugs.[361] A polymer-based "sandwich" structure was formed by plasma polymerization followed by the embedding of the drug between the two polymer films. The top polymer film was porous, allowing the drug to leak from the bilayer structure at a given rate. They showed that the rate of release could be adjusted by varying the thickness of the top polymer layer. While these systems do show promise, many of the systems are complex and time-consuming to fabricate. Hence, easy to manufacture systems capable of controlling the release of small molecules to a system is needed.

Poly (*N*-isopropylacrylamide) (pNIPAm) is by far the most extensively studied responsive polymer to date.[18, 39, 42, 170] It is well known to be thermoresponsive, exhibiting a lower critical solution temperature (LCST) at 32 °C in water. That is, < 32 °C the polymer has favorable interactions with water molecules and exists as a solvated, extended random coil. The polymer-

polymer interactions become dominant at > 32 °C, causing the polymer to desolvate and collapse into a dense globular conformation. Furthermore, the transition is fully reversible and can be repeated many times. As the LCST is close to physiological temperature, pNIPAm based materials, such as hydrogels and microgels have been widely exploited in biomedical and biological applications.

Like linear pNIPAm, pNIPAm-based hydrogel particles (microgels) have also been synthesized and are fully water swollen (large diameter) at T < 32 °C, while they are dehydrated (small diameter) at T > 32 °C.[18, 362-364] PNIPAm-based micro and nanogels are most easily synthesized via free radical precipitation polymerization.[38, 365] This approach is versatile in terms of the variety of chemical functionality that can be added to the microgels by simply adding functional monomers to the reaction prior to the initiation. Using this approach, pNIPAm-based microgels with a variety of chemical functionalities have been synthesized.[142, 366, 367] The most commonly used comonomer is acrylic acid (AAc), which renders the p(NIPAm-*co*-AAc) microgel pH responsive,[144, 367-369] and can also be used to further modify the microgels with other small molecules.[170, 171, 370-372] The pH responsivity is a result of the pK_a of the AAc group. That is, the pK_a for AAc is ~4.25, so when the pH of the environment is < 4.25, the AAc group are protonated and mostly neutral (a slight charge can exist depending on the initiator used), and when the pH > 4.25, the microgels are deprotonated and negatively charged. Therefore, at high pH, the microgels have attractive electrostatic interactions with positively charged species, while they have minimal interactions with positively charged species at low pH.

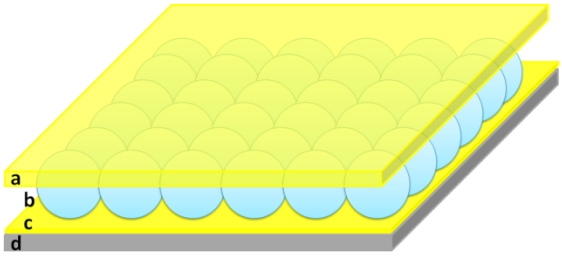

Figure 3-1. Structure of a pNIPAm microgel-based assemblies. (a) and (c) are 15 nm Au layers (with 2 nm Cr adhesion layer) sandwiching (b) a microgel layer all on a (d) glass substrate. Reproduced with permission from ref. 299, Copyright 2013, American Chemical Society.

Recently, our group developed color tunable materials by sandwiching pNIPAm-based microgels between two thin gold (Au) films resulting in the "mirror-dielectric-mirror" configuration of a device.[40, 130, 144, 155, 156, 161, 171, 373-375] The structure of the device is shown in Figure 3-1. When it is immersed in water, microgel layer swells, rendering them thermoresponsive. This allows the thickness of the microgel layer to be tuned by varying the water temperature. Since the color of the devices depends on the dielectric thickness, the color of the device can be dynamically tuned with temperature, which makes them good sensor devices.[373, 375] Using appropriately modified microgels, the device can also be made to change color as a function of pH,[130] and upon exposure to glucose.[171] We also demonstrated that polyelectrolytes can penetrate into the microgel-based layer by entering through the pores in the Au layer (overlayer) covering the microgels, which will, in turn, change the optical properties of the devices.[155] Finally, we showed that the Au overlayer's pore size can be varied by changing the thickness of the Au overlayer.[130, 156] That is, thick Au has fewer and smaller pores than thin Au. We have been able to exploit this phenomenon for sensing and biosensing applications.[374]

In the present work, we exploit the pH responsivity of p(NIPAm-*co*-AAc) microgels assemblies, and the pore size control of the top Au overlayers, to achieve devices capable of

delivering the small molecule tris (4-(dimethylamino)phenyl)methylium chloride (Crystal Violet, CV) to a system. The loading and release mechanism is illustrated Figure 3-2. CV molecules are positively charged and represented by the blue dots. As mentioned above, an increase in the solution pH to above the pK_a for AAc renders the microgels negatively charged. Thus, at high pH there is a strong electrostatic interaction between the microgels and the positively charged CV molecules, which facilitates CV adsorption into the microgel. Reducing the pH of the solution to below the pK_a of AAc renders the AAc groups neutral. Hence, the electrostatic interactions holding the CV into the microgels were destroyed, and the CV could exit the microgel layer. Here, we show that the rate of the release from the device depends on solution pH and the thickness of the Au overlayer.

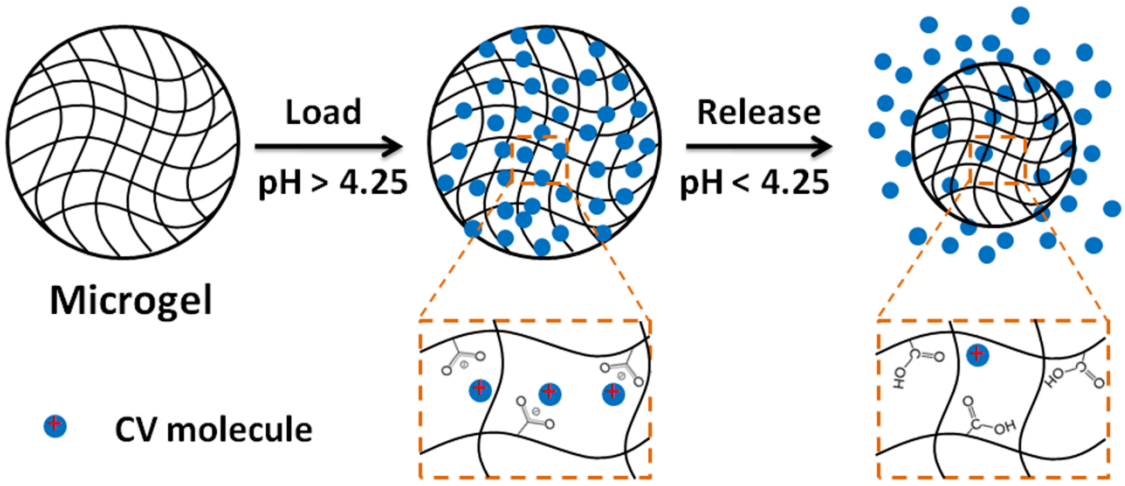

Figure 3-2. Loading and release mechanism of CV molecules into and out of p(NIPAm-*co*-AAc) microgels. Reproduced with permission from ref. 299, Copyright 2013, American Chemical Society.

3.2 Experimental section

Materials: *N*-isopropylacrylamide (NIPAm) was purchased from TCI (Portland, Oregon) and purified by recrystallization from hexanes (ACS reagentgrade, EMD, Gibbstown, NJ) prior to use. *N, N'*-methylenebisacrylamide (BIS) (99 %), acrylic acid (AAc) (99 %), and ammonium persulfate (APS) (98+ %) were obtained from Aldrich (St. Louis, MO) and were used as received. Sodium chloride was obtained from EMD (Millipore, Billerica, MA), and deionized (DI) water with a resistivity of 18.2 MΩ·cm was used. Cr/Au annealing was done in a Thermolyne muffle furnace from ThermoFisher Scientific (Ottawa, Ontario). Anhydrous ethanol was obtained from Commercial Alcohols (Brampton, Ontario). Sodium hydroxide (NaOH, 99.8 %) and hydrochloric acid were purchased from Caledon Chemicals (Georgetown, Ontario) and were used as received. Fisher's finest glass coverslips were 25 × 25 mm and obtained from Fisher Scientific (Ottawa, Ontario). Cr was 99.999 % and obtained from ESPI as flakes (Ashland, OR), while Au was 99.99 % and obtained from MRCS Canada (Edmonton, AB). Tris (4-(dimethylamino)phenyl)methylium chloride (Crystal Violet, CV) was obtained from Sigma-Aldrich.

Microgel synthesis: Microgels composed of poly (*N*–isopropylacrylamide)-*co*-acrylic acid (p(NIPAm-*co*-AAc)) were synthesized via free radical precipitation polymerization as described previously.[130] Briefly, a 3-necked round bottom flask was fitted with a reflux condenser, nitrogen inlet, and temperature probe, and charged with a solution of NIPAm (11.9 mmol) and BIS (0.703 mmol) in 99 mL deionized water, previously filtered through a 0.2 μm filter. The solution was bubbled with N_2 gas and allowed to heat to 70 °C over ~1 hour. AAc (1.43 mmol) was added to the heated reaction mixture in one aliquot. The reaction was then initiated with a solution of APS (0.2 mmol) in 1 mL of deionized water. The reaction was allowed to proceed at 70 °C for 4 hours

under a blanket of nitrogen. The resulting suspension was allowed to cool overnight, and then it was filtered through a Whatman #1 paper filter to remove any large aggregates. The microgel solution was then distributed into centrifuge tubes and purified via centrifugation at ~8300 rcf to form a pellet, followed by removal of the supernatant and resuspension with deionized water, 6x. The cleaned microgels were recombined and stored in a brown glass jar.

CV loaded device fabrication: CV loaded devices were fabricated using a previously published protocol[155] with slight modification. The process is shown in Figure 3-3. To fabricate the Au coated coverslips (etalon underlayer), 2 nm Cr followed by 15 nm of Au was thermally evaporated onto a 25 x 25 mm ethanol rinsed and N_2 gas dried glass coverslip (Fisher's Finest, Ottawa, ON) at a rate of 0.2 Å s^{-1}, and 0.1 Å s^{-1}, respectively (Torr International Inc., thermal evaporation system, Model THEUPG, New Windsor, NY). The Cr/Au substrates were annealed at 250 °C for 3 h (Thermolyne muffle furnace, Ottawa, ON) and cooled to room temperature prior to microgel film deposition. Approximately 10 mL of microgels solution was centrifuged at ~8300 rcf to form a pellet at the bottom of a centrifuge tube. The supernatant was removed and discarded, and the pellet was vortexed to loosen and homogenize the particles in the remaining solvent. A 40 µL aliquot of the concentrated microgels was put onto the substrate and then spread toward each edge using the side of a micropipette tip. The substrate was rotated 90°, and the microgel solution was spread again. The spreading and rotation continued until the microgel solution became too viscous to spread due to drying. The microgel solution was allowed to dry completely on the substrate for 2h with the hotplate temperature set to 35 °C. After that, the dry film was rinsed copiously with DI water to remove any excess microgels not bound directly to the Au. The film was then placed into a DI water bath and allowed to incubate overnight on a hot plate set to ~30 °C. Following this step, the substrate was again rinsed with DI water to further

remove any microgels not bound directly to the Au substrate surface. The samples were then rinsed with deionized water, dried with N_2, and then put into 20 mL of a CV solution (4 mg/mL, pH of 6.5) overnight. Excess CV was rinsed off the substrate with pH 6.5 solution (to not disturb the microgel-CV interaction) and incubated in pH 6.5 solution overnight followed by drying with N_2 gas. Another Au overlayer (2 nm Cr for adhesion, followed by deposition of different thicknesses of Au overlayers) was evaporated onto the CV loaded microgel layer. Since we were interested in understanding how the Au overlayer thickness affected the rate of CV release from the etalon, we sealed the etalon's edges with clear nail polish.

CV release: A Petri dish filled with 20 mL of pH solution was placed on a hot plate, and the solution temperature maintained at 25 ^{o}C. In our experiments, we use two pH values, 3.0 and 6.5. The solution in the Petri dish was stirred continuously at 260 RPM using a magnetic stir bar. The solution flowed through a cuvette in an Agilent 8453 UV-Vis spectrophotometer, equipped with an 89090A temperature controller, via a peristaltic pump. The CV loaded device was added to the Petri dish, and a timer started. The absorbance spectrum of the solution was collected every 30 s. The flow rate of the solution was measured before and after each experiment and was used (along with the time measurements) to calculate a volume.

3.3 Results and discussion

Microgel assemblies based devices have been reported by our group as an optical device that can be used to sense ions,[373] glucose,[171] or biomolecules.[374] It can also be used as a platform to study the penetration of macromolecules into confined spaces.[144] Here, we show that the structure can be used for controlled and triggered small molecule (or "drug") release to a system. To accomplish this, the p(NIPAm-*co*-AAc) microgel assemblies based device was fabricated using the protocol shown schematically in Figure 3-3. Initially, 2 nm Cr and 15 nm Au was

thermally evaporated on the glass substrate, followed by annealing and deposition of the microgel layer. The microgel layer was loaded with CV as detailed above; CV was used as a model drug. CV is hydrophilic, positively charged, and has an absorbance maximum at ~590 nm, which makes it easy to detect spectrophotometrically and the purple color of CV solution makes it easily visible.

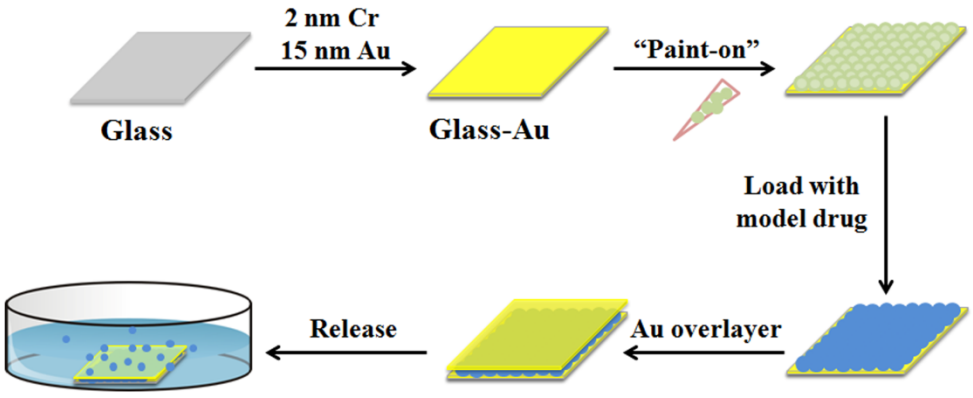

Figure 3-3. Schematic of the fabrication of CV (drug) loaded devices and the release process. Reproduced with permission from ref. 299, Copyright 2013, American Chemical Society.

Next, Au was deposited on the CV loaded microgel layer to form the top Au overlayer of the device. Again, the edges were sealed with clear nail polish to prevent CV leakage out of the sides and to ensure that the CV only exited the device through the Au overlayer. The device (in this example with a 500 nm overlayer) was added to a Petri dish containing pH 6.5 solution, and the solution's absorbance spectrum collected every 30 s. The UV-vis spectra are shown in Figure 3-4. The absorbance value at 590 nm was used to quantify the amount of CV in solution after releasing. As can be seen in Figure 3-4(a), in pH 6.5 solution the increase was quite minimal, this was in contrast to a CV-loaded device exposed to pH 3.0 solution, which is shown in Figure 3-4(b). From the data, it is clear that for a given Au overlayer thickness, we are able to control the

release rate with pH by modulating the CV-microgel interaction. It is worth noting here that the spectrum of CV was unaffected by the Au deposition process.

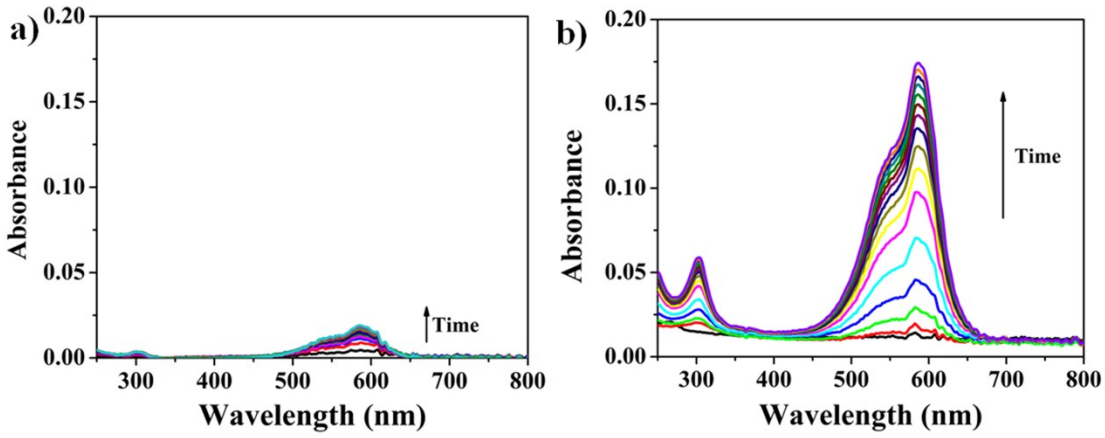

Figure 3-4. Release of CV over time, monitored via UV-vis spectrophotometer, in (a) pH 6.5 and (b) pH 3.0 solutions. The Au overlayer thickness o this sample was 500 nm. The maximum absorbance is at 590 nm, and the absorbance increases with time. The spectra were obtained every 30 s, and the total release time was 2 h; here we show spectra for the first 10 min of release. Reproduced with permission from ref. 299, Copyright 2013, American Chemical Society.

In order to evaluate how the rate of CV release from the device was affected by Au overlayer thickness, we constructed CV-loaded devices with four overlayer thicknesses 50, 200, 500 and 700 nm. The release profiles for the CV-loaded device with different Au overlayer thicknesses were evaluated at for the device exposed to pH 6.5 and then pH 3.0 solutions. For these experiments, we simply monitored the absorbance at 590 nm over time. Figure 3-5(a) shows CV molecule release from the device in pH 6.5 solution. The data show that at this pH, the release was slow due to the favorable electrostatic interactions between the CV and the microgels, as discussed above. Figure 3-5(b) shows CV release from the device at pH 3.0, and clearly, shows that the Au overlayer thickness plays a major role in controlling the release rate. It is important to mention here that volume, instead of time, was used as the x-axis since the flow

rate was variable from sample to sample. The 50 nm Au overlayer sample released the CV the fastest, while the 700 nm Au overlayer sample released CV the slowest. The rate of CV released appears to scale with Au overlayer thickness. In previous studies of our group, we have shown that the average pore size decreases with increasing Au overlayer thickness.[40] So we attribute the slower release kinetics as a function of increasing Au overlayer thickness to the decrease in Au pore size. It is interesting to note that the amount of CV released from each film varies with Au overlayer thickness. While this is not well understood, we attribute this to the thicker Au overlayers trapping the CV in a state in which it is not able to be released. For controls, we showed that ambient light and pH had no effect on the CV spectrum, as shown in Figure 3-6.

Finally, we show that the thermoresponsive nature of the pNIPAm-based microgels can be used to accelerate the release of the CV from the etalon at a given Au overlayer thickness. As can be seen in Figure 3-7, when a device with a 700 nm Au overlayer is initially immersed in pH 3.0 solution at 25 ^{o}C the release rate is much slower than when the solution temperature is increased to ~47 ^{o}C, showing that the collapse of the microgels in the assemblies can accelerate the release rate.

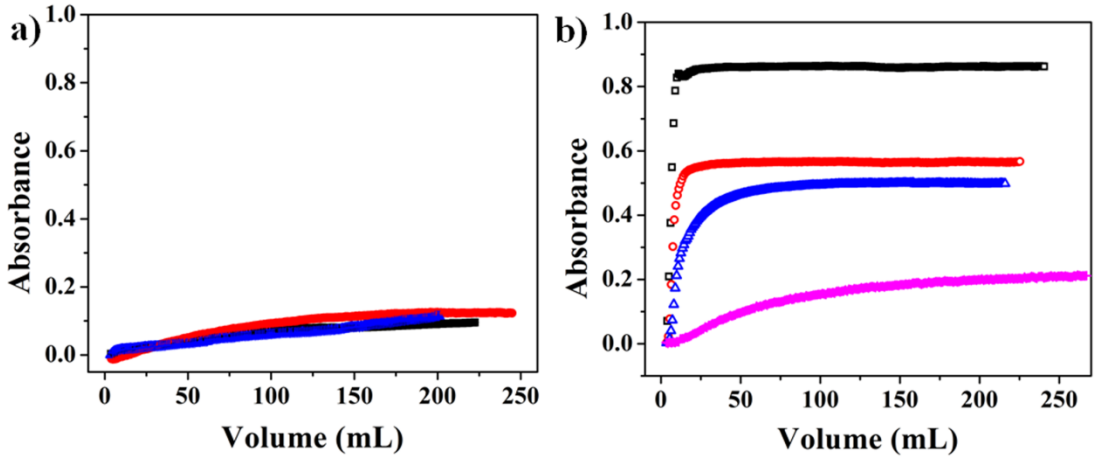

Figure 3-5. Release profiles for the microgel assemblies based devices in (a) pH 6.5 and (b) pH 3.0 solutions. The Au overlayer thicknesses were (■) 50 nm, (○) 200 nm, (Δ) 500 nm, and (+) 700 nm. In all cases, the total release times were 2 h. Since the flow rates were variable from experiment to experiment, the total volumes are slightly different, but allow for direct comparisons of the data with flow rate irrelevant. Reproduced with permission from ref. 299, Copyright 2013, American Chemical Society.

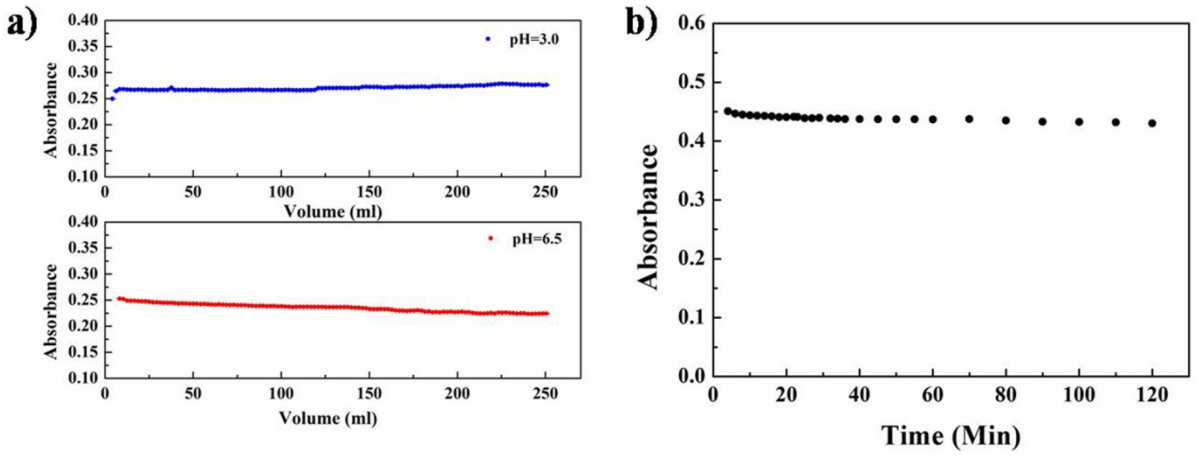

Figure 3-6. Control experiments showing that the ability of CV to absorb light is independent of (left) solution pH, and (right) exposure to ambient light. This was done by monitoring the lambda max for CV as a function of time.

We also point out here that the CV release rates for microgels in the devices are much faster than the same microgels in solution. We hypothesize that this is a result of the microgels being in a monolayer sandwiched between the two Au layers. The sandwiching process results in microgels that are approximately half their solution diameter, hence then have a smaller distance to diffuse into the solution, leading to an increased release rate compared to the larger microgels in solution. We also point out here that the microgels in solution were slightly aggregated after CV addition for microgel loading. This further increase the effective distance CV needs to travel

to get out of the microgels and into the solution. Although, the kinetics are so much different for microgels in devices versus in solution that there must be another process forcing the CV out of the microgel layer of the device. This may be a result of the microgel layer contracting when the solution pH is lowered to pH 3.0 due to the charge neutralization in the microgel layer. It is well known that p(NIPAm-*co*-AAc) microgels contract when AAc is neutralized when going from pH 6.5 to pH 3.0. This contraction could mechanically push the CV out of the microgel layer leading to an increased release rate.

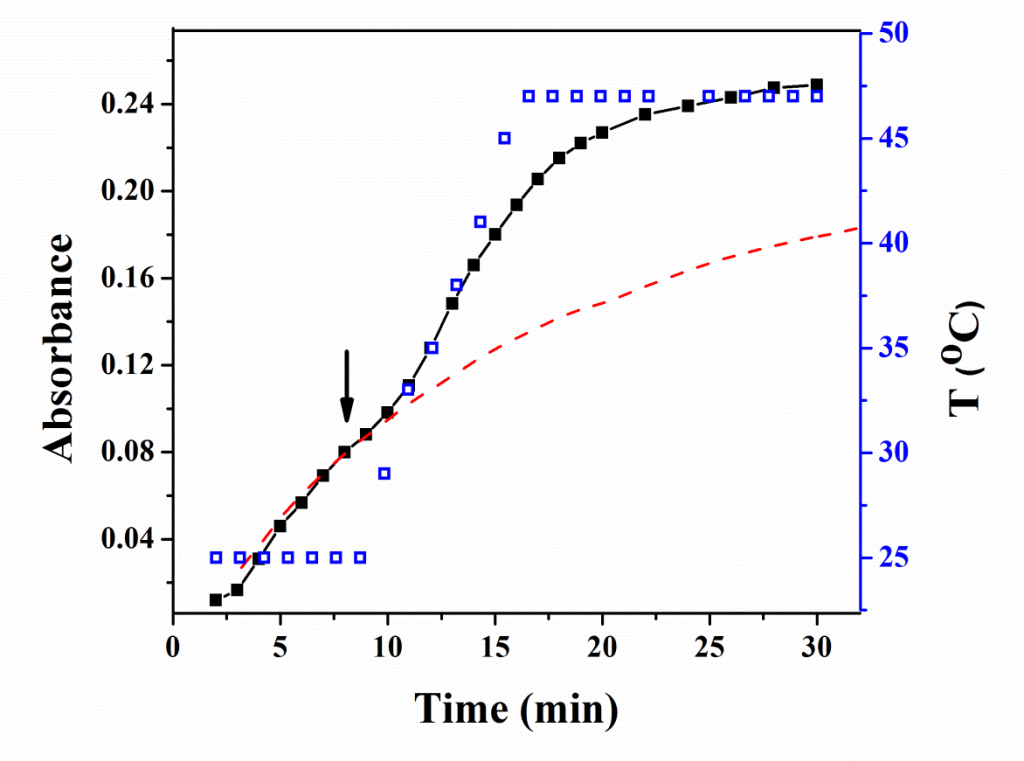

Figure 3-7. CV loaded device with a 700 nm Au overlayer was immersed in pH 3.0 solution at (□) 25 °C while the (■) CV release profile was collected. At 9 min, the solution temperature was increased to ~47 °C while the release profile was continuously monitored. As can be seen, the release rate dramatically increased when the solution temperature reached ~33 °C (>LCST for pNIPAm). The red dashed curve shows the predicted release profile if the solution temperature

was held continuously at 25 °C clearly illustrating the increased release rate. Reproduced with permission from ref. 299, Copyright 2013, American Chemical Society.

It has been clearly demonstrated that the microgel assemblies based device could be used to control the rate of release of a small molecule "drug" to a system. The ability to control the amount of the small molecule released in a given amount of time is also of importance to design on demand drug delivery systems. Figure 3-8 clearly shows that CV can be released from the device on demand, and the release halted by simply changing the pH. To accomplish this, we first immersed the CV-loaded device (500 nm Au overlayer) in pH 6.5 solution and monitored the release for 15 min. Following this period, we lowered the solution to pH 3.0 by adding hydrochloric acid, and after few minutes monitoring, the pH was increased to 6.5 again by adding sodium hydroxide (0.1 M). The solution pH was continuously monitored using a pH meter. This process was repeated, and as can be seen in the figure, the on-off process can be repeated many times.

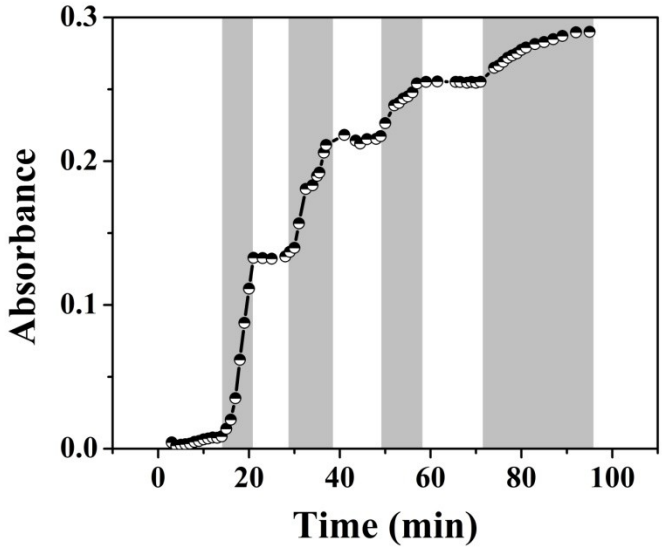

Figure 3-8. pH triggered release profile from an etalon with 500 nm Au overlayer. The dark regions represent where the solution pH was changed to 3.0, while the white regions are where the solution pH was 6.5. As mentioned, the solution pH was varied by adding either HCl or NaOH. Reproduced with permission from ref. 299, Copyright 2013, American Chemical Society.

3.4 Conclusion

In this Chapter, we developed a controlled and triggered drug delivery system utilizing p(NIPAm-*co*-AAc) microgel assemblies based device. The drug release can be triggered by varying the solution pH, with the release rate controlled by the thickness of the Au overlayer covering the microgels. Furthermore, we showed that the model drug could be released in a triggered fashion, turning on and off as a function of solution pH. In future, these devices will be used to release large macromolecular drugs from the confined microgel layers.

Chapter 4: Controlled Release Kinetics from Surface Modified Microgel Assemblies Based Reservoir[c]

In this chapter, surface modification of our previously developed microgel assemblies based devices shows improvement of the controlled release behavior. This study will discuss how the surface modification was done and effect on the releasing rate control experiment. In short, an easy fabricated, efficient and cheap method was developed to control the small molecule release rate by modifying the upper Au layer with a monolayer of silica.

4.1 Introduction

Stimuli-responsive polymer-based materials are often referred as "smart materials" due to their ability to respond to external stimuli, e.g., temperature,[347] pH,[144, 367, 368, 376] light,[349, 377, 378] magnetic field,[350] and electrical field.[14, 353] In the last few decades, functional stimuli-responsive materials such as porous materials,[341, 342, 379] microgels,[338] and nanogels[42, 339] have been used to encapsulate and release small molecules (or drugs) in a controlled and triggered fashion. Among stimuli-responsive polymers, poly (*N*-isopropylacrylamide) (pNIPAm) is by far the most extensively studied to date; a direct result of its thermoresponsive.[18, 39, 42, 170] As we discussed in previous Chapters, pNIPAm exhibits a lower critical solution temperature (LCST) of 32°C in water, which is close to physiological temperature. Above the LCST, pNIPAm undergoes a transition from a random coil (extended state) to a globule (collapsed state), expelling its solvating water in the process.

PNIPAm can be crosslinked into a polymer network, and hydrogel particles (nanogels or microgels, depending on diameter) can be synthesized. These networks also undergo a swollen-

[c] This Chapter has been adapted from the previously published article: S. Guo,[†] Y. Gao,[†] M. Wei, Q. Zhang, M. J. Serpe.* *J. Mater. Chem. B*, 2015, 3, 2516-2521.

to-collapsed transition in water at elevated temperature. Specifically, pNIPAm-based microgels transition from a swollen (large diameter) to a collapsed (small diameter) state at elevated temperature.[40, 380, 381] Like all temperature-induced conformational state changes of pNIPAm, the transition for pNIPAm-based microgels is fully reversible over many cycles. PNIPAm-based microgels can also be made responsive to other stimuli, in addition to temperature. For example, copolymerization of functional monomers or crosslinkers into the pNIPAm network can make them responsive to, e.g., pH, light and/or electric field.[353, 367, 377] A well-known pH-responsive pNIPAm-based microgel is pNIPAm-*co*-acrylic acid (p(NIPAm-*co*-AAc)), which is made by simply adding AAc at the time of synthesis.[144] We have shown that the charge switchability of the p(NIPAm-*co*-AAc) microgels allows oppositely charged molecules to bind and release at pH > pK_a, and pH < pK_a, respectively.[299]

In Chapter 3, we showed that microgel assemblies based devices could be generated by "sandwiching" a homogeneous monolayer of p(NIPAm-*co*-AAc) microgels between two thin Au layers.[40, 130, 144, 155, 156, 161, 171, 299, 374, 375, 382] The structure of this device has shown in Chapter 3. The optical properties of these devices have been studied in great detail, and they have been used for sensing a variety of species.[383, 384] We found that the structure could be used for controlled and triggered drug delivery as described in Chapter 3. Importantly, we determined that the release rate depended greatly on the thickness of the Au layer covering the microgel layer (Au overlayer), which systematically varied the pore size. Therefore, thick Au layers slowed the release properties compared to thin Au layers.[299]

We used Au layer thicknesses of up to 700 nm previously, which increases the device's cost and fabrication time dramatically. Therefore, new ways to control release rates are needed. In this study, we modify the Au overlayer porosity by adding a layer of silica via the hydrolysis

of tetraethyl orthosilicate (TEOS) vapor with water in the presence of ammonia. Using this approach, we were able to decrease the Au overlayer thickness to below 50 nm and subsequently modify the Au layer with silica to control the release rates. By varying the silica layer thickness by varying the modification time, the release rate could be effectively controlled and tuned, i.e., long modification time leads to slow release rates. This low-cost and effective method provides an alternative way to control and trigger drug release by using the microgel-based drug reservoir systems.

4.2 Experimental section

Materials: *N*-isopropylacrylamide (NIPAm) was purchased from TCI (Portland, Oregon) and purified by recrystallization from hexanes (ACS reagent grade, EMD, Gibbstown, NJ) prior to use. *N, N'*-methylenebisacrylamide (BIS) (99 %), acrylic acid (AAc) (99 %), and ammonium persulfate (APS) (98+ %) were obtained from Sigma-Aldrich (St. Louis, MO) and were used as received. Tris (4-(dimethylamino)phenyl)methylium chloride (Crystal Violet, CV) and tetraethyl orthosilicate (TEOS, 98 %) were obtained from Sigma-Aldrich (St. Louis, MO). Sodium chloride was obtained from EMD (Millipore, Billerica, MA), and deionized (DI) water with a resistivity of 18.2 MΩ•cm was used. Cr/Au annealing was done in a Thermolyne muffle furnace from ThermoFisher Scientific (Ottawa, Ontario). Anhydrous ethanol was obtained from Commercial Alcohols (Brampton, Ontario). Sodium hydroxide (NaOH, 99.8 %) and hydrochloric acid were purchased from Caledon Chemicals (Georgetown, Ontario) and were used as received. Fisher's finest glass coverslips were 25 × 25 mm and obtained from Fisher Scientific (Ottawa, Ontario). Cr was 99.999 % and obtained from ESPI as flakes (Ashland, OR), while Au was 99.99 % and obtained from MRCS Canada (Edmonton, AB).

Microgel synthesis: Temperature-ramp, surfactant-free, free radical precipitation polymerization was used to synthesize the microgels here, as previously described.[369] Briefly, a 3-necked round- bottom flask was fitted with a reflux condenser, nitrogen inlet, and temperature probe, and charged with a solution of the monomer mixture, comprised of NIPAm (11.9 mmol) and BIS (0.703 mmol) in 99 mL of deionized water, previously filtered through a 0.2 μm filter. The solution was bubbled with N_2 while stirring and heated to 70 °C over ~1 hour. 99 μL of AAc (1.43 mmol) was added to the heated reaction mixture with a micropipette in one aliquot. The reaction was then initiated with APS solution, prepared by dissolving 0.2 mmol ammonia persulfate in 1mL of deionized water. The reaction was then allowed to proceed at 70 ℃ for 4 hours under a blanket of nitrogen and vigorous stirring. The resulting suspension was allowed to cool overnight while stirring and then filtered through glass wool to remove any large aggregates. About 12 mL of the microgel suspension was then distributed into centrifuge tubes and washed via centrifugation at ~8500 rcf for 45 min to form a pellet at the bottom of centrifuge tubes, followed by removal of the supernatant. And then the pellet of microgel was re-suspended with original volume, 12 mL, of deionized water. This process was repeated to a total of six times to remove any unreacted monomers. The purified microgels were recombined and stored in a brown glass jar.

CV loaded device fabrication: CV loaded devices were fabricated by using a previously reported protocol with slight modification.[40] The process is shown in Figure 4-1. To fabricate the Au coated glass substrates, 2 nm Cr and 15 nm of Au was sequentially thermally evaporated at a rate of 0.2 Å s^{-1}, and 0.1 Å s^{-1}, respectively, (Torr International Inc., thermal evaporation system, Model THEUPG, New Windsor, NY) onto a 25 x 25 mm DI water/ethanol rinsed and N_2 gas dried glass substrate (Fisher's Finest, Ottawa, ON). The Cr/Au coated substrates were annealed

at 250 °C for 3 h (Thermolyne muffle furnace, Ottawa, ON) and cooled down to room temperature prior to microgel film painting. The annealed substrate was washed with deionized water and ethanol followed by drying with N_2 gas. Then a 40 µL aliquot of the concentrated microgels was dispensed onto the substrate and then spread toward each edge using the side of a micropipette tip. The substrate was rotated 90°, and the microgel solution was spread again. The spreading and rotation continued until the microgel solution became too viscous to spread due to drying. The microgel solution was allowed to dry completely on the substrate for 2 h with the hotplate temperature set to 35 °C. After that, the dry film was rinsed copiously with DI water to remove any excess microgels not directly bound to the Au. The microgel painted substrate was then placed into a DI water bath and allowed to incubate overnight on a hot plate set to 30 °C. Following this step, the substrate was again rinsed with DI water to further remove any microgels not bound directly to the Au substrate surface. The samples were then dried with N_2, and soaked in CV solution (4 mg/mL, pH of 6.5) for 5 hours. Then the samples were rinsed with pH 6.5 solution (to maintain the microgel-CV interaction) to remove excess CV, and incubated in pH 6.5 solution for 1 hour followed by drying with N_2 gas. Finally, another 2 nm Cr and 50 nm of Au metal layers were deposited on the microgel layer.

Au overlayer modification: Two 0.5 mL glass vessels were placed inside of a glass Petri dish. 0.4 mL of TEOS and NH_3 (28 % in water) were added separately into each vessel. Another Petri dish, with a CV-loaded device secured inside, was placed on top of the above Petri dish such that the Au overlayer was facing the TEOS/NH_3 vessels. Parafilm used to completely seal the system. The whole apparatus was held at room temperature, for different periods of time, to yield SiO_2 layers with various thicknesses. After silica layer formation, the etalon edges were sealed with clear nail polish, to ensure CV could only exit the microgel layer through the Au/silica overlayer.

CV release experiments: A Petri dish filled with 20 mL of water at pH 3 (ionic strength=2 mM) was placed on a hot plate, and the solution temperature was maintained at 25 ℃. The solution in the Petri dish was stirred continuously at 400 rpm using a magnetic stir bar. A peristaltic pump was used to pump the solution through a quartz cuvette in an Agilent 8453 UV-vis spectrophotometer, equipped with an 89090A temperature controller and Peltier heating device. The absorbance spectrum of the solution was collected every minute. The flow rate of the solution was set to a constant value, 0.042 mL/s (as measured).

4.3 Results and discussion

PNIPAm microgel assemblies based device loaded with the small molecule tris (4-(dimethylamino)phenyl)methylium chloride (Crystal Violet, CV) were generated. The procedure is outlined in Figure 4-1. Briefly, a glass substrate was coated with 2 nm Cr followed by 15 nm Au layer via thermal evaporation. Then p(NIPAm-*co*-AAc) microgels were painted on the Au surface and the excess microgels not directly bound to the Au layer rinsed away with deionized (DI) water. Then, positively charged CV was loaded into the p(NIPAm-*co*-AAc) microgel layer via soaking in a CV solution with a pH 6.5 that renders the microgels negatively charged. This layer was subsequently coated with another layer of Cr and Au, and the "sandwich" structure exposed to TEOS (as described in experimental) for various times. The reaction of TEOS with water to form silica is shown below and has been utilized previously for coating surfaces. [385-387]

$$Si(OCH_2CH_3)_4 + H_2O \xrightarrow{NH_3\ catalyst} (SiO_2)_n + CH_3CH_2OH$$

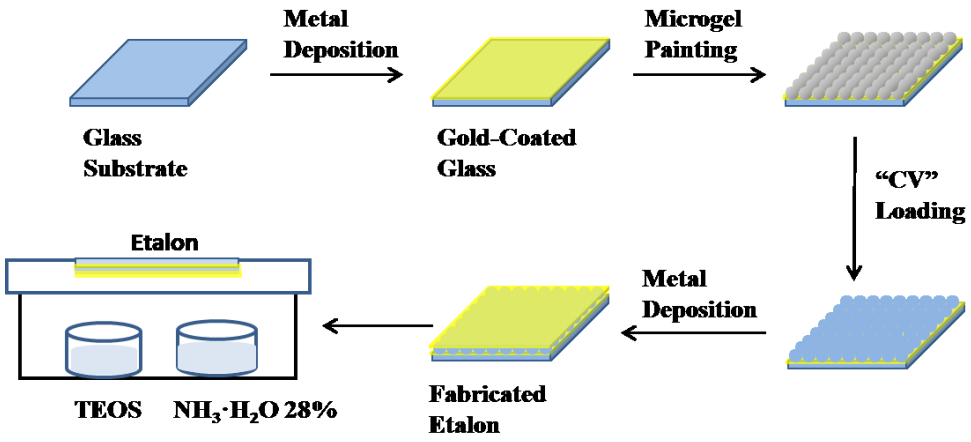

Figure 4-1. Schematic of the fabrication of Silica monolayer modified CV (drug) loaded devices process. Reproduced with permission from ref. 388, Copyright 2015, Royal Society of Chemistry.

A schematic depiction of the silica layer generation is shown in Figure 4-2. We hypothesize that the silica layer covers the surface of the Au overlayer, and fills in the Au overlayer pores to block the path of CV exiting the microgel layer to enter the surrounding solution. As the modification time is increased, the silica layer thickness should likewise increase, and more of the Au pores should be filled. The surface morphology of the resulting devices was investigated using atomic force microscopy (AFM, tapping mode, Asylum Research, Santa Barbara, CA) at room temperature. The images are shown in Figure 4-3. Prior to silica layer formation, the microgel curvature can be clearly seen. From the images, it can be seen that the microgel curvature is obvious before silica layer formation, while the curvature is largely diminished after silica layer formation. From the image, the apparent microgel diameter (diameter that can be measured, not necessarily the absolute diameter) before silica layer deposition was ~500 nm, while it appears to increase to ~700 nm as a result of silica layer deposition. The surface morphology is also clearly affected by the silica layer deposition. These observations allow us to conclude that the silica layers are forming on the Au overlayer.

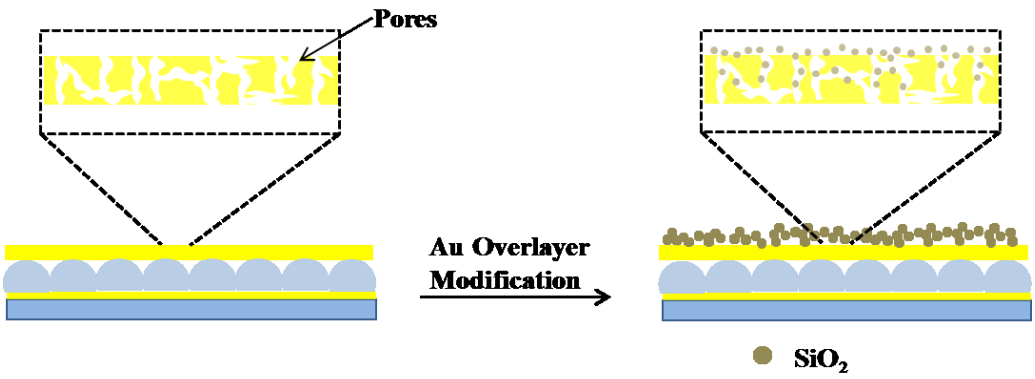

Figure 4-2. Schematic diagram of diffusion paths on thin Au overlayer and mechanism of paths blocked with SiO_2 layer. Reproduced with permission from ref. 388, Copyright 2015, Royal Society of Chemistry.

X-ray photoelectron spectroscopy (XPS) was also used to confirm the elemental composition of the overlayers after silica layer deposition, and how the atomic mole percent of silicon was affected by deposition time. The signal at 104 eV from the XPS spectrum (data not shown) was used to determine the atomic mole percent of Si^{4+}, which is evidence of the oxide state. Figure 4-4 shows that as the silica layer "growth" time increased, the amount of Si^{4+} also increased, with a concomitant decrease in the Au signal due to the silica layer covering it. Secondary ion mass spectrometry (SIMS) was conducted, and the data is shown in Figure 4-5 for the unmodified, 3 hours modified and 9 hours modified samples. The data shows that the Si layer formation is homogeneous on the Au surface. In fact, after 3 h deposition, the surface appears uniformly coated with Si, with little Au detectable over this area. The results after 9 h are similar. These data are consistent with thicker silica layers being deposited on the device's Au overlayer as a function of increasing deposition time.

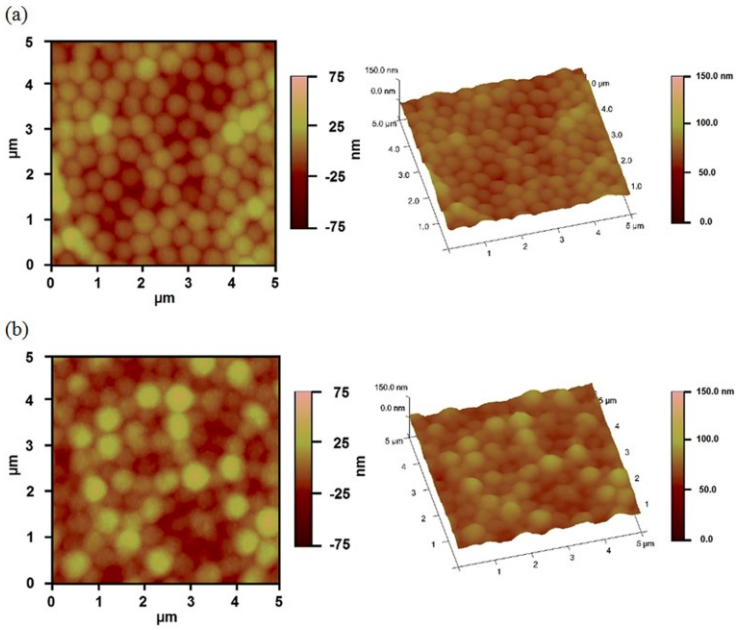

Figure 4-3. AFM images of surface morphology of sample device' upper Au layer before 9-hour treating (a), and after 9-hour treating (b). Reproduced with permission from ref. 388, Copyright 2015, Royal Society of Chemistry.

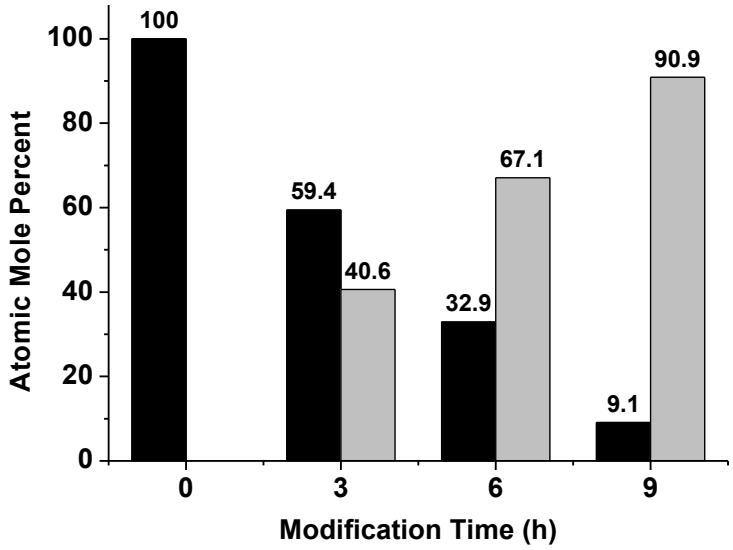

Figure 4-4. Relative atomic mole percentages of Au (Black) and Si (Grey) detected by XPS from upper Au surface of samples with varies of treating periods. Reproduced with permission from ref. 388, Copyright 2015, Royal Society of Chemistry.

Once silica layers could be deposited on the device Au overlayers, the CV release kinetics was investigated. We determined the release kinetics for devices with no silica layer, and devices after 3, 6, and 9 h TEOS exposure. These experiments were completed by adding CV loaded devices to a Petri dish containing 20 mL of pH 3.0 aqueous solutions. This pH neutralizes the microgel AAc groups allowing the CV to exit the devices. The solution from the Petri dish was pumped into a cuvette held in a UV-vis spectrometer, which was set up acquire a spectrum every 1 min for 240 min (4 h).The flow rate of the liquid was fixed at a constant value of 0.042 mL/s. CV, a water-soluble dye, has a maximum absorbance at ~590 nm. Therefore, based on Beers' law, and the constant solution volume, the magnitude of the absorbance at 590 nm is proportional to the amount of CV released. Figure 4-5a shows the full set of release kinetics. As is clearly seen, the release kinetics from the unmodified device is much faster than the modified

devices. The device exposed to TEOS for 9 h clearly has the slowest release kinetics, releasing only half the CV that the unmodified devices do in the given time period.

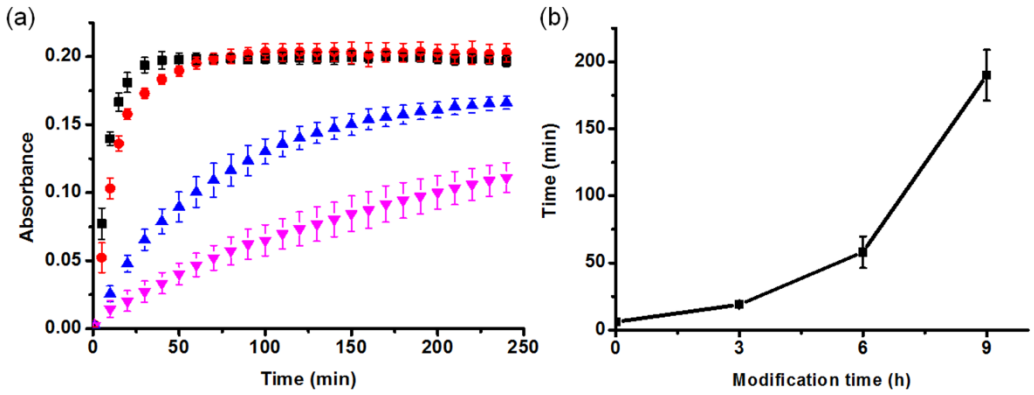

Figure 4-5. (a), Average release profiles for the microgel assemblies based devices in pH 3.0 solution. The modification time periods were (■) 0 hour, (●) 3 hours, (▲) 6 hours, (▼) 9 hours. There are 3 separate samples for each modification time period. And totally 12 samples are measured in experiments. In all cases, the total measuring time periods were 240 min (4h). Data were plotted for 10 minutes interval. (b), Time consumed by etalon devices with varied modification time release 50 % of loaded CV (absorbance 0.095) in pH 3.0 solutions. There are 3 separate samples for each modification time period. And totally 12 samples are measured in experiments. Reproduced with permission from ref. 388, Copyright 2015, Royal Society of Chemistry.

We went on to determine the long-term release characteristics of the devices. The release kinetics of samples modified for 6 and 9 hours were monitored up to 1200 minutes. And the highest value of absorbance was reached by 6-hour samples at around 650 min and by 9-hour samples at around 1000 min. And the final absorption values of solutions for all samples (modified and unmodified) are within the range of 0.185-0.205. By concluding the release kinetics data of all samples, we can find that different samples consume the significant different

amount of time to release 50 % of total amount of loaded CV which corresponding to the absorbance 0.195. (Figure 4-5b).

Based on this result, we can get that the silica monolayer generated by TEOS and ammonia do not have a significant effect on the total amount of CV released. In other words, this approach only slows down the release rate of small molecules but does not block the molecules in microgels forever. Overall, the silica monolayer is highly efficient in controlling the drug release rate and has small side effects on the function of this microgel-based drug delivery device. In future, silica monolayer is potentially able to be modified to adjust its ability and properties on drug delivery controlling and triggering.[389, 390]

4.4 Conclusion

In summary, based on the p(NIPAm-*co*-AAc) microgel-based drug release platform, we developed an easy fabricated, efficient and cheap method to control the small molecules' release rate by modifying the upper Au layer with a monolayer of silica. The silica layer is characterized and was shown to exhibit a dependence of hydrolysis reaction time of TEOS with ammonia. And by using a dye molecular, crystal violet, as a model drug to study the drug release behavior of this reservoir system, the releasing process was completely controllable through various surface morphologies by changing the modification time. Finally, the long-term efficiency of this drug delivery system shows the promise to be developed in medical science.

Chapter 5: Sequential and Controlled Release of Small Molecules from Poly (*N*-isopropylacrylamide) Microgel Assemblies Based Reservoir Devices[d]

In this chapter, we evaluated the sequential and controlled release of multi-drugs from our microgel assemblies based devices. Two different microgels are used for constructing the devices and drugs are easy to be loaded into the microgels separately. These systems represent a versatile approach to sequentially delivering small molecules, in a triggered fashion, with tunable release kinetics. With tuning the chemistry of microgels, it is able to further expand the multi-drugs release concept in future.

5.1 Introduction

Controlled and triggered drug delivery systems have played a major role in improved disease treatment over the past few decades.[222, 391-395] This is in part due to their ability to render otherwise toxic drug treatments relatively non-toxic by controlling dosages through controlled release rates. Most materials to date have been engineered to deliver a single small molecule drug to a system, and many are commercially available, such as the Cypher® stent from Johnson & Johnson, and the Taxus® stent from Boston Scientific. These and similar devices can be generated by mixing drug molecules with degradable polymers, which degrade under certain conditions to release a small molecule at a given rate. While these materials have certainly enhanced human health, many medical conditions are controlled by multiple biomolecules. Therefore, comprehensive treatment of certain diseases and conditions may be more effectively achieved by delivering more than one drug at a time to a system. Recently, the concept of multi-drug therapy was introduced[396-399] and systems that deliver multiple small molecules at the same

[d] This Chapter has been adapted from the previously published article: Y. Gao, K. Wong, A. Ahiabu, M. J. Serpe.* *J. Mater. Chem. B*, 2016, 4, 5144-5150.

time (co-delivery)[400] or sequentially[401] have been developed. For example, CombiPatch®, a transdermal patch marketed by Novogyne Pharmaceuticals, is a drug delivery system that can release both estradiol (an estrogen) and norethindrone acetate (a progestin) continuously upon application to the skin and delivers the medication in a steady and predictable manner for hormone replacement therapy. Similar approaches to drug delivery may provide great improvements to achieve enhanced therapies.

To yield enhanced delivery systems, various materials have been utilized, such as inorganic nanomaterials,[402] polymers,[222, 223, 403, 404] and biomacromolecules.[405-407] Among these, polymers have played an integral role in advanced drug delivery technologies, allowing both hydrophilic and hydrophobic drugs to be released at constant (or variable) rates over long periods of time. One approach utilized small molecule "drug" loaded polymer-based "reservoirs", which allowed for diffusion controlled drug release.[3,408] Another approach relied on covalently[409, 410] or non-covalently bonding[411] drug molecules onto/into a carrier; the bond between the drug and the carrier can be broken at certain environmental conditions,[226] e.g., in the presence of an enzyme,[412] and/or at certain pH values.[413]

Responsive polymers have also found their way into many drug delivery systems, with poly (*N*-isopropylacrylamide) (pNIPAm) being the most utilized to date.[18, 42, 170, 362] PNIPAm is well known to be thermoresponsive.[363, 364] Like linear pNIPAm, pNIPAm-based hydrogel particles (microgels) have also been synthesized as we introduced previously. PNIPAm-based micro and nanogels are most easily synthesized via free radical precipitation polymerization.[39, 365, 414, 415] This approach is versatile in terms of the variety of chemical functionality that can be added to the microgels by simply adding functional monomers to the reaction prior to the initiation. Using this approach, pNIPAm-based microgels with a variety of chemical

functionalities have been synthesized. The most commonly used comonomer is acrylic acid (AAc), which renders p(NIPAm-*co*-AAc) microgel pH-responsive.[144, 276, 368] AAc can also be used to couple other small molecules to the microgels by various coupling chemistries. The pH responsivity of the p(NIPAm-*co*-AAc) microgels is a direct result of the weak acidity of the AAc group and we have applied this pH responsivity into our microgels system as illustrated in Chapter 3. Similarly, other weak acid/base modified microgels can be synthesized, e.g., in this work, we generated boronic acid modified microgels by copolymerization of 3-(acrylamido) phenylboronic acid (APBA) into the microgels.[170, 171, 416, 417] APBA exhibits a pK_a of ~8.4 and is therefore negatively charged at pH > 8.4, while APBA is neutral at pH < 8.4. Like AAc-modified microgels, the APBA-modified microgels exhibit attractive interactions with positively charged species at high pH, while they are neutralized, and have minimal interactions with positively charged species at lower pH (< 8.4).

PNIPAm has found its way into controlled/triggered drug delivery devices mainly due to its above-described thermoresponsive, which occurs close to body temperature[117, 226, 228, 418] Recently, our group developed a pNIPAm microgel-based optical device (etalon) that we demonstrated to be very useful for sensing and biosensing.[40, 144, 160, 375, 419-421] We also showed that this device structure could be used as a "reservoir" for small molecules, allowing controlled and triggered release of the small molecules to a system.[298, 299, 384] Specifically, by localizing a small molecule into the microgel layer, we showed that the thickness of the Au layer covering the microgels (overlayer) allowed control over release rates; this due to the tunability of the Au pore size with its thickness.[40, 299] That is, thick Au has fewer and smaller pores than thin Au, which allows small molecules to exit the microgel layer either slow or fast, respectively.[299]

In the present study, we combined the ability to control the release rate of small molecules from our reservoir devices with the ability to tailor microgel chemistry to produce a system capable of delivering small molecules only at a specific solution pH and at controlled rates. This was accomplished by constructing reservoir devices from p(NIPAm-*co*-AAc) and p(NIPAm-*co*-APBA) microgels, which respond to pH by ionizing over drastically different ranges; the ionization (and neutralization) is what allows small molecules to be released only at drastically different solution pHs. We believe that these systems can provide more options for sequential and controlled drug release or multi-drug delivery approaches to therapy.

5.2 Experimental section

Materials: *N*-isopropylacrylamide (NIPAm) was purchased from TCI (Portland, Oregon) and purified by recrystallization from hexanes (ACS reagent grade, EMD, Gibbstown, NJ) prior to use. *N, N'*-methylenebisacrylamide (BIS) (99 %), acrylic acid (AAc) (99 %), 3-(Acrylamido) phenylboronic acid (APBA) and ammonium persulfate (APS) (98+ %) were obtained from Aldrich (St. Louis, MO) and were used as received. Sodium chloride was obtained from EMD (Millipore, Billerica, MA), and deionized (DI) water with a resistivity of 18.2 MΩ·cm was used. Cr/Au annealing was done in a Thermolyne muffle furnace from ThermoFisher Scientific (Ottawa, Ontario). Anhydrous ethanol was obtained from Commercial Alcohols (Brampton, Ontario). Sodium hydroxide (NaOH, 99.8 %) and hydrochloric acid were purchased from Caledon Chemicals (Georgetown, Ontario) and were used as received. Fisher's finest glass coverslips were 25 × 25 mm and obtained from Fisher Scientific (Ottawa, Ontario). Cr was 99.999 % and obtained from ESPI as flakes (Ashland, OR), while Au was 99.99 % and obtained from MRCS Canada (Edmonton, AB). Methylene blue was obtained from Sigma-Aldrich.

Microgel synthesis: Microgels composed of poly (*N*-isopropylacrylamide)-*co*-acrylic acid (p(NIPAm-*co*-AAc)) were synthesized via free radical precipitation polymerization as described previously.[48] Briefly, a 3-necked round bottom flask was fitted with a reflux condenser, nitrogen inlet, and temperature probe, and charged with a solution of NIPAm (11.9 mmol) and BIS (0.703 mmol) in 99 mL deionized water, previously filtered through a 0.2 μm filter. The solution was bubbled with N_2 gas and allowed to heat to 70 °C over ~1 hour. AAc (1.43 mmol) was added to the heated reaction mixture in one aliquot. The reaction was then initiated with a solution of APS (0.2 mmol) in 1 mL of deionized water. The reaction was allowed to proceed at 70 °C for 4 hours under a blanket of nitrogen. The resulting suspension was allowed to cool overnight, and then it was filtered through a Whatman #1 paper filter to remove any large aggregates. The microgel solution was then distributed into centrifuge tubes and purified via centrifugation at ~8300 rcf to form a pellet, followed by removal of the supernatant and resuspension with deionized water, 6x. The cleaned microgels were recombined and stored in a brown glass jar. Poly (N-isopropylacrlamide-3-(acrylamido) phenylboronic acid) (p(NIPAm-*co*-APBA)) microgels were synthesized in the same manner but replacing the AAc with APBA.

Loading MB into microgels: 250 μL of highly concentrated p(NIPAm-*co*-AAc) microgels, 250 μL of highly concentrated p(NIPAm-*co*-APBA) microgels, and 200 μL of aqueous MB solution (0.5 mg/mL) was added into 10.0 mL pH 10.0 solution (in a centrifuge tube), vortexed for 30 s and soaked for 3h. The solution was then centrifuged for 1 h at 10000 rpm, the supernatant solution containing the unbound MB was removed, and the microgels resuspended at the bottom in pH 10.0 solution. This pH allowed the unbound MB to be separated from the MB loaded microgels. This process of centrifugation and resuspension was repeated 3 times.

MB release from mixed microgels in solution: 25 μL of dye loaded mixed microgel solution was added to centrifuge tubes containing solutions with pH 2.0, 3.0, 4.0, 5.0, 6.0, 7.0, 8.0, 9.0, 10.0. The microgels were left exposed to these solutions for 3 h then centrifuged for 1 h at 10000 rpm. We also prepared mixed microgel solutions to investigate the kinetics of MB release from the microgels in solution. This was done by mixing 200 μL of each drug-loaded microgels into 10.0 mL pH 10.0 solution, incubating for some time, then centrifuging to isolate the microgels from the supernatant solution. 1 mL of the supernatant solution was analyzed each time, which was completely returned back to the original solution in the centrifuge tube. The process was repeated many times, and the solution pH was varied by adding 1.0 M HCl. The absorbance value at 664 nm (λ_{max} for MB) was collected from a UV-vis spectrum obtained with an Agilent 8453 UV-vis spectrophotometer, equipped with an 89090A temperature controller and Peltier heating device.

Microgel assemblies based reservoir device fabrication: 2 nm Cr followed by 15 nm of Au was deposited via thermal evaporated (Torr International Inc., thermal evaporation system, Model THEUPG, New Windsor, NY) onto a 25 x 25 mm ethanol rinsed and N_2 gas dried glass coverslip (Fisher's Finest, Ottawa, ON) at a rate of 0.2 Å s^{-1}, and 0.1 Å s^{-1}, respectively. The Cr/Au substrates were annealed at 250 °C for 3 h (Thermolyne muffle furnace, Ottawa, ON) and cooled to room temperature prior to microgel film deposition. Approximately 10 mL of microgel solution was centrifuged at ~8300 rcf to form a pellet at the bottom of a centrifuge tube. The supernatant was removed and discarded, and the pellet was vortexed to loosen and homogenize the particles in the remaining solvent. A 40 μL aliquot of the concentrated microgels was added onto the substrate and then spread toward each edge using the side of a micropipette tip. The substrate was rotated 90°, and the microgel solution was spread again. The spreading and

rotation continued until the microgel solution became too viscous to spread due to drying. The microgel solution was allowed to dry completely on the substrate for 2h with the hotplate temperature set to 35 °C. The dry film was then rinsed copiously with DI water to remove any excess microgels not bound directly to the Au. The film was then placed into a DI water bath and allowed to incubate overnight on a hot plate set to ~30 °C. Following this step, the samples were then rinsed with deionized water, dried with N_2, and then immersed into a 20 mL solution of MB (0.5 mg/mL, pH of 10.0) overnight. Excess MB was rinsed off the substrate with pH 10.0 solution (to not disturb the microgel-MB interaction) and incubated in pH 10.0 solution overnight followed by drying with N_2 gas. Another Au overlayer (2 nm Cr and 50 nm Au) was evaporated onto the MB loaded microgel layer. Since we were interested in understanding how the Au overlayer affected the rate of MB release from the etalon, we sealed the etalon's edges with clear nail polish to ensure that the MB was being released through the Au overlayer. Previous studies have confirmed that this is effective at preventing small molecules from releasing from the sides of the reservoir devices.[48] To fabricate devices with different ratios of microgels, we followed the same procedure as above, with slight modification. Briefly, to generate the 4:1 samples, we coated 80 % of the substrate with pAPBA-MG and 20 % with pAAc-MG. For the 1:1 samples, half of the substrate was coated with pAPBA-MG and the other half coated with pAAc-MG.

For loading MB and CV into pAPBA-MG and pAAc-MG, respectively, we exposed the portion of the substrate coated with pAPBA-MG to the MB solution (0.5 mg/mL, pH 10.0) and the portion coated with pAAc-MG to the CV solution (0.5 mg/mL in pH 7.0). After 3 h, the excess solutions were rinsed off the surfaces with pH 10.0 and pH 7.0 solutions, respectively.

The microgels were then coated with a given thickness of Au and the edges sealed to prevent the release from the side of the device.

MB release from reservoir devices: A Petri dish containing 20 mL of pH 10.0 solution was placed on a hot plate, and the solution temperature maintained at 25 ^{o}C. The solution in the Petri dish was stirred continuously at 260 RPM using a magnetic stir bar. The solution flowed through a cuvette (via a peristaltic pump) in an Agilent 8453 UV-vis spectrophotometer, equipped with an 89090A temperature controller and Peltier heating device. MB loaded etalons were added to the Petri dish, and a timer started. The absorbance spectrum of the solution was collected every 60 s and the solution pH adjusted by adding 0.1 M HCl.

5.3 Results and discussion

A schematic of the drug loading mechanism is shown in Figure 5-1. The model drug used in this study was methylene blue (MB). As the structure shows, MB is a positively charged molecule, which can interact strongly with negatively charged moieties. In this study, two sets of microgels were synthesized, p(NIPAm-*co*-AAc) (pAAc-MG) and p(NIPAm-*co*-APBA) (pAPBA-MG), which are both pH-responsive, The pH responsivity of the APBA-containing and AAc-containing microgels is shown in Figure 5-2. Specifically, these groups are negatively charged at pH > 4.25 and 8.4, respectively, but are neutral at pHs below these respective pH values. The microgels were loaded with MB by exposing them to solutions at pH 10.0, which was high enough to render both sets of microgels negatively charged, while the MB remained positively charged. This allowed the MB to be absorbed by the microgels via electrostatic interactions. After loading, and washing away the excess MB with pH 10.0 solution, the microgels exhibited a blue color; this confirmed that the MB was loaded into the microgel.

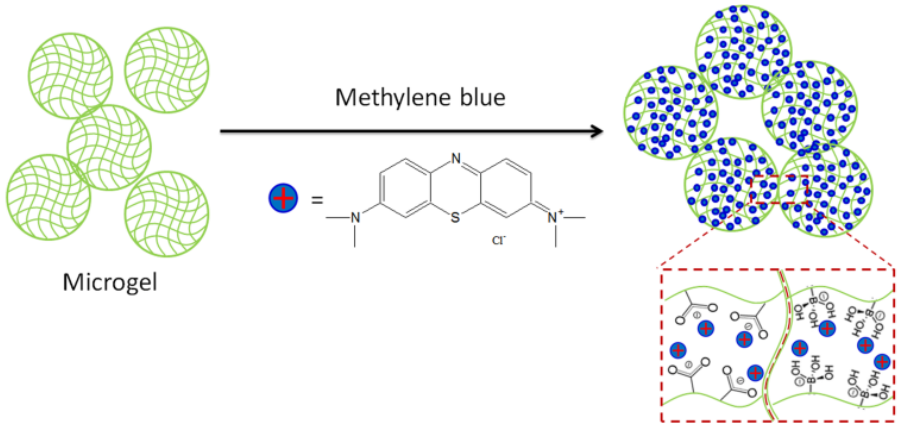

Figure 5-1. Positively charged methylene blue was used as a model drug molecule that can be loaded into pAAc-MG and pAPBA-MG at solution pH that renders them negatively charged. Reproduced with permission from ref. 159, Copyright 2016, Royal Society of Chemistry.

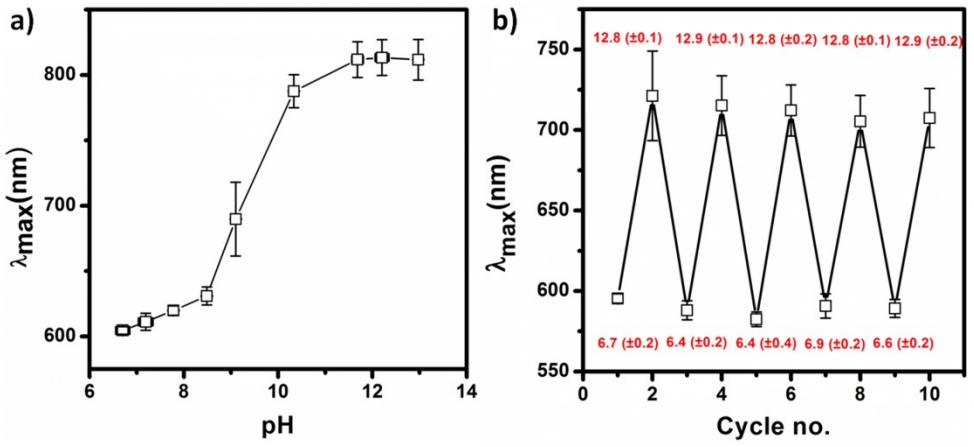

Figure 5-2. pH responsivity testing from pAPBA-MG. a) pAPBA-MG Peak shifting when changing pH for pAPBA-MG based etalon device. b) Continually change the pH to evaluate the reversible pH-responsive properties. Plots were done by averaging data from three individual sample tests.

After MB was loaded into the microgels, we investigated their ability to release MB in a pH-triggered fashion. Specifically, when the solution pH is > 8.4, both the pAPBA-MG and pAAc-MG will be negatively charged and bind the MB strongly. When the solution pH is

decreased below the pK_a for APBA, MB will be released from pAPBA-MG, while MB will still be bound to the pAAc-MG. MB will then be released from the pAAc-MG when the solution pH is below the AAc pK_a. The hypothesized mechanism is shown schematically in Figure 5-3.

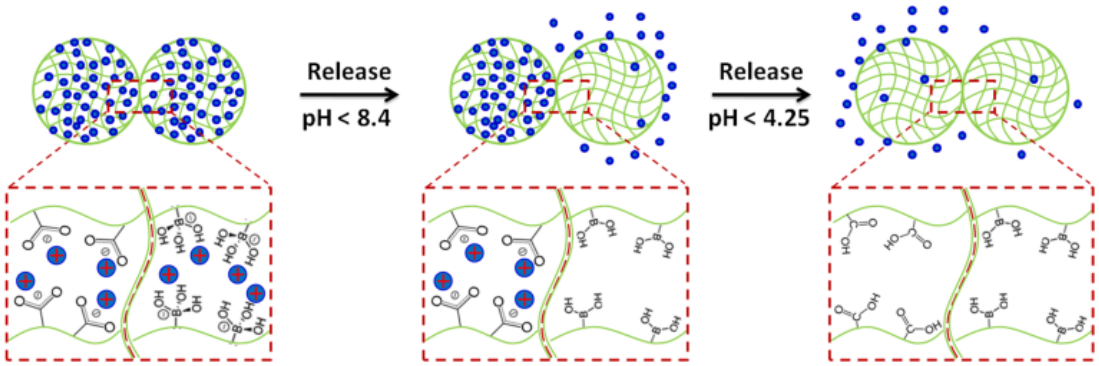

Figure 5-3. The pH-triggered MB release mechanism from pAPBA-MG and pAAc-MG. As each microgel is neutralized, the electrostatic interactions between the microgel and the MB are diminished, and the MB is released from the microgel. Reproduced with permission from ref. 159, Copyright 2016, Royal Society of Chemistry.

To test this hypothesis, we first investigated the pH-dependent release properties for the microgels in solution. To accomplish this, we first mixed 250 µL of pAAc-MG, 250 µL of pAPBA-MG, and 200 µL MB (0.5 mg/mL) and diluted into 10.0 mL pH 10.0 solution. This mixture was incubated for 3 h to load the MB into the microgels. The unbound MB was removed from the MB loaded microgels by multiple centrifugation/resuspension cycles, as detailed in the Experimental section. Then, 25 µL of the mixed concentrated microgel solution was exposed to various pH solutions to characterize their release behavior. Specifically, the microgels were incubated at each specific pH for 3 h (sufficient time for MB to diffuse out of microgels), then the microgels were centrifuged and the UV-vis spectrum of the supernatant solution was acquired. The absorbance value at 664 nm was then plotted as a function of solution pH. As can be seen in Figure 5-4, when the solution pH was 10.0, only a small amount of MB was released

from the microgels. At pH 10.0 to 7.0, there was a dramatic release of MB due to the neutralization of the APBA groups. At pH 7.0 to 5.0, there was minimal MB release, while another dramatic release event was observed when the solution pH was decreased to 4.0, which corresponds with the pAAc-MB interaction weakening due to AAc neutralization. Finally, at pH 4.0 to 2.0, all the MB was released, and the solution concentration of MB was stable. This result shows that sequential delivery of a small molecule from microgels is possible.

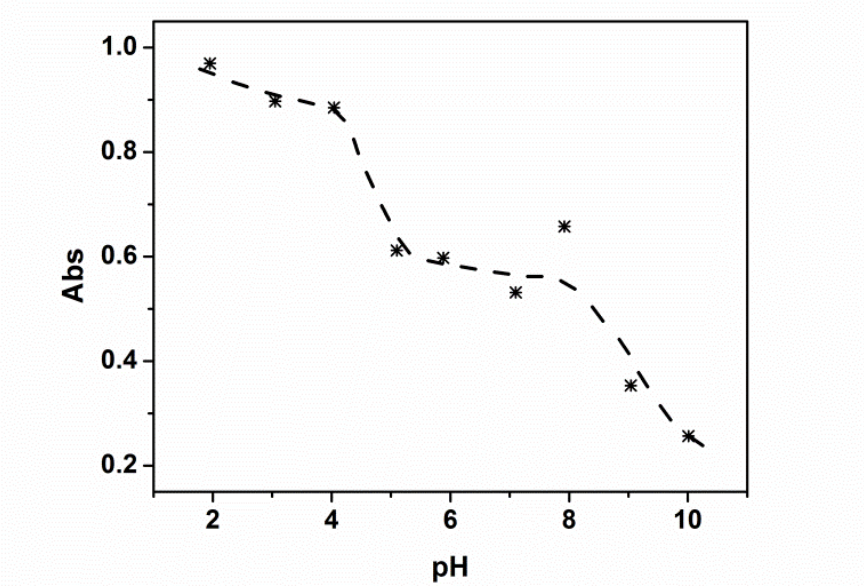

Figure 5-4. The maximum absorbance at 664 nm (max for MB) obtained from a UV-Vis of the supernatant solutions at each of the indicated solution pHs. In this case, the microgels were dispersed in solution at the indicated pH. Reproduced with permission from ref. 159, Copyright 2016, Royal Society of Chemistry.

Next, we wanted to demonstrate that the release rate of the MB could be controlled using microgel-based reservoir devices. The devices were constructed by "painting" the mixed microgels (mixed at a ratio of 1:1 (v/v) prior to painting) onto an Au-coated glass slide, following previously published protocols.[155] It is important to note that the microgels were first painted on the Au-coated glass slide, and then loaded with MB by soaking in an MB solution at

pH 10.0. Following MB loading, 50 nm of Au was deposited on the top of the microgel layer via thermal evaporation. Finally, the edges were sealed with clear nail polish to prevent MB release from the sides of the device.[299] The devices were soaked in a pH 10.0 solution, and the solution pH was systematically decreased. The release profiles for the devices at 37 ^{o}C and 25 ^{o}C are shown in Figure 5-5. As can be seen in Figure 5-5a (37 ^{o}C), the signal was stable until the solution pH was adjusted to 7.0 by addition of 0.1 M HCl. At this pH, the APBA microgels were neutralized, which caused them to release their loaded MB. After ~14 min, the solution absorbance stabilized, and then the solution pH was further decreased to 3.0. At this point, we observed another dramatic increase MB concentration in solution due to the AAc neutralization and their MB release. After some time (~25 min), the MB concentration in solution was stable due to the device being completely depleted of MB to release. The release behavior at 25 ^{o}C is shown in Figure 5-5b, and as can be seen, there is no considerable difference from the devices at 37 ^{o}C. We note that there is a significant initial increase of MB concentration in solution likely due to nonspecifically absorbed MB on the device becoming desorbed, which wasn't present on the other device at 37 ^{o}C. For comparison, we investigated the pH dependent MB release profile for the mixed microgels (1:1 (v/v)) in solution. This was done by mixing 200 μL of each of the drug-loaded microgels into 10.0 mL pH 10.0 solutions in a centrifuge tube. After soaking for 3 h, the whole sample was centrifuged to cause the microgels to be forced to the bottom of the centrifuge tube, and 1 mL of the supernatant solution was analyzed via UV-vis spectroscopy. The supernatant solution was returned to the original centrifuge tube and the solution was mixed and left to incubate for more time. As certain points, the solution pH was changed to pH 7.0 and 3.0, and the data can be seen in Figure 5-6. Compared to the microgel-based reservoir device, the free microgels release much more slowly and take much longer to completely release the MB.

Specifically, the release triggered from the first step takes ~4 h to stabilize, but the second pH-triggered release continues for days.

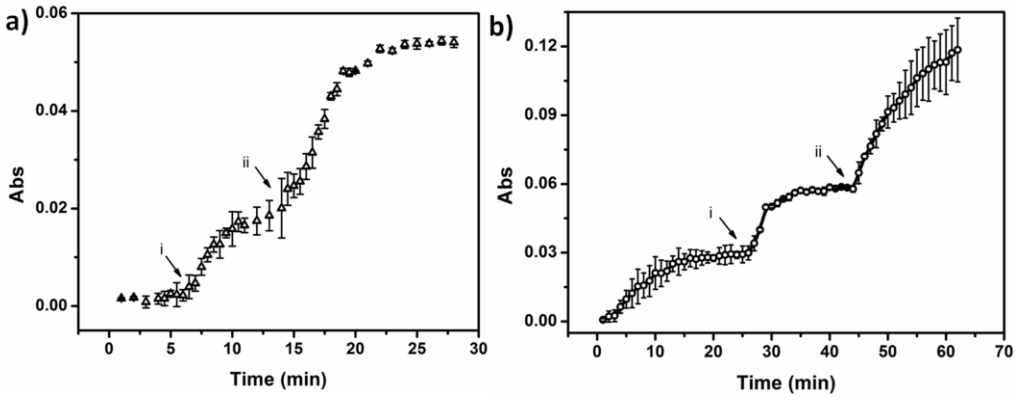

Figure 5-5. The maximum absorbance at 664 nm (λmax for MB) obtained from a UV-vis of the solution in a Petri dish containing a reservoir device with 1:1 pAPBA-MG and pAAc-MG and 50 nm Au overlayer at 37 ^{o}C (a) and 25 ^{o}C (b). The solution pH was changed from 10.0 to (arrow i) 7.0 and (arrow ii) 3.0. Each data point is an average value obtained from the analysis of two separate reservoir devices, with the error bars indicating the standard deviation. Reproduced with permission from ref. 159, Copyright 2016, Royal Society of Chemistry.

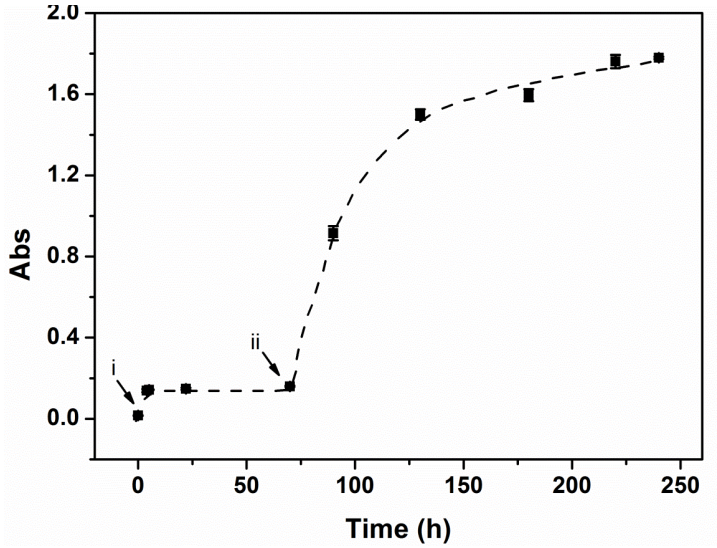

Figure 5-6. MB release from a solution composed of 1:1 (v/v) pAPBA-MG: pAAc-MG. The solution pH was changed from 10.0 to (arrow i) 7.0 and (arrow ii) 3.0.

To further prove that the release rate from the reservoir devices can be tuned by varying the thickness of the reservoir device's Au overlayer, we prepared samples with two different Au overlayer thicknesses, 50 nm, and 230 nm. To make the devices here, the painting procedure was varied slightly compared to what is described above. Specifically, to achieve the desired 1:1 ratio of pAPBA-MG : pAAc-MG, half of each substrate was painted with pAPBA-MG, and the other half was painted with pAAc-MG. This was done to offer more control over the microgel ratios in the reservoir devices. That is, the nature of the painting procedure produces "monolithic" monolayers of microgels on the Au coated surfaces. This ensures that each half of the surface is completely covered with a similar amount of the respective polymers. This is not something that can be said for painting the mixed microgel solutions. Regardless, the release profiles are shown in Figure 5-7. As can be seen, the device composed of a thin Au layer releases MB significantly faster than the devices composed of a relatively thick Au layer. This is due to the smaller pores of the thick Au overlayers restricting access of the MB to the bulk solution; thin Au has many

pores, which isn't as effective at restricting access of the MB to the solution as the thick Au.[48] We point out that the release profile for the devices made for this experiment is similar to what was observed in Figure 5-5 (painting the mixed microgels), which proves that the painting protocol used to make these devices doesn't greatly alter the observed release behavior.

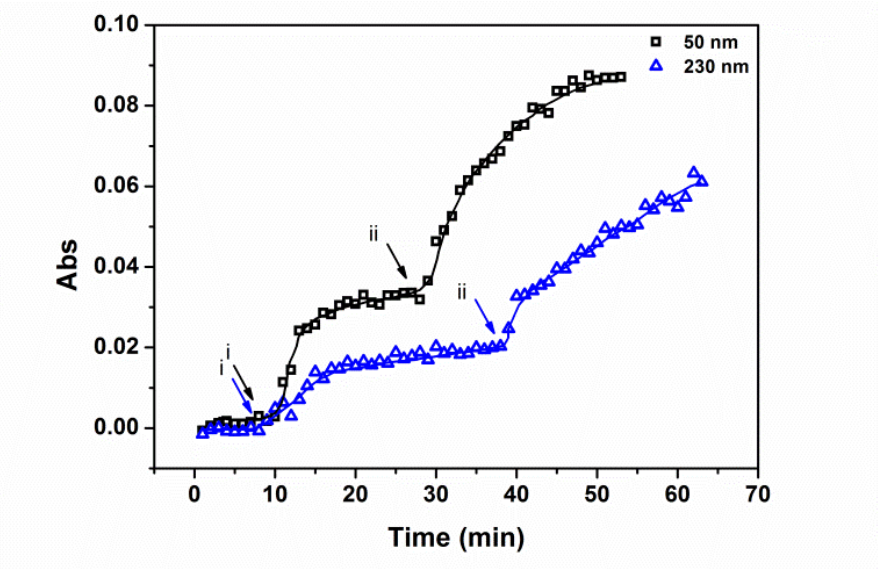

Figure 5-7. The maximum absorbance at 664 nm obtained from a UV-Vis of the solution in a Petri dish containing a reservoir device with 1:1 pAPBA-MG and pAAc-MG with an Au overlayer thickness of (□) 50 nm and (Δ) 230 nm. The solution pH was changed from 10.0 to (arrow i) 7.0 and (arrow ii) 3.0. Reproduced with permission from ref. 159, Copyright 2016, Royal Society of Chemistry.

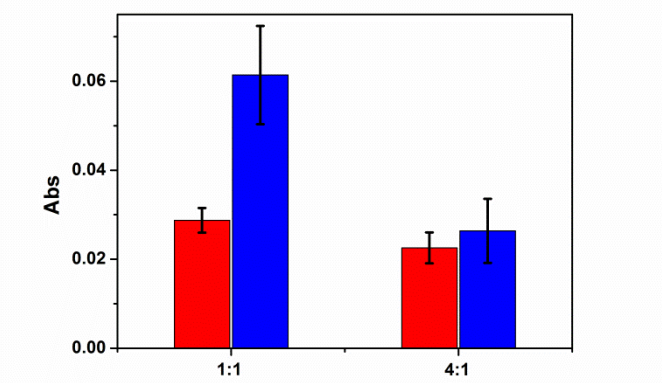

Figure 5-8. The absorbance values for the two separate pH-triggered releases observed for reservoir devices containing 1:1 and 4:1 pAPBA-MG: pAAc-MG. The red bars are the pAPBA-MG and the blue bars are the pAAc-MG. The values are an average of two separate measurements, and the error bars indicate the standard deviation. Reproduced with permission from ref. 159, Copyright 2016, Royal Society of Chemistry.

We point out that for all the experiments above, the ratio of pAPBA-MG : pAAc-MG was 1:1. As can be seen from the data, the amount of MB released as a result of the solution pH changes is not the same when stepping from pH 10.0 to 7.0 and from pH 7.0 to 3.0. This suggests that the pAPBA-MG and pAAc-MG have different capacities for releasing MB. This could be a result of the different microgel chemistries, which can influence their interactions with MB. This could also be a result of a mismatch in the number of each ionizable group in the respective microgels of the reservoir devices. Understanding this behavior would require more experimentation, which will be the subject of another investigation. For this investigation, we wanted to show that we could control the amount of MB released at the different pHs. In that case, we prepared reservoir devices by painting surface with 4:1 pAPBA-MG : pAAc-MG and 1:1 pAPBA-MG : pAAc-MG. The microgels were loaded with MB, and we investigated the pH-triggered release by UV-vis. The results can be seen in Figure 5-8. As can be seen, when the

ratio was 1:1, ~30 % of the release was from the pAPBA-MG (the pH 10.0 to 7.0 change) and ~70 % was from the pAAc-MG (pH 7.0 to 3.0 change). However, when the ratio was 4:1, the release from each of the microgels was approximately equal. This represents a very powerful yet simple approach to precisely control a number of small molecules delivered to a system. For example, an array of reservoir devices can be fabricated on a single substrate, each containing different ratios of microgels, which will allow one to rationally design the specific release characteristics. Furthermore, this can be combined with the tunable release kinetics (by changing the Au overlayer thickness) to provide even more control over small molecule doses.

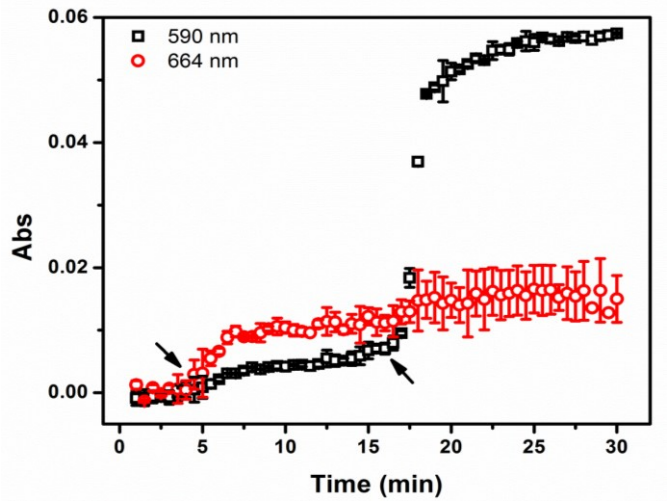

Figure 5-9. The release profile for a device made of pAPBA-MG and pAAc-MG loaded with MB and CV, respectively. The arrow at ~4 min shows the time the solution pH was adjuted to 7.0, while the arrow at ~17 min indicates when the solution pH was decreased to 3.0. The data points are averages obtained from two separate devices, and the error bars indicate the standard deviation. Reproduced with permission from ref. 159, Copyright 2016, Royal Society of Chemistry.

Finally, we determined the ability of the devices to release more than one small molecule when triggered by pH. For these experiments, MB and Crystal violet (CV), were used and were

separately loaded into pAPBA-MGs and pAAc-MGs. The release profile from these devices can be seen in Figure 5-9. As can be seen, when the solution pH was decreased to 7.0 at ~ 4 min, MB that was loaded in the APBA-MG was released. However, the CV in AAc-MG was not released until the solution pH was adjusted to 3.0. We point out that there was some overlap in the absorbance spectra for MB and CV, and therefore there was an increase in the CV signal (590 nm) when the MB was triggered to release, and vice versa. While this is the case, there may be some MB and CV released nonspecifically from the respective microgels. Regardless, the results suggest that the devices could be used to sequentially release small molecules to a system in a pH-dependent fashion.

5.4 Conclusion

In summary, we showed that microgel assemblies based reservoir devices could be fabricated from mixed microgels, specifically pAPBA-MG and pAAc-MG. We went on to show that these microgels could load positively charged MB, which could be released sequentially to a system, in a pH-dependent fashion. That is, when the solution pH was 10.0, both microgels were negatively charged and bound the MB strongly. When the solution pH was decreased to 7.0, the pAPBA-MG was neutralized and released MB; the pAAc-MG was neutralized and released its MB when the pH was decreased to pH 3.0. The data obtained from the reservoir devices was compared to microgels in solution, which exhibited much slower release kinetics. We also showed that the release kinetics from the reservoir devices could be tuned by varying the Au overlayer thickness. Additionally, we showed that the amount of MB delivered to a system as a result of the pH changes could be tuned by changing the ratio of the pAPBA-MG and pAAc-MG in the reservoir devices. Finally, we demonstrated that two different small molecules could be delivered to a system when triggered at specific pHs, e.g., pH 7.0 and 3.0. These systems

represent a versatile approach to sequentially delivering small molecules to a system, in a triggered fashion, with tunable release kinetics. Importantly, their release behavior can be easily tuned by simply changing the microgel chemistry, e.g., by generating reservoir devices from microgels that ionize at different solution pH. This would allow one to deliver various small molecules to a system triggered by a variety of solution pHs. This, combined with the tunable release kinetics and the ability to array these devices on a single substrate, makes this delivery platform extremely versatile, powerful, and unique.

Chapter 6: Free-Standing Poly (*N*-isopropylacrylamide) Microgel Assemblies[e]

In this chapter, a method was developed to remove the microgel assemblies on a glass substrate to generate free-standing device. We compared the properties of this device before and after separated from the substrate in different aspects. The advantages of this approach not only shows that the microgel assemblies based film could be completely released from the substrate but also gives the opportunity to transfer the film to different materials, which dramatically broaden the application of this device.

6.1 Introduction

Stimuli-responsive materials[6, 422, 423] or smart materials are able to "sense" changes in their environment by undergoing a chemical and/or physical transition. Ideally, the response is reversible, i.e., once the stimulus is removed, the responsive material returns to its initial state. A number of responsivities have been introduced into responsive materials including responsivity to: temperature, pH, ionic strength, light, electric and magnetic field.[6, 424-426] These materials have found a number of applications as electronic materials, for controlled/triggered drug delivery, as antibacterial coatings and for tissue engineering.[23] Considering all of the responsive polymer-based materials discovered to date, thermoresponsive poly (*N*-isopropylacrylamide) (pNIPAm) is by far the most extensively studied and used.[42] Colloidal pNIPAm-based hydrogels (microgels and nanogels depending on their diameter) can also be synthesized.[414, 427] Regardless of their dimensions, hydrogels can easily be modified with additional functional comonomers by

[e] This Chapter has been adapted from the previously published article: Y. Gao, W. Xu, M. J. Serpe.* *J. Mater. Chem. C*, 2014, 2, 5878-5884.

simple copolymerization,[18] which allow the microgels to be easily modified by further reaction with other functional molecules.

A wide variety of responsive polymer-based thin films have been fabricated using both polymerization (e.g., atom transfer radical polymerization[428-430]) and deposition techniques (e.g., layer-by-layer assembly[431-435]). While substrate-supported thin films are of utmost importance for a number of applications, there are instances where free-standing thin films are beneficial and have recently received a lot of attention. Compared to substrate-bound thin films, free-standing materials are: flexible; able to change size, shape, and/or conformation; easily accessible from all dimensions, and oftentimes more sensitive to environmental stimuli than substrate-supported thin films. A variety of approaches has been developed to fabricate free-standing responsive films,[436-438] one of the most facile ways to accomplish this is utilizing layer-by-layer (LbL) assembly. In one case (with charged components) a charged substrate is exposed alternately to solutions containing positively or negatively charged polymers (polyelectrolytes). The interactions between the substrate charges and the polyelectrolyte allow a substrate-attached thin film to be formed. Since these films are held together by electrostatics, they can be destabilized in solutions of extreme pHs and ionic strength.[434, 439]

We have discussed the device of a pNIPAm-based microgel layer sandwiched between two thin metal layers in previous chapters.[130, 144, 155, 375] A schematic depiction of the device can be seen in Figure 6-1a. As shown in Figure 6-1b, these devices exhibit unique multipeak reflectance spectra, which we have exploited for sensing applications.[171, 374] The position of the peaks in the reflectance spectrum depends on the distance between the device's two Au layers and the refractive index of microgels as shown in Equation (6-1).[144]

$$\lambda m = 2nd \cos\theta \qquad (6\text{-}1)$$

where λ is the wavelength maximum of the peak (s), m is the peak order, n is the refractive index of the dielectric, d is the spacing between the mirrors, and θ is the angle of incidence.

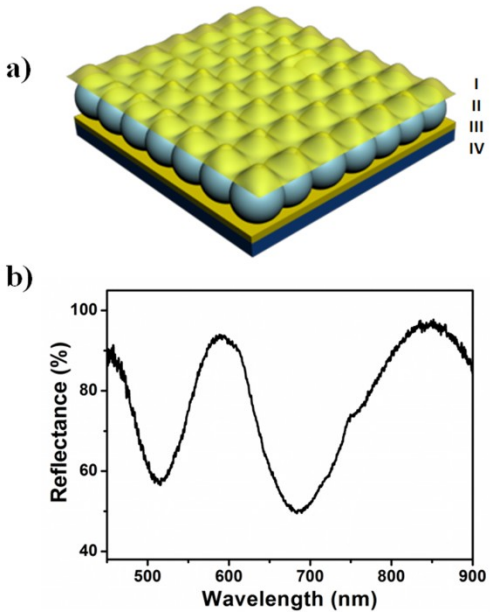

Figure 6-1. a) The basic construct of a microgel assemblies based device. (I) and (III) are 15 nm Au layers (a 2 nm Cr adhesion layer below the Au layer is not shown); (II) monolithic p(NIPAm-*co*-AAc) microgel layer; and (IV) glass substrate. b) Characteristic reflectance spectrum for a p(NIPAm-*co*-AAc) microgel-based device in water. Reproduced with permission from ref. 419, Copyright 2014, Royal Society of Chemistry.

While we have shown that microgel assemblies based devices can be fabricated on various planar substrates, there are some substrates that are difficult to coat with, e.g., curved surfaces, rods, and tubes. Furthermore, for our sensing and monitoring efforts, it is advantageous to fabricate devices that can be adhered to skin.[440-442] To achieve this, it would be beneficial to fabricate a device on planar substrates, followed by their desorption. The desorbed device can then adhere to any other substrate as needed. In this study, we describe the fabrication of free-standing p(NIPAm-*co*-AAc) microgel assemblies based devices that exhibit high-quality optical

properties, which are capable of being transferred to multiple substrates. The desorbed device exhibit similar optical properties to the substrate adhered one and retain their pH and temperature responsivity.

6.2 Experimental section

Materials: *N*-isopropylacrylamide was purchased from TCI (Portland, Oregon) and purified by recrystallization from hexanes (ACS reagent grade, EMD, Gibbstown, NJ) prior to use. *N, N'* -methylenebisacrylamide (99 %), acrylic acid (99 %), H_2O_2 (30 wt %) and ammonium persulfate (98+ %) were obtained from Aldrich (St. Louis, MO) and were used as received. Poly (diallyldimethylammonium chloride) (M_w = 100,000-200,000) (PDADMAC, 20 wt % in water) and poly (allylamine hydrochloride) (M_w = 55,000-65,000) (PAH) were obtained from Aldrich as solutions. Poly (sodium 4-styrenesulfonate) (M_w = 70,000) (PSS, Aldrich) and poly (acrylic acid) (M_w = 90,000) (PAA, Polysciences) were used as an anionic polyelectrolyte. H_2SO_4 (98 %) was purchased from Caledon Chemicals (Alberta) and was used as received. Anhydrous ethanol was obtained from Commercial Alcohols (Brampton, Ontario). Hydrochloric acid and sodium hydroxide were purchased from Caledon Chemicals (Alberta). All deionized water (DI) was 18.2 M Ω · cm and obtained from a Milli-Q Plus system from Millipore (Billerica, MA). Au annealing was performed in an Isotemp muffle furnace from Fisher Scientific (Ontario, Canada). Microscope glass slides were 25 mm × 75 mm × 1.0 mm and obtained from Fisher Scientific. Cr (99.999 %) was obtained from ESPI (Ashland, OR), while Au (99.99 %) was obtained from MRCS Canada (Edmonton, AB). Photographs of the films were taken with a Canon Power shot SD20 Digital ELPH SD.

Microgel synthesis: Microgels composed of poly (*N*-isopropylacrylamide-*co*-acrylic acid) (p(NIPAm-*co*-AAc)) were synthesized via surfactant-free, free radical precipitation

polymerization as described previously.[130, 144] The monomer mixture was comprised of 85 % *N* -isopropylacrylamide (NIPAm) and 10 % acrylic acid (AAc) with 5 % *N*, *N*'-methylenebisacrylamide (BIS) as the crosslinker. The monomer, NIPAm (11.9 mmol), and the crosslinker, BIS (0.703 mmol), were dissolved in DI water (99 mL) with stirring in a small beaker. The mixture was filtered through a 0.2 μm filter affixed to a 20 mL syringe into a 250 mL, 3-necked round bottom flask. The flask was then fitted with a temperature probe, a condenser/N_2 outlet, stir bar, and a N_2 inlet. The monomer solution was purged with N_2 gas for ≈ 1 hr with stirring, while the temperature was allowed to reach 70 °C. AAc (1.406 mmol) was added to the heated mixture with a micropipette. An aqueous solution of ammonium persulfate (APS, 0.046 g in 1.0 mL) was delivered to the monomer solution with a transfer pipette to initiate the reaction, and the reaction was continued for 4 h. Following completion of the reaction, the reaction mixture was filtered through glass wool to remove any large aggregates. The coagulum was rinsed with deionized water and the reaction solution was diluted to ≈ 120 mL. Aliquots of these particles (13 mL) in centrifuge tubes were centrifuged at a speed of ≈ 8500 relative centrifugal force (rcf) at 20 °C to produce a pellet. The supernatant was removed from the pellet of particles, which were then re-suspended to their original volume (13 mL) using deionized water. This process has completed a total of six times to remove the unreacted monomer and linear polymer from the microgels.

Sacrificial layer fabrication: 25 mm × 25 mm glass microscope slides were cleaned and hydroxylated in Piranha solution (a mixture of 7:3 (v/v) 98 % H_2SO_4 and 30 % H_2O_2) (*CAUTION*: Piranha solutions react violently with organic materials and should not be stored in closed containers). They were then rinsed copiously with deionized water and dried under a stream of nitrogen before use. Layer-by-layer self-assembly was used to form the sacrificial layer

on the glass substrate. Specifically, the freshly cleaned glass substrate was immersed in a PDADMAC aqueous solution (1 mg/mL, pH 6.5) for 15 min to obtain a cation-terminated surface and the substrate was then rinsed by immersion in deionized water for 15 min before the next layer was deposited. Next, the substrate was immersed into an aqueous PSS solution (1 mg/mL, pH 6.5) for 15 min to obtain an anion-terminated surface. The rinsing and adsorption steps were repeated until the desired number of bilayers was obtained. Finally, the prepared substrate was dried with nitrogen and used. PAH/PAA multilayers were assembled in the same way, although the pH of the PAH solution was adjusted to 7.5, while the pH of the PAA solution was 3.5. [439]

Device fabrication: Devices were prepared following a previously published method.[155] To fabricate etalons on the modified coverslips, 2 nm Cr and 15 nm of Au was thermally evaporated onto the substrate at a rate of 0.2 Å s^{-1}, and 0.1 Å s^{-1}, respectively (Torr International Inc., thermal evaporation system, Model THEUPG, New Windsor, NY). A 40 μL aliquot of concentrated microgels (from viscous pellet formed via centrifugation of a microgel solution) was added to the substrate and then spread toward each edge using the side of a micropipette tip. The film was rotated 90°, and the microgel solution was spread again. The spreading and rotation continued until the microgel solution became too viscous to spread due to drying. This process was done with extreme care as to not damage the sacrificial polymer layer on the glass. The microgel solution was allowed to dry completely on the substrate for 2 h with the hotplate temperature set to 35 °C. After that, the dry film was rinsed copiously with DI water to remove any excess microgels not bound directly to the Au. The film was then placed into a DI water bath and allowed to incubate overnight on a hot plate set to ~30 °C. Following this step, the substrate was again rinsed with DI water to further remove any microgels not bound directly to the Au

substrate surface. The samples were then dried with N_2 gas and another Au overlayer (2 nm Cr for adhesion layer) was evaporated. To yield a free-standing etalon, the whole substrate was immersed in an aqueous sodium hydroxide aqueous solution (1 M) to remove the sacrificial layer. The free-standing etalons were transferred to a variety of substrates with no previous treatment.

Reflectance spectroscopy: Reflectance measurements were conducted using a Red Tide USB650 spectrometer, a LS-1 tungsten light source, and a reflectance probe from Ocean Optics (Dunedin, FL). The spectra were recorded using Ocean Optics Spectra Suite Spectroscopy Software at room temperature over a wavelength range of 400-1000 nm. Measurements were conducted by placing the film in a Petri dish with water at room temperature. The probe tip was immersed in the water and its distance from the etalon surface adjusted for optimal signal. The probe remained undisturbed between measurements to ensure that all of the spectra were taken in the same manner. The film was moved under the probe and at least three measurements were taken for each film in different areas.

Scanning electron microscopy: SEM images were obtained with a JSM-6010LA JEOL (Peabody, MA) SEM. Samples were tilted 30° (unless otherwise indicated) relative to the source. Etalons were imaged by transferring the free-standing etalon onto a clean silica substrate and then dried under nitrogen gas flow.

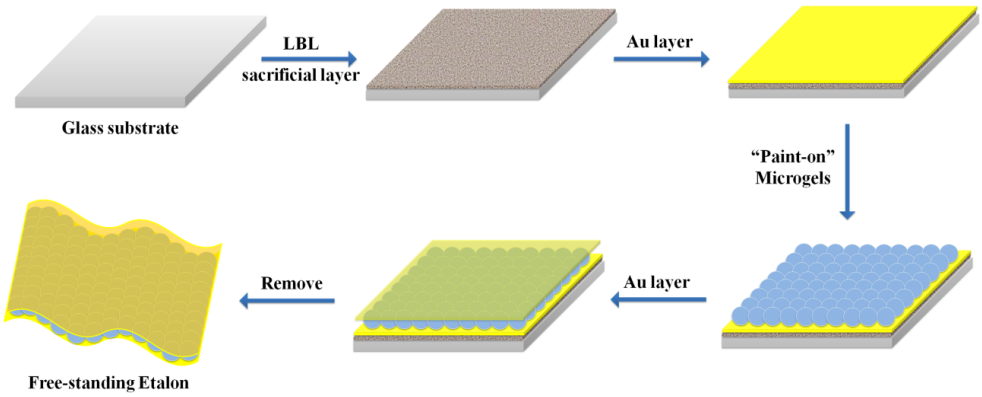

Figure 6-2. Schematic depiction of the device assembly and removal process. First, a sacrificial LbL-assembled film was deposited on the glass followed by the etalon fabrication on the sacrificial layer. Finally, the assembly was exposed to a 1 M NaOH aqueous solution, which dissolves the sacrificial layer, and releases the etalon. Reproduced with permission from ref. 419, Copyright 2014, Royal Society of Chemistry.

6.3 Results and discussion

To achieve free-standing device, microgel assemblies based devices were fabricated on LBL-deposited sacrificial thin polymer films, all on a glass substrate. A schematic of the fabrication protocol is shown in Figure 6-2. Specifically, a glass substrate was cleaned and hydroxylated by immersion in piranha solution for 4 h *(Caution, piranha solution is extremely dangerous -- handle with care)*. Then the LBL multilayer film was constructed on the glass surface. Here, two polyelectrolyte systems were used, poly (diallyl dimethyl ammonium chloride) (PDADMAC)/poly (sodium 4-styrenesulfonate) (PSS) and poly (allylamine hydrochloride) (PAH)/poly (acrylic acid) (PAA). Briefly, the glass was subsequently immersed into 1 mg/mL aqueous solution of PDADMAC solution (pH 6.5) for 15 min, followed by immersing in DI water for 15 min for rinsing. The substrate was then immersed in a 1 mg/mL solution of PSS (pH 6.5), for another 15 min, and again in DI water for 15 min. The process was repeated until 10

bilayers (PDADMAC/PSS is a bilayer) were formed on the glass. The $(PAH/PAA)_{10}$ layers were formed in the same way, using different solution pH's, as indicated in the experimental section.[439] Following thin film formation, 15 nm of Au was deposited (via thermal evaporation) on top of the LbL assembled thin film, followed by microgel deposition on the Au layer following our previously published painting protocol.[155] Another Au layer was subsequently deposited on top of the microgel layer to yield the etalon's Au-microgel-Au sandwich structure.

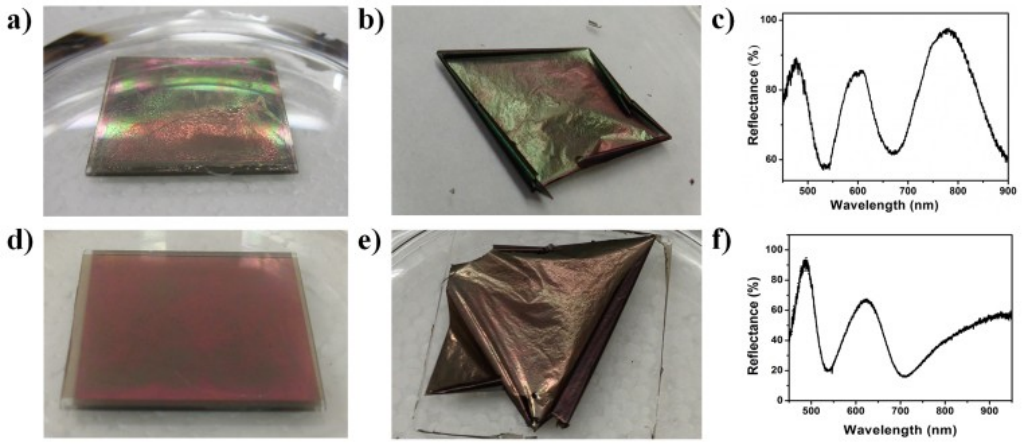

Figure 6-3. (a) Photograph of the substrate-bound device (PDADMAC/PSS sacrificial layer) immersed in 1 M NaOH solution and (b) after desorption. (c) After desorption, the device still exhibits the unique, multi-peak reflectance spectrum. (d) Photograph of the substrate-bound device (PAH/PAA sacrificial layer) immersed in 1 M NaOH solution and (e) after ~8 minutes NaOH exposure. (f) Again, after desorption, the device still exhibits the unique, multi-peak reflectance spectrum. The size of the glass substrate above was 2.5 cm × 2.5 cm. Reproduced with permission from ref. 419, Copyright 2014, Royal Society of Chemistry.

To generate a free-standing device, the assembly was immersed into a 1 M aqueous solution of NaOH. This causes the sacrificial layer to dissolve, and the device to be released from the glass substrate. The disassembly and release process is shown in Figure 6-3. As can be seen,

when the assembly was immersed into the high pH solution the corners began to delaminate from the glass after ~ 2 minutes, while the whole device was removed from the glass substrate within 10 min, see Figure 6-3(a, b) and Figure 6-3(d, e). In both cases, the device was released from the substrate due to a combination of effects. Considering the assembly on glass, it could be released from the substrate by breaking the polymer-glass, polymer-polymer, and/or polymer-Cr/Au interactions. In the case of the weak polyelectrolytes (PAH/PAA), the high pH most likely broke the polymer-polymer interactions, while a combination of these effects was most likely responsible for the disassembly of the PDADMAC/PSS layers. In fact, the device was removed from the substrate much faster with the PAH/PAA sacrificial layers. We point out here that the edges of the slide were scratched before immersion of the etalon into the high pH solution, which we found to assist with the peeling process. Figure 6-3b shows a free-standing etalon film in the basic solution. As can be seen in Figure 6-3c and Figure 6-3f, the optical properties of the free-standing microgel assemblies based devices were retained after peeling from the substrate surface. Additionally, the free-standing device can be dried and rehydrated with no apparent effect on the optical properties.

To investigate the structure of the free-standing device, and to verify the Au-microgel-Au structure was still intact after desorption from the glass substrate, scanning electron microscopy (SEM) was performed. To accomplish this, the free-standing device was transferred to a silicon substrate and imaged. As can be seen in Figure 6-4(a-c), the full structure remains intact after desorption, indicating that the pH treatment doesn't affect the device's structure and that the microgels are still sandwiched between the two Au layers. The free-standing film can be completely broken into small pieces by ultrasonication, as shown in Figure 6-4d. This result may

provide us a way to prepare a single microgel-based element in the future, which may have unique optical properties and potential applications for sensing and drug delivery.

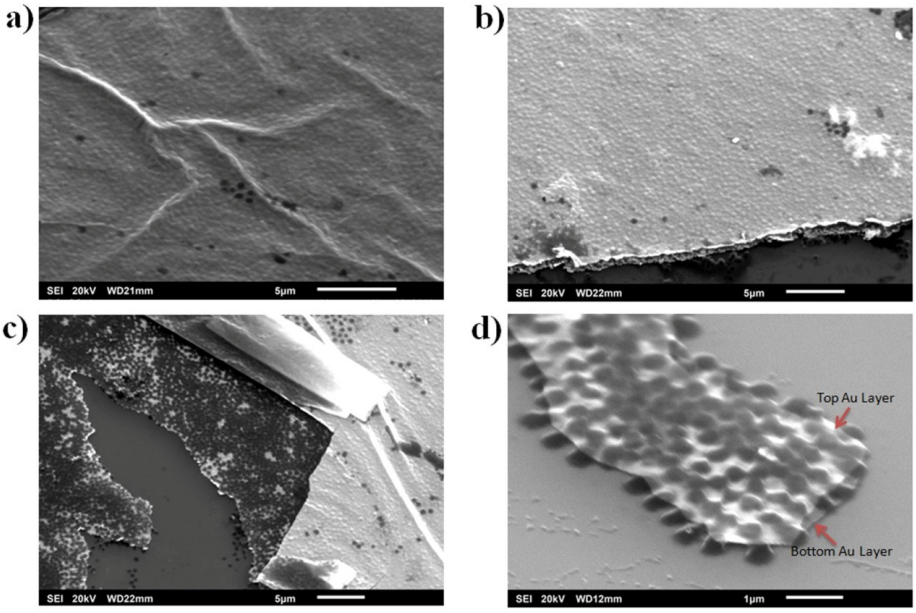

Figure 6-4. SEM images of a free standing device from (a,c) the top, (b,d) tilted 30°. As can be seen in (a,b), the structure remained intact after desorption from the solid substrate, and the microgels remained sandwiched between the two Au layers. As can be seen in (c), there are two Au layers present. (d) The structure of a device after sonication. Sonication breaks up into small pieces, which appear to retain the structure. Reproduced with permission from ref. 419, Copyright 2014, Royal Society of Chemistry.

Next, we wanted to confirm that the free-standing device could be transferred to different substrates and that their optical properties remained intact. To accomplish this, we desorbed it from the solid glass substrates and adhered them to different substrates, such as silicon, polydimethylsiloxane (PDMS), plastic and paper. After the free-standing films were transferred onto the different substrates, the reflectance spectra were collected; the results are shown in Figure 6-5. As can be seen in Figure 6-5a, the reflectance spectrum of the film on a silicon

substrate shows multiple peaks similar to the original device made on a glass substrate. As can be seen in Figure 6-5(b-d), similar spectra could be observed for a free-standing etalon transferred to PDMS, plastic, and paper, respectively. For the "plastic" substrate, we used a piece of a nitrile lab gloves as an example. When the device was transferred onto the nitrile, it was not flat based due to its deposition on the elastic substrate, but it still exhibited a reflectance spectrum that is characteristic to the device (Figure 6-5c). Finally, filter paper was used as a substrate of the film in Figure 6-5d. While the optical properties of this film were comparable to the initial substrate-bound device, there were some differences due to the porosity of the paper. The porosity, combined with the capillary effects of the paper made the device difficult to hydrate.

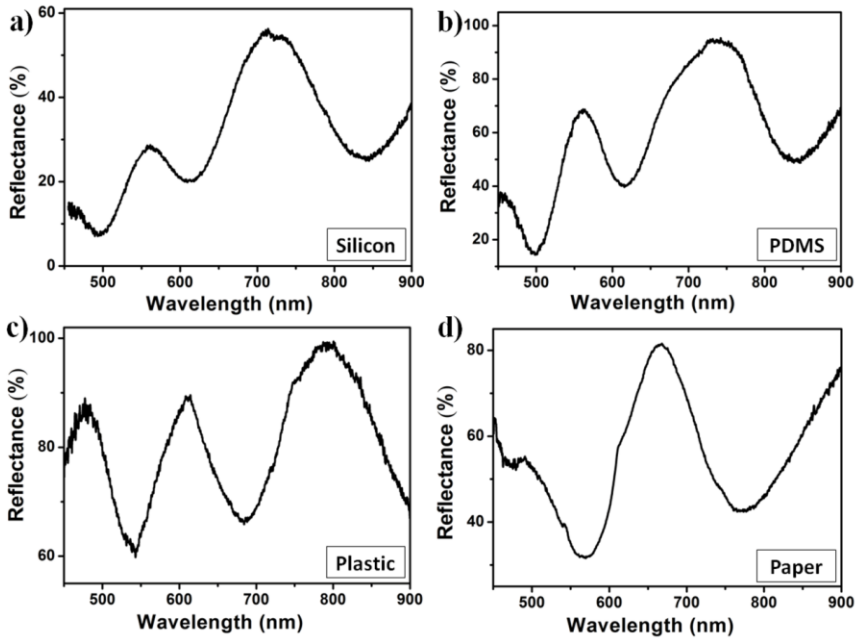

Figure 6-5. Reflectance spectra for devices desorbed from the initial glass substrate and transferred to: (a) silicon; (b) PDMS; (c) plastic/nitrile and (d) paper. Reproduced with permission from ref. 419, Copyright 2014, Royal Society of Chemistry.

Additionally, we wanted to show the utility of the approach for coating curved surfaces and even skin. This could find applications in the biomedical area and for real-time health monitoring applications.[441-445] To accomplish this, we desorbed the device from a glass substrate and (like above) and transferred it to the outside of a glass tube with a diameter of 1 cm. The resultant device can be seen in Figure 6-6a. The structure remains intact and retains its optical properties as can be seen in Figure 6-6b. Furthermore, a free-standing device was transferred to the human skin, as shown in Figure 6-6c. Similarly, it remained intact and the optical properties were unaffected.

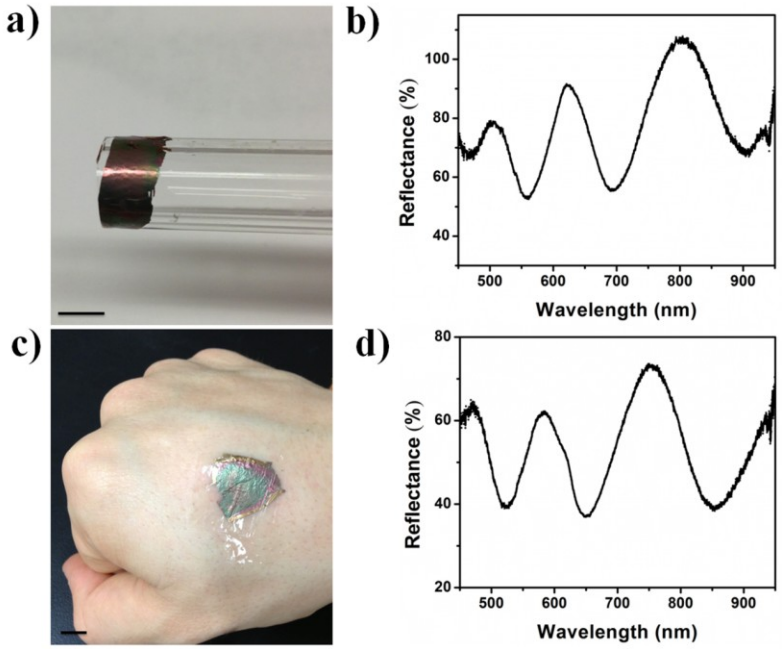

Figure 6-6. A free-standing device transferred to (a) a glass tube, and (c) skin. (b, d) The reflectance spectra obtained from the devices. The scale bar is 0.5 cm. Reproduced with permission from ref. 419, Copyright 2014, Royal Society of Chemistry.

In our previous chapters, we showed that microgel assemblies based devices have unique responsivity to a variety of stimuli, specifically, they are very sensitive to temperature and pH changes (among other things).[144, 155, 161, 374, 446] Therefore, we investigated the responsivity and

sensitivity of the free-standing devices to temperature and pH. To accomplish this, the free-standing device was desorbed from the initial glass substrate and added to a bare silicon substrate. The results are shown in Figure 6-7. Figure 6-7a shows that it is extremely sensitive to solution pH, i.e., the reflectance peak red shifts a total of ~330 nm upon increasing the solution pH from 3.17 to 9.32. This is due to the deprotonation of AAc at high pH, which leads to enhanced Coulombic repulsion in the microgel network and swelling. The temperature-dependent optical properties are shown in Figure 6-7b at different solution pH. We found that it was fully responsive to temperature at pH 3.0, while it was minimally responsive to temperature at high pH. This behavior is similar to that have not been desorbed from the glass substrate and is a result of the charges in the microgels at high pH preventing the microgel collapse at elevated temperature.[40, 144] At pH 3.0, the AAc groups are neutral and therefore there is no barrier for the microgel deswelling at elevated temperature.

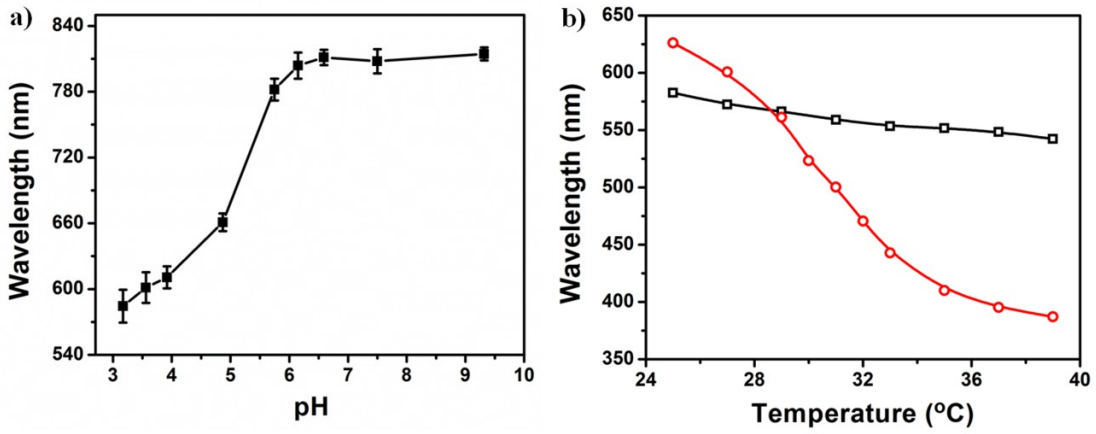

Figure 6-7. (a) The response of the free-standing devices to pH, and (b) temperature at different pH's. As can be seen in (b), the device responds to temperature at pH= 3.0 (red), while the thermal response is hindered at pH= 6.0 (black). This is due to the deprotonated AAc groups preventing the collapse of the microgels. Reproduced with permission from ref. 419, Copyright 2014, Royal Society of Chemistry.

Finally, to further demonstrate the applicability of the free-standing devices, we showed that they could be used to release a small molecule model drug once absorbed onto a polymer matrix. To accomplish this, the small molecule crystal violet (CV, model drug) was loaded into the microgel layer at a given pH, while it was released at another pH. Specifically, at pH > 4.25 (pK_a for AAc) the microgels were negatively charged, while the CV is positively charged, thus the microgels were able to absorb the CV via electrostatic interactions. When the pH was lowered to < 4.25 the AAc groups were neutralized, releasing the CV.[299] To load the free-standing etalon with CV, it was immersed into 20 mL of an aqueous solution of CV (0.5 g/L, pH 6.5) for 4 h. It was then transferred to a glass substrate (used as a support) and gently rinsed with pH 6.5 solution to remove the excess CV. Finally, the edges of etalon were sealed with epoxy and put in direct contact with a pNIPAm-based hydrogel (15 mm x 15 mm x 2.5 mm) synthesized following standard protocol.[447] The hydrogels were swollen with different pH solutions, by soaking them for more than 5 h in solutions of pH 3.0 (release) and pH 6.5 (no release). We point out that the pNIPAm-based hydrogel was used purely out of convenience, and only served as a generic polymer matrix in this case. The results are shown in Figure 6-8, which reveals that the hydrogel immersed in pH 3.0 solution was able to induce the etalon to release the loaded CV (by protonating the AAc groups), while the hydrogel immersed in pH 6.5 solution did not because the electrostatic interactions were still strong. These results show that the free-standing devices could be adhered to "foreign" substrates, e.g., skin, and be triggered to release small molecules in a controlled fashion. This specifically demonstrates the utility of the devices for drug delivery applications.

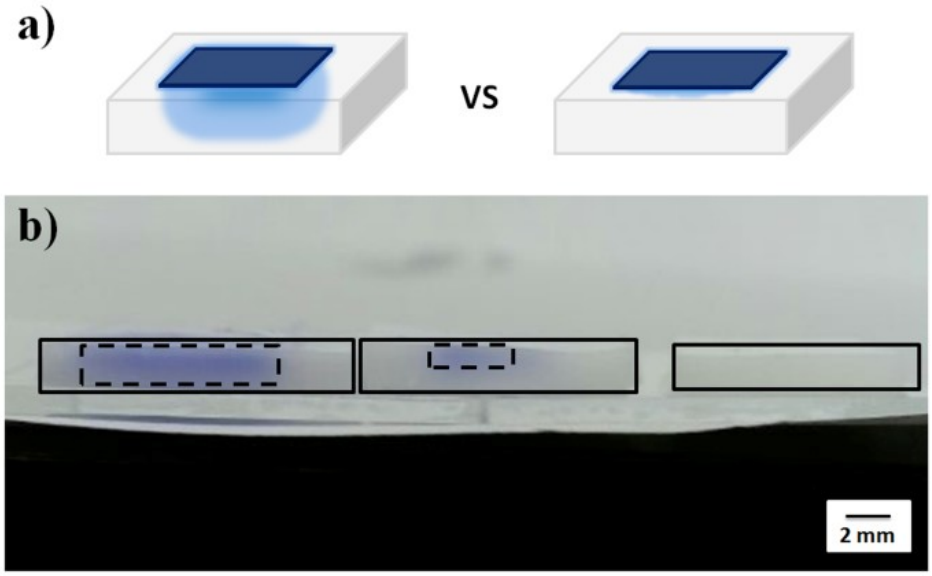

Figure 6-8. (a) Schematic showing that a "drug" loaded free-standing device can be transferred to a hydrogel that was swollen in solutions of (left) pH 3.0 and (right) 6.5. (b) As can be seen, the small molecule can be released from the etalon at (left) pH 3.0, while minimal CV was released at (middle) pH 6.5 (right). The hydrogel before contact with the CV loaded free-standing device. The black dashed lines indicate the region in the hydrogel where CV was located, while the black solid lines indicate the individual hydrogel boundaries. Reproduced with permission from ref. 419, Copyright 2014, Royal Society of Chemistry.

6.4 Conclusion

In summary, a simple method for fabricating free-standing microgel assemblies based device was developed by introducing a sacrificial layer between the device and glass substrate. The sacrificial layer was prepared by LbL assembly, which could be destroyed in solutions at high pH; destroying the film releases the device from the substrate. The free-standing microgel assemblies based device can be easily transferred to substrates with different chemistries and shapes. We found that its optical properties are retained after desorption from the solid substrate, which continues to exhibit very sensitive responses to solution pH and temperature. Finally, we

demonstrate that the devices could be transferred to another surface, in this case, a hydrogel, and be triggered to release a small molecule drug. In the future, the free-standing microgel assemblies based device will be used for light filtering applications, biosensing, we will further the drug delivery concept.

Chapter 7: Light-Induced Color Changes and Drug Release from Microgel Assemblies Based Device[f]

In this chapter, we will introduce a light-responsive system that changes the color of microgel assemblies based devices and controls the release behavior of this devices. By applying a photoacid into the system, which can release protons under light irradiation, the non-light-responsive microgel will respond to light and the interesting phenomenon will be observed.

7.1 Introduction

Photonic materials are composed of periodic arrays of contrasting refractive index materials, which interact with incident light (via reflection, refraction, and/or diffraction) to produce unique optical properties.[448-452] The refractive index periodicity can be in one, two, or three dimensions; while the specific optical properties depend on the spacing between the material's periodic elements and their refractive index. These materials often yield visually stimulating optical properties, but they also have numerous practical applications, such as photonic circuits,[453] optical filters,[454] and in communications.[455]

The most basic photonic materials are composed of elements with fixed positions and refractive indices. While these "static" structures are of utmost importance, the tunability of the spacing and/or the refractive indices of the photonic material's elements can make these devices even more useful.[456, 457] The fabrication and development of materials and structures, which exhibit dynamically tunable optical properties ("color tunability") have also been extensively studied.[427, 456, 458, 459] Various studies have shown the optical properties to be tunable with: light,[460] electric field,[461] magnetic field,[462, 463] temperature,[460, 464, 465] pH,[466] ionic strength,[467]

[f] This Chapter has been adapted from the previously published article: Y. Gao, M. J. Serpe.* *ACS Appl. Mater. Interfaces*, 2014, 6, 8461-8466.

solvent compositions, and humidity.[468, 469] Among of these, light has a high level of control which can be delivered to a subtle adjustment in terms of wavelength, duration and intensity. Light can also allow localized excitation and certain wavelengths can be selected to penetrate materials, e.g., skin. Which come with an important application of the light trigger, controlled drug delivery. In this research area, the place can be exploited through a light-controlled reaction for drug liberation to give control of the quantity of drug released, the timing of the release event, and its location. Light-triggered reaction can cause the change of environment to induced responsive behaviors, like pH change. Furthermore, it is very simple to modulate responses by simply turning on and off the source.

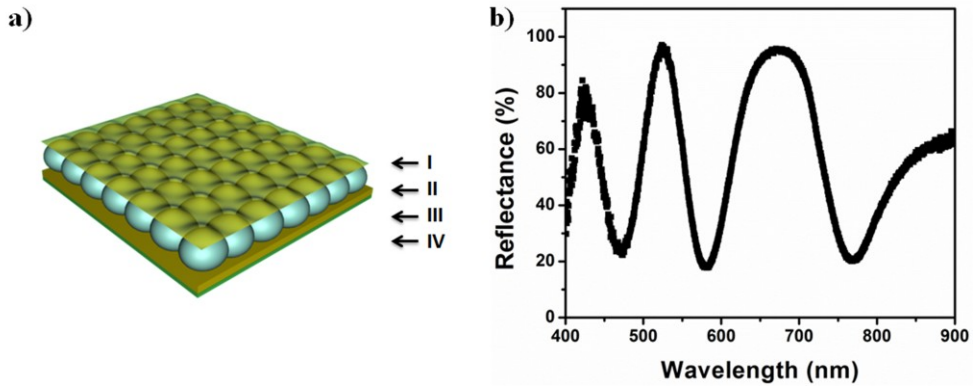

Figure 7-1. a) The structure of a standard microgel-based etalon composed of (I and III) two Au layers sandwiching microgel layer(II) on a glass support(IV). b) typical reflectance spectrum obtained from a microgel-based etalon immersed in deionized water. Reproduced with permission from ref. 420, Copyright 2014, American Chemical Society.

In our previous chapters, we reported on polymer-based optical materials that exhibit unique optical properties and visual color, which can be tuned with temperature and other stimuli.[130, 144, 375, 470] These devices were constructed by sandwiching a responsive polymer layer between two Au layers all supported on a glass substrate. This structure is akin to the mirror-

dielectric-mirror structure of a classic Fabry-Perot etalon (etalon), see Figure 7-1. In this novel structure (shown in Figure 7-1a), the responsive polymer layer is composed of assembled thermoresponsive poly (*N*-isopropylacrylamide) (pNIPAm)-based hydrogel particles (microgels). PNIPAm is well known to be water soluble at temperatures below 32 °C, becoming "insoluble" at higher temperatures.[18, 42, 414] As part of this transition, pNIPAm undergoes a random coil (extended) to a globule (collapsed) transition. Likewise, pNIPAm-based microgels undergo a swollen to collapsed transition as the temperature of the water they are in is increased to > 32 °C. The addition of comonomers into the microgels adds chemical functionality and can alter the microgel responsivity. Acid comonomers, such as acrylic acid (AAc),[18, 144] adds pH responsivity to the already thermoresponsive microgels. Specifically, the AAc monomer has a pK_a of ~ 4.25, so when p(NIPAm-*co*-AAc) microgels are exposed to a solution with a pH above the pK_a for AAc the collapse transition is hindered. Furthermore, the microgels swell, which are both a result of Coulombic repulsion between the deprotonated AAc in the microgel. These effects are fully reversible by lowering the solution pH to below 4.25.

As indicated above, pNIPAm microgel-based etalons were constructed, which exhibit interesting optical properties, i.e., color and multipeak reflectance spectra (shown in Figure 7-1b). The position of the reflectance peaks can be predicted from Equation (7-1):[130, 144]

$$\lambda m = 2nd \cos\theta \qquad (7\text{-}1)$$

where λ is the wavelength maximum of the peak (s), m is the peak order, n is the refractive index of the dielectric, d is the spacing between the mirrors, and θ is the angle of incidence.

Therefore, since the microgel solvation state can be modulated with pH variations, and the microgels define the distance between the etalon's Au layers, the position of the reflectance peaks (and the etalon color) should depend on solution pH. That is, when the solution pH is

above the pK_a of AAc, the AAc groups become negatively charged, which results in microgel swelling and a concomitant increase in the distance between two Au layers. However, when the solution pH is again lowered to below AAc's pK_a, the microgels decrease in diameter due to the AAc protonation; this results in a decrease in the distance between the etalon's Au layers. As can be predicted from equation 1, the increase and decrease in the distance between the Au layers result in a red shift and blue shift of the etalon's reflectance peaks, respectively.

7.2 Experimental section

Materials: *N*-isopropylacrylamide was purchased from TCI (Portland, Oregon) and purified by recrystallization from hexanes (ACS reagent grade, EMD, Gibbstown, NJ) prior to use. *N, N'* -methylenebisacrylamide (99 %), acrylic acid (99 %), *o*-Nitrobenzaldehyde (*o*-NBA) and ammonium persulfate (98+ %) were obtained from Aldrich (St. Louis, MO) and were used as received. Polydimethylsiloxane (PDMS) (Sylgard 184) was purchased from Dow Corning Corporation and used as received. Anhydrous ethanol was obtained from Commercial Alcohols (Brampton, Ontario). All deionized water was 18.2 M Ω · cm and obtained from a Milli-Q Plus system from Millipore (Billerica, MA). Au annealing was performed in an Isotemp muffle furnace from Fisher Scientific (Ontario, Canada). Glass cover slides were 25 mm × 25 mm and obtained from Fisher Scientific. Cr (99.999 %) was obtained from ESPI (Ashland, OR), while Au (99.99 %) was obtained from MRCS Canada (Edmonton, AB). Photographs of the films were taken with a Canon Power shot SD20 Digital ELPH SD.

Microgel synthesis: P(NIPAm-*co*-AAc) microgels were synthesized via free radical precipitation polymerization as described previously. The monomer mixture was comprised of 85 % *N*-isopropylacrylamide (NIPAm) and 10 % acrylic acid (AAc) with 5 % *N, N'*-methylenebisacrylamide (BIS) crosslinker. The monomer, NIPAm (11.9 mmol), and the

crosslinker, BIS (0.703 mmol), were dissolved in 18.2 M Ω · cm deionized water (99 mL) with stirring in a small beaker. The mixture was filtered through a 0.2 μm filter affixed to a 20 mL syringe into a 250 mL, 3-neck round bottom flask. The flask was then fitted with a temperature probe, a condenser/N_2 outlet, stir bar, and a N_2 inlet. The monomer solution was purged with N_2 gas for ≈ 1 hr with stirring, while the temperature was allowed to reach 70 °C. AAc (1.406 mmol) was added to the heated mixture with a micropipette. An aqueous solution of ammonium persulfate (APS; 0.046 g in 1.0 mL) was delivered to the monomer solution with a transfer pipette to initiate the reaction, and reaction will continue for 4 h. Following completion of the reaction, the reaction mixture was filtered through glass wool to remove any large aggregates. The coagulum was rinsed with deionized water and the reaction solution was diluted to ≈ 120 mL. An aliquot of these particles (13 mL) in centrifuge tubes was centrifuged at a speed of ≈ 8500 relative centrifugal force (rcf) at 20 °C to produce a pellet. The supernatant was removed from the pellet of particles, which were then re-suspended to their original volume (13 mL) using deionized water. This process has completed a total of six times to remove the unreacted monomer and linear polymer from the microgels. For poly (*N*-isopropylacrylamide) microgels, the monomer mixture was comprised of 95 % *N*-isopropylacrylamide (NIPAm) and 5 % *N, N'*-methylenebisacrylamide (BIS) crosslinker. The process is the same as above. The diameter of both the synthetic microgels is ~ 600 nm.

Etalon fabrication: Etalon was prepared as previously described. To fabricate the Au coated coverslips (etalon underlayer), 2 nm Cr and 15 nm of Au was added to a 25 x 25 mm ethanol rinsed and N_2 gas dried glass coverslip (Fisher's Finest, Ottawa, ON) at a rate of 1 Å s^{-1}, and 0.1 Å s^{-1}, respectively (Torr International Inc., thermal evaporation system, Model THEUPG, New Windsor, NY). The Cr/Au substrates were annealed at 250 °C for 3 h (Thermolyne muffle

furnace, Ottawa, ON) and cooled to room temperature prior to microgel film deposition. Approximately 5-10 mL of microgel solution was centrifuged at ~8300 rcf to form a pellet. The supernatant was removed and discarded, and the pellet was vortexed to loosen and homogenize the particles in the remaining solvent. A 40 µL aliquot of concentrated microgels were spread onto an annealed 25 mm x 25 mm Au-coated glass coverslip at 30 °C. The film was allowed to dry on a 35 °C hot plate for 120 minutes before the excess microgels were rinsed with deionized water. The samples were soaked overnight at 30 °C in a deionized water bath. The samples were then rinsed with deionized water, dried with N_2, and another Au overlayer (2 nm Cr for adhesion, followed by 15 nm Au) was added. The completed device was soaked overnight in deionized water at 30 °C before spectral analysis.

Reflectance spectroscopy: Reflectance measurements were conducted using a Red Tide USB650 spectrometer, a LS-1 tungsten light source, and a reflectance probe from Ocean Optics (Dunedin, FL). The spectra were recorded using Ocean Optics Spectra Suite Spectroscopy Software at room temperature over a wavelength range of 400-1000 nm. Measurements were conducted by placing the film in a Petri dish with water at room temperature. The probe tip was immersed in the water and its distance from the etalon surface adjusted for optimal signal. The probe remained undisturbed between measurements to ensure that all of the spectra were taken in the same manner. The UV irradiation was done by using a Blak-Ray® B-100AP High-Intensity UV Lamp with a wavelength of 365 nm.

7.3 Results and discussion

In this study, we developed a p(NIPAm-*co*-AAc) microgel assemblies based device (etalon) that are capable of changing its optical properties and visual color in response to solution pH changes induced by UV light irradiation. To accomplish this we utilized the photoacid *o*-

nitrobenzaldehyde (*o*-NBA); its structure and UV light-induced reaction are shown in Figure 7-2. The photoacid *o*-NBA was used because its behavior is well characterized and has been used in a variety of applications over a number of years.[57, 471-473] As illustrated in Figure 7-2a, the molecule releases a proton under UV irradiation (UV Source: 365 nm long wave UV), which causes the solution pH to decrease, which was already proposed and studied by other researchers.[474, 475] To investigate the rate and efficiency of this process, we prepared aqueous solutions of various *o*-NBA concentrations (1 mM, 5 mM and 10 mM) and adjusted their pH to ~7.00 by adding aliquots of 1 M NaOH solution. Each solution was continuously irradiated with UV light for the indicated time while recording the solution pH every 10 sec. As can be seen in Figure 7-2b, when the solution concentration increases from 1 mM to 5 mM, the rate of pH change increases, while there is no change upon further increase of the solution concentration. Therefore, for subsequent experiments, we chose to work with 5 mM *o*-NBA solutions. The pH of this solution was capable of a total pH change of ~3.6 pH units (pH 7.0 to 3.4). We also performed the same experiment in the absence of *o*-NBA and found a negligible change in solution pH upon UV exposure.

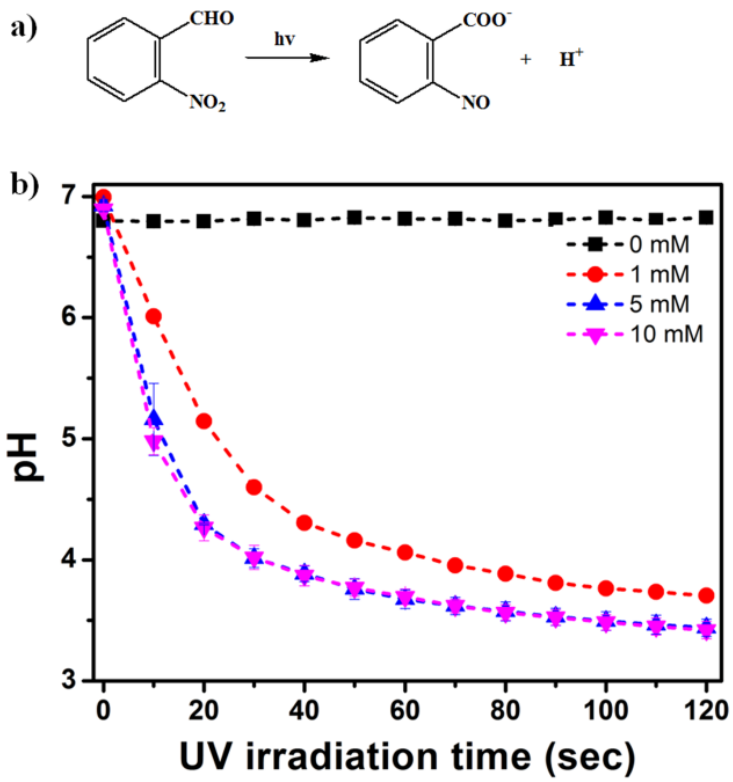

Figure 7-2. a) The reaction of *o*-NBA induced by exposure to UV irradiation and b) the observed change in solution pH after exposure to an aqueous solution of the indicated *o*-NBA concentrations to UV irradiation for the indicated elapsed times. Reproduced with permission from ref. 420, Copyright 2014, American Chemical Society.

The proton release mechanism of *o*-NBA in response to UV irradiation is illustrated in Figure 7-3. As early as 1901, Ciamician and Silberz[476] had observed that *o*-NBA undergoes a phototransformation to give o-nitrosobenzoic acid. Since then, several investigators have examined this reaction in detail, in attempts to understand the mechanism of the transformation.[477-483] An intramolecular hydrogen transfer in 2-nitrobenzaldehyde initiates a sequence of ground-state reactions that leads to 2-nitrosobenzoic acid. The transient species detected has been tentatively assigned to ketene from a biradical structure. On the picosecond time scale, the molecule undergoes hydrogen transfer, yielding a ketene intermediate, internal

conversion recovering the starting material, and intersystem crossing.[484] The latter molecule is a moderately strong acid and dissociates in aqueous solutions so that the photochemistry of 2-nitrobenzaldehyde can be used to create a rapid pH-jump in solution. Many biological macromolecules, such as proteins and nucleic acids, show pH-dependent conformational changes. Those changes can be monitored in real time by using the light-induced pH-jump.

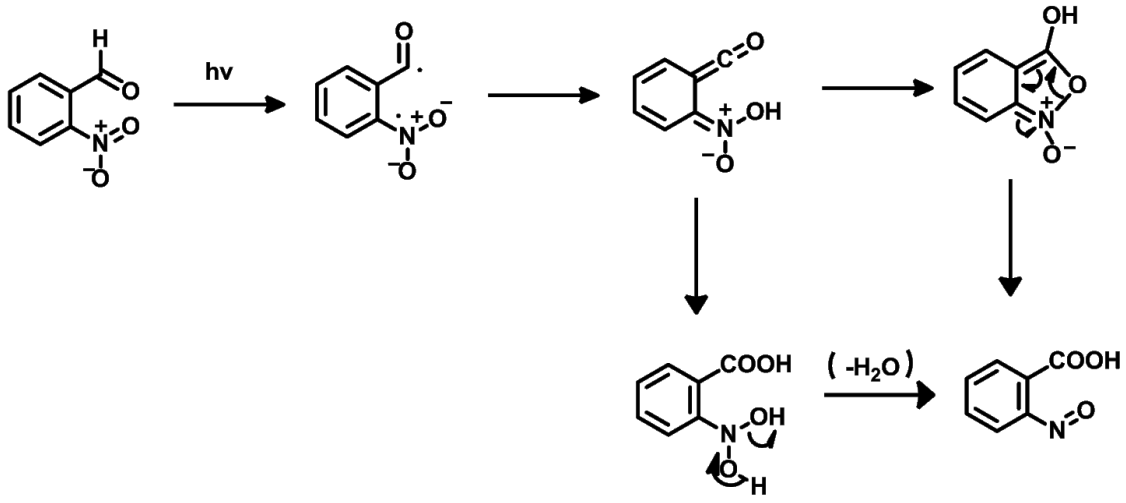

Figure 7-3. Photochemistry of o-NBA molecules, structure change response to UV light.

As can be seen in Figure 7-4, a decrease of the solution pH occurs each time UV light was exposed to the solution and stabilized after the light was turned off. This quick pH change proves that the photochemical reaction finished and stabilized in seconds, and provides a solution with a homogeneous pH. The concentration of *o*-NBA we used here is 5 mM. The result also shows that the resultant pH drop isn't as pronounced after multiple exposures to UV, which we propose is a result of the decrease in *o*-NBA concentration.

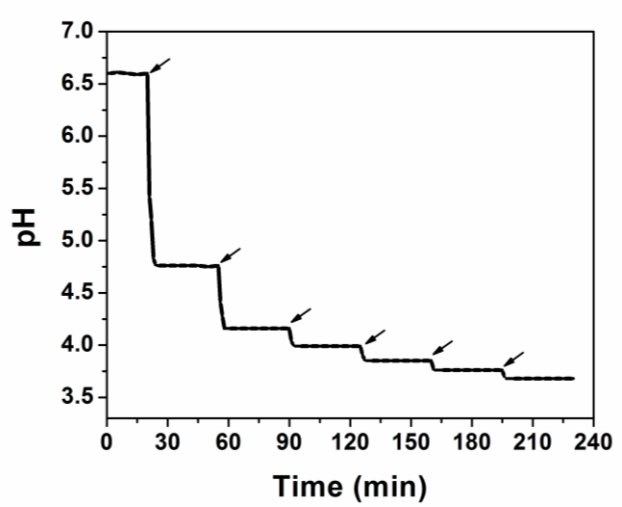

Figure 7-4. Solution pH profile induced by exposing the *o*-NBA solution to UV light for 10 sec (arrows) followed by stabilization.

With the ability to tune the pH of the *o*-NBA solution with UV irradiation, we determined if the optical properties of a p(NIPAm-*co*-AAc) microgel-based etalon could be tuned with UV irradiation. This is illustrated schematically in Figure 7-5. Initially, the p(NIPAm-*co*-AAc) microgel-based etalon was added to a Petri dish and 5 mM *o*-NBA solution (pH 7.00) was added. The etalon was allowed to incubate for ~60 min until the reflectance spectrum was stable, i.e., there was no observable change in the position of the reflectance peaks for at least 30 min. Since the initial solution pH was greater than the microgel's pK_a, the microgels were swollen and the mirrors were relatively far apart. Exposure of the system to the UV light caused the solution pH to decrease, as shown in Figure 7-4, resulting in a spectral shift from the etalon as can be seen in Figure 7-6. As can be seen, exposing the system to UV light for 10 sec, followed by stabilization in the absence of UV light caused the solution pH to decrease by approximately 2 units resulting in a blue shift in the position of the reflectance peak. This is expected since the microgel's AAc groups were protonated. Furthermore, the system was again exposed to UV light for 10 sec, followed by stabilization in the absence of UV light exposure. The solution pH subsequently

dropped again, resulting in a spectral blue shift. As can be seen, the total wavelength shift was 160 nm. From this large spectral shift, we hypothesized that this system could be used to visually change the color of the etalons.

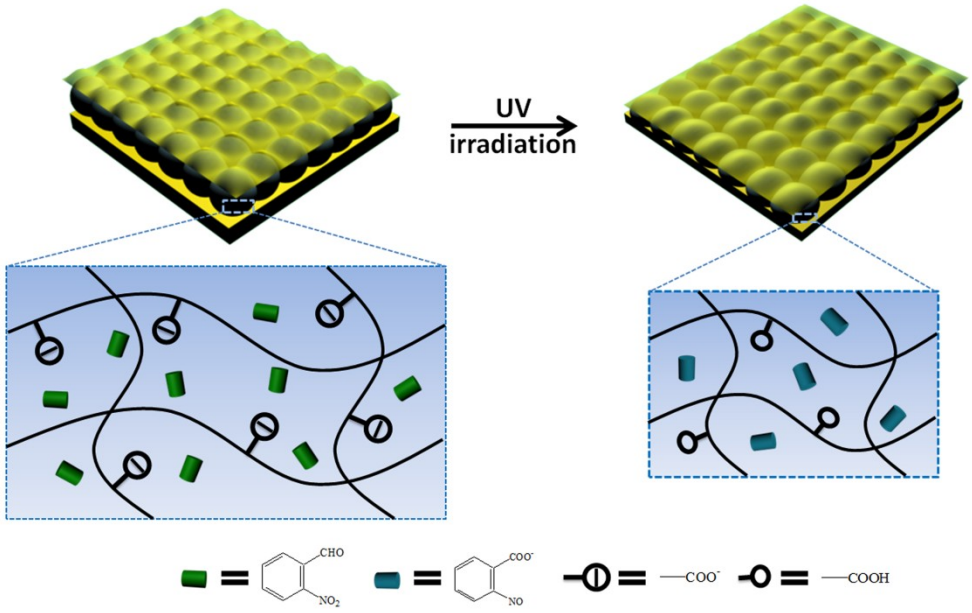

Figure 7-5. Schematic illustration of the reaction of the pNIPAm microgel assemblies based etalon system upon exposure to UV irradiation. Upon UV exposure, the *o*-NBA produces a proton, which lowers the pH of the solution. The decrease in solution pH results in protonation of the p(NIPAm-*co*-AAc) microgels, which alters their solvation state and the optical properties of the etalon. Reproduced with permission from ref. 420, Copyright 2014, American Chemical Society.

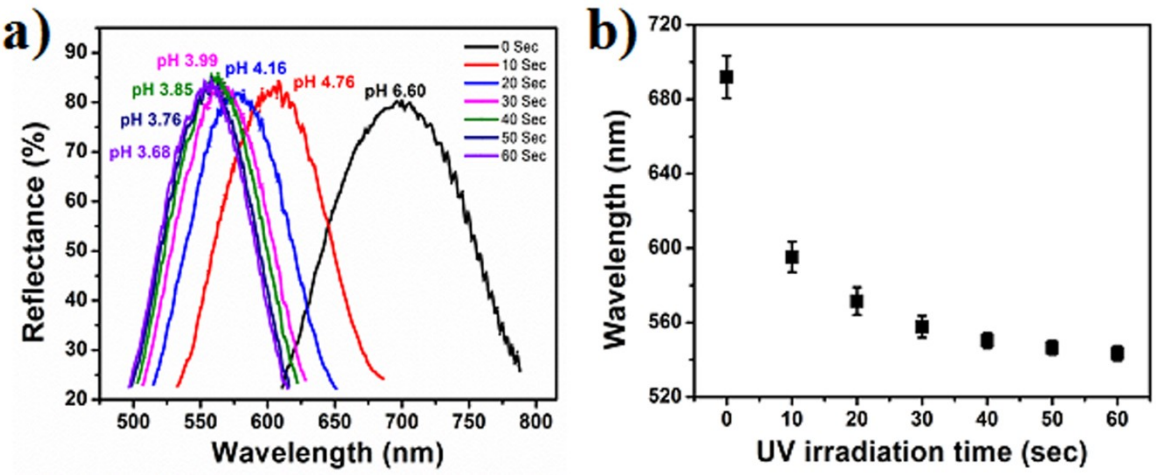

Figure 7-6. a) Reflectance spectrum for a device in *o*-NBA solution after exposure to UV irradiation for the indicated times. For these experiments, the device was initially stabilized in an *o*-NBA solution (5 mM) of pH 6.60, then exposed to UV irradiation for the indicated times (total irradiation times). After exposure to UV irradiation for the indicated times, the UV light was removed and the device allowed to stabilize. b) The final peak positions as a function of total irradiation time. Each point is the average obtained by analyzing 3 separate etalons and the error bars indicate the standard deviation. Reproduced with permission from ref. 420, Copyright 2014, American Chemical Society.

To investigate this, we constructed an etalon with a specific region masked off with poly(dimethylsiloxane) (PDMS, Sylgard 184). The PDMS mask was cut in such a way as to cover part of the etalon while exposing the rest. In this case, we cut the PDMS mask to expose the etalon such that the letters “UA” are formed. To accomplish this, the prepared PDMS mask (see Experimental section) was added to the top of the etalon and sealed by applying pressure. This assembly was subsequently exposed to a 5 mM *o*-NBA solution with a pH close to 7. The unmasked "UA" region was in direct contact with the solution, while the masked region remained unexposed. After soaking for several minutes, the system was exposed to UV light for

60 sec to trigger the solution pH change, which leads to a dramatic color change in the patterned, exposed region. As can be seen in Figure 7-7, the protected region was covered with PDMS and remained blue, while the region exposed to the solution was initially red, which changed to green upon ~1 min UV exposure and wait for few mins to stable. This is clearly depicted in the UA patterned region of the photograph. What is interesting is the initial color of the patterned region could be regenerated by replenishing the *o*-NBA. Furthermore, the color of the patterned region could be switched again by exposure to UV light. This color change can be repeated over many cycles with great fidelity and reproducibility, as can be seen in Figure 7-8. We also determined that further exposure of the system to UV irradiation, past the 60 sec exposure, has no effect on the pH, and hence no effect on the etalon's color.

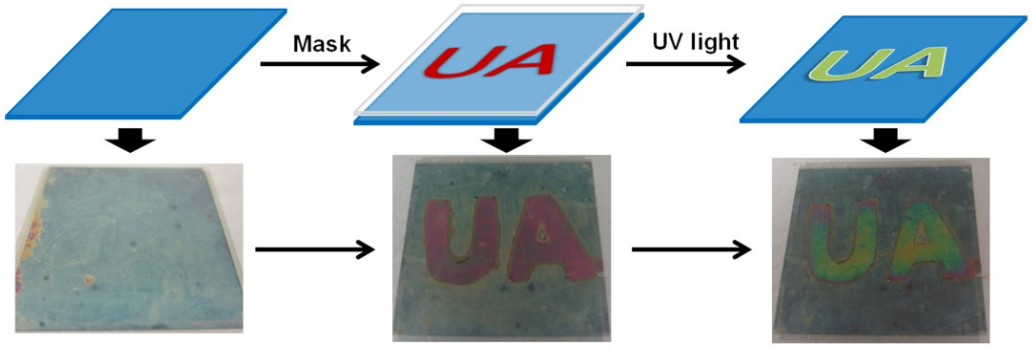

Figure 7-7. The color change of an etalon exposed to an *o*-NBA solution (5 mM) only in a specific region, which was defined by a PDMS mask. Upon UV exposure, the color of the device visually changes. Reproduced with permission from ref. 420, Copyright 2014, American Chemical Society.

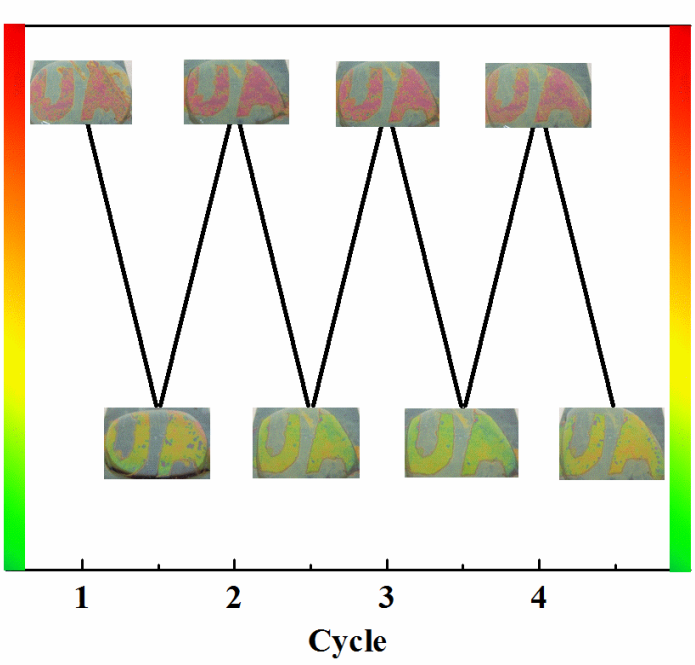

Figure 7-8. The reversibility of the etalon's color by repeated exposure to UV irradiation followed by the addition of fresh *o*-NBA solution. Reproduced with permission from ref. 420, Copyright 2014, American Chemical Society.

Finally, we patterned a single substrate such that a defined region contained pH-responsive microgels, while other regions contained non-pH responsive microgels. Specifically, we synthesized pNIPAm-based microgels with and without AAc, such that they were both approximately the same diameter (~600 nm). Using a PDMS mask, part of the etalon was covered and non-pH responsive pNIPAm microgels painted in the uncovered region -- in this case, the mask was in the shape of a maple leaf. Following this step, the mask was removed and the microgels allowed to dry and were rinsed following our defined protocol to yield a monolayer of microgel in that region.[144] Then, the rest of the substrate (the maple leaf region) was painted with p(NIPAm-*co*-AAc) microgels. Again, our previously described protocol was used to yield a single microgel layer in that region.[144] Following the coating of the respective regions of the substrate with microgels, the whole substrate was covered with a thin layer of Au

to yield an etalon. As can be seen in Figure 7-9, after soaking the device in the 5 mM *o*-NBA solution with pH ~7, the different regions appeared similar in color, showing the uniformity of the patterned regions. The system was then exposed to UV irradiation and a photograph of the device taken every one minute. The device clearly changes color in the region where the p(NIPAm-*co*-AAc) were painted, while the region containing the pNIPAm microgels remained unchanged. Again, the region containing the p(NIPAm-*co*-AAc) microgels is reacting to the UV-induced solution pH changes, changing the distance between the etalon's Au layers, while the pNIPAm microgels remain unresponsive to the solution pH changes. The maple leaf color change also can be repeated by immersing the etalon into a fresh *o*-NBA solution and re-exposure to UV light.

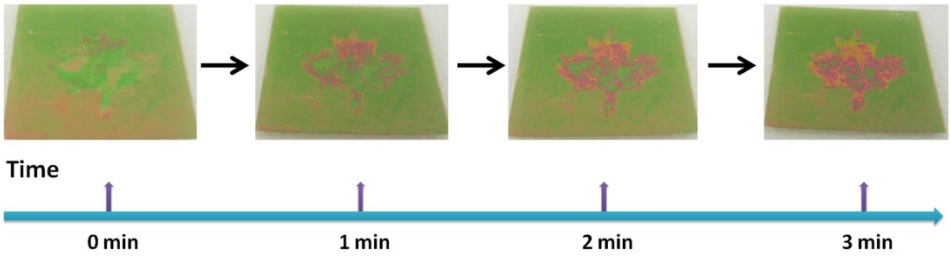

Figure 7-9. The response of a patterned etalon immersed in *o*-NBA solution (5 mM) after exposure to UV irradiation for the indicated times. In this case, the maple leaf region was composed of pH-responsive p(NIPAm-*co*-AAc) microgels, while the rest of the device was composed of non-pH responsive pNIPAm microgels. Reproduced with permission from ref. 420, Copyright 2014, American Chemical Society.

Furthermore, we study the light controlled drug release behavior from this device and the results are shown in Figure 7-10. The costumed slide is put into the cuvette and fill with pH 6.5 solution with *o*-NBA (5 mM), after exposed to a different time of UV irradiation, the release profile is plotted as well as the pH is monitored during the releasing process. We can see clearly

that the release rate is well controlled by the irradiation time. With longer irradiation, the releasing is faster, however, with short irradiation, the releasing is slower. This proves the concept that this system can be used to develop a light triggered drug release system.

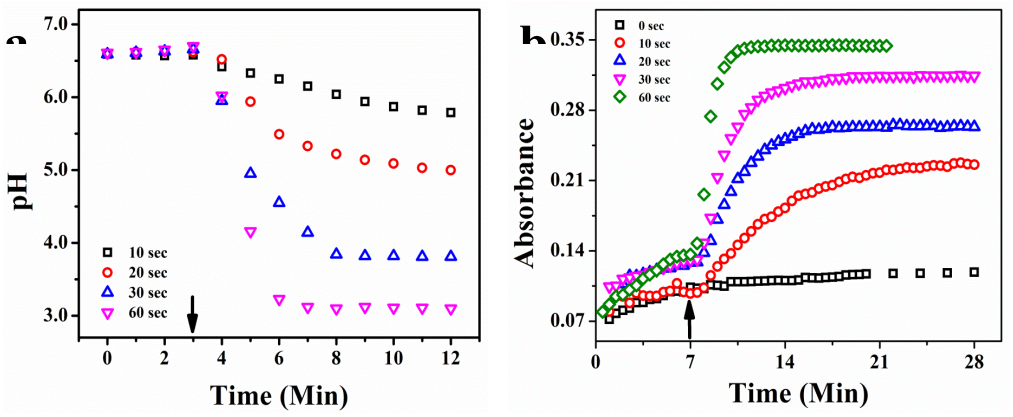

Figure 7-10. pH change with UV irradiation time and relatively drug release profile from this device.

7.4 Conclusion

In conclusion, we show that UV light could be used to decrease the pH of an aqueous solution containing *o*-NBA. This is a direct result of the UV light inducing the *o*-NBA to release a proton. Furthermore, by immersing a p(NIPAm-*co*-AAc) microgel assemblies based device in this solution, we were able to tune its optical properties upon UV irradiation. This was a direct result of the p(NIPAm-*co*-AAc) microgels changing solvation state in response to the solution pH changes, which directly alters the optical properties of the device. We were able to fabricate patternes on it and change the visual color in those specific regions. Finally, the optical properties of the devices were reversible by simply adding fresh *o*-NBA solution and reexposing the device to UV light. These unique properties will be exploited in the future for display technologies and controlled/triggered drug delivery.

Chapter 8: Controlled Drug Release from the Aggregation-Disaggregation Behavior of pH-Responsive Microgels[g]

In this chapter, pH-responsive microgels based system with controllable aggregation and disaggregation was developed and controlled drug release behavior was studied. Specifically, pH-responsive microgels exhibit opposite charges over a given solution pH range were synthesized. We showed that the microgels aggregated when they are mixed in one pH range, which could be used to trap/load a small molecule model drug. Changing the pH will induce the disaggregation and release the payload.

8.1 Introduction

Polymer microgels are colloidally stable crosslinked hydrogel particles, which have a swollen network structure in a suitable "good" solvent.[116, 118, 123, 485] Microgels have attracted much attention in theoretical studies of soft matter[486-488] and for various applications[489, 490] over the past several decades. In particular, they have rapidly gained considerable importance in materials science owing to their potential applications in drug delivery,[264, 491] sensing,[374, 492, 493] photonic crystal fabrication,[144, 465, 494] and separation and purification technologies.[495] Most of these applications are a direct result of their ability to be rendered responsive to external stimuli, i.e., they can be engineered to undergo reversible solvation state changes in response to environmental stimuli such as pH,[18, 460] temperature,[116, 121] ionic strength of the surrounding medium,[496] light, [497, 498] electric field[499] and magnetic field.[500] The solvation state of the microgels is often a result of the imbalance/balance between repulsive and attractive forces acting on the particles. Small molecules are easily introduced into microgels via

[g] This Chapter has been adapted from the previously published article: Y. Gao,[†] A. Ahiabu,[†] M. J. Serpe.* *ACS Appl. Mater. Interfaces*, 2014, 6, 13749-13756.

copolymerization of functional comonomers into the microgels, or post-polymerization modification, that can lead to these forces and the resultant responsivity.[121, 501]

Poly (*N*-isopropylacrylamide) (pNIPAm) is by far the most extensively studied responsive polymer to date.[13, 502,503-505] PNIPAm-based hydrogel particles (microgels) have the ability to be fully water swollen (large diameter) and dehydrated (small diameter) by changing the temperature. PNIPAm-based micro and nanogels are most easily synthesized via free radical precipitation polymerization.[506, 507] This approach is versatile in terms of the variety of chemical modifications that can be made to the microgels by simply adding functional monomers to the reaction solution prior to the initiation. Using this approach, pNIPAm-based microgels with a variety of chemical functionalities have been synthesized.[170, 508] The most commonly used comonomer is acrylic acid (AAc),[144] which renders the p(NIPAm-*co*-AAc) microgel pH-responsive, and can also be used to further modify the microgels with other small molecules.[171] The pH responsivity is a result of the pK_a of the AAc group. That is, the pK_a for AAc is ~4.25,[509] so when the pH of the environment is < 4.25, the AAc groups are protonated and neutral (although a slight microgel charge can exist depending on the initiator used), and when the pH > 4.25, the microgels are deprotonated and negatively charged. Similarly, positively charged microgels can be obtained by copolymerizing with amine-containing comonomers like, *N*-[3-(Dimethylamino)propyl]methacrylamide (DMAPMA), whose pK_a is ~8.4.[510] Therefore, at pH < 8.4, these microgels are positively charged and exhibit attractive electrostatic interactions with negatively charged species,[511, 512] while they have minimal interactions with negatively charged species at high pH (>8.4). This behavior is completely reversed for AAc-modified microgels, which exhibit attractive interactions with positively charged species at pH > 4.25. Thus, these microgels are protonated at higher pH and neutral at lower pH.

Stimuli-responsive microgels have been used and developed for drug delivery systems in the past.[117, 264, 513, 514] A variety of different stimuli have been engineered into these systems to allow the release of small molecules in a triggered and controlled fashion. The primary triggers for release from microgel-based drug delivery systems are temperature and pH. Microgels have been used as drug carriers by exploiting different forces, such as electrostatic interactions,[299] hydrogen bonding,[515] or bioconjugate interactions.[117] The drug molecules can diffuse out of the microgels by exposure to an external environment that interrupts these interactions. In most of the cases, the drug loading process is complex[516] and the loading efficiency of the microgels (or microgel-based systems) is typically limited owing to the size of the microgels. In light of this, it is imperative to find a more effective way of minimizing these disadvantages, making microgel-based technologies viable for drug delivery.

In this study, we developed a facile method to entrap a small molecule model drug methylene blue (MB) into microgels by aggregating microgels of opposite charges in the presence of MB. P(NIPAm-*co*-AAc) and p(NIPAm-*co*-DMAPMA) microgels were used as negatively and positively charged microgel moieties, respectively. The electrostatic interaction between these two microgels (at given pH) can cause the formation of large aggregates and concomitant loading of the drug. Using this approach, we envisage that the drug loading efficiency will be dramatically increased. The pH-triggered aggregation of the microgels and the resultant release of MB from the microgels due to disaggregation at certain pH were investigated and were shown to be a viable option for a drug delivery system.

8.2 Experimental section

Materials: Unless otherwise specified, all reagents were purchased from Sigma-Aldrich. *N*-Isopropylacrylamide (NIPAm) was purified by recrystallization from hexanes prior to use. *N*, *N'*-

Methylene(bisacrylamide) (BIS), acrylic acid (AAc), *N*-[3-(dimethylamnino)propyl] methacrylamide (DMAPMA) and ammonium persulfate (APS) were used without further purification. Methylene blue (MB) was used as the model drug. UV-Vis spectrometer (Hewlett-Packard Diode Array Spectrometer) was used to monitor the release of the model drug. pH meter (JENCO 6173 pH) was used to prepare the pH solutions using sodium hydroxide (NaOH) and hydrochloric acid (HCl) to adjust the pH. Millipore water (18.2 MΩ cm) from a Milli-Q Plus system (Fisher, Z00QSVC01) was used in this experiment. Scanning electron microscope (SEM) (JSM-6010LA JEOL, Peabody, MA.) was used to image the aggregates.

Synthesis of p(NIPAm-*co*-AAc) microgels: p(NIPAm-*co*-AAc) The microgels were synthesized following a previously published procedure.[18, 144] A 3-necked flask was fitted with a reflux condenser, nitrogen inlet, and temperature probe), and charged with a solution of NIPAm (11.9 mmol) and BIS (0.703 mmol) in 99 mL deionized water, previously filtered through a 0.2 μm filter. The solution was purged with N_2 and allowed to heat to 70 °C for 1.5 hr. AAc (1.43 mmol) was added to the heated reaction mixture in one aliquot, and immediately initiating the reaction with a solution of APS (0.2 mmol) in 1 mL of deionized water. The reaction was then allowed to proceed at 70 °C for 4 hours under a blanket of nitrogen. The resulting suspension was allowed to cool overnight, and filtered through a Whatman #1 filter paper to remove any large aggregates. The microgel solution was then distributed into centrifuge tubes and purified via centrifugation at ~10000 rpm for ~30 min to form a pellet, followed by removal of the supernatant and resuspending in deionized water, 6x.

Synthesis of p(NIPAm-*co*-DMAPMA) microgels: These microgels were synthesized similarly to the above protocol. A 3-necked flask was fitted with a reflux condenser, nitrogen inlet, and temperature probe), and charged with a solution of NIPAm (11.9 mmol) and BIS

(0.703 mmol) in 99 mL deionized water, previously filtered through a 0.2 μm filter. The solution was purged with N_2 and allowed to heat to 70 °C for 1.5 hr. DMAPMA (1.43 mmol) was added to the heated reaction mixture in one aliquot, and immediately initiating the reaction with a solution of APS (0.2 mmol) in 1 mL of deionized water. The reaction was then allowed to proceed at 70 °C for 2 hours under a blanket of nitrogen. The resulting suspension was allowed to cool overnight, and filtered through a pad of glass wool to remove any large aggregates. The microgel solution was then distributed into centrifuge tubes and purified via centrifugation at ~10000 rpm for ~30 min to form a pellet, followed by removal of the supernatant and resuspending in deionized water, 6x.

Aggregation of microgels: A 1:1 (v/v) ratio (50:50 μL) concentrated microgels of p(NIPAm-*co*-AAc) and p(NIPAm-*co*-DMAPMA) were mixed in a glass vial containing1000 μL pH solutions (pH 2, 4, 5, 7, 9, 10 and 12). The pH solutions were prepared using HCl and NaOH with the ionic strength adjusted to 2.0 mM using NaCl.

UV-vis spectroscopy: The absorbance of the supernatant solutions from the aggregation studies was measured. In each case, 200 μL of the supernatant from all pH solutions were diluted with 2000 μL of a solution with the same pH.

Drug release: Efficient aggregation was observed for microgels mixed at pH 5 and 7, so the drug was loaded at this pH and released at pH 2 and 10 (where no or little aggregates were observed). The aggregated microgels were kept in a vial and placed in a beaker containing either 5 mL pH 2 or 10 solutions and covered. The temperature was set to 25 °C and with a stirring rate of 80 rpm. The release of the drug was monitored every 5 min for 1 h, and every 10 min for another 1 h and finally every 20 min until the release profile plateaued. We showed the controlled release of the drug by loading the drug at pH 5, and released at pH 10 for 4 h, after

which 0.1 M HCl was added to drop the pH of the solution from 10 to 2, monitoring the release for another 4 h.

Characterization of Aggregates: Scanning electron microscopy (SEM) was done on the mixed microgels at different pH. The samples were taken from pH 2, 5, 7 and 12, and dried for 2 days. Before doing the SEM, samples were coated with ~10 nm layer of Au by sputter.

8.3 Results and discussion

As mentioned above, the microgels used in this study were synthesized via free radical precipitation polymerization, as previously described.[144] The microgels were composed of functional groups that render them negatively and positively charged at certain pH, while they are neutral otherwise. This is due to the different pK_a values for AAc (~4.25) and DMAPMA (~8.4); therefore when the pH is below the pK_a of AAc group, p(NIPAm-*co*-AAc) microgels are neutral and p(NIPAm-*co*-DMAPMA) microgel are positively charged, while when the pH of the solution is greater than the pK_a for DMAPMA, the p(NIPAm-*co*-AAc) microgels are negatively charged, while the p(NIPAm-*co*-DMAPMA) are neutral. In the range of pH 4.25 - 8.4 both sets of microgels are charged to different extents, which leads to various degrees of p(NIPAm-*co*-AAc)/p(NIPAm-*co*-DMAPMA) microgel aggregation when they are mixed. During the aggregation, small molecule model drugs in the surrounding solution can be trapped inside the aggregates, as depicted in Scheme 8-1. This phenomenon is in accordance with the scrambled egg model.[512] In this study, we used a dye molecule (methylene blue, MB) as a model drug, the structure is also presented in Scheme 8-1, and it is a positively charged molecule, independent of solution pH.

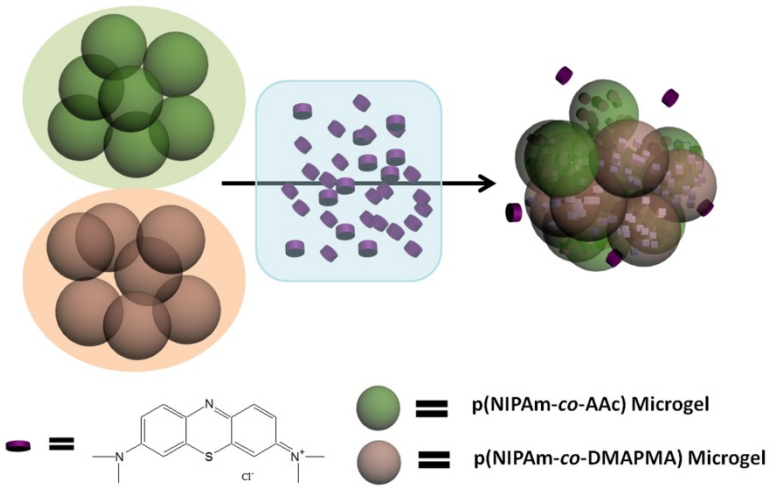

Scheme 8-1. Aggregate formation and model drug (methylene blue) trapping when microgels are mixed at pH that renders them both charged. Reproduced with permission from ref. 298, Copyright 2014, American Chemical Society.

To evaluate the aggregation behavior, the microgels were mixed together at various pH. A photograph image of the aggregated microgels themselves without MB at different solution pH is shown in Figure 8-1. We noted that the microgels at pH 2 and 12 do not visually aggregate, and the microgel solution remains turbid indicative of the microgels remaining dispersed in the solution. This is quite different when the microgels are mixed together at pH 5 and 7, where the microgels visually aggregate into large structures. To further investigate the aggregation behavior, their size and morphology were evaluated using SEM, and the results can be seen in Figure 8-2. At pH 2 and 12, the SEM images clearly show that the microgels are not aggregated and appear individually on a substrate. However, at pH 5 and 7, large aggregates were formed and the size is around 2 mm x 4 mm, which is big enough to be seen visually. Most of the microgels were involved in the formation of the aggregates, which left the solution less turbid (because there were minimal microgels left unaggregated in the solution). The relative differences in the sizes of aggregates are shown in Figure 8-3. The SEM images show that the

aggregates are tightly bound to one another, which increases their ability to uptake model small molecule drugs. This is due to the interstices between the aggregated microgels effectively trapping the small molecule, as we have shown previously for water remediation applications.[495, 517-519]

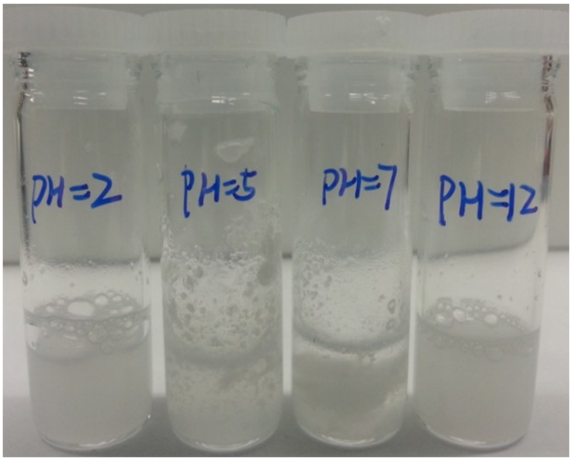

Figure 8-1. Photograph of microgel-based aggregates in solutions of the indicated pH.

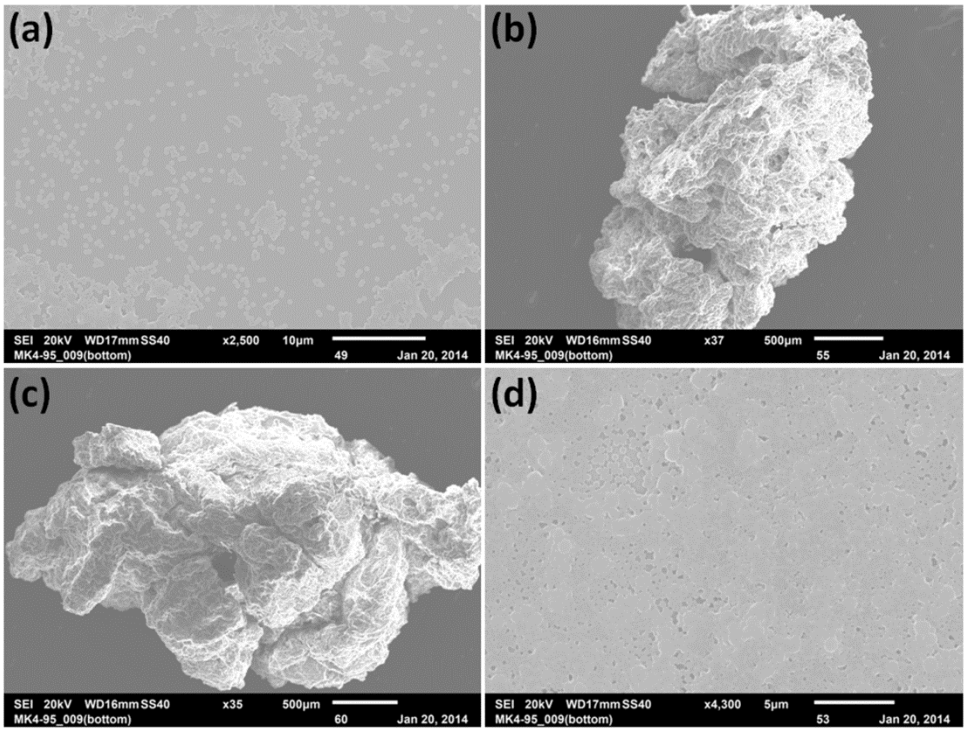

Figure 8-2. Scanning electron microscope (SEM) images of samples recovered after the two sets of microgels were mixed in solutions of pH (a) 2; (b) 5; (c) 7; (d) 12. Reproduced with permission from ref. 298, Copyright 2014, American Chemical Society.

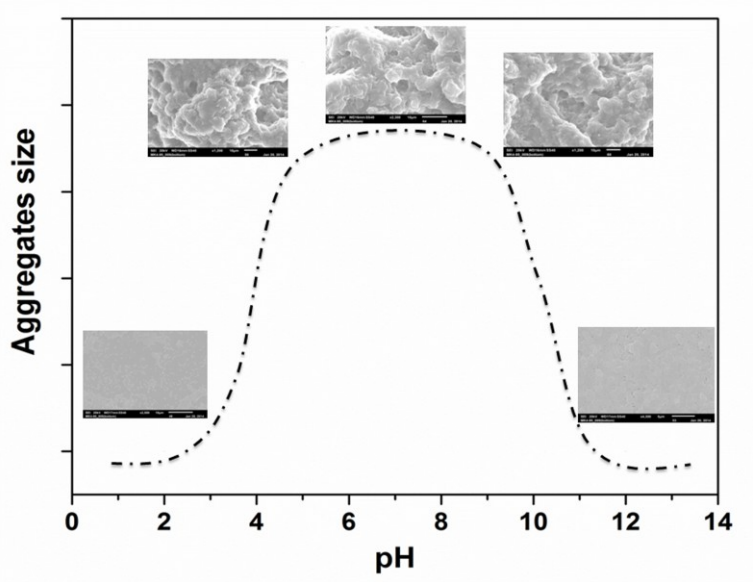

Figure 8-3. SEM images showing the relative aggregate sizes of the microgels at different pH.

When aggregates are formed in the presence of the dye molecule MB, we expect the most efficient trapping at pH 5, 7 and 9, while we expect the least amount of aggregation at pH 2 and 12. To generate the aggregates in the presence of MB, 1.0 mL of 0.5 mg/mL MB solution was added to individual glass vials, and diluted to a total volume of 10 mL with the appropriate pH solution, bringing the final concentration of MB to 0.05 mg/mL. For these experiments, solution pH of 2, 4, 5, 7, 9, 10, 12 was used, and the solutions were vivid blue in each case, as can be seen in Figure 8-4a. Then 50 μL of each microgel, taken directly from a centrifuged microgel pellet (see experimental section), was added one at a time to these pH solutions; p(NIPAm-*co*-AAc) microgels were always added to the solution first followed immediately by pNIPAm-*co*-DMAPMA microgels. The aggregates formed immediately upon addition of the two microgels to the appropriate pH solution. As can be seen in Figure 8-4b, the dye was trapped inside the microgels aggregated in solutions of certain pH as is evidenced by the color of the aggregates and the associated decoloration of the solution. As can be seen from the results, almost no visual aggregates were formed in solutions of pH 2 and 12 (where one of the microgels is neutral, while the other is charged), while large aggregates were formed at pH 5, 7 and 9. Some aggregates were formed at pH 4 and 10 (near the two different pK_a values), but these aggregates were much less efficient at trapping MB. In order to investigate whether the MB dye molecules contribute to the formation of the aggregates, two control experiments were conducted. The addition of only one set of microgels to MB solutions of the various pH had no effect on the aggregation state of the microgels, meaning that the aggregation is achieved only when the different microgels are together in their charged state.

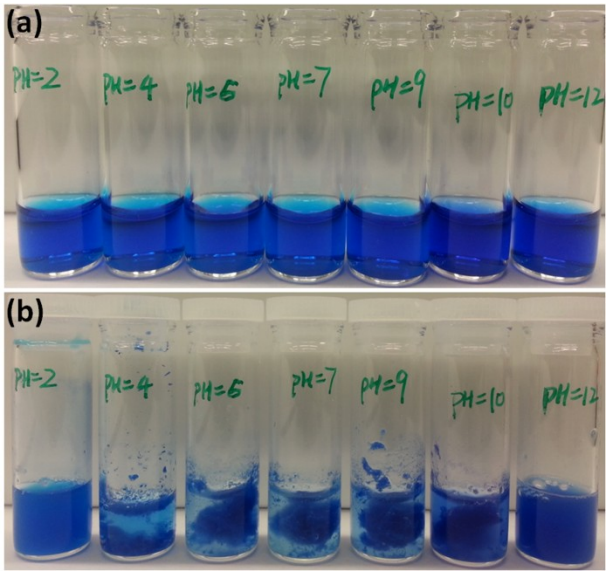

Figure 8-4. Photographs of methylene blue (MB) solutions at the indicated pH (a) before and (b) after addition and aggregation of the individual sets of microgels. Reproduced with permission from ref. 298, Copyright 2014, American Chemical Society.

Before studying the drug release properties of the aggregates, the ability of the aggregates to trap MB at the different pH was further investigated. To do this, the absorbances of MB solutions were measured by UV-vis spectroscopy, before and after aggregates were formed, and removed from the MB solutions. Specifically, 200 μL of the MB solution (0.05 mg/mL) was diluted with 2.0 mL of a given pH solution, and the initial absorbance measured. In this case, we measured the absorbance value at MB's λ_{max} of 664 nm, and the results are shown in Figure 8-5. As can be seen, the solution pH minimally affects the MBs optical properties. Similar to what was observed above, the amount of MB left in solution after aggregation of the microgels depends dramatically on pH; at pH values where the most efficient aggregation take place, almost all of the MB were removed from the solution. However, the absorbance of the remaining solutions when the "aggregates" were formed at pH 2 and 12 was high due to the excess MB present. It must be noted that p(NIPAm-*co*-AAc) microgels are negatively charged at high pH,

which can allow them to electrostatically bind with MB. However, we have shown that the aggregation has a much greater effect on the uptake than electrostatics alone, see Figure 8-6. In this case, there are no aggregates formed but the negative p(NIPAm-*co*-AAc) microgels will electrostatically interact with positive MB molecules. Also, zeta potential measurements of the individual p(NIPAm-*co*-AAc) and p(NIPAm-*co*-DMAPMA) microgels further confirm this aggregation behavior. At the extreme pH values (i.e., pH 2 and 12), only one set of the microgels is charged (for example, pNIPAm-*co*-AAc is negatively at pH 12 while p(NIPAm-*co*-DMAPMA) is positively charged at pH 2. However, at pH ranges between these shaded portions, the two sets of microgels have strong opposite charges, which have a high tendency of allowing the formation of aggregates.

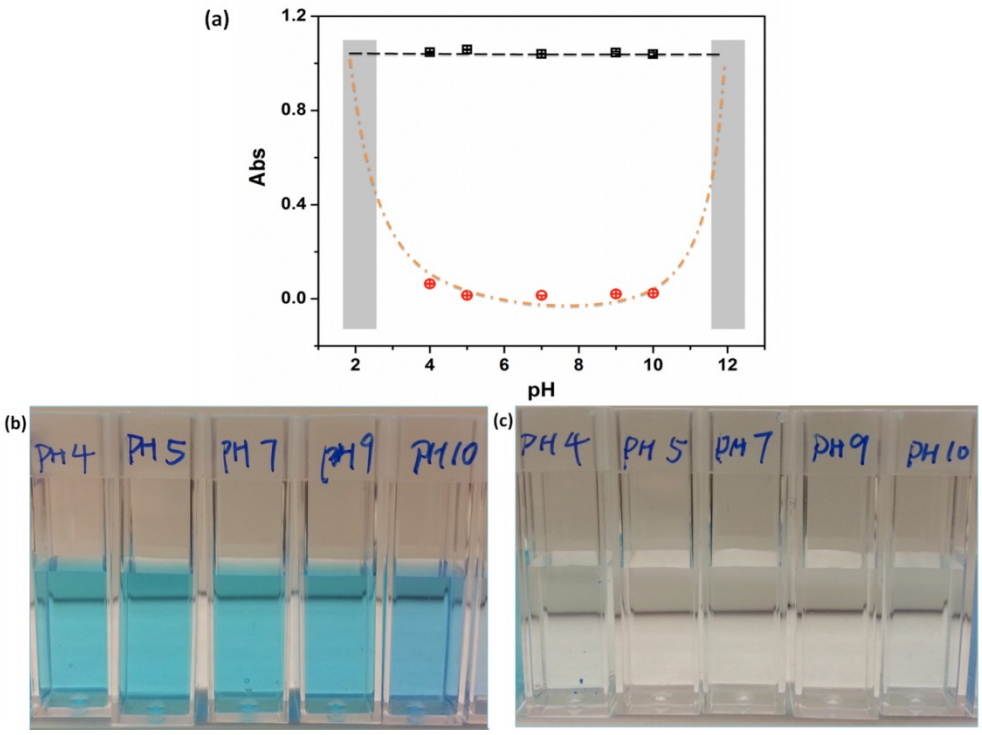

Figure 8-5. a) UV-vis absorbance values from MB solutions at the indicated pH (□) before and (O) after microgel aggregation (and removal from solution). Photographs of the remaining

solutions at the indicated pH b) before and c) after microgel aggregation. Reproduced with permission from ref. 298, Copyright 2014, American Chemical Society.

Next, the ability of the aggregates to release MB at different pH was investigated. This was done by isolating the aggregates formed at pH 5 and 7 and exposing the aggregates to solutions that have pH values that render one of the sets of microgels neutral. To do this, a glass vessel containing 5.0 mL aqueous solution (either pH 2 or 10) was placed on a hot plate to control the solution temperature at 25 ^{o}C, while the solution was stirred at a rate of 80 RPM. Then a small vial containing the MB loaded aggregates was immersed into the glass container such that the liquid filled the small vial and contacted the aggregates. At this point, a timer was started. The whole assembly was covered with a glass slide to prevent the water from evaporating. The aggregates were placed in the small vial to keep them from becoming damaged from the stirring. At a given time intervals, 2.0 mL of the solution was removed from the release vessel, and a UV-vis spectrum acquired. In pH 2, the absorbance was taken every 5 min for the first 1 h, then every 10 min in the second hour and every 20 min in the third hour, until the release profile plateaued. In pH 10, the release was slow (due to the AAc charge), so absorbance was taken at less frequent intervals. Following each UV-vis measurement, all the liquid was carefully returned to the release vessel. The results are shown in Figure 8-7. Figure 8-7a shows the release profiles for aggregates formed at pH 5. As can be seen, the MB is released very quickly from the aggregates at pH 2, with the release completing in ~ 5 h. However, at pH 10, the release was so slow that the absorbance was still lower than 0.2 even after 50 h, which is much slower than releasing in pH 2 (absorbance reached this value in 15 min). Therefore, the MB can be released at a rate that is controlled by pH. Figure 8-7b shows the same experiments, but for the aggregates formed at pH 7. As can be seen, the same phenomenon was observed for these aggregates; very fast release for

the aggregates exposed to pH 2 solution, while very slow release at pH 10. When in lower pH (~2), the electrostatic interaction between microgels disappeared and disaggregation occurred, making the diffusion of the MB molecules out of the microgels much easier. At the same time, pNIPAm-*co*-DMAPMA microgels are positively charged at this pH, which will form a repulsive force with the positively charged MB molecules, hence dramatically increasing the diffusion of MB out of the microgel aggregates. Therefore, the disaggregation and repulsive forces, in combination with the AAc neutralization, are the collective forces that contribute to the faster release at pH 2. However, at pH 10, while the aggregates still broke up due to the neutralization of the p(NIPAm-*co*-DMAPMA) microgels, the p(NIPAm-*co*-AAc) microgels are fully negatively charged, which cause them to form attractive electrostatic interactions with MB molecules (Figure 8-5). This makes the release of MB from the aggregates much slower. We can clearly see that even after releasing, the solution color turned blue in pH 2, while it is almost colorless in pH 10.

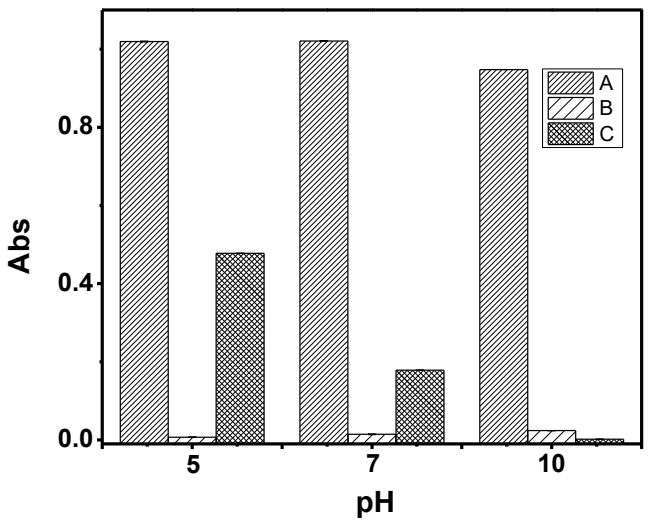

Figure 8-6. Absorbance values for MB solutions at the indicated pH. A) MB solutions before addition of microgels, (B) after microgel aggregation, and (C) after addition of just the

p(NIPAm-*co*-AAc) microgels alone and centrifugation to remove the microgels from solution. Reproduced with permission from ref. 298, Copyright 2014, American Chemical Society.

The electrostatic interaction between MB and the p(NIPAm-*co*-AAc) microgels becomes stronger as the solution pH increases, leading to more uptakes of MB, and less left over in solution. Although, at the pH here, the amount of MB left over in solution after aggregation is the same indicating that the aggregates are able to trap MB, in addition to the electrostatic interactions.

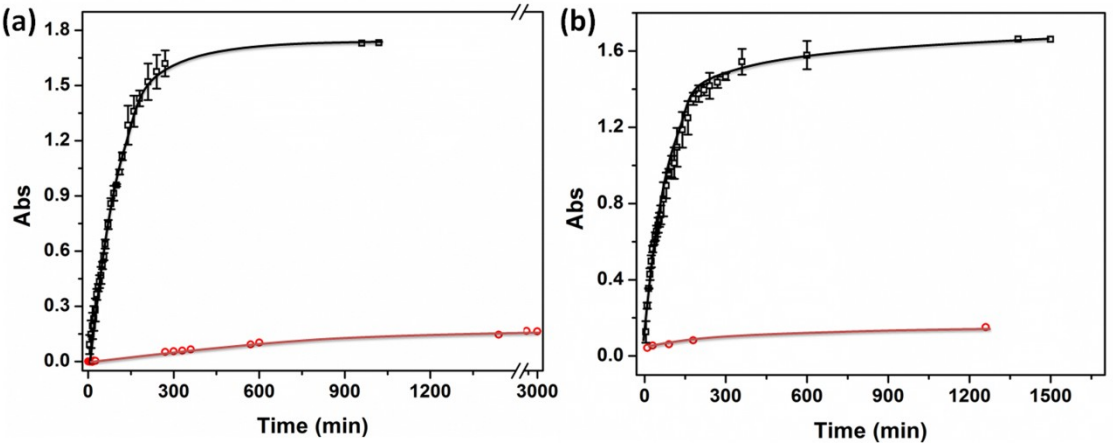

Figure 8-7. Drug release profiles in (□) pH=2 and (O) pH=10 solutions for aggregates formed at (a) pH=5 and (b) pH=7. Each point is the average of 3 individual experiments, while the error bars are the standard deviations. Reproduced with permission from ref. 298, Copyright 2014, American Chemical Society.

Following this, we investigated the ability of the aggregates to release MB in a pH-triggered fashion. To do this, the aggregates were first immersed in a pH 10 solution and the release profile was measured over ~4 h. The solution pH was then reduced from pH 10 to 2, by the addition of HCl, and the release was continuously measured. The results are shown in Figure 8-8. When the pH was changed from 10 to 2 at 270 min, the absorbance increased immediately,

eventually stabilizing at 0.8. This result shows that changing the pH can trigger the release of the model drug MB.

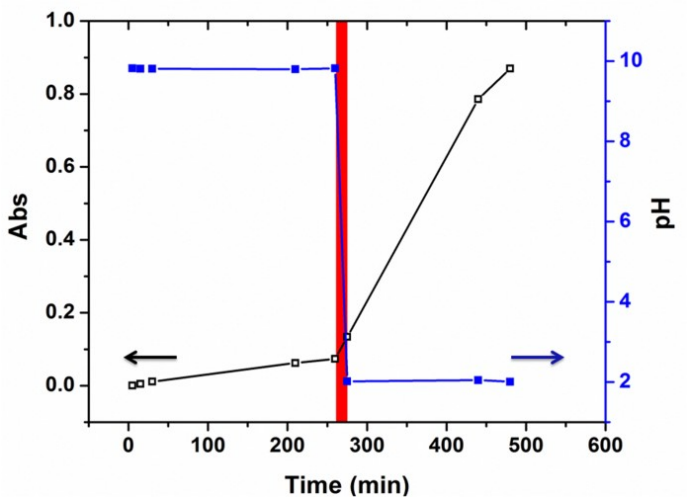

Figure 8-8. Triggered small molecule release from the microgel-based aggregates upon changing the solution pH from 10 to 2 at the same time indicated by the shaded region. Reproduced with permission from ref. 298, Copyright 2014, American Chemical Society.

8.4 Conclusion

In conclusion, we synthesized pH-responsive microgels, which exhibit opposite charges over a given solution pH range. We showed that the microgels aggregated when they are mixed in this pH range, which could be used to trap/load a small molecule model drug methylene blue. We showed that the loading efficiency was greater when the microgels aggregated, compared to simply relying on electrostatic interactions for loading. Finally, we showed that the methylene blue could be released in a pH-dependent fashion over many hours/days at certain pH conditions. This is a clear demonstration of how microgel-based technology could be used for health-related applications, which could be used to release biologically relevant molecules at low pH environments typically found at tumor sites.

Chapter 9: Supramolecular Microgels Fabricated from Supramonomers[h]

In this chapter, we employed the concept of supramonomers for the fabrication of supramolecular microgels. Supramonomer-based crosslinker was prepared by the host-gust interaction between tri-peptides and curcubit[8]uril, and this crosslinker was applied to chemically synthesize the supramolecular microgels. The supramolecular microgels exhibit not only thermal responsive properties as conventional microgels but also dynamic and degradable properties due to the introduction of supramonomers.

9.1 Introduction

Supramonomers are bifunctional monomers that are generated via their noncovalent interaction with a chemical unit that holds them together, which can be utilized in the fabrication of supramolecular polymers.[520] Different from the traditional supramolecular polymerization,[521-533] supramonomers are first fabricated through noncovalent synthesis, and then supramolecular polymers are constructed through traditional (covalent) polymerization of the supramonomers. In the past few years, efforts have been made for the synthesis of supramolecular polymers from various types of supramonomers through different polymerization methods, demonstrating its general applicability in the fabrication of supramolecular polymers.[534-539] Meanwhile, it is of significant importance to employ the dynamic nature of supramonomers for the fabrication of functional supramolecular materials.

Poly (*N*-isopropylacrylamide) (pNIPAm)-based microgels are well-known temperature responsive (i.e., thermoresponsive) materials that can be used for a variety of applications.[38, 116, 121, 158, 540-543] For example, they have been used for sensing,[130, 132, 544-547] chemical separation,[548]

[h] This Chapter has been adapted from the previously published article: Q. Song,[†] Y. Gao,[†] J. Xu, B. Qin, M. J. Serpe,* X. Zhang.* *ACS Macro Lett.*, 2016, 5, 1084-1088.

drug delivery,[117, 299, 549] and artificial muscles.[550-552] PNIPAm-based microgels are typically synthesized by copolymerizing NIPAm with various functional monomers using *N*, *N*'-methylenebis(acrylamide) (BIS) as cross-linker in aqueous solution. Microgels fabricated in this way are of thermoresponsive, however with BIS as cross-linker, the covalently cross-linked microgels are undegradable, which might limit their use in certain conditions, such as biological and environmental.

In this work, supramonomers were used as a supramolecular cross-linker to fabricate supramolecular microgels. The dynamic nature of supramonomers may endow the supramolecular microgels with stimuli-responsive and degradable properties. As shown in Scheme 9-1, we first designed and synthesized a guest molecule, Phe-Gly-Gly linked with an acrylate moiety via esterification reaction (FGG-EA). Based on the specific host-guest supramolecular complexation, the tripeptide derivative FGG-EA was allowed to complex with cucurbit[8]uril (CB[8]) in a molar ratio of 2:1 to give supramonomers with one acrylate moiety at each end.[553-558] Then the supramonomers were used as a supramolecular cross-linker to copolymerize with NIPAm in aqueous solution, obtaining supramolecular microgels, which we hypothesize, will exhibit both the thermoresponsive of the pNIPAm-based microgels and degradable properties attributed to the supramonomers. The concept of supramonomers provides us a facile strategy towards the fabrication of supramolecular microgels, which may greatly enrich the application of microgels.

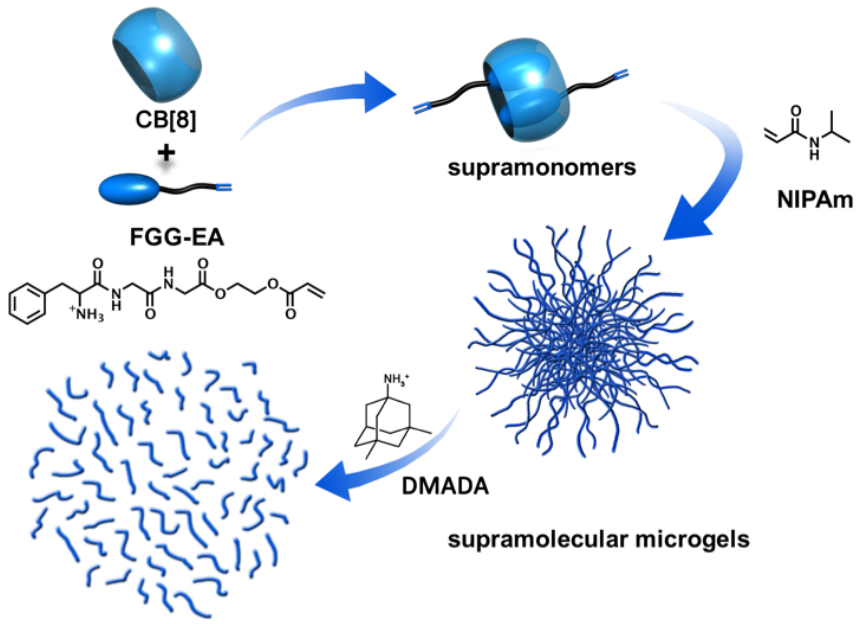

Scheme 9-1. Fabrication of supramolecular microgels from supramonomers. Reproduced with permission from ref. 166, Copyright 2016, American Chemical Society.

9.2 Experimental section

Materials preparation: Boc-FGG-EA: Boc-FGG 1.0 g (2.64 mmol) was dissolved into 60 mL dry CH_2Cl_2 and *N, N'*-carbonyldiimidazole 0.5 g (3.13 mmol) was then added to the solution. The mixture was stirred for 5 h at room temperature until lots of white precipitates appeared. Then 600 μL (5.71 mmol) 2-hydroxyethyl acrylate was added into the solution. The mixture was stirred for 20 h at room temperature to acquire a transparent solution. After mixed with 50 mL NaCl saturated aqueous solution (with 1 mM HCl), the solution was extracted with 100 mL CH_2Cl_2. Then the organic phase was dried with anhydrous Na_2SO_4 and filtered. The solvent was evaporated under reduced pressure. The crude product was purified via column chromatography (silica, CH_2Cl_2: methanol=10:1) to give the product as colorless oil (700 mg, yield: 56 %). ^{1}H NMR (JOEL JNM-ECA400, 400 MHz, $CDCl_3$, 25 °C): δ (ppm) = 1.39 (9H), 3.08 (2H), 3.98

(4H), 4.31 (1H), 4.38 (4H), 5.05 (1H), 5.88 (1H), 6.14 (1 H), 6.43 (1H), 6.70 (1H), 6.89 (1H), 7.26 (5H).

FGG-EA: Boc-FGG-EA 0.7 g (1.47 mmol) was dissolved in 10 mL CH_2Cl_2 and 2 mL CF_3COOH was then added into the solution. After stirring for 5 h at room temperature, the solvent was removed under reduced pressure and dissolved in 5 mL methanol. After precipitated in diethyl ether, FGG-EA was collected by filtration as a white powder (0.58 g, yield: 80 %). ^{1}H NMR (JOEL JNM-ECA400, 400 MHz, D_2O, 25 °C): δ (ppm) = 3.23 (2H), 3.94 (2H), 4.02 (2H), 4.30 (1H), 4.44 (4H), 5.98 (1H), 6.19 (1H), 6.43 (1H), 7.30 (2H), 7.39 (3H). as shown in Figure 9-1.

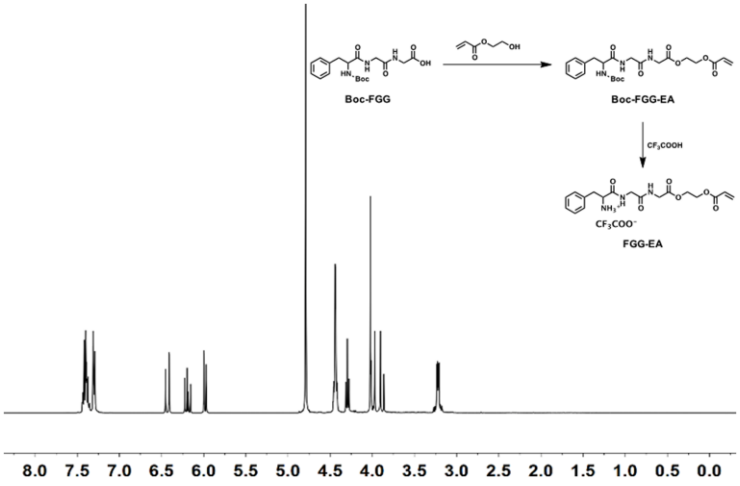

Figure 9-1. Synthesis of FGG-EA molecular and ^{1}H NMR of FGG-EA (400 MHz, D2O).

Microgel preparation: Supramolecular microgels were prepared by copolymerization of NIPAm and supramonomers. For a typical experiment, NIPAm (219.4 mg, 1.9 mmol), FGG-EA (98.28 mg, 0.2 mmol), CB[8] (161.6 mg, 0.1 mmol) were dissolved in 100 mL deionized water. Then the solution was heated to 70 °C under N_2 atmosphere. 14.0 mg ammonium persulphate (APS) was added to initiate the polymerization. After 2.5 h, the reaction mixture was allowed to cool down to room temperature and filtered through glass wool to remove any large aggregates.

Then the reaction mixture was centrifuged to produce a pellet at the bottom of the centrifuge tube. The supernatant was removed from the pellet of microgels, which was then resuspended to the original volume using deionized water. This process was repeated 3 times until the microgels were cleaned.

Methods: ^{1}H NMR spectra were recorded on either JOEL JNM-ECA400 apparatus (400 MHZ) or Agilent/Varian Inova spectrometer (four channel 500 MHz or two channel 400 MHz). UV-via spectra were obtained using a Hewlett-Packard diode array spectrometer. ITC (Isothermal Titration Calorimetry) experiment was carried out with a Microcal VP-ITC apparatus at 298.15 K. Size of the microgels was measured by Malvern ZEN3690 Zetasizer. Microscopic images were obtained using Olympus IX71. ESI mass spectrum was recorded by Agilent Technologies, 6220, Accurate-Mass-OATOF.

9.3 Results and discussion

The supramonomers were prepared by simply mixing FGG-EA and CB[8] in a molar ratio of 2:1 in aqueous solution. The formation of supramonomers was studied by ^{1}H NMR. As shown in Figure 9-2a, peaks at ~7.25 ascribed to the aromatic ring of FGG shifted to higher field after the complexation of FGG with CB[8] while no residual signals from free FGG were detected, indicating that FGG-EA and CB[8] formed a complex and the binding ratio should be 2:1. Moreover, ITC results further confirmed the formation of supramonomers. As shown in Figure 9-2b, there was an abrupt transition at a molar ratio of 2.0. By fitting the titration curve, the binding constant can be calculated to be 2.0×10^{11} M^{-2}. Therefore, the high binding affinity guarantees the formation of supramonomers with well-defined composition.

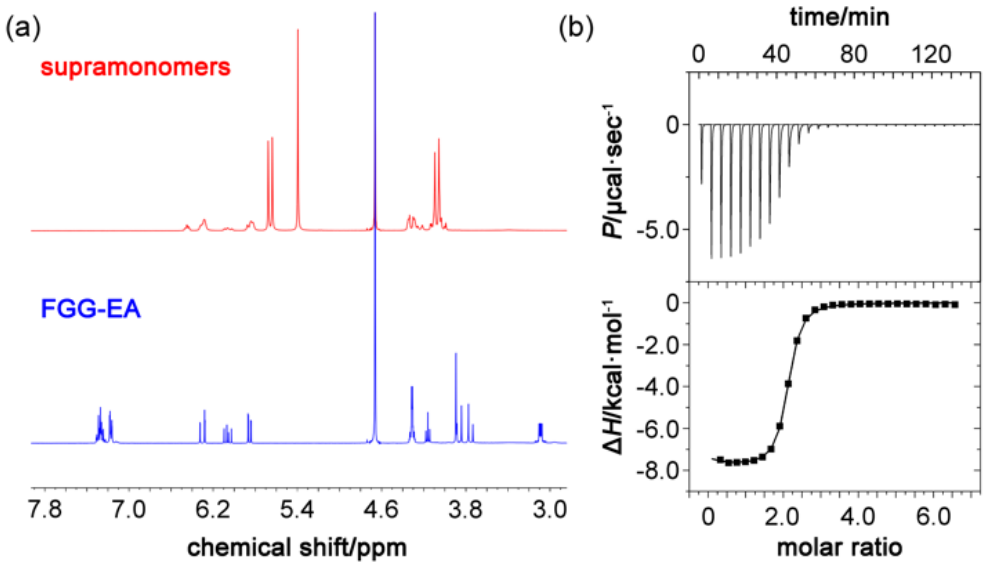

Figure 9-2. (a) Partial 1H NMR spectra of supramonomers and FGG-EA. (b) ITC data for titration of CB[8] (0.1 mM) with FGG-EA (2.0 mM) in 50 mM NaAc/HAc buffer (pH = 4.7) at 25 °C. Fitting data using two sets of the binding site model gave a binding constant of 2.0×10^{11} M-2. Reproduced with permission from ref. 166, Copyright 2016, American Chemical Society.

Furthermore, as can be seen in the electrospray ionization mass spectrometry (ESI-MS) spectrum in Figure 9-3, a molecular ion peak with a mass/charge ratio of 1042.36 was observed, which is in good agreement with the calculated molecular weight of the supramonomer with two positive charges. This suggests that the supramonomer is formed in the ratio of 2:1 of FGG-EA and CB[8].

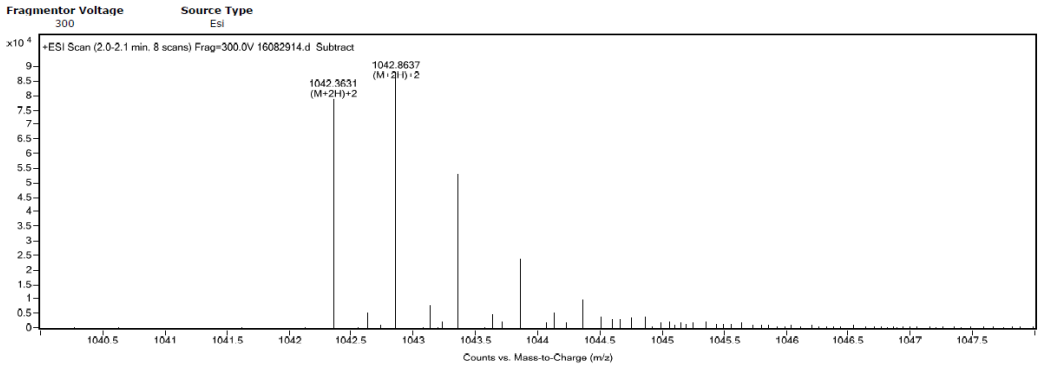

Formula Calculator Results

Formula	Ion Species	Mass	Calc. Mass	m/z	Calc. m/z	Diff (mDa)	Diff(ppm)	DBE	Ion	Score
C84 H94 N38 O28	C84 H96 N38 O28	2082.7109	2082.71	1042.3631	1042.3623	-0.95	-0.45	57	(M+2H)+2	95.85

Figure 9-3. ESI-MS spectrum of supramonomer.

Supramolecular microgels were then synthesized through the copolymerization of NIPAm and supramonomers with the supramonomer molar percentage of 5 %.[559] As shown in the transmission electron microscope (TEM) images, spherical microgels in the dry state with diameter around 400 nm were observed (Figure 9-4a). Furthermore, DLS gave detailed size information about the microgels (Figure 9-4b). The hydrated diameter of the microgels was ~900 nm at 25 °C, which decreased to ~550 nm at 45 °C, demonstrating the thermoresponsive. The lower critical solution temperature (LCST) of the microgels was measured based on turbidimetric analysis attributed to light scattering. The absorbance (i.e., scattering) of the microgel aqueous dispersions was investigated by measuring UV-vis spectra at various temperatures. By plotting the absorbance at 250 nm against temperature, as shown in Figure 9-4c, the LCST of microgels is around 37 °C. In addition, we cycled the temperature between 25 °C and 45 °C over many times. The size of the supramolecular microgels was consistent from cycle to cycle, as in Figure 9-5, showing good reversibility and stability, which guarantees its practical application as conventional pNIPAm-based microgels.

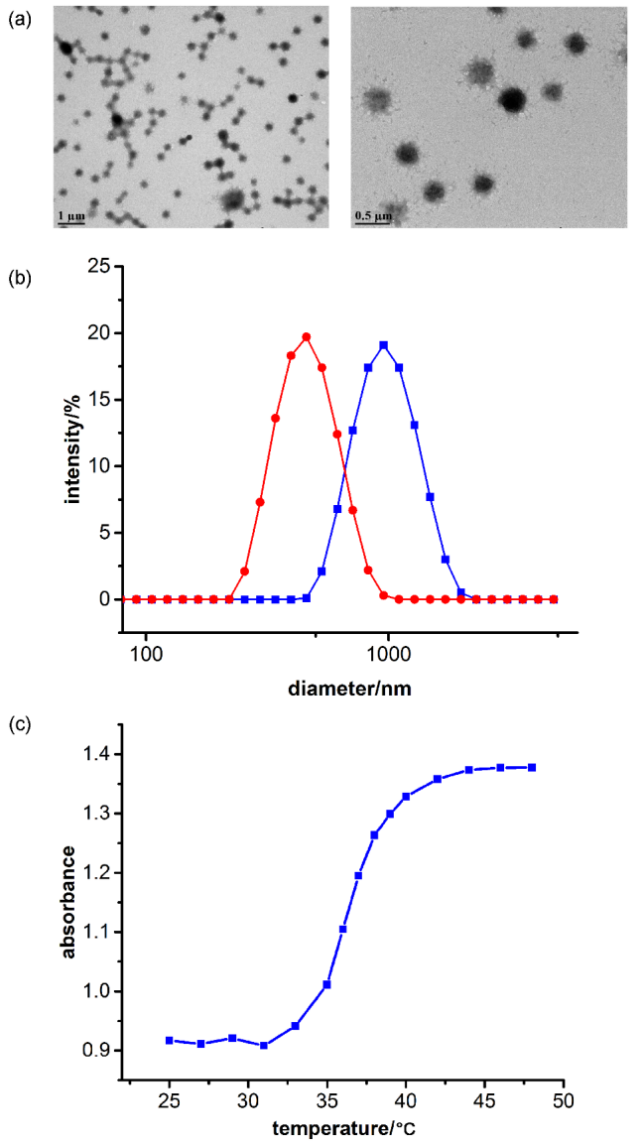

Figure 9-4. (a) TEM images of supramolecular microgels. (b) DLS data of supramolecular microgels at 25 °C and 45 °C. (c) LCST of supramolecular microgels monitored by UV/vis spectroscopy. Reproduced with permission from ref. 166, Copyright 2016, American Chemical Society.

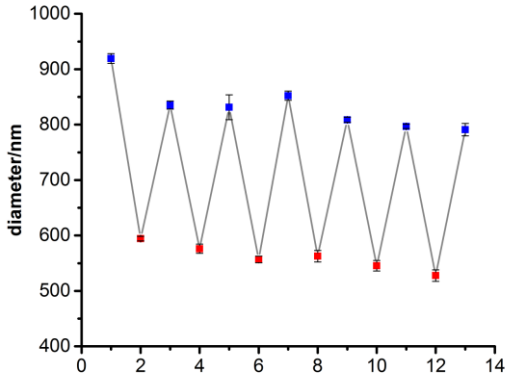

Figure 9-5. Diameter of supramolecular microgels at 25 °C and 45 °C at different cycles, monitored by DLS.

To confirm that the supramonomers did act as a cross-linker during the formation of supramolecular microgels, ^{1}H NMR of the microgels was collected. As can be seen in Figure 9-6, the microgels showed broad signals due to their polymeric nature, and peaks ascribed to CB[8] could be observed. At the same time, no peaks belonging to the double bonds of free supramonomers were detected, which indicated that the supramonomers act as a cross-linker instead of the monomer. Moreover, by integrating peaks assigned to the supramonomer and pNIPAm, the molar percentage of the supramonomer was calculated to be 5.4 %, which was close to the initial ratio used for the supramolecular microgel fabrication. We further investigated the ^{1}H NMR of supramolecular microgels under different temperature. And the results in Figure 9-6b shows that the similar structure of microgels.

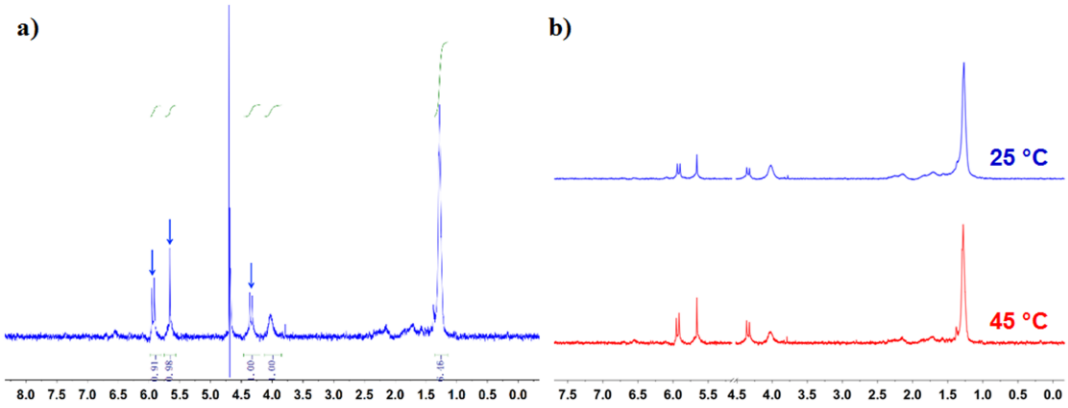

Figure 9-6. (a) ^{1}H NMR of supramolecular microgels (400 MHz, D_2O). Arrows show peaks belonging to CB[8]. By integrating peaks ascribed to supramonomers and pNIPAm, the ratio percentage of the supramonomer was calculated to be 5.4%, which was close to the initial ratio used for the supramolecular microgel fabrication. (b) ^{1}H NMR of supramolecular microgels at 25 °C (up) and 45 °C (below) (400 MHz, D_2O).

Benefitting from the dynamic nature of the supramonomers, the microgels can undergo degradation when exposed to certain stimuli. 3, 5-Dimethyl-1-adamantanamine hydrochloride (DMADA), which has a much higher binding constant with CB[8] (4.33×10^{11} M^{-1}) than FGG-EA,[49] can be utilized as chemical stimuli to destroy the supramonomers. When adding the equimolar amount of DMADA into the solution of supramonomers, as revealed by ^{1}H NMR spectra, shown in Figure 9-7, peaks belonging to FGG-EA shifted back, suggesting the dissociation of the supramonomers.

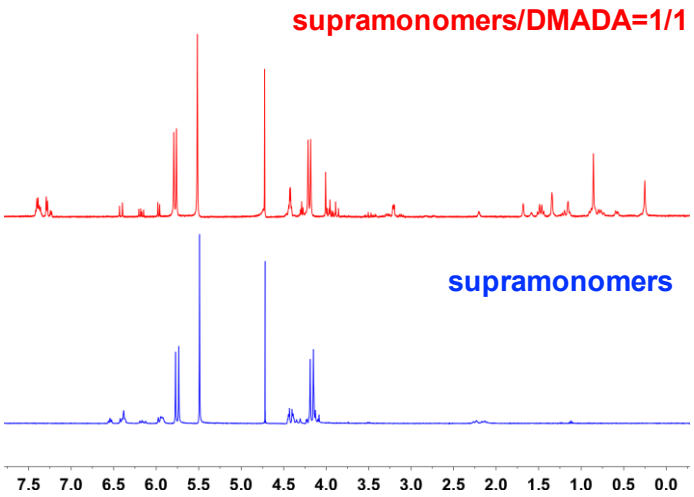

Figure 9-7. ^{1}H NMR of supramonomers with and without DMADA (400 MHz, D2O).

As shown in Figure 9-8a, upon adding DMADA into the aqueous solution of microgels, the translucent solution became transparent suggesting that the microgels were thoroughly degraded. It is also possible to monitor the degradation process *in situ* via microscopy (Figure 9-8c). After dripping one droplet of the microgel aqueous dispersion onto the microscope slide, microgels were found in both water phase and dry phase after water evaporation. However, after adding DMADA into the microgel drop on the slide *in situ*, microgels in the water phase vanished while microgels in the dry phase remained unchanged. As indicated by DLS (Figure 9-8b), after adding DMADA, only small aggregates with a diameter below 100 nm were detected, supporting the degradation of microgels. In the meantime, conventional microgels using BIS as cross-linker were prepared as a control. DLS showed no clear change upon adding DMADA (data not shown here).

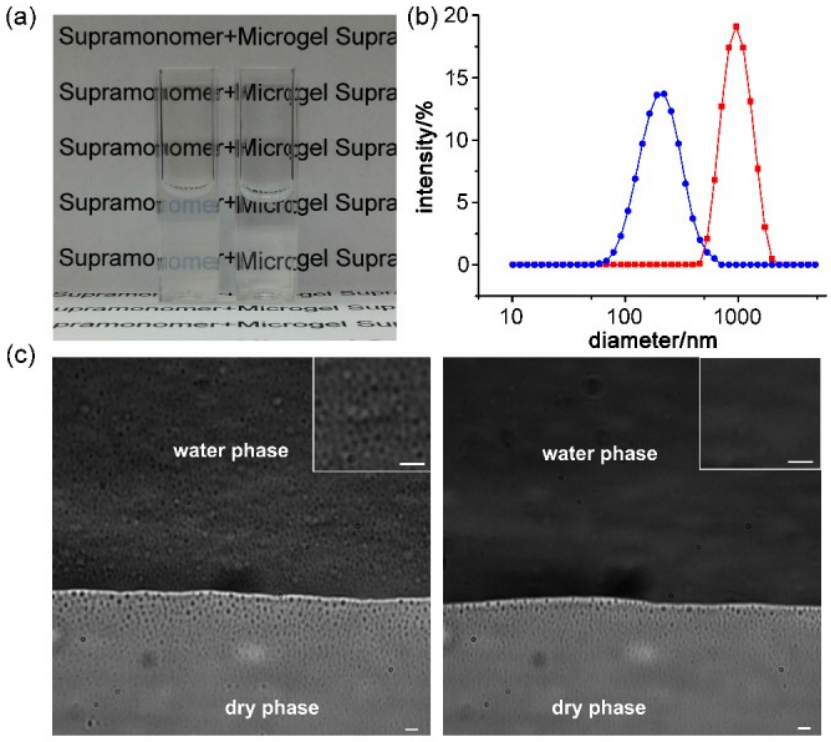

Figure 9-8. (a) Photo of supramolecular microgels before (left) and after (right) adding DMADA. (b) DLS data of supramolecular microgels before (red) and after (blue) adding DMADA. (c) Microscopic images of supramolecular microgels before (left) and after (right) adding DMADA (Scale bar: 4 μm). Reproduced with permission from ref. 166, Copyright 2016, American Chemical Society.

We also wanted to determine if the microgel degradation process could be attributed to the disassociation of the supramonomers. To answer this question, ^{1}H NMR spectrum of microgels after adding DMADA was conducted. Peaks ascribed to CB[8] were found to become much sharper than that of the microgels, suggesting the disappearance of large aggregates. In the meantime, peaks at ~7.3 ppm could be assigned to free FGG moieties, also indicating the specific noncovalent interactions between FGG and CB[8] were disrupted. Therefore, it is the

DMADA that causes the disassociation of the supramonomers, followed by the degradation of the microgels.

Moreover, the degradation kinetics of the microgels can also be revealed by UV/vis spectroscopy. By monitoring the change in absorbance at 260 nm against time after the addition of DMADA, the relationship between microgel degradation ratio and degradation time could be obtained. Simulated according to the principle of the first-order reaction, the degradation rate constant is about 2.96×10^{-3} s^{-1}. It should be noted that the degradation rate constant in microgels is much smaller than the dissociation rate of CB[8]-related association and disassociation. Therefore, the slow diffusion of DMADA into the microgels could be responsible for the low degradation rate.

It is assumed that the degradation kinetics relates greatly to the structure of the microgels. As is known, the thermoresponsive microgels tend to expel their water of solvation and de-swell when heated above LCST and re-swell when cooled below LCST. Below LCST, the microgels exhibit fully swelled structure, making the relatively small molecule DMADA easy to diffuse in. However, above LCST, the microgels exhibit dense and collapsed structure, making the DMADA molecule hard to diffuse in. In other words, the degradation kinetics should be quite different below and above LCST. In this regard, the degradation kinetics at different temperatures was investigated. According to the degradation rate constant at different temperatures, the apparent activation energy (E_a) as well as preexponential factor (A) below LCST (15.0 °C, 17.5 °C, 20.0 °C, 22.5 °C, 25.0 °C) and above LCST (45.0 °C, 47.5 °C, 50.0 °C, 52.5 °C, 55.0 °C) could be calculated based on Arrhenius formula, respectively, as shown in Figure 9-9. The preexponential factor A above LCST ($A = 1.79 \times 10^{6}$ s^{-1}) is much smaller than that below LCST ($A = 9.80 \times 10^{7}$ s^{-1}), indicating that it is much more difficult for DMADA to

diffuse into the microgels above LCST. In the meantime, the apparent activation energy E_a above LCST (E_a = 52.7 kJ/mol) is slightly smaller than that below LCST (E_a = 59.9 kJ/mol), which could be attributed to the relatively higher local CB[8] concentration in the microgels above LCST, making it easier for DMADA to destroy the crosslinking points once it has already diffused into the microgels.

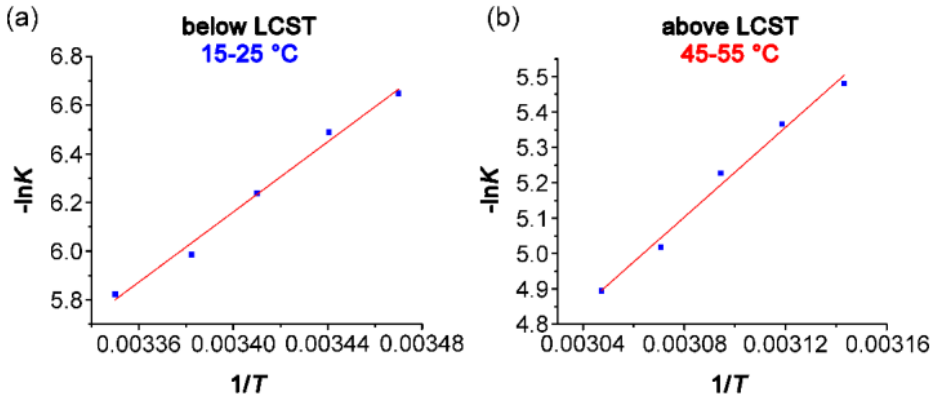

Figure 9-9. Fitting of degradation rate constant (K) to degradation temperature (T) based on Arrhenius Equation to give the apparent activation energy (Ea) and preexponential factor (A) below LCST (a) and above LCST (b). Reproduced with permission from ref. 166, Copyright 2016, American Chemical Society.

To further confirm the influence of microgel structure on the degradation kinetics, degradation process upon a time at 35 °C and 38 °C was studied and compared. As shown in Figure 9-10, the degradation is much faster at 35 °C (swelled structure) than 38 °C (collapsed structure), proving that the degradation kinetics are closely related to the microgel structure. We can explain this based on the microgel structure at different temperatures. Firstly, we know that the LCST of the supramolecular microgels is around 37 °C, which means 35 °C is slightly lower and microgels are fully swollen, and 38 °C is a little bit higher and microgels are fully collapsed as shown in Figure 9-10b. The faster degradation at a lower temperature is attributed to the many

pores that exist when the microgels are swollen, which allows for relatively fast diffusion of DMADA into the microgels compared to the less porous microgels at elevated temeprature. Therefore, this study provides a facile way to tune the degradation kinetics of the supramolecular microgels.

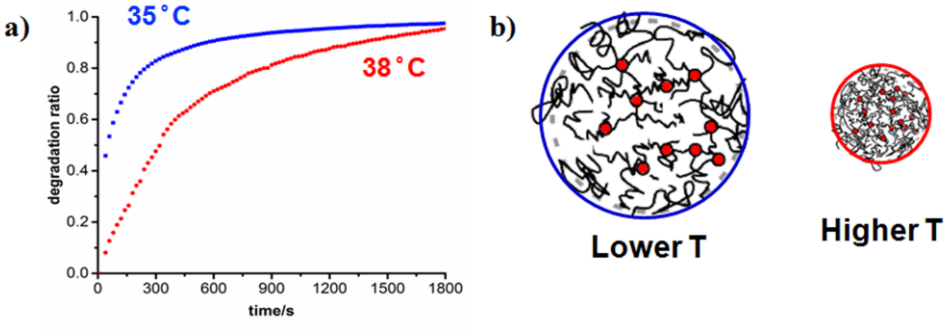

Figure 9-10. a) Degradation kinetics at 35 °C and 38 °C, and b) the possible mechanism of DMADA diffusion into microgels under different temperature.

It should be pointed out that the supramolecular microgels can undergo degradation under various stimuli. For example, triethylamine (TEA) can destroy the multiple hydrogen bonding between FGG-EA and CB[8], leading to the disassociation of the supramonomers, thus causing the degradation of the microgels, which could be proved by DLS as well as the naked eye. The microgel solution also becomes cloudy when TEA is added, as shown in Figure 9-11. One thing to note is that after the degradation of microgels, we still see some small particles in the solution according to DLS measurements. We propose that this may cause by the degradation of microgels, which produced small pNIPAm fragments with random molecular weight distribution. And these polymer fragments still maintain the temperature-responsive property of NIPAm itself.

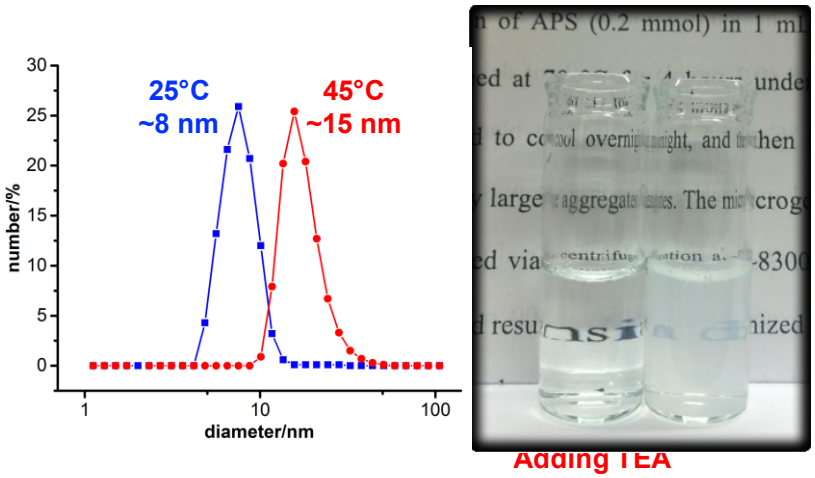

Figure 9-11. DLS of supramolecular microgels adding TEA (left); photo of supramolecular microgels before and after adding TEA (right).

For further prove that this approach to synthesize supramolecular microgels is independent of the monomers components, we verified the percentage of the supramonomer ratio and the results are shown in Figure 9-12. Supramolecular microgels with lower supramonomer ratio (2.5%) were synthesized by the same procedure described above. For comparison, we characterized the size, phase transition and degradation properties of the supramolecular microgels. The diameter of the supramolecular microgels with the lower supramonomer ratio at 25 °C was ~950 nm, which decreased to ~300 nm at 45 °C (Figure 9-12a). The LCST was measured to be around 42 °C, higher than the microgels with 5% supramonomer ratio (Figure 9-12b), which is attributed to the loosely cross-linked structure and hydrophilic dynamic supramolecular cross-linker. Adding DMADA could also lead to the degradation of the supramolecular microgels, as indicated by DLS in Figure 9-12c. The larger size distribution of degraded microgels comes from the higher molecular weight of pNIPAm fragment when starting from a higher percentage of reaction monomers.

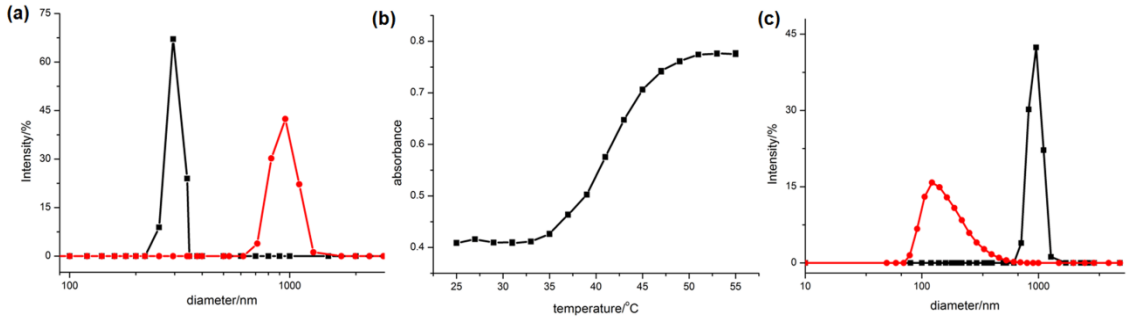

Figure 9-12. Supramolecular microgels with lower supramonomer ratio (2.5 %). (a) DLS data of supramolecular microgels at 25 °C and 45 °C. (b) LCST of supramolecular microgels monitored by UV/vis spectroscopy. (c) DLS data of supramolecular microgels before (red) and after (blue) adding DMADA.

Finally, I want to point out is that the way to apply non-covalent interaction into the synthesis of microgels is not limited to just these studies. We have shown that pNIPAm-based microgels can be successfully prepared by combining covalent bonds and non-covalent interaction, which gives new properties for responsive microgels. For example, after adding the degradation agent, the microgels will partially degrade, make the microgel size larger and more porous. We can pursue more studies on the controlled drug delivery system based on this interesting phenomenon.

9.4 Conclusion

In conclusion, for the first time, we have employed the concept of supramonomers for the fabrication of supramolecular microgels. The supramolecular microgels exhibit not only thermal responsive properties as conventional microgels but also dynamic and degradable properties due to the introduction of supramonomers. In principle, supramonomers with various architectures can be constructed on the basis of different noncovalent interactions. Different monomers could be used to copolymerize with supramonomers to form supramolecular microgels. Therefore, it is

highly anticipated that the similar strategy can be extended to fabricate various supramolecular microgels with tailor-made structure and function.

Chapter 10: Conclusion and Future Outlook

10.1 Conclusion

In this dissertation, the overall goal of the work was to study the stimuli-responsive microgels assemblies based devices and their applications. In particular, their role as suitable carriers for controlled drug release systems was explored. Here, we will provide concluding remarks for these studies and propose future research directions.

Microgels from pNIPAm have excellent thermoresponsive properties with a conformation change in the temperature of physiological range, which promoted them as a controlled drug release vehicle. By incorporating various functional monomers or post-functionalization, microgels responsive to other stimuli and multi-responsive microgels could be prepared, such as pH-responsive microgels, light-responsive microgels as illustrated in the chapters. Owing to the porous network structure and tunable properties, responsive microgels, and their constructed materials or systems have been investigated as controlled drug delivery devices for many years. Herein, the microgel assemblies based device that we proposed showed unique properties, particularly, as a reservoir device for controlled drug release.

Controlled and triggered drug release system utilizing p(NIPAm-*co*-AAc) microgel assemblies based device was developed in Chapter 3. The p(NIPAm-*co*-AAc) microgel was charged at high pH to load the drug by electrostatic interaction, and released the drug at low pH through protonation. Furthermore, we showed that the model drug could be released in a triggered fashion, turning on and off as a function of solution pH. The main contribution to this study is that the release rate could be controlled by the thickness of the Au overlayer covering the microgels. The results showed that when the Au layer thickness increases to more than 500

nm, there is a prominent decrease of the release rate. However, it increases the cost and limits the application of the prepared device.

To reduce the Au layer thickness, we developed an easily fabricated and efficient method to control small molecule release rate by modifying the upper Au layer with a monolayer of silica in Chapter 4. The upper Au layer can be dramatically reduced to 50 nm. Silica layer is characterized and was shown to exhibit a thickness dependence on hydrolysis reaction time of TEOS with ammonia. The release process was completely controllable through various surface morphologies by changing the modification time. Finally, the results showed a long-term efficiency of this drug delivery system. In the future, the upper Au layer coated with a biodegradable polymer or porous polymer layer may provide more options for this research direction.

We further proved that microgel assemblies based reservoir devices could be fabricated from mixed microgels, specifically pAPBA-MG and pAAc-MG, to show sequentially release of multi-drugs in a controlled manner in Chapter 5. We went on to show that these microgels could load positively charged MB, which could be released sequentially to a system, in a pH-dependent fashion. When the solution pH was higher, both microgels were negatively charged strongly bound the MB. When the solution pH was decreased to neutral, the pAPBA-MG was neutralized and released MB; the pAAc-MG was neutralized and released its MB at lower pH. The data obtained from the reservoir devices was compared to microgels in solution, which exhibited much slower release kinetics. We also showed that the release kinetics from the reservoir devices could be tuned by varying the Au overlayer thickness. Finally, we showed that the amount of MB delivered to a system as a result of the pH changes could be tuned by changing the ratio of the pAPBA-MG and pAAc-MG in the reservoir devices. These systems represent a versatile

approach to sequentially deliver small molecules, in a triggered fashion, with tunable release kinetics. Importantly, their release behavior can be easily tuned by simply changing the microgel chemistry, e.g., by generating reservoir devices from microgels that ionize at different solution pH. This would allow the delivery of various small molecules to a system triggered by a variety of solution pH. This, combined with the tunable release kinetics and the ability to array these devices on a single substrate, makes this delivery platform extremely versatile, powerful, and unique.

A simple method for fabricating free-standing microgel assemblies based device was developed by introducing a sacrificial layer between the device and glass substrate in Chapter 6. The sacrificial layer was prepared by LbL assembly, which could be destroyed in solutions at high pH; destroying this approach releases the device from the substrate. The free-standing microgel assemblies based device can be easily transferred to other substrates with different chemistries and shapes. We found that its optical properties are retained after desorption from the solid substrate, which continues to exhibit very sensitive responses to solution pH and temperature. Finally, we demonstrated that the devices could be transferred to another surface, in this case, a hydrogel, and can be triggered to release a small drug molecule. In the future direction, the free-standing microgel assemblies based device could be used for light filtering applications, biosensing, to further the drug delivery concept.

In Chapter 7, we developed a light-responsive system for the non-light-responsive microgels. UV light could be used to decrease the pH of an aqueous solution containing *o*-NBA. This is a direct result of the UV light inducing the *o*-NBA to release a proton. Furthermore, by immersing a p(NIPAm-*co*-AAc) microgel assemblies based device in this solution, we were able to tune its optical properties upon UV irradiation. which directly changes the p(NIPAm-*co*-AAc)

microgels solvation state in response to the solution pH changes alters the optical properties of the device. We were able to fabricate patterns on the device and changed the visual color in those specific regions. Finally, the optical properties of the devices were reversible by simply adding fresh *o*-NBA solution and reexposing the device to UV light. We also showed that this unique property can be exploited for controlled/triggered drug delivery and for display technologies in the future.

In Chapter 8, we synthesized various pH-responsive microgels, p(NIPAm-*co*-AAc) and p(NIPAm-*co*-DMAPMA), which exhibited opposite charges over a given solution pH range. We showed that the microgels aggregated when they are mixed in this pH range, which was used to trap/load a small molecule model drug methylene blue. We showed that the loading efficiency was greater when the microgels aggregated, compared to simply relying on electrostatic interactions for loading. Finally, we showed that the methylene blue was released in a pH-dependent fashion over many hours/days at certain pH conditions. This is a clear demonstration of how microgel-based technology can be used for health-related applications to release biologically relevant molecules at low pH environments typically found at tumor sites.

We have employed the concept of supramonomers for the fabrication of supramolecular microgels in Chapter 9. The supramolecular microgels exhibit not only thermal responsive properties as conventional microgels but also dynamic and degradable properties due to the introduction of supramonomers. In principle, supramonomers with various architectures can be constructed on the basis of different noncovalent interactions. Different monomers could be used to copolymerize with supramonomers to form supramolecular microgels. Therefore, it is highly anticipated that the similar strategy can be extended to fabricate various supramolecular microgels with tailor-made structure and function.

Chemistry of the microgels will give more opportunities for device versatility. The p(NIPAm-*co*-AAc) microgels can reversibly trap and release positively charged molecules based on electrostatic interaction under pH variation because of the pH-responsivity. Other responsive microgels may apply to this system to generate increasing novelty in future. This brings the concept that we can customize the drug releasing process by designing microgels.

10.2 Future outlook

Although several systems have been developed and well characterized on the controlled drug releasing behaviors in this dissertation, there still exists some drawbacks and further research is really necessary. Numerous other experiments can be done in order to understand and make progress in various aspects of the work presented, some of which will be described here.

Firstly, the film from microgel monolayer is too fragile to be used for the application. In order to make the film robust, there are several strategies, for example, by using a thin polymer layer under the microgel monolayer to reinforce the toughness of the film. The mechanism is that the stronger polymer film will tolerate all the forces and keep the microgels together. The experiment can be done by spin coating a strong polymer thin film on the substrate ahead of preparing the microgels monolayer. Another approach is linking the microgels by chemical modification, which will covalently connect all the microgels to enhance resistant to fracture. The experiment can be done by incorporating a monomer with reactive moieties, like epoxy groups, to covalently connect the microgels. This double cross-linked network will provide extra forces to enhance the toughness of this microgel monolayer.

Secondly, the versatile chemistry of microgels allows the application of different stimuli to this system to achieve different purposes. For example, incorporating light-responsive monomer or cross-linker will bring either conformation change or degradable ability under light for

microgels. There are many choices for this topic as have been described in Chapters 1 and 2. As an example to illustrate, we can synthesize an *o*-nitrobenzyl alcohol based cross-linker, which will degrade under the light. This will directly disrupt the microgel and release the payloads.

Thirdly, there is an opportunity to develop microgel-inorganic nanoparticle hybrid systems for controlled drug delivery. Many systems of polymer nanoparticles have been studied and the synthesis of new functional nanoparticles replenishes the polymeric-based systems, for example, dopamine nanoparticle. The experiment can be done by incorporating dopamine nanoparticle into microgels and to develop photothermal therapy system. The increase of temperature induced by NIR irradiation to above the VPTT of the microgel will cause rapid deswelling, followed by the release of drug in an on-demand manner.

Finally, microgels monolayer with a unique two-dimensional microenvironment can not only used for controlled drug delivery but also for other biomedical applications, like tissue engineering. So far, the field of tissue engineering has not full-filled its grand potential of engineering such combinatorial scaffolds for engineering functional tissues. This is primarily due to the many challenges associated with finding the right micro-architectures and extracellular matrix compositions for optimal tissue regeneration. Our microgels monolayer with various microenvironments can contribute to the developed tissue engineering scaffolds, composed of native-like cellular micro-architectures resembling vascularised and bone marrow tissue architectures. This high-throughput platform can be used to examine stem cell fate within such heterogeneous micro constructs, enabling a cost-effective development of new tissue engineering strategies.

References

1. M. V. Gandhi and B. Thompson, *Smart materials and structures*, Springer Science & Business Media, 1992.
2. W. G. Lynn, *American Journal of Anatomy*, 1931, **49**, 97-139.
3. B. M. Walton and A. F. Bennett, *Physiological Zoology*, 1993, 270-287.
4. J. Fondeville, H. A. Borthwick and S. Hendricks, *Planta*, 1966, **69**, 357-364.
5. D. Hodick and A. Sievers, *Planta*, 1988, **174**, 8-18.
6. M. A. C. Stuart, W. T. Huck, J. Genzer, M. Müller, C. Ober, M. Stamm, G. B. Sukhorukov, I. Szleifer, V. V. Tsukruk and M. Urban, *Nature Materials*, 2010, **9**, 101-113.
7. D. Roy, J. N. Cambre and B. S. Sumerlin, *Progress in Polymer Science*, 2010, **35**, 278-301.
8. M. W. Urban, *Handbook of stimuli-responsive materials*, Wiley Online Library, 2011.
9. A. S. Hoffman, *Advanced Drug Delivery Reviews*, 2013, **65**, 10-16.
10. Y. Zhao and T. Ikeda, *Smart light-responsive materials: azobenzene-containing polymers and liquid crystals*, John Wiley & Sons, 2009.
11. O. Bertrand and J.-F. Gohy, *Polymer Chemistry*, 2017, **8**, 52-73.
12. H. G. Schild, *Progress in Polymer Science*, 1992, **17**, 163-249.
13. M. Heskins and J. E. Guillet, *Journal of Macromolecular Science—Chemistry*, 1968, **2**, 1441-1455.
14. I. C. Kwon, Y. H. Bae and S. W. Kim, *Nature,* 1991, **354**, 291-293.
15. G. Filipcsei, J. Feher and M. Zrınyi, *Journal of Molecular Structure*, 2000, **554**, 109-117.

16. C. Katsuno, A. Konda, K. Urayama, T. Takigawa, M. Kidowaki and K. Ito, *Advanced Materials*, 2013, **25**, 4636-4640.

17. D. M. Lynn, M. M. Amiji and R. Langer, *Angewandte Chemie International Edition*, 2001, **40**, 1707-1710.

18. J. D. Debord and L. A. Lyon, *Langmuir*, 2003, **19**, 7662-7664.

19. A. Kawamura and T. Miyata, *Encyclopedia of Polymeric Nanomaterials*, 2015, 1619-1626.

20. S. Dai, P. Ravi and K. C. Tam, *Soft Matter*, 2008, **4**, 435-449.

21. Q. Yan, R. Zhou, C. Fu, H. Zhang, Y. Yin and J. Yuan, *Angewandte Chemie*, 2011, **123**, 5025-5029.

22. S. Dong, Y. Luo, X. Yan, B. Zheng, X. Ding, Y. Yu, Z. Ma, Q. Zhao and F. Huang, *Angewandte Chemie International Edition*, 2011, **50**, 1905-1909.

23. T. Miyata, N. Asami and T. Uragami, *Nature*, 1999, **399**, 766-769.

24. S. J. Rowan and J. B. Beck, *Faraday Discussions*, 2005, **128**, 43-53.

25. J. Hu, G. Zhang and S. Liu, *Chemical Society Reviews*, 2012, **41**, 5933-5949.

26. R. V. Ulijn, *Journal of Materials Chemistry*, 2006, **16**, 2217-2225.

27. M. Zelzer, S. J. Todd, A. R. Hirst, T. O. McDonald and R. V. Ulijn, *Biomaterials Science*, 2013, **1**, 11-39.

28. T. Okano, in *Responsive Gels: Volume Transitions II*, Springer, 1993, pp. 179-197.

29. R. Bernstein, C. Cruz, D. Paul and J. Barlow, *Macromolecules*, 1977, **10**, 681-686.

30. J. Seuring and S. Agarwal, *Macromolecular Rapid Communications*, 2012, **33**, 1898-1920.

31. A. Shultz and P. Flory, *Journal of the American Chemical Society*, 1952, **74**, 4760-4767.

32. J. M. Cowie and I. J. McEwen, *Journal of the Chemical Society, Faraday Transactions 1: Physical Chemistry in Condensed Phases*, 1976, **72**, 526-533.

33. M. R. Aguilar and J. Roman, *Smart polymers and their applications*, Elsevier, 2014.

34. F. Meeussen, E. Nies, H. Berghmans, S. Verbrugghe, E. Goethals and F. Du Prez, *Polymer*, 2000, **41**, 8597-8602.

35. Z. Hu, T. Cai and C. Chi, *Soft Matter*, 2010, **6**, 2115-2123.

36. T. Nishi and T. Kwei, *Polymer*, 1975, **16**, 285-290.

37. R. Hoogenboom, *Angewandte Chemie International Edition*, 2009, **48**, 7978-7994.

38. R. Pelton and P. Chibante, *Colloids and Surfaces*, 1986, **20**, 247-256.

39. G. Zhang and C. Wu, *Journal of the American Chemical Society*, 2001, **123**, 1376-1380.

40. M. C. Carter, C. D. Sorrell and M. J. Serpe, *The Journal of Physical Chemistry B*, 2011, **115**, 14359-14368.

41. C. Scherzinger, A. Schwarz, A. Bardow, K. Leonhard and W. Richtering, *Current Opinion in Colloid & Interface Science*, 2014, **19**, 84-94.

42. C. Wu and S. Zhou, *Macromolecules*, 1995, **28**, 8381-8387.

43. C. Tanford, *The Hydrophobic Effect: Formation of Micelles and Biological Membranes 2d Ed*, J. Wiley., 1980.

44. G. Kocak, C. Tuncer and V. Butun, *Polymer Chemistry*, 2017, **8**, 144-176.

45. I. F. Tannock and D. Rotin, *Cancer Research*, 1989, **49**, 4373-4384.

46. H. Jiang, S. Kelch and A. Lendlein, *Advanced Materials*, 2006, **18**, 1471-1475.

47. C. De las Heras Alarcón, S. Pennadam and C. Alexander, *Chemical Society Reviews*, 2005, **34**, 276-285.

48. P. Theato, B. S. Sumerlin, R. K. O'Reilly and T. H. Epps III, *Chemical Society Reviews*, 2013, **42**, 7055-7056.

49. Y.-L. Zhao and J. F. Stoddart, *Langmuir*, 2009, **25**, 8442-8446.

50. S. Tamesue, Y. Takashima, H. Yamaguchi, S. Shinkai and A. Harada, *Angewandte Chemie International Edition*, 2010, **49**, 7461-7464.

51. G. S. Kumar and D. Neckers, *Chemical Reviews*, 1989, **89**, 1915-1925.

52. Y. Yu, M. Nakano and T. Ikeda, *Nature*, 2003, **425**, 145-145.

53. A. Ryabchun, I. Raguzin, J. Stumpe, V. Shibaev and A. Bobrovsky, *ACS Applied Materials & Interfaces*, 2016, **8**, 27227-27235.

54. M.-Q. Zhu, L. Zhu, J. J. Han, W. Wu, J. K. Hurst and A. D. Li, *Journal of the American Chemical Society*, 2006, **128**, 4303-4309.

55. R. Klajn, *Chemical Society Reviews*, 2014, **43**, 148-184.

56. G. Berkovic, V. Krongauz and V. Weiss, *Chemical Reviews*, 2000, **100**, 1741-1754.

57. H. Zhao, E. S. Sterner, E. B. Coughlin and P. Theato, *Macromolecules*, 2012, **45**, 1723-1736.

58. S. Wang, Y. Song and L. Jiang, *Journal of Photochemistry and Photobiology C: Photochemistry Reviews*, 2007, **8**, 18-29.

59. K. Ichimura, S.-K. Oh and M. Nakagawa, *Science*, 2000, **288**, 1624-1626.

60. Z. Xu, B. Yan, J. Riordon, Y. Zhao, D. Sinton and M. G. Moffitt, *Chemistry of Materials*, 2015, **27**, 8094-8104.

61. D. S. Achilleos, T. A. Hatton and M. Vamvakaki, *Journal of the American Chemical Society*, 2012, **134**, 5726-5729.

62. B. Scrosati, *Applications of electroactive polymers*, Springer, 1993.

63. G. G. Wallace, P. R. Teasdale, G. M. Spinks and L. A. Kane-Maguire, *Conductive electroactive polymers: intelligent polymer systems*, CRC press, 2008.

64. Y. Bar-Cohen, *Electroactive polymer (EAP) actuators as artificial muscles: reality, potential, and challenges*, SPIE press, 2004.

65. V. Guarino, S. Zuppolini, A. Borriello and L. Ambrosio, *Polymers*, 2016, **8**, 185.

66. Y. Bar-Cohen and Q. Zhang, *MRS Bulletin*, 2008, **33**, 173-181.

67. A. Hunt, Z. Chen, X. Tan and M. Kruusmaa, *Smart Materials and Structures*, 2016, **25**, 035016.

68. K. J. Kim and S. Tadokoro, *Artificial Muscles and Sensors*, 2007.

69. A. Punning, K. J. Kim, V. Palmre, F. Vidal, C. Plesse, N. Festin, A. Maziz, K. Asaka, T. Sugino and G. Alici, *Scientific Reports*, 2014, **4**, 6913.

70. R. J. Mortimer, *Chemical Society Reviews*, 1997, **26**, 147-156.

71. F. Carpi and E. Smela, *Biomedical applications of electroactive polymer actuators*, John Wiley & Sons, 2009.

72. M. Radisic, *Nature Materials*, 2016, **15**, 596-597.

73. K. Ren, Y. Liu, H. Hofmann, Q. Zhang and J. Blottman, *Applied Physics Letters*, 2007, **91**, 132910.

74. L. J. Romasanta, M. Lopez-Manchado and R. Verdejo, *Progress in Polymer Science*, 2015, **51**, 188-211.

75. H. Kawai, *Japanese Journal of Applied Physics*, 1969, **8**, 975.

76. M. Portugall, H. Ringsdorf and R. Zentel, *Macromolecular Chemistry and Physics*, 1982, **183**, 2311-2321.

77. A. Gugliuzza and E. Drioli, *Journal of Membrane Science*, 2013, **446**, 350-375.

78. O. Borisova, L. Billon, R. Richter, E. Reimhult and O. Borisov, *Langmuir*, 2015, **31**, 7684-7694.

79. J. Thévenot, H. Oliveira, O. Sandre and S. Lecommandoux, *Chemical Society Reviews*, 2013, **42**, 7099-7116.

80. M. Zrínyi, L. Barsi and A. Büki, *The Journal of Chemical Physics*, 1996, **104**, 8750-8756.

81. N. S. Satarkar and J. Z. Hilt, *Journal of Controlled Release*, 2008, **130**, 246-251.

82. J. Ge, Y. Hu and Y. Yin, *Angewandte Chemie International Edition*, 2007, **46**, 7428-7431.

83. Y. Min, S. Huang, Y. Wang, Z. Zhang, B. Du, X. Zhang and Z. Fan, *Macromolecules*, 2015, **48**, 316-322.

84. J. Fan, J. Zou, X. He, F. Zhang, S. Zhang, J. E. Raymond and K. L. Wooley, *Chemical Science*, 2014, **5**, 141-150.

85. R. J. Wojtecki, M. A. Meador and S. J. Rowan, *Nature Materials*, 2011, **10**, 14-27.

86. H. Zhang, H. Xia, J. Wang and Y. Li, *Journal of Controlled Release*, 2009, **139**, 31-39.

87. J. Folk and J. Finlayson, *Advances in Protein Chemistry*, 1977, **31**, 1-133.

88. E. Dickinson and Y. Yamamoto, *Journal of Food Science*, 1996, **61**, 811-816.

89. J. J. Sperinde and L. G. Griffith, *Macromolecules*, 1997, **30**, 5255-5264.

90. P. D. Thornton, R. J. Mart and R. V. Ulijn, *Advanced Materials*, 2007, **19**, 1252-1256.

91. F. Huang and O. A. Scherman, *Chemical Society Reviews*, 2012, **41**, 5879-5880.

92. A. Tanaka, Y. Fukuoka, Y. Morimoto, T. Honjo, D. Koda, M. Goto and T. Maruyama, *Journal of the American Chemical Society*, 2015, **137**, 770-775.

93. Y. Ding, Y. Kang and X. Zhang, *Chemical Communications*, 2015, **51**, 996-1003.

94. I. Cobo, M. Li, B. S. Sumerlin and S. Perrier, *Nature Materials*, 2015, **14**, 143-159.

95. A. Sagi, R. Weinstain, N. Karton and D. Shabat, *Journal of the American Chemical Society*, 2008, **130**, 5434-5435.

96. S. Kim and K. E. Healy, *Biomacromolecules*, 2003, **4**, 1214-1223.

97. M. Nakahata, Y. Takashima, H. Yamaguchi and A. Harada, *Nature Communications*, 2011, **2**, 511.

98. N. Kamaly, B. Yameen, J. Wu and O. C. Farokhzad, *Chemical Reviews*, 2016, **116**, 2602-2663.

99. N. Ma, Y. Li, H. Xu, Z. Wang and X. Zhang, *Journal of the American Chemical Society*, 2009, **132**, 442-443.

100. R. Cheng, F. Meng, C. Deng, H.-A. Klok and Z. Zhong, *Biomaterials*, 2013, **34**, 3647-3657.

101. K. Rahimian-Bajgiran, N. Chan, Q. Zhang, S. M. Noh, H.-i. Lee and J. K. Oh, *Chemical Communications*, 2013, **49**, 807-809.

102. J. Yang, W. Liu, M. Sui, J. Tang and Y. Shen, *Biomaterials*, 2011, **32**, 9136-9143.

103. H. Cho, J. Bae, V. K. Garripelli, J. M. Anderson, H.-W. Jun and S. Jo, *Chemical Communications*, 2012, **48**, 6043-6045.

104. H. Fu, D. M. Policarpio, J. D. Batteas and D. E. Bergbreiter, *Polymer Chemistry*, 2010, **1**, 631-633.

105. A. Napoli, M. Valentini, N. Tirelli, M. Müller and J. A. Hubbell, *Nature Materials*, 2004, **3**, 183-189.

106. H. Xu, W. Cao and X. Zhang, *Accounts of Chemical Research*, 2013, **46**, 1647-1658.

107. N. Ma, Y. Li, H. Ren, H. Xu, Z. Li and X. Zhang, *Polymer Chemistry*, 2010, **1**, 1609-1614.

108. O. Nuyken, V. Burkhardt, T. Pöhlmann and M. Herberhold, *Macromolecular Symposia*, 1991, **44**, 195-206.

109. S. Maeda, Y. Hara, T. Sakai, R. Yoshida and S. Hashimoto, *Advanced Materials*, 2007, **19**, 3480-3484.

110. W. Baker, *Rubber Chemistry and Technology*, 1949, **22**, 935-955.

111. T. Tanaka, D. Fillmore, S.-T. Sun, I. Nishio, G. Swislow and A. Shah, *Physical Review Letters*, 1980, **45**, 1636.

112. T. Tanaka and D. J. Fillmore, *The Journal of Chemical Physics*, 1979, **70**, 1214-1218.

113. T. Tanaka, *Physica A: Statistical Mechanics and its Applications*, 1986, **140**, 261-268.

114. X. Wu, R. Pelton, A. Hamielec, D. Woods and W. McPhee, *Colloid & Polymer Science*, 1994, **272**, 467-477.

115. C. Wu, *Polymer*, 1998, **39**, 4609-4619.

116. R. Pelton, *Advances in Colloid and Interface Science*, 2000, **85**, 1-33.

117. J. K. Oh, R. Drumright, D. J. Siegwart and K. Matyjaszewski, *Progress in Polymer Science*, 2008, **33**, 448-477.

118. J. Zhang, S. Xu and E. Kumacheva, *Journal of the American Chemical Society*, 2004, **126**, 7908-7914.

119. M. J. Snowden, B. Z. Chowdhry, B. Vincent and G. E. Morris, *Journal of the Chemical Society, Faraday Transactions*, 1996, **92**, 5013-5016.

120. I. Berndt and W. Richtering, *Macromolecules*, 2003, **36**, 8780-8785.

121. T. Hoare and R. Pelton, *Macromolecules*, 2004, **37**, 2544-2550.

122. K. Tam, S. Ragaram and R. Pelton, *Langmuir*, 1994, **10**, 418-422.

123. H. Senff and W. Richtering, *The Journal of Chemical Physics*, 1999, **111**, 1705-1711.

124. W. Su, M. Yang, K. Zhao and T. Ngai, *Macromolecules*, 2016, **49**, 7997-8008.

125. C. M. Nolan, M. J. Serpe and L. A. Lyon, *Biomacromolecules*, 2004, **5**, 1940-1946.

126. M. J. Serpe, K. A. Yarmey, C. M. Nolan and L. A. Lyon, *Biomacromolecules*, 2005, **6**, 408-413.

127. J.-T. Zhang, N. Smith and S. A. Asher, *Analytical Chemistry*, 2012, **84**, 6416-6420.

128. J.-T. Zhang, L. Wang, X. Chao and S. A. Asher, *Langmuir*, 2011, **27**, 15230-15235.

129. J.-T. Zhang, L. Wang, J. Luo, A. Tikhonov, N. Kornienko and S. A. Asher, *Journal of the American Chemical Society*, 2011, **133**, 9152-9155.

130. C. D. Sorrell and M. J. Serpe, *Advanced Materials*, 2011, **23**, 4088-4092.

131. M. R. Islam, A. Ahiabu, X. Li and M. J. Serpe, *Sensors*, 2014, **14**, 8984-8995.

132. Y. Gao, X. Li and M. J. Serpe, *RSC Advances*, 2015, **5**, 44074-44087.

133. H. Kawaguchi, *Polymer International*, 2014, **63**, 925-932.

134. J. Gao and B. J. Frisken, *Langmuir*, 2003, **19**, 5212-5216.

135. X. Hu, Z. Tong and L. A. Lyon, *Langmuir*, 2011, **27**, 4142-4148.

136. J. Bonham, M. Faers and J. Van Duijneveldt, *Soft Matter*, 2014, **10**, 9384-9398.

137. A. Pich and W. Richtering, in *Chemical Design of Responsive Microgels*, Springer, 2010, pp. 1-37.

138. C. L. Sieglaff, *Journal of Polymer Science*, 1959, **41**, 319-326.

139. H. Kojima, F. Tanaka, C. Scherzinger and W. Richtering, *Journal of Polymer Science Part B: Polymer Physics*, 2013, **51**, 1100-1111.

140. P. W. Zhu and D. H. Napper, *Chemical Physics Letters*, 1996, **256**, 51-56.

141. F. Tanaka, T. Koga, H. Kojima, N. Xue and F. o. M. Winnik, *Macromolecules*, 2011, **44**, 2978-2989.

142. S. Zhou and B. Chu, *The Journal of Physical Chemistry B*, 1998, **102**, 1364-1371.

143. L. Zha, J. Hu, C. Wang, S. Fu, A. Elaissari and Y. Zhang, *Colloid and polymer science*, 2002, **280**, 1-6.

144. C. D. Sorrell, M. C. Carter and M. J. Serpe, *Advanced Functional Materials*, 2011, **21**, 425-433.

145. S. Schmidt, T. Hellweg and R. von Klitzing, *Langmuir*, 2008, **24**, 12595-12602.

146. M. J. Serpe and L. A. Lyon, *Chemistry of Materials*, 2004, **16**, 4373-4380.

147. A. S. J. Iyer and L. A. Lyon, *Angewandte Chemie International Edition*, 2009, **48**, 4562-4566.

148. T. Hellweg, *Angewandte Chemie International Edition*, 2009, **48**, 6777-6778.

149. S. A. Asher, J. Holtz, L. Liu and Z. Wu, *Journal of the American Chemical Society*, 1994, **116**, 4997-4998.

150. A. W. Bridges, N. Singh, K. L. Burns, J. E. Babensee, L. A. Lyon and A. J. García, *Biomaterials*, 2008, **29**, 4605-4615.

151. S. Schmidt, M. Zeiser, T. Hellweg, C. Duschl, A. Fery and H. Möhwald, *Advanced Functional Materials*, 2010, **20**, 3235-3243.

152. J. Weng, X. Li, Y. Guan, X. Zhu and Y. Zhang, *Langmuir*, 2016, **32**, 12876-12884.

153. X. Li, J. Weng, Y. Guan and Y. Zhang, *Langmuir*, 2016, **32**, 3977-3982.

154. D. Suzuki, J. G. McGrath, H. Kawaguchi and L. A. Lyon, *The Journal of Physical Chemistry C*, 2007, **111**, 5667-5672.

155. C. D. Sorrell, M. C. Carter and M. J. Serpe, *ACS Applied Materials & Interfaces*, 2011, **3**, 1140-1147.

156. J. B. Smiley-Wiens and M. J. Serpe, *Colloid and Polymer Science*, 2013, **291**, 971-979.

157. Y. Hertle and T. Hellweg, *Journal of Materials Chemistry B*, 2013, **1**, 5874-5885.

158. L. A. Lyon, Z. Meng, N. Singh, C. D. Sorrell and A. S. John, *Chemical Society Reviews*, 2009, **38**, 865-874.

159. Y. Gao, K. Y. Wong, A. Ahiabu and M. J. Serpe, *Journal of Materials Chemistry B*, 2016, **4**, 5144-5150.

160. Q. M. Zhang, A. Ahiabu, Y. Gao and M. J. Serpe, *Journal of Materials Chemistry C*, 2015, **3**, 495-498.

161. M. R. Islam and M. J. Serpe, *Macromolecules*, 2013, **46**, 1599-1606.

162. A. Pich, K. Wiemer, U. Simon, G. Agrawal, K. Doermbach, J. Mayer, I. Slabu, F. Schrader, T. Caumanns and J. Steitz, *Journal of Materials Chemistry B*, 2017, **5**, 1284-1292.

163. S. Cho, Y. Li, M. Seo and E. Kumacheva, *Angewandte Chemie International Edition*, 2016, **55**, 14014-14018.

164. C. D. Jones and L. A. Lyon, *Macromolecules*, 2000, **33**, 8301-8306.

165. A. J. Schmid, J. Dubbert, A. A. Rudov, J. S. Pedersen, P. Lindner, M. Karg, I. I. Potemkin and W. Richtering, *Scientific Reports*, 2016, **6**, 22736

166. Q. Song, Y. Gao, J.-F. Xu, B. Qin, M. J. Serpe and X. Zhang, *ACS Macro Letters*, 2016, **5**, 1084-1088.

167. D. Schmitz and A. Pich, *Polymer Chemistry*, 2016, **7**, 5687-5697.

168. K. Gawlitza, A. Radulescu, R. von Klitzing and S. Wellert, *Polymer*, 2014, **55**, 6717-6724.

169. L. Nyström, R. Nordström, J. Bramhill, B. R. Saunders, R. n. Álvarez-Asencio, M. W. Rutland and M. Malmsten, *Biomacromolecules*, 2016, **17**, 669-678.

170. T. Hoare and R. Pelton, *Macromolecules*, 2007, **40**, 670-678.

171. C. D. Sorrell and M. J. Serpe, *Analytical and Bioanalytical Chemistry*, 2012, **402**, 2385-2393.

172. M. R. Islam, K. C. Johnson and M. J. Serpe, *Analytica Chimica Acta*, 2013, **792**, 110-114.

173. Q. M. Zhang, D. Berg, S. M. Mugo and M. J. Serpe, *Chemical Communications*, 2015, **51**, 9726-9728.

174. J. Bratby, *Coagulation and flocculation in water and wastewater treatment*, IWA publishing, 2006.

175. S. A. Parsons and B. Jefferson, *Introduction to potable water treatment processes*, Blackwell publishing, 2006.

176. R. J. Hall, V. T. Pinkrah, B. Z. Chowdhry and M. J. Snowden, *Colloids and Surfaces A: Physicochemical and Engineering Aspects*, 2004, **233**, 25-38.

177. G. E. Morris, B. Vincent and M. J. Snowden, *Journal of Colloid and Interface Science*, 1997, **190**, 198-205.

178. D. Menne, F. Pitsch, J. E. Wong, A. Pich and M. Wessling, *Angewandte Chemie International Edition*, 2014, **53**, 5706-5710.

179. T. Ngai, S. H. Behrens and H. Auweter, *Chemical Communications*, 2005, 331-333.

180. G. Liu, M. Cai, X. Wang, F. Zhou and W. Liu, *ACS Macro Letters*, 2016, **5**, 144-148.

181. T. M. Allen and P. R. Cullis, *Science*, 2004, **303**, 1818-1822.

182. K. Park, *Journal of Controlled Release*, 2014, **190**, 3-8.

183. E. Mathiowitz, J. S. Jacob, Y. S. Jong and G. P. Carino, *Nature*, 1997, **386**, 410.

184. L. M. Ensign, R. Cone and J. Hanes, *Advanced Drug Delivery Reviews*, 2012, **64**, 557-570.

185. J. Huang, Q. Shu, L. Wang, H. Wu, A. Y. Wang and H. Mao, *Biomaterials*, 2015, **39**, 105-113.

186. K. Thanki, R. P. Gangwal, A. T. Sangamwar and S. Jain, *Journal of Controlled Release*, 2013, **170**, 15-40.

187. A. S. Puranik, L. P. Pao, V. M. White and N. A. Peppas, *European Journal of Pharmaceutics and Biopharmaceutics*, 2016, **108**, 196-213.

188. S. Zhang, A. M. Bellinger, D. L. Glettig, R. Barman, Y.-A. L. Lee, J. Zhu, C. Cleveland, V. A. Montgomery, L. Gu and L. D. Nash, *Nature Materials*, 2015, **14**, 1065-1071.

189. R. J. Levy, V. Labhasetwar, S. A. Strickberger, T. Underwood and J. Davis, *Drug Delivery*, 1996, **3**, 137-142.

190. A. Hatefi and B. Amsden, *Journal of Controlled Release*, 2002, **80**, 9-28.

191. B. Jeong, Y. H. Bae, D. S. Lee and S. W. Kim, *Nature*, 1997, **388**, 860-862.

192. A. Paul, A. Hasan, H. A. Kindi, A. K. Gaharwar, V. T. Rao, M. Nikkhah, S. R. Shin, D. Krafft, M. R. Dokmeci and D. Shum-Tim, *ACS Nano*, 2014, **8**, 8050-8062.

193. K. Vulic and M. S. Shoichet, *Journal of the American Chemical Society*, 2011, **134**, 882-885.

194. G. Molinaro, J.-C. Leroux, J. Damas and A. Adam, *Biomaterials*, 2002, **23**, 2717-2722.

195. J.-A. Yang, J. Yeom, B. W. Hwang, A. S. Hoffman and S. K. Hahn, *Progress in Polymer Science*, 2014, **39**, 1973-1986.

196. L. Li, B. Yan, J. Yang, L. Chen and H. Zeng, *Advanced Materials*, 2015, **27**, 1294-1299.

197. M. Shin, S.-G. Park, B.-C. Oh, K. Kim, S. Jo, M. S. Lee, S. S. Oh, S.-H. Hong, E.-C. Shin and K.-S. Kim, *Nature Materials*, 2017, **16**, 147-152.

198. M. R. Prausnitz and R. Langer, *Nature Biotechnology*, 2008, **26**, 1261-1268.

199. M. R. Prausnitz, *Advanced Drug Delivery Reviews*, 2004, **56**, 581-587.

200. S. Y. Yang, E. D. O'Cearbhaill, G. C. Sisk, K. M. Park, W. K. Cho, M. Villiger, B. E. Bouma, B. Pomahac and J. M. Karp, *Nature Communications*, 2013, **4**, 1702.

201. S. Henry, D. V. McAllister, M. G. Allen and M. R. Prausnitz, *Journal of Pharmaceutical Sciences*, 1998, **87**, 922-925.

202. J. A. Mikszta, J. B. Alarcon, J. M. Brittingham, D. E. Sutter, R. J. Pettis and N. G. Harvey, *Nature Medicine*, 2002, **8**, 415-419.

203. S. P. Sullivan, D. G. Koutsonanos, M. del Pilar Martin, J. W. Lee, V. Zarnitsyn, S.-O. Choi, N. Murthy, R. W. Compans, I. Skountzou and M. R. Prausnitz, *Nature Medicine*, 2010, **16**, 915-920.

204. P. C. DeMuth, A. V. Li, P. Abbink, J. Liu, H. Li, K. A. Stanley, K. M. Smith, C. L. Lavine, M. S. Seaman and J. A. Kramer, *Nature Biotechnology*, 2013, **31**, 1082-1085.

205. J. Yu, Y. Zhang, Y. Ye, R. DiSanto, W. Sun, D. Ranson, F. S. Ligler, J. B. Buse and Z. Gu, *Proceedings of the National Academy of Sciences*, 2015, **112**, 8260-8265.

206. P. C. DeMuth, J. J. Moon, H. Suh, P. T. Hammond and D. J. Irvine, *ACS Nano*, 2012, **6**, 8041-8051.

207. D. A. LaVan, T. McGuire and R. Langer, *Nature Biotechnology*, 2003, **21**, 1184-1191.

208. R. Langer, *Pharmacology & Therapeutics*, 1983, **21**, 35-51.

209. J. M. Anderson, *European Journal of Pharmaceutics and Biopharmaceutics*, 1994, **40**, 1-8.

210. R. Langer, *Nature Biotechnology*, 1994, **12**, 689-693.

211. J. N. Brown, J. M. Miller, R. A. Altschuler and A. L. Nuttall, *Hearing Research*, 1993, **70**, 167-172.

212. C. D. Saudek, J.-L. Selam, H. A. Pitt, K. Waxman, M. Rubio, N. Jeandidier, D. Turner, R. E. Fischell and M. A. Charles, *New England Journal of Medicine*, 1989, **321**, 574-579.

213. H. J. Hirsch, D. Gillis, D. Strich, B. Chertin, A. Farkas, T. Lindenberg, H. Gelber and I. M. Spitz, *Pediatrics*, 2005, **116**, e798-e802.

214. J. Folkman, D. M. Long and R. Rosenbaum, *Science*, 1966, **154**, 148-149.

215. R. Langer and J. Folkman, 1976.

216. R. Langer and D. A. Tirrell, *Nature*, 2004, **428**, 487-492.

217. D. G. Anderson, J. A. Burdick and R. Langer, *Science*, 2004, **305**, 1923-1924.

218. J. P. Rolland, B. W. Maynor, L. E. Euliss, A. E. Exner, G. M. Denison and J. M. DeSimone, *Journal of the American Chemical Society*, 2005, **127**, 10096-10100.

219. J. Y. Kelly and J. M. DeSimone, *Journal of the American Chemical Society*, 2008, **130**, 5438-5439.

220. K.-S. Lee, R. H. Kim, D.-Y. Yang and S. H. Park, *Progress in Polymer Science*, 2008, **33**, 631-681.

221. S. Sershen and J. West, *Advanced Drug Delivery Reviews*, 2002, **54**, 1225-1235.

222. K. E. Uhrich, S. M. Cannizzaro, R. S. Langer and K. M. Shakesheff, *Chemical Reviews*, 1999, **99**, 3181-3198.

223. W. B. Liechty, D. R. Kryscio, B. V. Slaughter and N. A. Peppas, *Annual Review of Chemical and Biomolecular Engineering*, 2010, **1**, 149-173.

224. O. Pillai and R. Panchagnula, *Current Opinion in Chemical Biology*, 2001, **5**, 447-451.

225. A. Bajpai, S. K. Shukla, S. Bhanu and S. Kankane, *Progress in Polymer Science*, 2008, **33**, 1088-1118.

226. S. Mura, J. Nicolas and P. Couvreur, *Nature Materials*, 2013, **12**, 991-1003.

227. R. Langer and J. Folkman, *Nature*, 1976, **263**, 797-800.

228. D. Schmaljohann, *Advanced Drug Delivery Reviews*, 2006, **58**, 1655-1670.

229. Y. Qiu and K. Park, *Advanced Drug Delivery Reviews*, 2001, **53**, 321-339.

230. A. Chilkoti, M. R. Dreher, D. E. Meyer and D. Raucher, *Advanced Drug Delivery Reviews*, 2002, **54**, 613-630.

231. P. Bawa, V. Pillay, Y. E. Choonara and L. C. Du Toit, *Biomedical Materials*, 2009, **4**, 022001.

232. C. J. Kearney and D. J. Mooney, *Nature Materials*, 2013, **12**, 1004-1017.

233. A. S. Hoffman, *Journal of Controlled Release*, 2008, **132**, 153-163.

234. P. T. Wong and S. K. Choi, *Chemical Reviews*, 2015, **115**, 3388-3432.

235. N. A. Peppas and B. Narasimhan, *Journal of Controlled Release*, 2014, **190**, 75-81.

236. A. N. F. Versypt, D. W. Pack and R. D. Braatz, *Journal of Controlled Release*, 2013, **165**, 29-37.

237. M. Grassi and G. Grassi, *Current Drug Delivery*, 2005, **2**, 97-116.

238. C. Ferrero, D. Massuelle and E. Doelker, *Journal of Controlled Release*, 2010, **141**, 223-233.

239. J. Crank, *The mathematics of diffusion*, Oxford university press, 1979.

240. S. Koutsopoulos, L. D. Unsworth, Y. Nagai and S. Zhang, *Proceedings of the National Academy of Sciences*, 2009, **106**, 4623-4628.

241. L. Serra, J. Doménech and N. A. Peppas, *Biomaterials*, 2006, **27**, 5440-5451.

242. P. I. Lee and N. A. Peppas, *Journal of Controlled Release*, 1987, **6**, 207-215.

243. B. Narasimhan, *Advanced Drug Delivery Reviews*, 2001, **48**, 195-210.

244. J. Heller, R. Baker, R. Gale and J. Rodin, *Journal of Applied Polymer Science*, 1978, **22**, 1991-2009.

245. B. Narasimhan and N. A. Peppas, *Journal of Pharmaceutical Sciences*, 1997, **86**, 297-304.

246. J. Siepmann, H. Kranz, R. Bodmeier and N. Peppas, *Pharmaceutical Research*, 1999, **16**, 1748-1756.

247. S. Dash, P. N. Murthy, L. Nath and P. Chowdhury, *Acta Poloniae Pharmaceutica*, 2010, **67**, 217-223.

248. D. R. Paul and F. W. Harris, *Controlled release polymeric formulations*, ACS Publications, ACS Symposium Series, 1976.

249. A. Hixson and J. Crowell, *Industrial & Engineering Chemistry*, 1931, **23**, 1160-1168.

250. H. Hopfenberg, in *Controlled Release Polymeric Formulations*, ACS Publications, ACS Symposium Series, 1976, vol. 33, pp. 26-32.

251. S. N. Rothstein, W. J. Federspiel and S. R. Little, *Biomaterials*, 2009, **30**, 1657-1664.

252. M. M. Pakulska, S. Miersch and M. S. Shoichet, *Science*, 2016, **351**, aac4750.

253. K. Vulic, M. M. Pakulska, R. Sonthalia, A. Ramachandran and M. S. Shoichet, *Journal of Controlled Release*, 2015, **197**, 69-77.

254. V. Delplace, J. Obermeyer and M. S. Shoichet, *ACS Nano*, 2016, **10**, 6433-6436.

255. K. Vulic and M. S. Shoichet, *Biomacromolecules*, 2014, **15**, 3867-3880.

256. H. Duan, L. Zhu, J. Hou, J. Peng, H. Xie, Y. Lin, C. Liu, W. Li, H. Xu and C. Wang, *Organic & Biomolecular Chemistry*, 2016, **14**, 11342-11346.

257. N. X. Wang and H. A. Von Recum, *Macromolecular Bioscience*, 2011, **11**, 321-332.

258. S. E. Sakiyama-Elbert and J. A. Hubbell, *Journal of Controlled Release*, 2000, **65**, 389-402.

259. C. C. Lin and A. T. Metters, *Journal of Biomedical Materials Research Part A*, 2007, **83**, 954-964.

260. A. S. Fu, T. R. Thatiparti, G. M. Saidel and H. A. Von Recum, *Annals of Biomedical Engineering*, 2011, **39**, 2466-2475.

261. K. C. Koehler, K. S. Anseth and C. N. Bowman, *Biomacromolecules*, 2013, **14**, 538-547.

262. M. B. Yatvin, J. N. Weinstein, W. H. Dennis and R. Blumenthal, *Science*, 1978, **202**, 1290-1293.

263. M. Karimi, P. Sahandi Zangabad, A. Ghasemi, M. Amiri, M. Bahrami, H. Malekzad, H. Ghahramanzadeh Asl, Z. Mahdieh, M. Bozorgomid and A. Ghasemi, *ACS Applied Materials & Interfaces*, 2016, **8**, 21107-21133.

264. J. K. Oh, D. I. Lee and J. M. Park, *Progress in Polymer Science*, 2009, **34**, 1261-1282.

265. S. G. Lévesque and M. S. Shoichet, *Bioconjugate Chemistry*, 2007, **18**, 874-885.

266. D. S. Muggli, A. K. Burkoth, S. A. Keyser, H. R. Lee and K. S. Anseth, *Macromolecules*, 1998, **31**, 4120-4125.

267. D. Steinhilber, M. Witting, X. Zhang, M. Staegemann, F. Paulus, W. Friess, S. Küchler and R. Haag, *Journal of Controlled Release*, 2013, **169**, 289-295.

268. X. Li, Y. Gao and M. J. Serpe, *Canadian Journal of Chemistry*, 2015, **93**, 685-689.

269. N. Murthy, Y. X. Thng, S. Schuck, M. C. Xu and J. M. Fréchet, *Journal of the American Chemical Society*, 2002, **124**, 12398-12399.

270. D. Neugebauer, J. Rydz, I. Goebel, P. Dacko and M. Kowalczuk, *Macromolecules*, 2007, **40**, 1767-1773.

271. N. Bhuchar, R. Sunasee, K. Ishihara, T. Thundat and R. Narain, *Bioconjugate Chemistry*, 2011, **23**, 75-83.

272. M. Motornov, Y. Roiter, I. Tokarev and S. Minko, *Progress in Polymer Science*, 2010, **35**, 174-211.

273. H. Bysell, R. Månsson, P. Hansson and M. Malmsten, *Advanced Drug Delivery Reviews*, 2011, **63**, 1172-1185.

274. N. Smeets and T. Hoare, *Journal of Polymer Science Part A: Polymer Chemistry*, 2013, **51**, 3027-3043.

275. M. Laurenti, P. Guardia, R. Contreras-Cáceres, J. Pérez-Juste, A. Fernandez-Barbero, E. Lopez-Cabarcos and J. Rubio-Retama, *Langmuir*, 2011, **27**, 10484-10491.

276. F. Zhang and C.-C. Wang, *Langmuir*, 2009, **25**, 8255-8262.

277. M. Boularas, E. Gombart, J. F. Tranchant, L. Billon and M. Save, *Macromolecular Rapid Communications*, 2015, **36**, 79-83.

278. O. Yassine, A. Zaher, E. Q. Li, A. Alfadhel, J. E. Perez, M. Kavaldzhiev, M. F. Contreras, S. T. Thoroddsen, N. M. Khashab and J. Kosel, *Scientific Reports*, 2016, **6**, 28539

279. K. Gupta and H. Gangadharappa, *American Journal of Drug Discovery and Development*, 2011, **1**, 24-48.

280. P. Gupta, K. Vermani and S. Garg, *Drug Discovery Today*, 2002, **7**, 569-579.

281. V. Delplace and J. Nicolas, *Nature Chemistry*, 2015, **7**, 771-784.

282. A. R. Khare and N. A. Peppas, *Journal of Biomaterials Science, Polymer Edition*, 1993, **4**, 275-289.

283. N. A. Peppas and A. R. Khare, *Advanced Drug Delivery Reviews*, 1993, **11**, 1-35.

284. M. Am Ende, D. Hariharan and N. Peppas, *Reactive Polymers*, 1995, **25**, 127-137.

285. E. O. Akala, P. Kopečková and J. Kopeček, *Biomaterials*, 1998, **19**, 1037-1047.

286. A. Gutowska, J. S. Bark, I. C. Kwon, Y. H. Bae, Y. Cha and S. W. Kim, *Journal of Controlled Release*, 1997, **48**, 141-148.

287. V. Carelli, S. Coltelli, G. Di Colo, E. Nannipieri and M. Serafini, *International Journal of Pharmaceutics*, 1999, **179**, 73-83.

288. B. Lu, M. Tarn, N. Pamme and T. Georgiou, *Journal of Materials Chemistry B*, 2016, **4**, 3086-3093.

289. B. Lu, M. Tarn, N. Pamme and T. Georgiou, *Journal of Materials Chemistry B*, 2015, **3**, 4524-4529.

290. X. Zhang, S. Malhotra, M. Molina and R. Haag, *Chemical Society Reviews*, 2015, **44**, 1948-1973.

291. T. Rossow, J. A. Heyman, A. J. Ehrlicher, A. Langhoff, D. A. Weitz, R. Haag and S. Seiffert, *Journal of the American Chemical Society*, 2012, **134**, 4983-4989.

292. A. L. Sisson and R. Haag, *Soft Matter*, 2010, **6**, 4968-4975.

293. X. Zhang, K. Achazi and R. Haag, *Advanced Healthcare Materials*, 2015, **4**, 585-592.

294. D. Steinhilber, T. Rossow, S. Wedepohl, F. Paulus, S. Seiffert and R. Haag, *Angewandte Chemie International Edition*, 2013, **52**, 13538-13543.

295. M. C. Parrott, J. C. Luft, J. D. Byrne, J. H. Fain, M. E. Napier and J. M. DeSimone, *Journal of the American Chemical Society*, 2010, **132**, 17928-17932.

296. Z.-Y. Qiao, R. Zhang, F.-S. Du, D.-H. Liang and Z.-C. Li, *Journal of Controlled Release*, 2011, **152**, 57-66.

297. Y.-Y. Liu, Y.-H. Shao and J. Lü, *Biomaterials*, 2006, **27**, 4016-4024.

298. Y. Gao, A. Ahiabu and M. J. Serpe, *ACS Applied Materials & Interfaces*, 2014, **6**, 13749-13756.

299. Y. Gao, G. P. Zago, Z. Jia and M. J. Serpe, *ACS Applied Materials & Interfaces*, 2013, **5**, 9803-9808.

300. T. Hoare and R. Pelton, *Langmuir*, 2008, **24**, 1005-1012.

301. A. Barhoumi, Q. Liu and D. S. Kohane, *Journal of Controlled Release*, 2015, **219**, 31-42.

302. V. Marturano, P. Cerruti, M. Giamberini, B. Tylkowski and V. Ambrogi, *Polymers*, 2016, **9**, 8.

303. C. Alvarez‐Lorenzo, L. Bromberg and A. Concheiro, *Photochemistry and Photobiology*, 2009, **85**, 848-860.

304. D. Wang and S. Wu, *Langmuir*, 2016, **32**, 632-636.

305. M. J. Hansen, W. A. Velema, M. M. Lerch, W. Szymanski and B. L. Feringa, *Chemical Society Reviews*, 2015, **44**, 3358-3377.

306. J. Cao, S. Huang, Y. Chen, S. Li, X. Li, D. Deng, Z. Qian, L. Tang and Y. Gu, *Biomaterials*, 2013, **34**, 6272-6283.

307. B. Yan, J.-C. Boyer, D. Habault, N. R. Branda and Y. Zhao, *Journal of the American Chemical Society*, 2012, **134**, 16558-16561.

308. J. Jiang, X. Tong, D. Morris and Y. Zhao, *Macromolecules*, 2006, **39**, 4633.

309. R. Luo, Y. Cao, P. Shi and C. H. Chen, *Small*, 2014, **10**, 4886-4894.

310. H. Wang, J. Di, Y. Sun, J. Fu, Z. Wei, H. Matsui, A. del C Alonso and S. Zhou, *Advanced Functional Materials*, 2015, **25**, 5537-5547.

311. L. Zhang, Y. Li, Z. Jin, C. Y. Jimmy and K. M. Chan, *Nanoscale*, 2015, **7**, 12614-12624.

312. K. Khaletskaya, J. Reboul, M. Meilikhov, M. Nakahama, S. p. Diring, M. Tsujimoto, S. Isoda, F. Kim, K.-i. Kamei and R. A. Fischer, *Journal of the American Chemical Society*, 2013, **135**, 10998-11005.

313. H. Kim, D. Lee, J. Kim, T.-i. Kim and W. J. Kim, *ACS Nano*, 2013, **7**, 6735-6746.

314. W. Yin, L. Yan, J. Yu, G. Tian, L. Zhou, X. Zheng, X. Zhang, Y. Yong, J. Li and Z. Gu, *ACS Nano*, 2014, **8**, 6922-6933.

315. F. Kong, X. Zhang, H. Zhang, X. Qu, D. Chen, M. Servos, E. Mäkilä, J. Salonen, H. A. Santos and M. Hai, *Advanced Functional Materials*, 2015, **25**, 3330-3340.

316. A. K. Rengan, A. B. Bukhari, A. Pradhan, R. Malhotra, R. Banerjee, R. Srivastava and A. De, *Nano Letters*, 2015, **15**, 842-848.

317. T. Kawano, Y. Niidome, T. Mori, Y. Katayama and T. Niidome, *Bioconjugate Chemistry*, 2009, **20**, 209-212.

318. S. M. Lee, H. Park, J. W. Choi, Y. N. Park, C. O. Yun and K. H. Yoo, *Angewandte Chemie International Edition*, 2011, **50**, 7581-7586.

319. R. Contreraseras International EditionPark, C. O. Yun and K. H. Yoo, oo, vastava and A. De, Dacifico, T. Hellweg, A. Fernández‐Barbero and L. M. Liz‐Marzán, *Advanced Materials*, 2008, **20**, 1666-1670.

320. M. S. Yavuz, Y. Cheng, J. Chen, C. M. Cobley, Q. Zhang, M. Rycenga, J. Xie, C. Kim, K. H. Song and A. G. Schwartz, *Nature Materials*, 2009, **8**, 935-939.

321. J. H. Kim and T. Randall Lee, *Drug Development Research*, 2006, **67**, 61-69.

322. A. Agarwal, M. A. Mackey, M. A. El-Sayed and R. V. Bellamkonda, *ACS Nano*, 2011, **5**, 4919-4926.

323. G. Saravanakumar, J. Lee, J. Kim and W. J. Kim, *Chemical Communications*, 2015, **51**, 9995-9998.

324. H. Zhang, X. Fan, R. Suo, H. Li, Z. Yang, W. Zhang, Y. Bai, H. Yao and W. Tian, *Chemical Communications*, 2015, **51**, 15366-15369.

325. S. Son, E. Shin and B.-S. Kim, *Biomacromolecules*, 2014, **15**, 628-634.

326. J. Sun, R. Gui, H. Jin, N. Li and X. Wang, *RSC Advances*, 2016, **6**, 8722-8728.

327. Y. Hu, M. Deng, H. Yang, L. Chen, C. Xiao, X. Zhuang and X. Chen, *Polymer*, 2017.

328. X. Wang, J. Zhang, Y. Wang, C. Wang, J. Xiao, Q. Zhang and Y. Cheng, *Biomaterials*, 2016, **81**, 114-124.

329. Y. Zhang, C. Fu, Y. Li, K. Wang, X. Wang, Y. Wei and L. Tao, *Polymer Chemistry*, 2017.

330. R. Roy, M. Bhagyalalitha, P. Choudhury and P. Dastidar, *Chemical Communications*, 2016, **52**, 13811-13814.

331. Q. Hu, W. Sun, C. Wang and Z. Gu, *Advanced Drug Delivery Reviews*, 2016, **98**, 19-34.

332. J. P. Wu, B. Cheng, S. R. Roffler, D. J. Lundy, C. Y. Yen, P. Chen, J. J. Lai, S. H. Pun, P. S. Stayton and P. C. Hsieh, *Science Translational Medicine*, 2016, **8**, 365ra160.

333. A. GhavamiNejad, M. SamariKhalaj, L. E. Aguilar, C. H. Park and C. S. Kim, *Scientific Reports*, 2016, **6**, 33594.

334. J. Kost and R. Langer, *Advanced Drug Delivery Reviews*, 2001, **46**, 125-148.

335. J. L. West, *Nature Materials*, 2003, **2**, 709-710.

336. A. Nelson, *Nature Materials*, 2008, **7**, 523-525.

337. H. Ichikawa and Y. Fukumori, *Journal of Controlled Release*, 2000, **63**, 107-119.

338. T. Hoare and R. Pelton, *Langmuir*, 2008, **24**, 1005-1012.

339. J. Zhang, Z.-F. Yuan, Y. Wang, W.-H. Chen, G.-F. Luo, S.-X. Cheng, R.-X. Zhuo and X.-Z. Zhang, *Journal of the American Chemical Society*, 2013, **135**, 5068-5073.

340. N. Singh, A. Karambelkar, L. Gu, K. Lin, J. S. Miller, C. S. Chen, M. J. Sailor and S. N. Bhatia, *Journal of the American Chemical Society*, 2011, **133**, 19582-19585.

341. I. I. Slowing, B. G. Trewyn, S. Giri and V. Y. Lin, *Advanced Functional Materials*, 2007, **17**, 1225-1236.

342. P. Nadrah, U. Maver, A. Jemec, T. Tišler, M. Bele, G. Dražić, M. Benčina, A. Pintar, O. Planinšek and M. Gaberšček, *ACS Applied Materials & Interfaces*, 2013, **5**, 3908-3915.

343. E. Choleris, S. R. Little, J. A. Mong, S. V. Puram, R. Langer and D. W. Pfaff, *Proceedings of the National Academy of Sciences*, 2007, **104**, 4670-4675.

344. B. S. Aytar, M. R. Prausnitz and D. M. Lynn, *ACS Applied Materials & Interfaces*, 2012, **4**, 2726-2734.

345. A. Elbakry, A. Zaky, R. Liebl, R. Rachel, A. Goepferich and M. Breunig, *Nano Letters*, 2009, **9**, 2059-2064.

346. D. He, X. He, K. Wang, M. Chen, Y. Zhao and Z. Zou, *Journal of Materials Chemistry B*, 2013, **1**, 1552-1560.

347. L. E. Bromberg and E. S. Ron, *Advanced Drug Delivery Reviews*, 1998, **31**, 197-221.

348. G. Liu, W. Liu and C.-M. Dong, *Polymer Chemistry*, 2013, **4**, 3431-3443.

349. K. Niikura, N. Iyo, Y. Matsuo, H. Mitomo and K. Ijiro, *ACS Applied Materials & Interfaces*, 2013, **5**, 3900-3907.

350. B. Sahoo, K. S. P. Devi, R. Banerjee, T. K. Maiti, P. Pramanik and D. Dhara, *ACS Applied Materials & Interfaces*, 2013, **5**, 3884-3893.

351. H. J. Kim, H. Matsuda, H. Zhou and I. Honma, *Advanced Materials*, 2006, **18**, 3083-3088.

352. S.-F. Lee, X.-M. Zhu, Y.-X. J. Wang, S.-H. Xuan, Q. You, W.-H. Chan, C.-H. Wong, F. Wang, J. C. Yu and C. H. Cheng, *ACS Applied Materials & Interfaces*, 2013, **5**, 1566-1574.

353. J. Ge, E. Neofytou, T. J. Cahill III, R. E. Beygui and R. N. Zare, *ACS Nano*, 2011, **6**, 227-233.

354. S. J. McInnes, E. J. Szili, S. A. Al-Bataineh, J. Xu, M. E. Alf, K. K. Gleason, R. D. Short and N. H. Voelcker, *ACS Applied Materials & Interfaces*, 2012, **4**, 3566-3574.

355. P. Horcajada, C. Serre, G. Maurin, N. A. Ramsahye, F. Balas, M. Vallet-Regi, M. Sebban, F. Taulelle and G. Férey, *Journal of the American Chemical Society*, 2008, **130**, 6774-6780.

356. Z. Zhang, D. Balogh, F. Wang and I. Willner, *Journal of the American Chemical Society*, 2013, **135**, 1934-1940.

357. Z. Zhang, D. Balogh, F. Wang, R. Tel-Vered, N. Levy, S. Y. Sung, R. Nechushtai and I. Willner, *Journal of Materials Chemistry B*, 2013, **1**, 3159-3166.

358. T. D. Nguyen, Y. Liu, S. Saha, K. C.-F. Leung, J. F. Stoddart and J. I. Zink, *Journal of the American Chemical Society*, 2007, **129**, 626-634.

359. J. T. Santini, M. J. Cima and R. Langer, *Nature*, 1999, **397**, 335-338.

360. G. Jeon, S. Y. Yang, J. Byun and J. K. Kim, *Nano Letters*, 2011, **11**, 1284-1288.

361. K. Vasilev, N. Poulter, P. Martinek and H. J. Griesser, *ACS Applied Materials & Interfaces*, 2011, **3**, 4831-4836.

362. H. Kawaguchi, K. Fujimoto and Y. Mizuhara, *Colloid and Polymer Science*, 1992, **270**, 53-57.

363. I. Berndt and W. Richtering, *Macromolecules*, 2003, **36**, 8780-8785.

364. R. Pelton, H. Pelton, A. Morphesis and R. Rowell, *Langmuir*, 1989, **5**, 816-818.

365. J. Wiedemair, M. J. Serpe, J. Kim, J.-F. Masson, L. A. Lyon, B. Mizaikoff and C. Kranz, *Langmuir*, 2007, **23**, 130-137.

366. Z. Meng, J. K. Cho, S. Debord, V. Breedveld and L. A. Lyon, *The Journal of Physical Chemistry B*, 2007, **111**, 6992-6997.

367. M. Karg, Y. Lu, E. Carbo-Argibay, I. Pastoriza-Santos, J. Perez-Juste, L. M. Liz-Marzan and T. Hellweg, *Langmuir*, 2009, **25**, 3163-3167.

368. O. Zavgorodnya and M. J. Serpe, *Colloid and Polymer Science*, 2011, **289**, 591-602.

369. A. Burmistrova and R. von Klitzing, *Journal of Materials Chemistry*, 2010, **20**, 3502-3507.

370. Z. Meng, G. R. Hendrickson and L. A. Lyon, *Macromolecules*, 2009, **42**, 7664-7669.

371. W. H. Blackburn, E. B. Dickerson, M. H. Smith, J. F. McDonald and L. A. Lyon, *Bioconjugate Chemistry*, 2009, **20**, 960-968.

372. S. Nayak, H. Lee, J. Chmielewski and L. A. Lyon, *Journal of the American Chemical Society*, 2004, **126**, 10258-10259.

373. L. Hu and M. J. Serpe, *Chemical Communications*, 2013, **49**, 2649-2651.

374. M. R. Islam and M. J. Serpe, *Chemical Communications*, 2013, **49**, 2646-2648.

375. L. Hu and M. J. Serpe, *Polymers*, 2012, **4**, 134-149.

376. E. Ayano, M. Karaki, T. Ishihara, H. Kanazawa and T. Okano, *Colloids and Surfaces B: Biointerfaces*, 2012, **99**, 67-73.

377. Q. M. Zhang, X. Li, M. R. Islam, M. Wei and M. J. Serpe, *Journal of Materials Chemistry C*, 2014, **2**, 6961-6965.

378. W. Fischer, M. A. Quadir, A. Barnard, D. K. Smith and R. Haag, *Macromolecular Bioscience*, 2011, **11**, 1736-1746.

379. L. Y. Chu, T. Yamaguchi and S.-i. Nakao, *Advanced Materials*, 2002, **14**, 386-389.

380. X. Ma, Y. Cui, X. Zhao, S. Zheng and X. Tang, *Journal of colloid and interface science*, 2004, **276**, 53-59.

381. J. Rubio-Retama, N. E. Zafeiropoulos, C. Serafinelli, R. Rojas-Reyna, B. Voit, E. Lopez Cabarcos and M. Stamm, *Langmuir*, 2007, **23**, 10280-10285.

382. M. R. Islam and M. J. Serpe, *Biosensors and Bioelectronics*, 2013, **49**, 133-138.

383. M. R. Islam and M. J. Serpe, *APL Materials*, 2013, **1**, 052108.

384. M. R. Islam, Y. Gao, X. Li and M. J. Serpe, *Journal of Materials Chemistry B*, 2014, **2**, 2444-2451.

385. J. Ferguson, E. Smith, A. Weimer and S. George, *Journal of The Electrochemical Society*, 2004, **151**, G528-G535.

386. X. Deng, L. Mammen, H.-J. Butt and D. Vollmer, *Science*, 2012, **335**, 67-70.

387. Y. Kobayashi, H. Katakami, E. Mine, D. Nagao, M. Konno and L. M. Liz-Marzán, *Journal of Colloid and Interface Science*, 2005, **283**, 392-396.

388. S. Guo, Y. Gao, M. Wei, Q. M. Zhang and M. J. Serpe, *Journal of Materials Chemistry B*, 2015, **3**, 2516-2521.

389. C. Kneuer, M. Sameti, E. G. Haltner, T. Schiestel, H. Schirra, H. Schmidt and C.-M. Lehr, *International Journal of Pharmaceutics*, 2000, **196**, 257-261.

390. Y. Lu, Y. Yin, B. T. Mayers and Y. Xia, *Nano Letters*, 2002, **2**, 183-186.

391. R. Langer, *Nature*, 1998, **392**, 5-10.

392. R. Langer, *Science*, 1990, **249**, 1527-1533.

393. Y. Qiu and K. Park, *Advanced Drug Delivery Reviews*, 2012, **64**, 49-60.

394. B. Chertok, M. J. Webber, M. D. Succi and R. Langer, *Molecular Pharmaceutics*, 2013, **10**, 3531-3543.

395. S. J. Liu, S. Wen Wenser, M. D. Succi and R. Langer, *Journal of Biomedical Materials research*, 2002, **63**, 807-813.

396. N. S. Rejinold, T. Baby, K. Chennazhi and R. Jayakumar, *Journal of Biomedical Nanotechnology*, 2015, **11**, 392-402.

397. M. S. Aw, J. Addai-Mensah and D. Losic, *Chemical Communications*, 2012, **48**, 3348-3350.

398. Q. He, Y. Gao, L. Zhang, Z. Zhang, F. Gao, X. Ji, Y. Li and J. Shi, *Biomaterials*, 2011, **32**, 7711-7720.

399. H.-C. Shin, A. W. Alani, D. A. Rao, N. C. Rockich and G. S. Kwon, *Journal of Controlled Release*, 2009, **140**, 294-300.

400. F.-M. Chen, M. Zhang and Z.-F. Wu, *Biomaterials*, 2010, **31**, 6279-6308.

401. A. C. Le Meur, C. Aymonier and V. Héroguez, *ChemPhysChem*, 2012, **13**, 692-694.

402. T. Sun, Y. S. Zhang, B. Pang, D. C. Hyun, M. Yang and Y. Xia, *Angewandte Chemie International Edition*, 2014, **53**, 12320-12364.

403. T. Vermonden, R. Censi and W. E. Hennink, *Chemical Reviews*, 2012, **112**, 2853-2888.

404. Y. Jiang, G. Liu, X. Wang, J. Hu, G. Zhang and S. Liu, *Macromolecules*, 2015, **48**, 764-774.

405. M. Malmsten, H. Bysell and P. Hansson, *Current Opinion in Colloid & Interface Science*, 2010, **15**, 435-444.

406. H. Zhang, M. Oh, C. Allen and E. Kumacheva, *Biomacromolecules*, 2004, **5**, 2461-2468.

407. X. Hu, G. Liu, Y. Li, X. Wang and S. Liu, *Journal of the American Chemical Society*, 2014, **137**, 362-368.

408. P. J. Blackshear, *Scientific American*, 1979, **241**, 66.

409. J. Khandare and T. Minko, *Progress in Polymer Science*, 2006, **31**, 359-397.

410. J. Kopeček, *Advanced Drug Delivery Reviews*, 2013, **65**, 49-59.

411. J. Ding, L. Chen, C. Xiao, L. Chen, X. Zhuang and X. Chen, *Chemical Communications*, 2014, **50**, 11274-11290.

412. M. R. Lee, K. H. Baek, H. J. Jin, Y. G. Jung and I. Shin, *Angewandte Chemie International Edition*, 2004, **43**, 1675-1678.

413. K. T. Oh, H. Yin, E. S. Lee and Y. H. Bae, *Journal of Materials Chemistry*, 2007, **17**, 3987-4001.

414. R. Pelton and P. Chibante, *Colloids and Surfaces*, 1986, **20**, 247-256.

415. J. Yin, X. Guan, D. Wang and S. Liu, *Langmuir*, 2009, **25**, 11367-11374.

416. D. Wang, T. Liu, J. Yin and S. Liu, *Macromolecules*, 2011, **44**, 2282-2290.

417. V. Lapeyre, I. Gosse, S. Chevreux and V. Ravaine, *Biomacromolecules*, 2006, **7**, 3356-3363.

418. T. Hoare, B. P. Timko, J. Santamaria, G. F. Goya, S. Irusta, S. Lau, C. F. Stefanescu, D. Lin, R. Langer and D. S. Kohane, *Nano Letters*, 2011, **11**, 1395-1400.

419. Y. Gao, W. Xu and M. J. Serpe, *Journal of Materials Chemistry C*, 2014, **2**, 5878-5884.

420. Y. Gao and M. J. Serpe, *ACS Applied Materials & Interfaces*, 2014, **6**, 8461-8466.

421. Q. M. Zhang, W. Xu and M. J. Serpe, *Angewandte Chemie*, 2014, **126**, 4927-4931.

422. I. Tokarev and S. Minko, *Soft Matter*, 2009, **5**, 511-524.

423. I. Tokarev, M. Motornov and S. Minko, *Journal of Materials Chemistry*, 2009, **19**, 6932-6948.

424. T. Chen, R. Ferris, J. Zhang, R. Ducker and S. Zauscher, *Progress in Polymer Science*, 2010, **35**, 94-112.

425. L. Zhai, *Chemical Society Reviews*, 2013, **42**, 7148-7160.

426. G. Stoychev, S. Turcaud, J. W. Dunlop and L. Ionov, *Advanced Functional Materials*, 2013, **23**, 2295-2300.

427. J. D. Debord, S. Eustis, S. Byul Debord, M. T. Lofye and L. A. Lyon, *Advanced Materials*, 2002, **14**, 658-662.

428. J.-S. Wang and K. Matyjaszewski, *Journal of the American Chemical Society*, 1995, **117**, 5614-5615.

429. J.-S. Wang and K. Matyjaszewski, *Macromolecules*, 1995, **28**, 7901-7910.

430. K. Matyjaszewski and J. Xia, *Chemical Reviews*, 2001, **101**, 2921-2990.

431. G. Decher, *Science*, 1997, **277**, 1232-1237.

432. Y. Lvov, K. Ariga, I. Ichinose and T. Kunitake, *Journal of the American Chemical Society*, 1995, **117**, 6117-6123.

433. F. Caruso, K. Niikura, D. N. Furlong and Y. Okahata, *Langmuir*, 1997, **13**, 3422-3426.

434. C. Jiang, S. Markutsya and V. V. Tsukruk, *Advanced Materials*, 2004, **16**, 157-161.

435. C. Jiang and V. V. Tsukruk, *Advanced Materials*, 2006, **18**, 829-840.

436. K. E. Shopsowitz, H. Qi, W. Y. Hamad and M. J. MacLachlan, *Nature*, 2010, **468**, 422-425.

437. D. Xu, Q. Xu, K. Wang, J. Chen and Z. Chen, *ACS Applied Materials & Interfaces*, 2013, **6**, 200-209.

438. S. H. Wibowo, E. H. Wong, A. Sulistio, S. N. Guntari, A. Blencowe, F. Caruso and G. G. Qiao, *Advanced Materials*, 2013, **25**, 4619-4624.

439. S. S. Shiratori and M. F. Rubner, *Macromolecules*, 2000, **33**, 4213-4219.

440. Z. Bian, J. Song, R. C. Webb, A. P. Bonifas, J. A. Rogers and Y. Huang, *RSC Advances*, 2014, **4**, 5694-5697.

441. W. H. Yeo, Y. S. Kim, J. Lee, A. Ameen, L. Shi, M. Li, S. Wang, R. Ma, S. H. Jin and Z. Kang, *Advanced Materials*, 2013, **25**, 2773-2778.

442. R. C. Webb, A. P. Bonifas, A. Behnaz, Y. Zhang, K. J. Yu, H. Cheng, M. Shi, Z. Bian, Z. Liu and Y.-S. Kim, *Nature Materials*, 2013.

443. L. Persano, C. Dagdeviren, Y. Su, Y. Zhang, S. Girardo, D. Pisignano, Y. Huang and J. A. Rogers, *Nature Communications*, 2013, **4**, 1633.

444. D.-H. Kim, N. Lu, Y. Huang and J. A. Rogers, *MRS Bulletin*, 2012, **37**, 226-235.

445. X. Huang, W.-H. Yeo, Y. Liu and J. A. Rogers, *Biointerphases*, 2012, **7**, 1-9.

446. I. N. Heppner and M. J. Serpe, *Colloid and Polymer Science*, 2013, 1-6.

447. A. Rotzetter, C. Schumacher, S. Bubenhofer, R. Grass, L. Gerber, M. Zeltner and W. Stark, *Advanced Materials*, 2012, **24**, 5352-5356.

448. G. A. Ozin and S. Yang, *Advanced Functional Materials*, 2001, **11**, 95-104.

449. J. E. Wijnhoven and W. L. Vos, *Science*, 1998, **281**, 802-804.

450. P. V. Braun and P. Wiltzius, *Nature*, 1999, **402**, 603-604.

451. P. Jiang, J. F. Bertone and V. L. Colvin, *Science*, 2001, **291**, 453-457.

452. V. L. Colvin, *MRS Bulletin*, 2001, **26**, 637-641.

453. P. J. Pauzauskie and P. Yang, *Materials Today*, 2006, **9**, 36-45.

454. S.-y. Lin, J. Fleming, D. Hetherington, B. Smith, R. Biswas, K. Ho, M. Sigalas, W. Zubrzycki, S. Kurtz and J. Bur, *Nature*, 1998, **394**, 251-253.

455. M. Deubel, G. Von Freymann, M. Wegener, S. Pereira, K. Busch and C. M. Soukoulis, *Nature Materials*, 2004, **3**, 444-447.

456. C. I. Aguirre, E. Reguera and A. Stein, *Advanced Functional Materials*, 2010, **20**, 2565-2578.

457. A. R. Parker and H. E. Townley, *Nature Nanotechnology*, 2007, **2**, 347-353.

458. A. C. Arsenault, D. P. Puzzo, I. Manners and G. A. Ozin, *Nature Photonics*, 2007, **1**, 468-472.

459. O. Sato, S. Kubo and Z.-Z. Gu, *Accounts of Chemical Research*, 2008, **42**, 1-10.

460. A. Garcia, M. Marquez, T. Cai, R. Rosario, Z. Hu, D. Gust, M. Hayes, S. A. Vail and C.-D. Park, *Langmuir*, 2007, **23**, 224-229.

461. T. J. White, M. E. McConney and T. J. Bunning, *Journal of Materials Chemistry*, 2010, **20**, 9832-9847.

462. J. Ge and Y. Yin, *Advanced Materials*, 2008, **20**, 3485-3491.

463. J. Ge and Y. Yin, *Journal of Materials Chemistry*, 2008, **18**, 5041-5045.

464. J. H. Holtz and S. A. Asher, *Nature*, 1997, **389**, 829-832.

465. J. D. Debord and L. A. Lyon, *The Journal of Physical Chemistry B*, 2000, **104**, 6327-6331.

466. Y. F. Yue, M. A. Haque, T. Kurokawa, T. Nakajima and J. P. Gong, *Advanced Materials*, 2013.

467. K. Lee and S. A. Asher, *Journal of the American Chemical Society*, 2000, **122**, 9534-9537.

468. Z. Wang, J. Zhang, J. Xie, C. Li, Y. Li, S. Liang, Z. Tian, T. Wang, H. Zhang and H. Li, *Advanced Functional Materials*, 2010, **20**, 3784-3790.

469. J. Huang, C.-a. Tao, Q. An, C. Lin, X. Li, D. Xu, Y. Wu, X. Li, D. Shen and G. Li, *Chemical Communication*, 2010, **46**, 4103-4105.

470. L. Hu and M. J. Serpe, *Journal of Materials Chemistry*, 2012, **22**, 8199-8202.

471. B. Zhao, J. S. Moore and D. J. Beebe, *Science*, 2001, **291**, 1023-1026.

472. E. Cabane, V. Malinova and W. Meier, *Macromolecular Chemistry and Physics*, 2010, **211**, 1847-1856.

473. P. C. DeMuth, Y. Min, B. Huang, J. A. Kramer, A. D. Miller, D. H. Barouch, P. T. Hammond and D. J. Irvine, *Nature Materials*, 2013, **12**, 367-376.

474. G. Ciamician and P. Silber, *Berichte der deutschen chemischen Gesellschaft*, 1901, **34**, 1530-1543.

475. M. L. Donten, P. Hamm and J. VandeVondele, *The Journal of Physical Chemistry B*, 2011, **115**, 1075-1083.

476. G. Ciamician and P. Silber, *European Journal of Inorganic Chemistry*, 1901, **34**, 1530-1543.

477. P. A. Leighton and F. A. Lucy, *The Journal of Chemical Physics*, 1934, **2**, 756-759.

478. F. A. Lucy and P. A. Leighton, *The Journal of Chemical Physics*, 1934, **2**, 760-766.

479. A. Tench and P. Coppens, *The Journal of Physical Chemistry*, 1963, **67**, 1378-1380.

480. S. Laimgruber, W. J. Schreier, T. Schrader, F. Koller, W. Zinth and P. Gilch, *Angewandte Chemie International Edition*, 2005, **44**, 7901-7904.

481. M. Gaplovsky, Y. V. Il'ichev, Y. Kamdzhilov, S. V. Kombarova, M. Mac, M. A. Schwörer and J. Wirz, *Photochemical & Photobiological Sciences*, 2005, **4**, 33-42.

482. S. Laimgruber, T. Schmierer, P. Gilch, K. Kiewisch and J. Neugebauer, *Physical Chemistry Chemical Physics*, 2008, **10**, 3872-3882.

483. T. Schmierer, G. Ryseck, T. Villnow, N. Regner and P. Gilch, *Photochemical & Photobiological Sciences*, 2012, **11**, 1313-1321.

484. M. George and J. Scaiano, *The Journal of Physical Chemistry*, 1980, **84**, 492-495.

485. I. A. Eydelnant, B. B. Li and A. R. Wheeler, *Nature Communications*, 2015, **5**, 7513.

486. R. Mezzenga, P. Schurtenberger, A. Burbidge and M. Michel, *Nature Materials*, 2005, **4**, 729-740.

487. S. Nayak and L. A. Lyon, *Angewandte Chemie International Edition*, 2005, **44**, 7686-7708.

488. D. Heyes and A. Brańka, *Soft Matter*, 2009, **5**, 2681-2685.

489. J. Mattsson, H. M. Wyss, A. Fernandez-Nieves, K. Miyazaki, Z. Hu, D. R. Reichman and D. A. Weitz, *Nature*, 2009, **462**, 83-86.

490. B. R. Saunders and B. Vincent, *Advances in Colloid and Interface Science*, 1999, **80**, 1-25.

491. M. Malmsten, *Microgel Suspensions: Fundamentals and Applications*, 2011, 375-405.

492. G. R. Hendrickson and L. A. Lyon, *Soft Matter*, 2009, **5**, 29-35.

493. S. Su, M. M. Ali, C. D. Filipe, Y. Li and R. Pelton, *Biomacromolecules*, 2008, **9**, 935-941.

494. L. A. Lyon, J. D. Debord, S. B. Debord, C. D. Jones, J. G. McGrath and M. J. Serpe, *The Journal of Physical Chemistry B*, 2004, **108**, 19099-19108.

495. D. Parasuraman and M. J. Serpe, *ACS Applied Materials & Interfaces*, 2011, **3**, 2732-2737.

496. B. Zhao and J. S. Moore, *Langmuir*, 2001, **17**, 4758-4763.

497. S. Dai, P. Ravi and K. C. Tam, *Soft Matter*, 2009, **5**, 2513-2533.

498. Q. M. Zhang, W. Xu and M. J. Serpe, *Angewandte Chemie International Edition*, 2014, **53**, 4827-4831.

499. D. Klinger and K. Landfester, *Polymer*, 2012, **53**, 5209-5231.

500. B. Brugger and W. Richtering, *Advanced Materials*, 2007, **19**, 2973-2978.

501. S. Nayak and L. A. Lyon, *Angewandte Chemie International Edition*, 2004, **43**, 6706-6709.

502. S. Fujishige, K. Kubota and I. Ando, *The Journal of Physical Chemistry*, 1989, **93**, 3311-3313.

503. T. Okano, N. Yamada, H. Sakai and Y. Sakurai, *Journal of Biomedical Materials Research*, 1993, **27**, 1243-1251.

504. T. Hoare, J. Santamaria, G. F. Goya, S. Irusta, D. Lin, S. Lau, R. Padera, R. Langer and D. S. Kohane, *Nano Letters*, 2009, **9**, 3651-3657.

505. J. Kost and R. Langer, *Advanced Drug Delivery Reviews*, 2012, **64**, 327-341.

506. X. Wu, R. Pelton, A. Hamielec, D. Woods and W. McPhee, *Colloid and Polymer Science*, 1994, **272**, 467-477.

507. C. D. Jones and L. A. Lyon, *Macromolecules*, 2003, **36**, 1988-1993.

508. M. Das, N. Sanson and E. Kumacheva, *Chemistry of Materials*, 2008, **20**, 7157-7163.

509. K. C. Johnson, F. Mendez and M. J. Serpe, *Analytica Chimica Acta*, 2012, **739**, 83-88.

510. I. Eke, B. Elmas, M. Tuncel and A. Tuncel, *Colloids and Surfaces A: Physicochemical and Engineering Aspects*, 2006, **279**, 247-253.

511. D. Suzuki and K. Horigome, *Langmuir : the ACS Journal of Surfaces and Colloids*, 2011, **27**, 12368-12374.

512. J. Kaur, S. L. Harikumar and A. Kaur, *International Research Journal of Pharmacy*, 2012, **3**, 58-62.

513. K. Soppimath, T. Aminabhavi, A. Dave, S. Kumbar and W. Rudzinski, *Drug Development and Industrial Pharmacy*, 2002, **28**, 957-974.

514. L. Zha, B. Banik and F. Alexis, *Soft Matter*, 2011, **7**, 5908-5916.

515. T. R. Hoare and D. S. Kohane, *Polymer*, 2008, **49**, 1993-2007.

516. D. Kakde, D. Jain, V. Shrivastava, R. Kakde and A. T. Patil, *Journal of Applied Pharmaceutical Science*, 2011, **01**, 01-10.

517. D. Parasuraman, A. K. Sarker and M. J. Serpe, *ChemPhysChem*, 2012, **13**, 2507-2515.

518. D. Parasuraman, E. Leung and M. J. Serpe, *Colloid and Polymer Science*, 2012, **290**, 1053-1064.

519. D. Parasuraman, A. K. Sarker and M. J. Serpe, *Colloid and Polymer Science*, 2013, **291**, 1795-1802.

520. L. Yang, X. Liu, X. Tan, H. Yang, Z. Wang and X. Zhang, *Polymer Chemistry*, 2014, **5**, 323-326.

521. L. Yang, X. Tan, Z. Wang and X. Zhang, *Chemical Reviews*, 2015, **115**, 7196-7239.

522. C. Fouquey, J. M. Lehn and A. M. Levelut, *Advanced Materials*, 1990, **2**, 254-257.

523. L. Brunsveld, B. Folmer, E. Meijer and R. Sijbesma, *Chemical Reviews*, 2001, **101**, 4071-4098.

524. T. F. De Greef, M. M. Smulders, M. Wolffs, A. P. Schenning, R. P. Sijbesma and E. Meijer, *Chemical Reviews*, 2009, **109**, 5687-5754.

525. X. Yan, F. Wang, B. Zheng and F. Huang, *Chemical Society Reviews*, 2012, **41**, 6042-6065.

526. S. J. Barrow, S. Kasera, M. J. Rowland, J. del Barrio and O. A. Scherman, *Chemical Reviews*, 2015, **115**, 12320-12406.

527. Y. Liu, Y. Yu, J. Gao, Z. Wang and X. Zhang, *Angewandte Chemie*, 2010, **122**, 6726-6729.

528. Y. Liu, K. Liu, Z. Wang and X. Zhang, *Chemistry–A European Journal*, 2011, **17**, 9930-9935.

529. Z. Huang, L. Yang, Y. Liu, Z. Wang, O. A. Scherman and X. Zhang, *Angewandte Chemie International Edition*, 2014, **53**, 5351-5355.

530. L. Yang, Y. Bai, X. Tan, Z. Wang and X. Zhang, *ACS Macro Letters*, 2015, **4**, 611-615.

531. J.-F. Xu, Z. Huang, L. Chen, B. Qin, Q. Song, Z. Wang and X. Zhang, *ACS Macro Letters*, 2015, **4**, 1410-1414.

532. P. Wei, X. Yan, T. R. Cook, X. Ji, P. J. Stang and F. Huang, *ACS Macro Letters*, 2016, **5**, 671-675.

533. L. Rui, L. Liu, Y. Wang, Y. Gao and W. Zhang, *ACS Macro Letters*, 2015, **5**, 112-117.

534. N. Roy, E. Buhler and J.-M. Lehn, *Polymer Chemistry*, 2013, **4**, 2949-2957.

535. J.-F. Xu, Y.-Z. Chen, L.-Z. Wu, C.-H. Tung and Q.-Z. Yang, *Organic Letters*, 2013, **15**, 6148-6151.

536. Q. Song, F. Li, X. Tan, L. Yang, Z. Wang and X. Zhang, *Polymer Chemistry*, 2014, **5**, 5895-5899.

537. Q. Song, F. Li, L. Yang, Z. Wang and X. Zhang, *Polymer Chemistry*, 2015, **6**, 369-372.

538. Z. Huang, Y. Fang, Q. Luo, S. Liu, G. An, C. Hou, C. Lang, J. Xu, Z. Dong and J. Liu, *Chemical Communications*, 2016, **52**, 2083-2086.

539. X. Liu, J.-F. Xu, Z. Wang and X. Zhang, *Polymer Chemistry*, 2016, **7**, 2333-2336.

540. M. Ballauff and Y. Lu, *Polymer*, 2007, **48**, 1815-1823.

541. Q. M. Zhang, W. Xu and M. J. Serpe, *Angewandte Chemie International Edition*, 2014, **53**, 4827-4831.

542. W. Zhang, W. Zhang, Z. Cheng, N. Zhou, J. Zhu, Z. Zhang, G. Chen and X. Zhu, *Macromolecules*, 2011, **44**, 3366-3373.

543. S. Sun, P. Wu, W. Zhang, W. Zhang and X. Zhu, *Soft Matter*, 2013, **9**, 1807-1816.

544. T. Liu, J. Hu, J. Yin, Y. Zhang, C. Li and S. Liu, *Chemistry of Materials*, 2009, **21**, 3439-3446.

545. X. Li, Y. Gao and M. J. Serpe, *Macromolecular Rapid Communications*, 2015, **36**, 1382-1392.

546. X. Zheng, J. Qian, F. Tang, Z. Wang, C. Cao and K. Zhong, *ACS Macro Letters*, 2015, **4**, 431-435.

547. Q. Yuan, J. Gu, Y.-n. Zhao, L. Yao, Y. Guan and Y. Zhang, *ACS Macro Letters*, 2016, **5**, 565-568.

548. D. Parasuraman and M. J. Serpe, *ACS Applied Materials & Interfaces*, 2011, **3**, 4714-4721.

549. Y. Guan and Y. Zhang, *Soft Matter*, 2011, **7**, 6375-6384.

550. M. R. Islam, X. Li, K. Smyth and M. J. Serpe, *Angewandte Chemie International Edition*, 2013, **52**, 10330-10333.

551. X. Li and M. J. Serpe, *Advanced Functional Materials*, 2014, **24**, 4119-4126.

552. X. Li and M. J. Serpe, *Advanced Functional Materials*, 2016, **26**, 3282-3290.

553. L. M. Heitmann, A. B. Taylor, P. J. Hart and A. R. Urbach, *Journal of the American Chemical Society*, 2006, **128**, 12574-12581.

554. H. D. Nguyen, D. T. Dang, J. L. Van Dongen and L. Brunsveld, *Angewandte Chemie*, 2010, **122**, 907-910.

555. D. T. Dang, J. Schill and L. Brunsveld, *Chemical Science*, 2012, **3**, 2679-2684.

556. C. Hou, J. Li, L. Zhao, W. Zhang, Q. Luo, Z. Dong, J. Xu and J. Liu, *Angewandte Chemie International Edition*, 2013, **52**, 5590-5593.

557. X. Tan, L. Yang, Y. Liu, Z. Huang, H. Yang, Z. Wang and X. Zhang, *Polymer Chemistry*, 2013, **4**, 5378-5381.

558. M. Ramaekers, S. P. Wijnands, J. L. van Dongen, L. Brunsveld and P. Y. Dankers, *Chemical Communications*, 2015, **51**, 3147-3150.

559. S. Liu, C. Ruspic, P. Mukhopadhyay, S. Chakrabarti, P. Y. Zavalij and L. Isaacs, *Journal of the American Chemical Society*, 2005, **127**, 15959-15967.

Appendix

The appendixes are providing supporting information for this dissertation as well as some of the unpublished data from other projects that relatively to this topic. Appendix A-E is the unfinished projects that I did during the Ph.D. program. The main data will provide for each project and the describe of the data will be shown.

Appendix A: Understanding the Drug Uptake and Release Behavior of Microgels and Their Assemblies

In this project, we prepared three microgels with different percentage of AAc groups, MG1 (NIPAm : AAc : BIS=85 % : 10 % : 5 %), MG2 (NIPAm : AAc : BIS=75 % : 20 % : 5 %), MG3 (NIPAm : AAc : BIS=65 % : 30 % : 5 %), respectively, to study the uptaking and releasing behavior of p(NIPAm-*co*-AAc) microgels. Based on the electrostatic interaction between the positively charged CV molecules and negatively charged microgels, we evaluate the ability that microgels uptaking CV molecules as well as the kinetics of this process. The schematic shown was shown in Figure B-1 represent how CV was uptake by microgels.

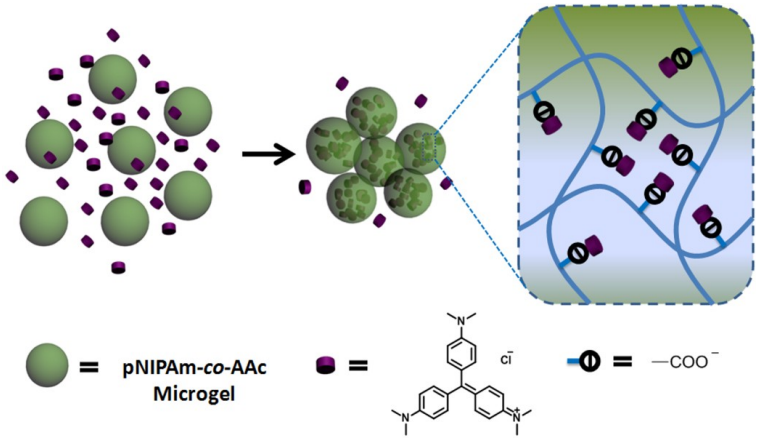

Figure A-1. Schematic illustration drug uptaking process and electrostatic interaction between p(NIPAm-*co*-AAc) microgels

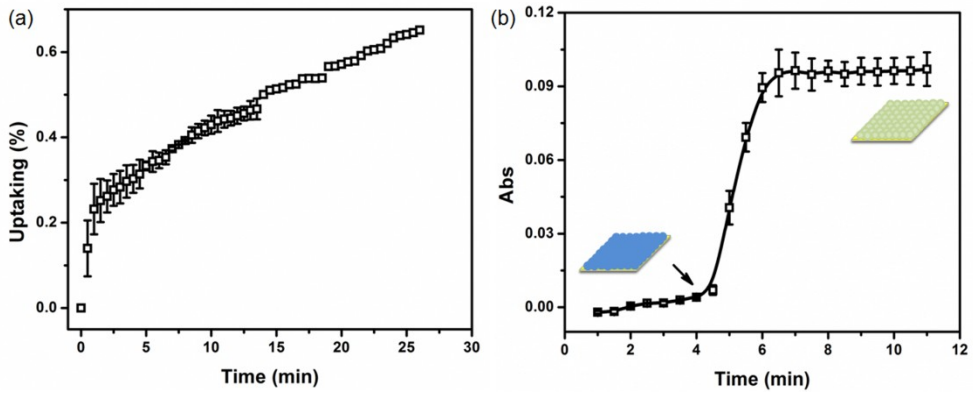

Figure A-2. Uptaking kinetics (a) and releasing behavior (b) of MG1 microgels-based assemblies.

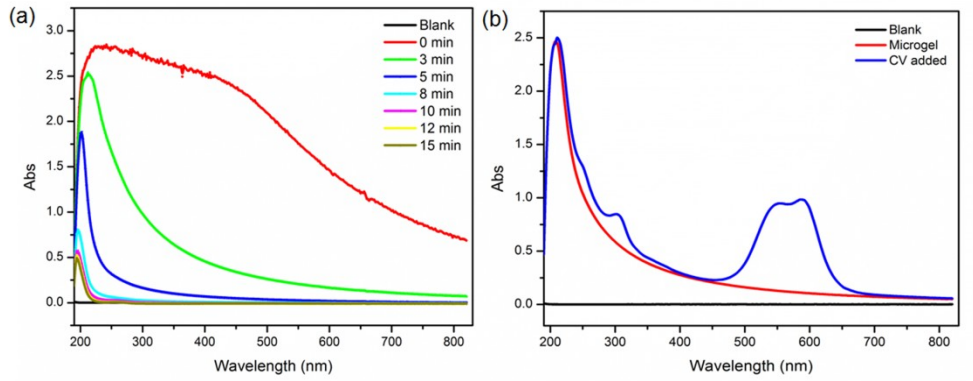

Figure A-3. (a) Evaluation of drug uptaking under different time scale. (b) UV-vis spectrum of microgel before and after uptaking CV, shown both the peaks of microgels and CV individually.

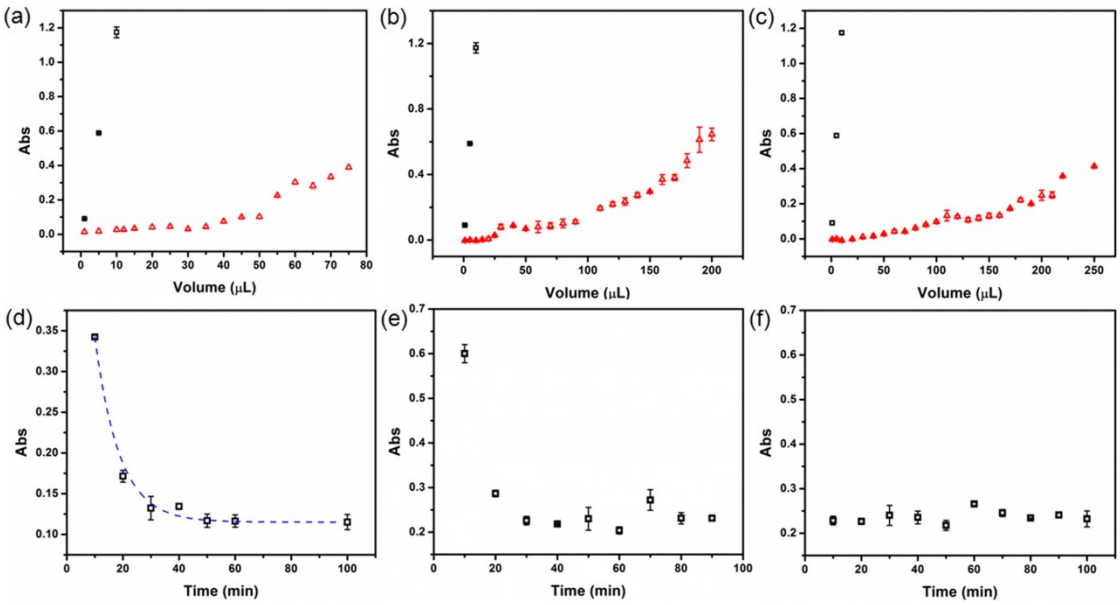

Figure A-4. Drug uptaking ability (a-c) and kinetics (d-f) for different microgels. MG1, (a) and (d). MG2, (b) and (e). MG3, (c) and (f).

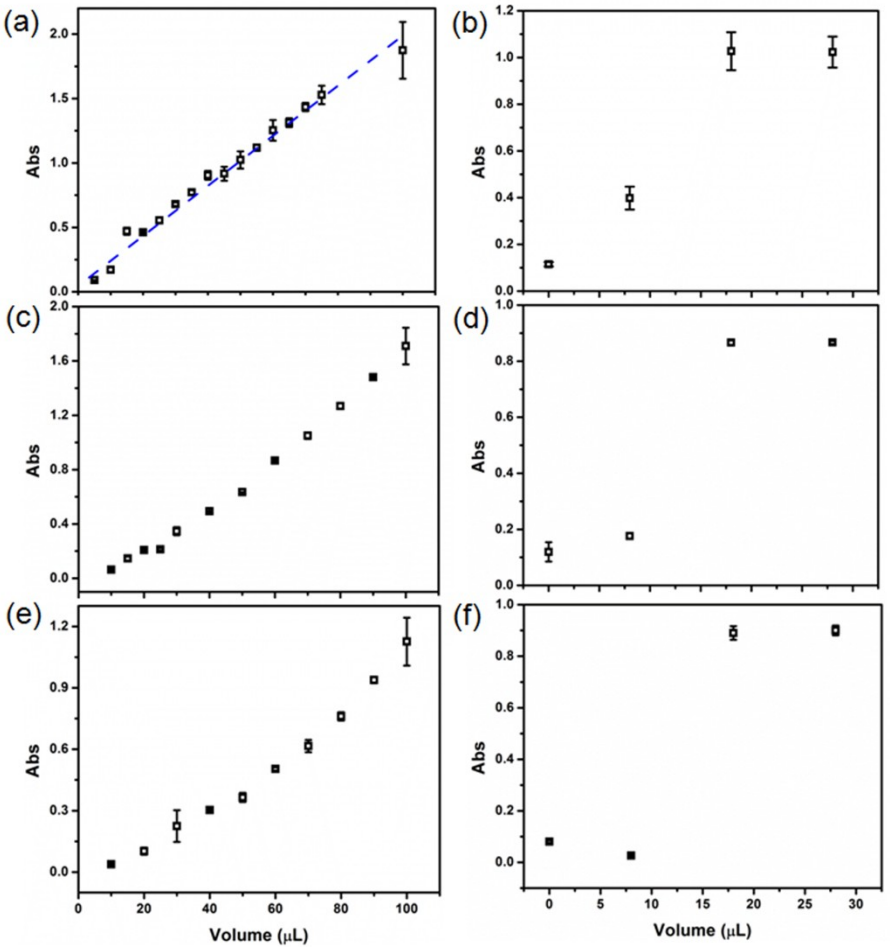

Figure A-5. Drug releasing behavior from different microgels, MG1, (a) and (b). MG2, (c) and (d). MG3, (e) and (f).

Appendix B: Polymer Brush-Based Optical Device with Multiple Responsivities[i]

In this Appendix, we constructed a stimuli-responsive optical device that changes its optical properties in response to multiple environmental stimuli, including temperature, pH, and humidity. The device's responsivity is a direct result of the pNIPAm-based layer changing conformation when exposed to these stimuli, which directly changes the distance between the device's Au layers. The device is easily prepared using standard ATRP polymerization and is extremely versatile regarding the functionality that can be added to the brush layer. For example, by reacting the resultant AAc groups with other functional molecules, the brush can exhibit responses to other stimuli and can be used for sensing or drug delivery applications.

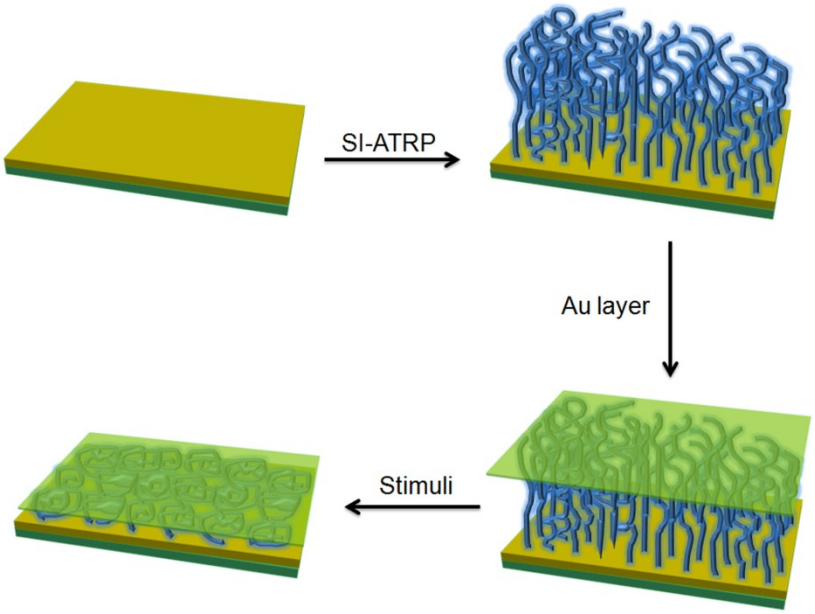

Figure B-1. Illustration of the device fabrication process and its response to a stimulus. First, an ATRP initiator was attached to the Au surface by a self-assembly process in anhydrous ethanol. Following this step, surface-initiated atom transfer radical polymerization (SI-ATRP) was

[i] This Appendix has been adapted from the previously published article: M. Wei,[†] Y. Gao,[†] M. J. Serpe.* *J. Mater. Chem. B*, 2015, 3, 744-747.

conducted to produce the desired brush. Finally, another 15 nm Au layer was thermally evaporated onto the resultant polymer brush. This yields a layered structure, which is capable of interacting with light to produce color.

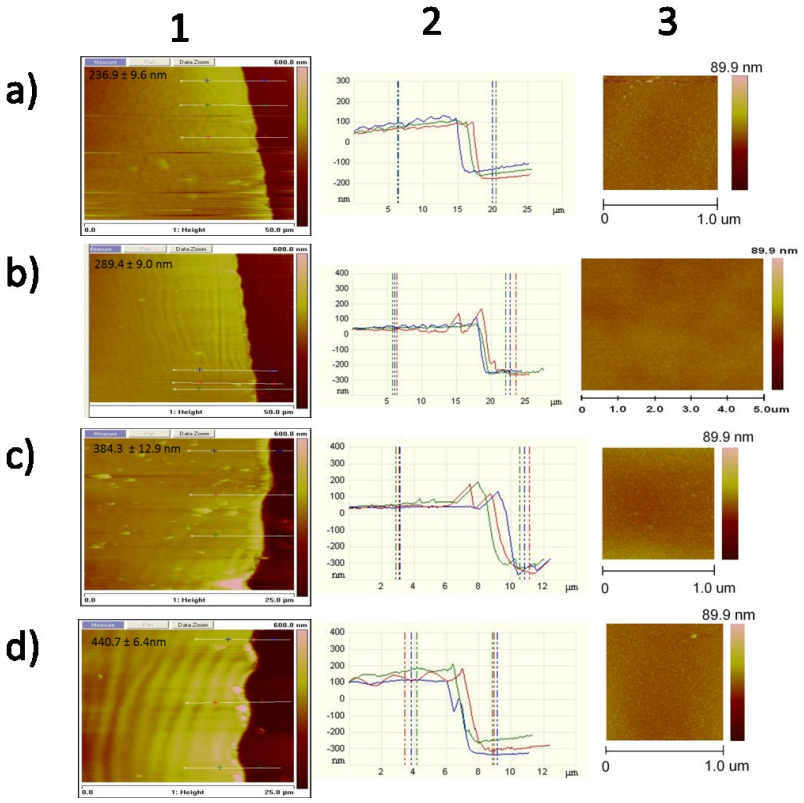

Figure B-2. AFM images of pNIPAm brush-based devices. Column 1 is images acquired in the air of a scratched portion of the device. The scratches were made with a razor blade. Column 2 is the line traces for the images in column 1. Column 3 shows the images of the films acquired away from the scratch.

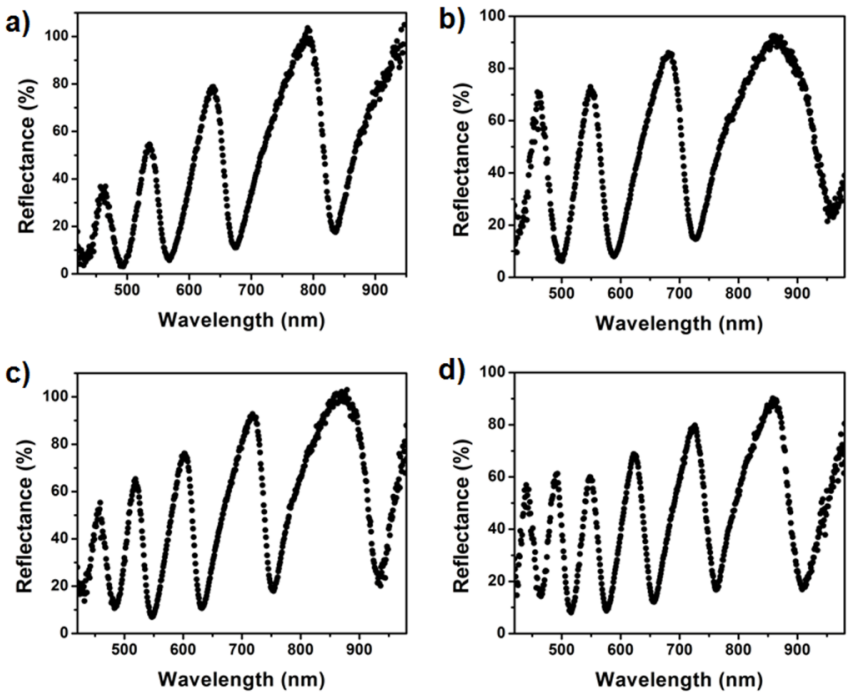

Figure B-3. Reflectance spectra for pNIPAm polymer brush-based devices with brush thicknesses of: (a) 237 ± 9 nm, (b) 289 ± 9 nm, (c) 380 ± 10 nm, and (d) 441 ± 6 nm. The thicknesses were measured using AFM. As can be seen, as the brush thickness of the brush is increased, the number of peaks in the reflectance spectrum increases. This is a direct result of more orders of reflection being possible when the etalons dielectric thickness increases, as we mention in previous chapters.

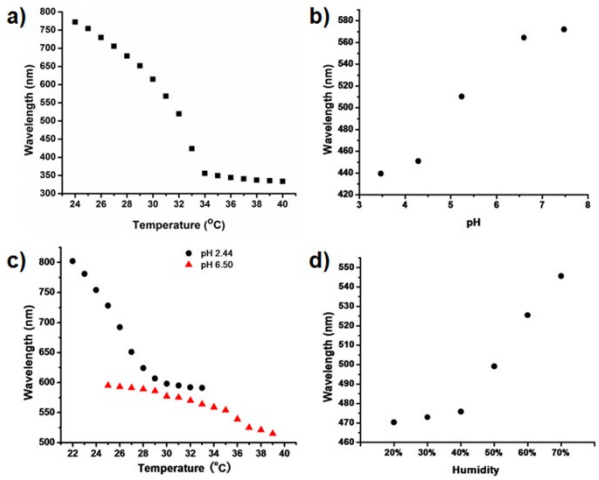

Figure B-4. Stimuli-responsive properties of polymer brush-based devices. (a) Temperature responsivity of the pNIPAm brush-based device. the device's reflectance peak shifted an impressive ~ 500 nm when the water temperature was changed from 24 to 40 ^{o}C. Additionally, the visible color of the device changed dramatically; (b) pH responsivity of p(NIPAm-*co*-AAc) brush-based device. The reflectance peaks red shift from 440 nm to 570 nm as the pH is raised above AAc's pK_a, and goes back to the original position once the pH is returned to < 4.25; (c) temperature responsivity of p(NIPAm-*co*-AAc) brush based device at the indicated solution pH. At pH 2.44, the wavelength shifted from 800 nm to 600 nm as the temperature was increased from 22 to 34 ^{o}C. At pH 6.50, the wavelength shifts from 600 nm to 500 nm when the temperature in increased from 24 to 40 ^{o}C. The minimal temperature responsivity is a result of the negative charges in the brush preventing the collapse at high temperature; (d) humidity responsivity of p(NIPAm-*co*-AAc) brush based device. The wavelength shifts from 470 nm to 550 nm as the relative humidity increases.

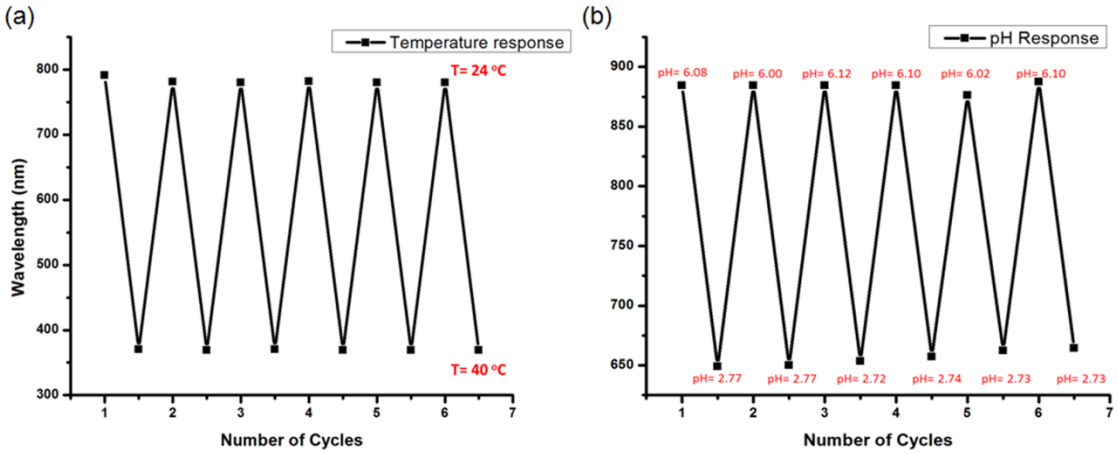

Figure B-5. Evaluation of the reproducibility of temperature and pH response. (a) PNIPAm brushes response to temperature change from 24 °C to 40 °C for 6 cycles. (b) For pH response reproducibility of p(NIPAm-*co*-AAc) brushes, the pH was changed from ~ 2.7 to ~ 6.2 and back to ~ 2.7 for several runs.

Appendix C: Novel Responsive Microgels Synthesis and Characterization

In this project, we prepared two microgels with different functions, poly (N-isopropylacrylamide-*co*-glycidyl methacrylate) (p(NIPAm-*co*-GMA)), and poly (N-isopropylacrylamide-*co*-3-(Trimethoxysilyl)propyl methacrylate) (p(NIPAm-*co*-TPM)). The epoxy group in p(NIPAm-*co*-GMA) microgels are reactive to multiple groups under gentle condition makes it lots of opportunities for post-functionalization. Tuning the percentage of TPM will give the properties of p(NIPAm-*co*-TPM) microgels will stay between soft pNIPAm microgels and solid silica nanoparticles, which will promote interesting phenomenon.

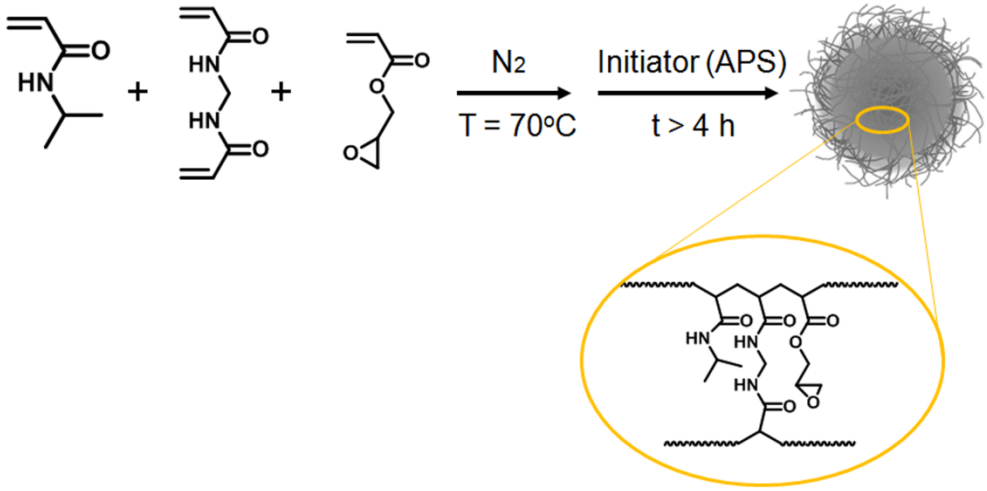

Figure C-1. Synthesize of p(NIPAm-*co*-GMA) microgel by free-radical polymerization.

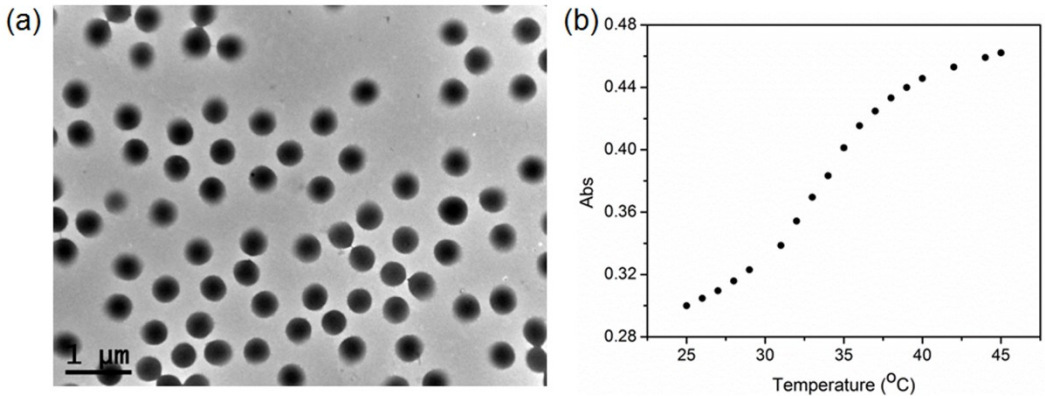

Figure C-2. (a) Morphology characterization of p(NIPAm-*co*-GMA) microgel by TEM and (b) thermal responsive properties test. LCST shift to ~ 35 ^{o}C.

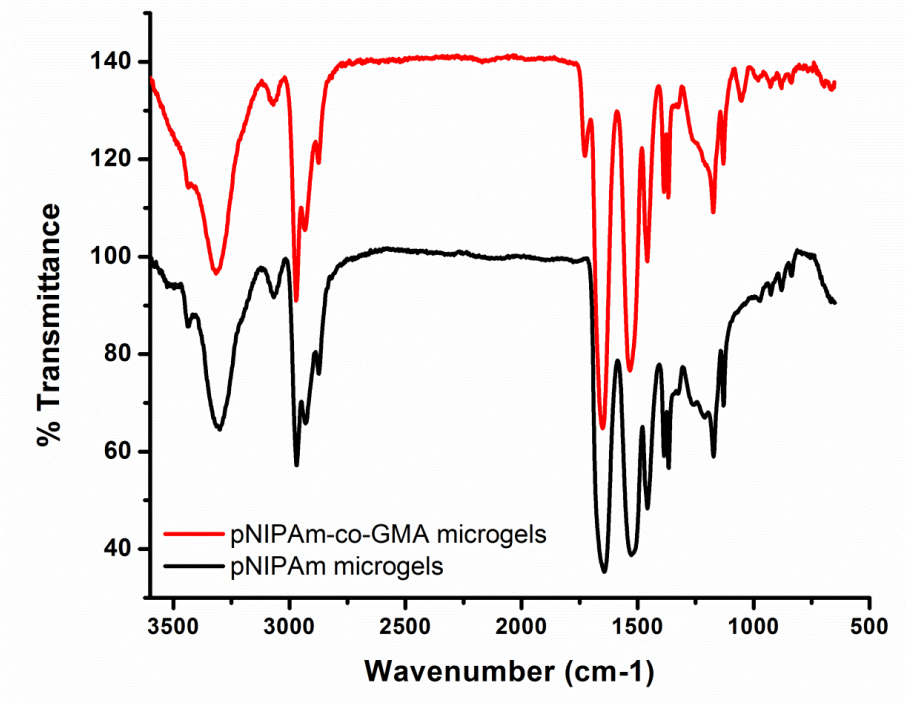

Figure C-3. FTIR comparison of p(NIPAm-*co*-GMA) and pNIPAm microgels. The peaks at 1727 cm^{-1} and 1052 cm^{-1} represent the present of GMA monomer in microgels.

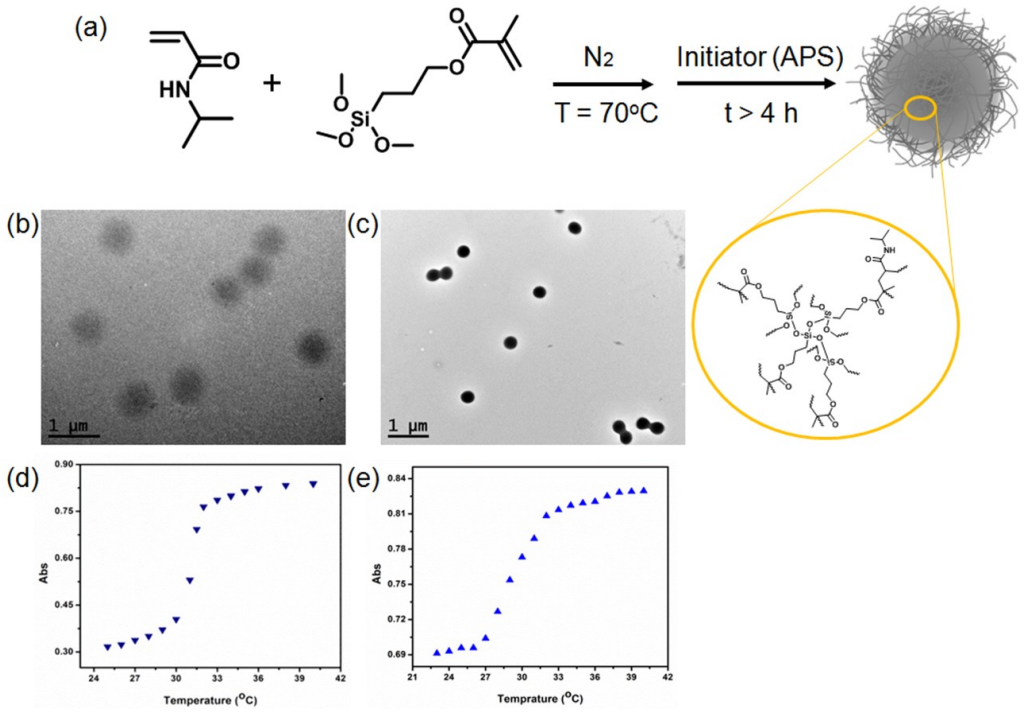

Figure C-4. (a) Synthesize of p(NIPAm-*co*-TPM) microgel by free-radical polymerization without adding crosslinker. Morphology of p(NIPAm-*co*-TPM) microgel by TEM with different percentage of TPM added, 1 % (b) and 5 % (c). Thermal responsive properties test for 1 % (d), the LCST is ~31 ^{o}C and 5 % (e), LCST shift to ~ 30 ^{o}C.

Appendix D: Core-Shell Microgels Assemblies for Controlled Drug Release

In this project, core-shell microgels were prepared to study the controlled drug release behavior. The p(NIPAm-*co*-AAc) core works as a drug reservoir to load the drug and the pNIPAm shell as a rate control membrane to tune the drug release rate. The core-shell microgels were assembled on the surface to form a monolayer to study the drug release. Latterly, different shell thickness could be prepared with varies of releasing rate.

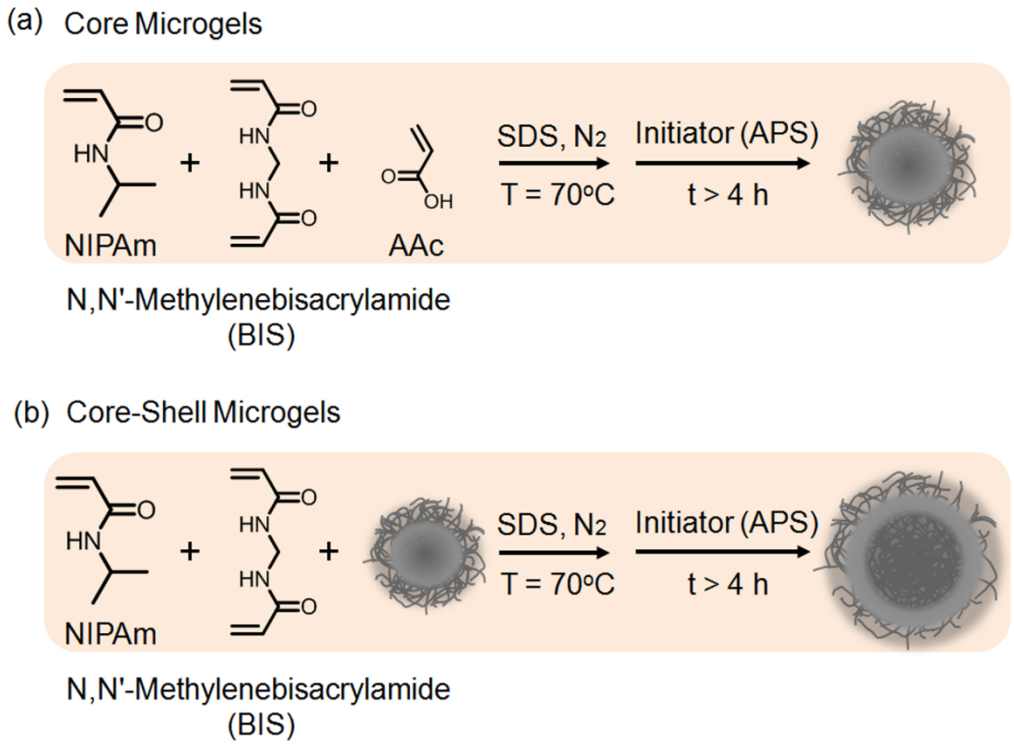

Figure D-1. Strategies of core-shell microgels synthesis from free radical polymerization.

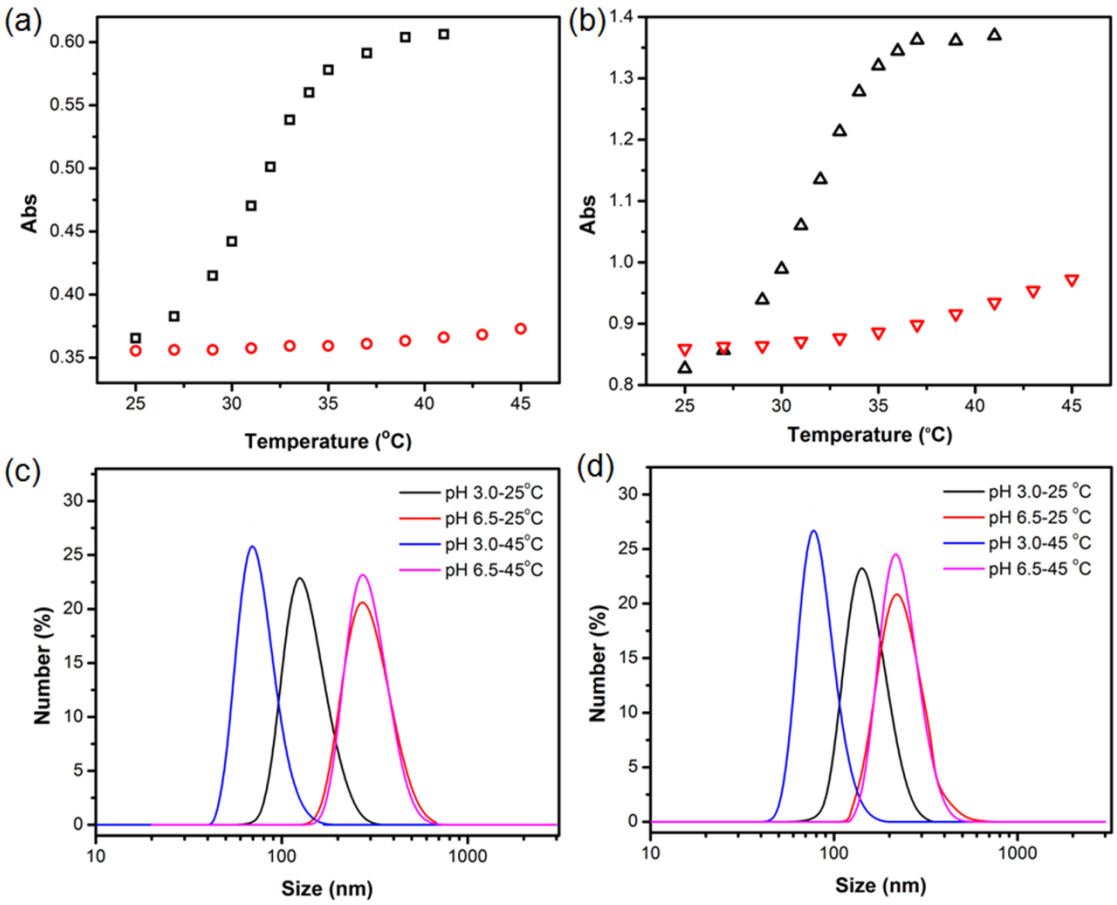

Figure D-2. LCST and size distribution characterization of p(NIPAm-*co*-AAc) core microgel. (a) LCST of p(NIPAm-*co*-AAc) core microgel under different pH 3.0 (black) and 6.5 (red). (b) LCST of p(NIPAm-*co*-AAc)@pNIPAm core-shell microgel under different pH 3.0 (black) and 6.5 (red). (c) Size distribution of p(NIPAm-*co*-AAc) core microgel under different pH and temperature. (d) Size distribution of p(NIPAm-*co*-AAc)@pNIPAm core-shell microgel under different pH and temperature.

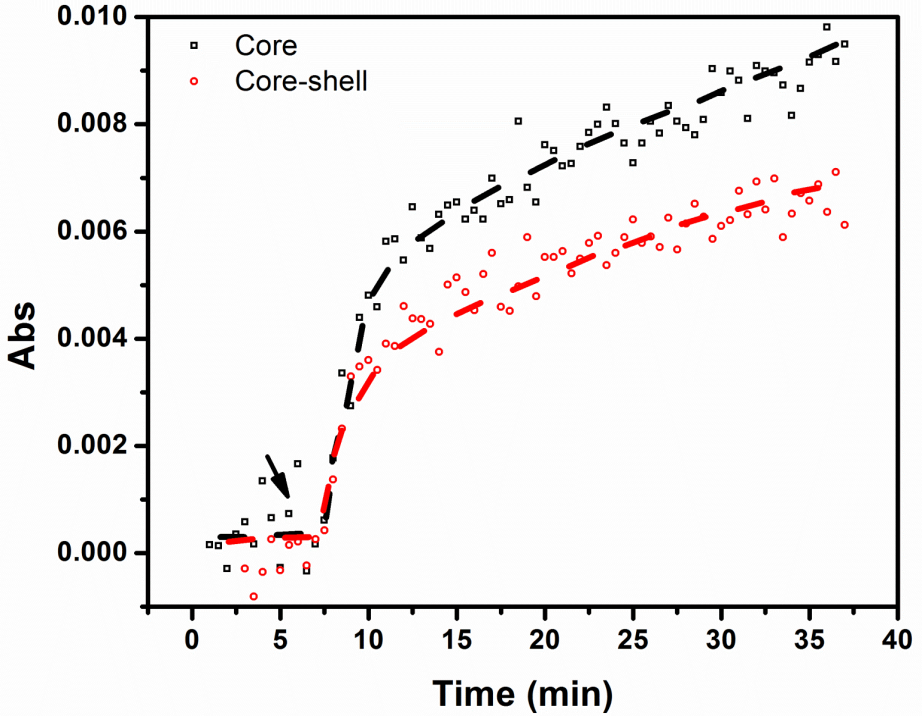

Figure D-3. Drug release profiles from p(NIPAm-*co*-AAc) core microgel (black) and p(NIPAm-*co*-AAc)@pNIPAm core-shell microgels (red) at 25 ^{o}C.

Appendix E: Stimuli-Responsive Microgel-Based Patches for Controlled Drug Release

In this project, we proposed to design a microgel-based patch to study the release behavior by controlling the porosity of the polymer film. The patch is prepared in the following way: firstly, a clean glass substrate was treated with Piranha solution, then poly (vinyl formal) (PVF) polymer with different concentration was spin coated, here a sacrificial layer can be used for better removing of the film in later step, and water soluble porous generation agent, like PEG, surfactant, are used to create the pores in the film. Followed by 50 nm Au evaporated, microgels were painted on the surface and excess were removed. Then drug was loaded and another polymer layer was coated as a cover layer to prevent the drug linkage and improve attachment further. Finally, the whole film was peeled off and transfer to another substrate for the test.

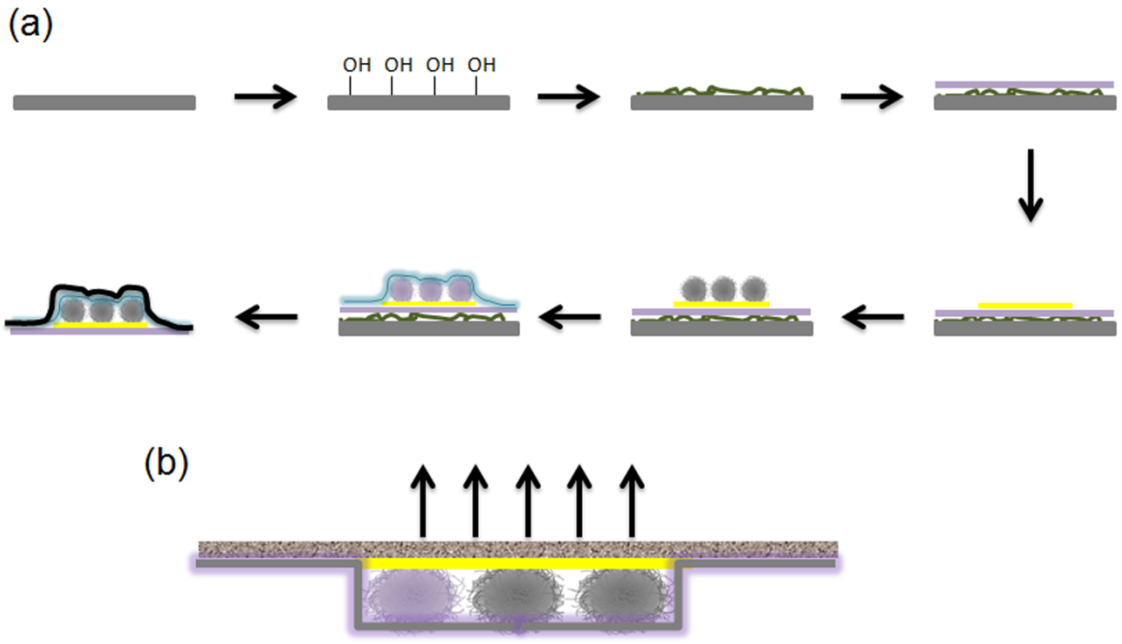

Figure E-1. Schematic illustration of the preparation of microgels-based patches drug reservoir (a) and (b) the structure of the patch and rate control polymer film.

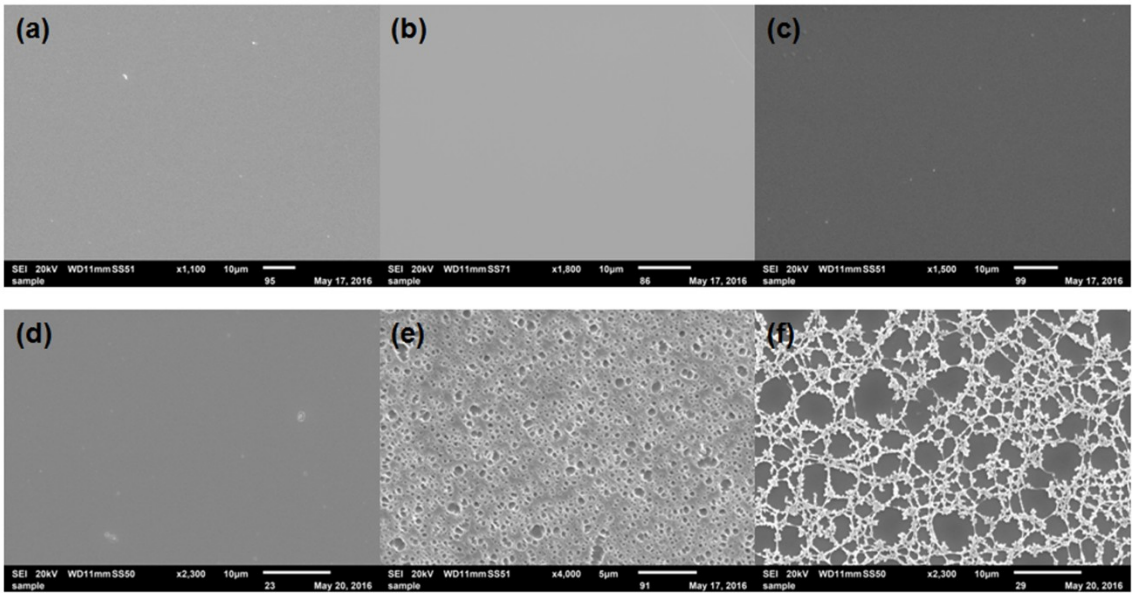

Figure E-2. SEM images of the porous polymer film from different ratio of PVF-PEG, (a) control, (b) 6:1, (c) 2:1, (d) 1:1, (e) 1:2 and (f) 1:4.

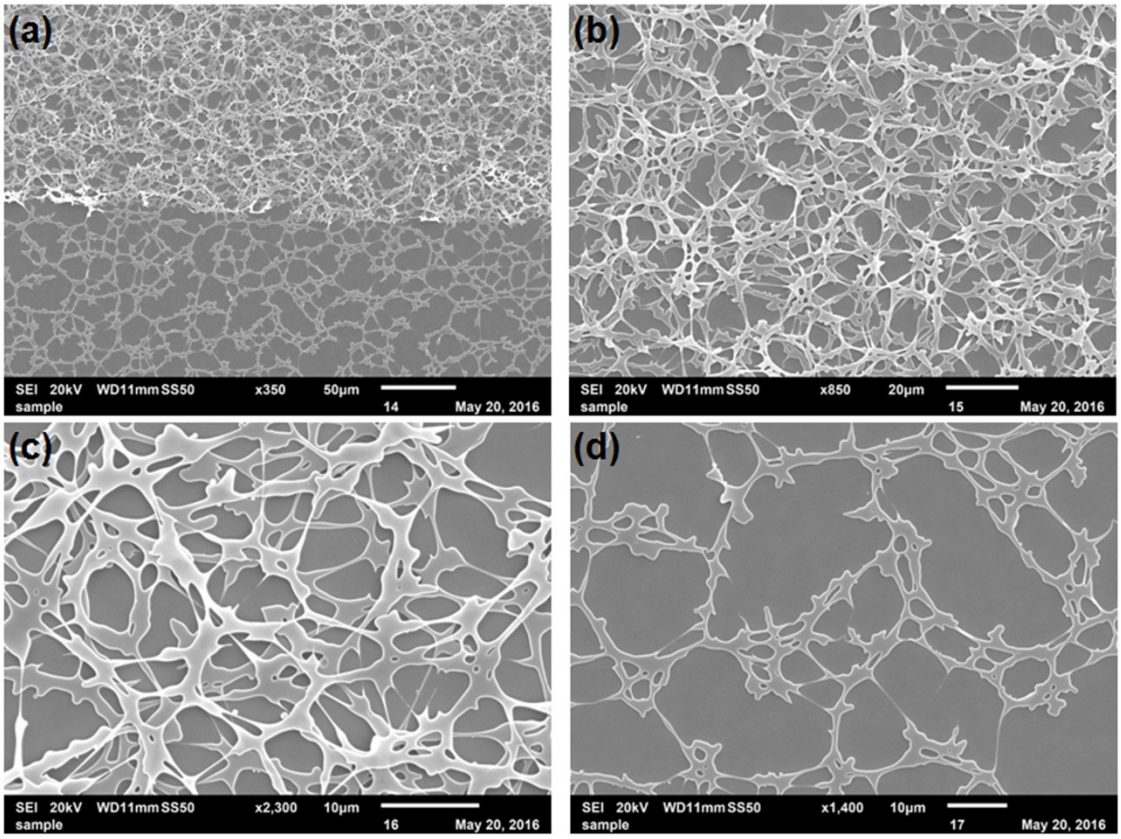

Figure E-3. SEM images with different magnification of the porous polymer film from PVF-Surfactant.

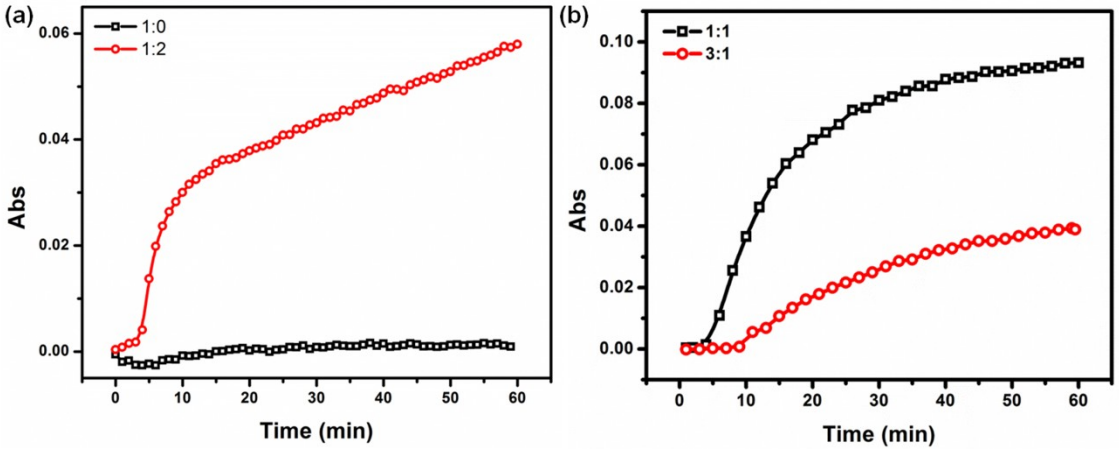

Figure E-4. Releasing profile of the prepared patches from PVF-PEG (a) and PVF-Surfactant (b).